

Charged Polymer Brushes: Design, Synthesis and Microbiological Evaluation

Department of Chemistry, Institute of Pharmacy
University of Hamburg

Dissertation

A thesis submitted for the degree of
Dr. rer. nat.

Nils Burmeister

Hamburg 2024

- 1. Academic supervisor:** Prof. Dr. Wolfgang Maison
- 2. Academic supervisor:** Prof. Dr. Sebastian G. Wicha
- 3. Academic supervisor:** Prof. Dr. Henk J. Busscher

Date of disputation (oral examination): 14.06.2024

“I am still confused – but on a higher level.”

Enrico Fermi

Danksagung

Mein besonderer und aufrichtiger Dank gilt Prof. Dr. Wolfgang Maison: Vielen Dank einerseits dafür, dass ich als ein Teil des Arbeitskreises bei dieser interessanten Themenstellung mitwirken durfte. Andererseits danke ich für die allzeit hilfsbereite fachliche Betreuung, die sich von meinem Pharmazie-Studium bis hin zum Einreichen dieser Dissertation erstreckte. Des Weiteren danke ich auch für die außerfachlichen Ratschläge und Hilfestellungen, die mich nachhaltig auf meinem Werdegang begleiten.

Darüber hinaus gilt mein weiterer Dank Prof. Dr. Sebastian Wicha für die Übernahme des Zweitgutachtens. Außerdem bedanke ich mich für die stetig unproblematischen Kooperationen und vor allem der Nutzung des S2 Labors. Zudem danke ich Ihnen ebenfalls für jegliche Expertise und jeglichen Beistand während des Studiums und während meiner Promotion. Zusätzlich danke Ich Prof. Dr. Louisa Temme und Prof. Dr. Ralph Holl für die Teilnahme an der Prüfungskommission.

Daran anschließend möchte ich mich auch bei dem gesamten AK Wicha für die umfangreiche Hilfsbereitschaft und Unterstützung bei Fragestellungen bedanken. Insbesondere gilt mein Dank Aneeq Farooq, Miklas Martens und Niklas Krömer, die mir jederzeit Platz, Material und gelegentlich helfende Hände zur Verfügung gestellt haben.

Einen weiteren Dank möchte ich an meine Kooperationspartner Dr. Nico Scharnagl (Hereon Geesthacht), Dr. Marcus Rohnke (JLU Gießen), Dr. Tomi Mantel (TUHH) und Lena Preuss (AG Streit) aussprechen, ohne deren Unterstützung ein Großteil der Publikationen nicht möglich gewesen wäre. Ferner danke ich allen Mitgliedern des Projekts AFOULs der Continental AG und insbesondere Dr. Fabrizio Pagnanelli für die stets gute Zusammenarbeit und dafür, dass ich ein Teil dieses progressiven Projekts sein durfte.

Natürlich danke ich den ehemaligen Mitgliedern des AK Maison: Dr. Serge Kliewer, Dr. Malte Holzapfel, Dr. Erik Ruf, Dr. Tim Naundorf, Dr. Sharah Chandralingam, Dr. Silke Schmidt, Dr. Tom Seddig, die mich sehr herzlich aufgenommen haben und mir jederzeit mit Rat und Tat zur Seite standen. Vor allem gilt mein Dank den aktuellen Arbeitsmitgliedern: Svenja Kerpa, Michelle Kobus, Erica Moretto, Shirin Mesgarha, Hauke Eggert, Laurens Ballentin, Lennart Spickschen, Timo Friedrich, Darius Ludolfs, Donovan Timm und Lasse Outzen. Insbesondere Michelle, Timo und Donovan danke ich für das Korrekturlesen dieser Arbeit. Ein besonderer Dank gilt in diesem Rahmen jedoch Eilika Zorn, die mir seit Beginn des Studiums, über die gesamte Promotion und darüber hinaus zur Seite steht. Danke, dass es dich gibt und ich hoffe, dass du mich, als meine engste Freundin auch weiterhin immer begleitest.

Bedanken möchte ich mich auch bei meinen Praktikanten Jule, Hannah, Hannah, Anna, Josefine, Leevke, Nick, Duc, Finn, Lennart und Dominik für euer Engagement und die hilfreiche Zusammenarbeit.

Weiterhin Danken möchte ich meinen engsten Freunden: Katja Scholz, Ole Hinrichs, Daniel Egor, Max Rembrink, Timo Westerfeld und Jonas Geweke. Vielen Dank, dass ihr meine Freizeit immer angenehm gestaltet, und hoffentlich immer gestalten werdet.

Der besonderste Dank gilt Anastasia. Ich danke dir von tiefstem Herzen, dass es dich gibt und du jederzeit für mich da bist. Vor allem, danke ich dir für dein Verständnis und deine unglaubliche Unterstützung mit deinem Zuspruch und deinem Vertrauen. Du hast mir diesen Weg als mein täglicher Sonnenschein erleichtert.

Zu guter Letzt gilt mein größter Dank meiner Familie. Vor allem aber meinen Eltern und meinem Bruder Lars (Brover). Vielen Dank, dass ihr mich bis hierhin unterstützt habt, ihr jederzeit für mich da seid und ihr immer für mich da sein werdet. Ich hoffe ich mache euch stolz.

The following results were obtained in Prof. Dr. Wolfgang Maison's research group at the Institute of Pharmacy of the University of Hamburg from April 2020 until November 2023.

List of Publications

- 1) Zwitterionic surface modification of polyethylene via atmospheric plasma-induced polymerization of (vinylbenzyl-)sulfobetaine and evaluation of antifouling properties**

Burmeister, N., Vollstedt, C., Kröger, C., Friedrich, T., Scharnagl, N., Rohnke, M., Zorn, E., Wicha, S.G., Streit, W.R., Maison, W.

Colloids and Surfaces B: Biointerfaces **2023** Vol. 224

(Impact factor: 5.8)

- 2) Low-Fouling and Antibacterial Polymer Brushes via Surface-Initiated Polymerization of a Mixed Zwitterionic and Cationic Monomer**

Burmeister, N., Zorn, E., Preuss, L., Timm, D., Scharnagl, N., Rohnke, M., Wicha, S.G., Streit, W.R., Maison, W.

Langmuir **2023**

(Impact factor: 3.9)

- 3) Surface-Grafted N-Oxides have Low-Fouling and Antibacterial Properties**

Burmeister, N., Zorn, E., Farooq, A., Preuss, L., Vollstedt C., Friedrich, T. Mantel, T., Scharnagl, N., Rohnke, M., Ernst, M. Wicha, S.G., Streit, W.R., Maison, W.

Advanced Materials Interfaces **2023**

(Impact factor: 5.4)

- 4) Contact-biocide TiO₂ Surfaces by Surface-Initiated Atom Transfer Radical Polymerization with Chemically Stable Phosphonate Initiators**

Zorn, E., Knaack J. I. H., Burmeister, N., Scharnagl, N., Rohnke, M., Wicha, S.G., Streit, W.R., Maison, W.

Langmuir **2023**

(Impact factor: 3.9)

Supplementary Publications and Unpublished Work

5) Charged polymers grafted from elastomers for offshore applications

Burmeister, N., Maison, W., Pagnanelli, F.

Unpublished Manuscript

Project (AFOUL) in cooperation with Continental AG, 2020-2022

6) Bio Resistant Zwitterionic Modification of Polyethylene Foils *via* Plasma Induced Polymerization

Burmeister, N., Maison, W.

Poster Presentation

DPhG Conference, Marburg 2022

7) Surface-Grafted N-Oxides have Low-Fouling and Antibacterial Properties

Burmeister, N., Maison, W.

Poster Presentation

DPhG Conference, Tübingen 2023

8) Interactions of Charged Surfaces with Bacteria and Biofilms

Burmeister, N., Zorn E., Maison, W.

Conference Talk, Poster Presentation

NordInfect Conference, Hamburg 2023

9) Medicinal Chemistry of Drugs with N-oxide Functionalities

Kobus, M., Friedrich, T., Zorn, E., Burmeister, N., Maison, W.

Perspective, under review (unpublished)

Journal of Medicinal Chemistry 2024

Patent Applications

Material mit langfristigen Antifouling Eigenschaften (2022P02354 DE (HACT))

Inventors: Pagnanelli F., Maison W., Burmeister N.

Partner: Dunlop Oil & Marine Ltd.

Submitted on: 12.10.2022

Content

1. Zusammenfassung	1
2. Abstract	5
3. Introduction	9
3.1 Relevance of Biofouling	9
3.1.1 Biofilm Formation	11
3.1.2 Marine Biofouling	13
3.2 Cell-Surface Interaction	17
3.2.1 Antifouling Strategies	19
3.2.2 Surface-Initiated Graft Polymerization	21
3.3.3 Monomer Design	26
3.3.4 Surface Topography	30
4. Aim of the Work	33
5. Results and Discussion (cumulative part)	35
5.1. Zwitterionic Surface Modification	35
5.2 Combined Low-Fouling and Contact-Active Surface Modification	49
5.3 Polymeric <i>N</i>-oxides for the Modulation of Biofilms	63
6. Modification of Elastomers	79
6.1 Charged Polymers Grafted from Elastomers for Offshore Applications	79
6.1.1 Introduction	80
6.1.2 Materials and Methods	82
6.1.3 Results and Discussion	88
6.1.4 Conclusion	99
6.1.5 Acknowledgements	100
7. Discussion - Critical Summary and Outlook	101
7.1 Methodology	101
7.2 Bioactivities	103
7.3 Novel but Restricted?	107

7.4 Future Directions	108
8. Literature	109
9. Appendix	123
9.1 Supplementary Materials	123
9.1.1 Zwitterionic surface modification of polyethylene <i>via</i> atmospheric plasma-induced polymerization of (vinylbenzyl-)sulfobetaine and evaluation of antifouling properties	123
9.1.2 Low-fouling and antibacterial polymer brushes <i>via</i> surface-initiated polymerization of a mixed zwitterionic and cationic monomer	138
9.1.3 Surface grafted N-Oxides have Low-Fouling and Antibacterial Properties ..	158
9.2 Supplementary Experimental Section	185
9.3. Hazardous Material	189
Declaration	193

List of Abbreviations

AMP	Antimicrobial peptides
ATR	Attenuated total reflected
ATRP	Atom transfer radical polymerization
CB	Carboxybetaine
C-di-GMP	Cyclic diguanylate
COSY	Correlated spectroscopy
CTA	Chain transfer agent
CTAC	Cetyltrimethylammonium chloride
d	Doublet
DABCO	1,4 diazabicyclo [2.2.2] octane
dd	Doublet of doublets
DLVO	Dejarguin, Landau, Verwey, Overbeek
DVB	Divinylbenzene
<i>E. coli</i>	<i>Escherichia coli</i>
EPM	Extracellular polymeric matrix
EPR	Electron paramagnetic resonance
EPS	Extracellular polymeric substance
Eq	Equivalent
ESI	Electrospray ionization
EtOAc	Ethyl acetate
EtOH	Ethanol
FLNG	Floating liquified natural gas
FPSO	Floating production storage and offloading unit
FRP	Free radical polymerization
FTIR	Fourier transform infrared spectroscopy
HMBC	Heteronuclear multiple bond correlation
HSQC	Heteronuclear single quantum coherence
iPrOH	Isopropanol
IR	Infrared spectroscopy
J	Scalar coupling constant
KTL	natural rubber/ styrene-butadiene rubber
LAP	Living anionic polymerization
LCP	Living cationic polymerization
LNG	Liquified natural gas

m	Multiplet
MCPBA	<i>meta</i> -Chloroperoxybenzoic acid
MIC	Minimal inhibitory concentration
MNNG-HOS	Human osteo sarcoma cells after treatment with <i>N</i> -methyl- <i>N'</i> -nitro- <i>N</i> -nitrosoguanidine
MS	Mass spectrometry
NMP	Nitroxide mediated polymerization
NMR	Nuclear magnetic resonance
NR	Natural rubber
OEG	Oligo- (ethylene glycol)
p-(VBTAC-co-VBSB)	A copolymer of monomers: Vinylbenzyl trimethylammonium chloride and vinylbenzyl (sulfobetaine)
<i>P. aeruginosa</i>	<i>Pseudomonas aeruginosa</i>
PA 6.6	Polyamide 6.6
PE	Polyethylene
PEG	Poly- (ethylene glycol)
PIMP	Photoiniferter-mediated polymerization
PP	Polypropylene
ppm	parts per million
PVC	Polyvinylchloride
QAC	Quaternary ammonium compound
QAS	Quaternary ammonium salt
QS	quorum sensing
Ra	2-dimensional average surface roughness
RAFT	Reversible addition-fragmentation transfer polymerization
RI	Radical initiator
RNA seq	Ribonucleic acid sequencing
ROP	Ring-opening polymerization
ROS	Reactive oxygen species
rt	Room temperature
s	Singlet
<i>S. aureus</i>	<i>Staphylococcus aureus</i>
Sa	3-dimensional average surface roughness
SAM	Self-assembled-monolayer
SB	Sulfobetaine

SBR	Styrene-butadiene rubber
SD	Standard deviation
SIMS	Secondary ion mass spectrometry
SPM	Scanning probe microscopy
SWI	Seawater intake system
t	Triplet
T+	Rubber compound KTL vulcanized with polyamide 6.6 wrapping tape
TBT	Tributyltin
TGA	Thermogravimetry analysis
Ti	Titanium
TMAO	Trimethylamine <i>N</i> -oxide
TNTC	Too numerous to count
ToF	Time of flight
UV	Ultraviolet
<i>V. gazogenes</i>	<i>Vibrio gazogenes</i>
VBDSB	3-(4-(4-Vinylbenzyl)-1,4-diazabicyclo [2.2.2]-octan-1,4-dium-1-yl) propane-1-sulfonate
VBNOx	Vinylbenzyl-(<i>N</i> -Oxide)
VBSB	Vinylbenzyl-(sulfobetaine)
VBTAC	Vinylbenzyltrimethylammonium chloride
WCA	Water contact angle
WHO	World Health Organization
XPS	X-ray photoelectron-spectroscopy
δ	Chemical shift

1. Zusammenfassung

Der Eingriff in die initialen Anheftungsprozesse von Mikroorganismen an Oberflächen stellt einen Schlüsselschritt für die Entwicklung antiadhäsiver (Antifouling) und antibakterieller Materialoberflächen dar. Insbesondere die Variation der Polarität und der Ladung auf Biofilm-assoziierten Oberflächen ermöglicht hierbei eine gezielte Modifikation der Zell-Oberflächen-Interaktionen. Die nötige chemische Funktionalisierung der Materialoberflächen, ihre Analyse sowie die mikrobiologische Evaluierung sind herausfordernd. Darüber hinaus sind die Wechselwirkungen der Mikroorganismen mit den funktionalisierten Oberflächen unzureichend verstanden. In diesem Kontext beschreibt die vorliegende Arbeit die Synthese und systematische Untersuchung geladener Polymerbürsten auf Biofilm-relevanten Oberflächen.

In einer ersten Arbeit erfolgte die Immobilisierung von Vinylbenzyl-Sulfobetain (VBSB), einem zwitterionischen Styrol-Derivat, auf Polyethylen (PE). Die Modifizierung des chemisch inerten PE wurde über Atmosphärendruck-Plasma-Aktivierung mit anschließender Sprühbeschichtung durchgeführt, welche im Vergleich zur ursprünglich genutzten Lösungsbeschichtung eine skalierbare, industriell adaptierbare Methode darstellt. Die resultierenden zwitterionischen Propfpolymerer zeigten Schichtdicken im Bereich von 50-100 nm, eine Ladungsdichte von $> 10^{16}$ zugänglicher anionischer Sulfonat-Gruppen pro cm^2 und damit einhergehenden stark hydrophilen Eigenschaften (Wasser-Kontaktwinkel $< 10^\circ$). Zur Bestimmung der zwitterionischen Ladungsdichte wurde ein neuartiges Kristallviolett-Assay, basierend auf einem Ionenaustausch-Mechanismus, entwickelt und validiert. Die elementare Zusammensetzung und Präsenz des VBSB-Polymers auf PE wurde über XPS, ToF-SIMS und FT-IR bestätigt. Die mikrobiologische Evaluation hinsichtlich der passiven Antifouling-Eigenschaften wurde in einem bakteriellen Adhäsionstest gegen Gram-positive Bakterien (*S. aureus*) belegt. Darüber hinaus wurde ein langfristiger Antifouling-Mechanismus in natürlichem Seewasser über einen Zeitraum von 21 Tagen beobachtet. Dieses erstmals beschriebene, effiziente und skalierbare Protokoll zur Herstellung zwitterionischer Polymerbürsten bildete weiterführend die Grundlage für die Modifizierung von marin-genutzten Elastomeren (Sektion 6, nicht kumulativer Part).

Die Verifizierung der antiadhäsiven Wirksamkeit von Sulfobetain-Gruppen und der belegten Kontakt-Bioziden-Wirkung von quaternären Ammoniumgruppen, lieferte die Grundlage für die Entwicklung des neuartigen Styrol-Monomers (VBDSB), welches beide genannten Funktionalitäten vereint. Die oberflächeninitiierte Polymerisation dieses Monomers auf Titan- und Polyethylen-Grundmaterial ergab bifunktionelle Polymerbürsten mit Schichtdicken von über 750 nm, die durch ToF-SIMS-SPM-Messungen bestätigt wurde. Die chemische Zusammensetzung der Bürstenpolymere wurde durch XPS- und FT-IR-Analysen bestätigt. Die Oberflächenladung, charakterisiert durch das Zeta- (ζ -) Potenzial, war unabhängig vom pH-

Wert positiv, und die Anzahl der für Lösungsmittel zugänglichen Ammoniumgruppen betrug $\sim 10^{16} \text{ N}^+/\text{cm}^2$. Dies führte zu einer starken antibakteriellen Aktivität gegen Gram-positive und Gram-negative Bakterien. Die Bestätigung der bifunktionellen Wirksamkeit wurde abschließend über Zelladhäsionstests gegenüber Gram-positiven und Gram-negativen Bakterien festgestellt. Die Darstellung, Propfpolymerisation und Charakterisierung dieses neuartigen Monomers begründet die neue Stoffklasse der polymeren „Diammonium-Sulfonate“ als erste derartige Kombination von aktiven und passiven Wirkmechanismen.

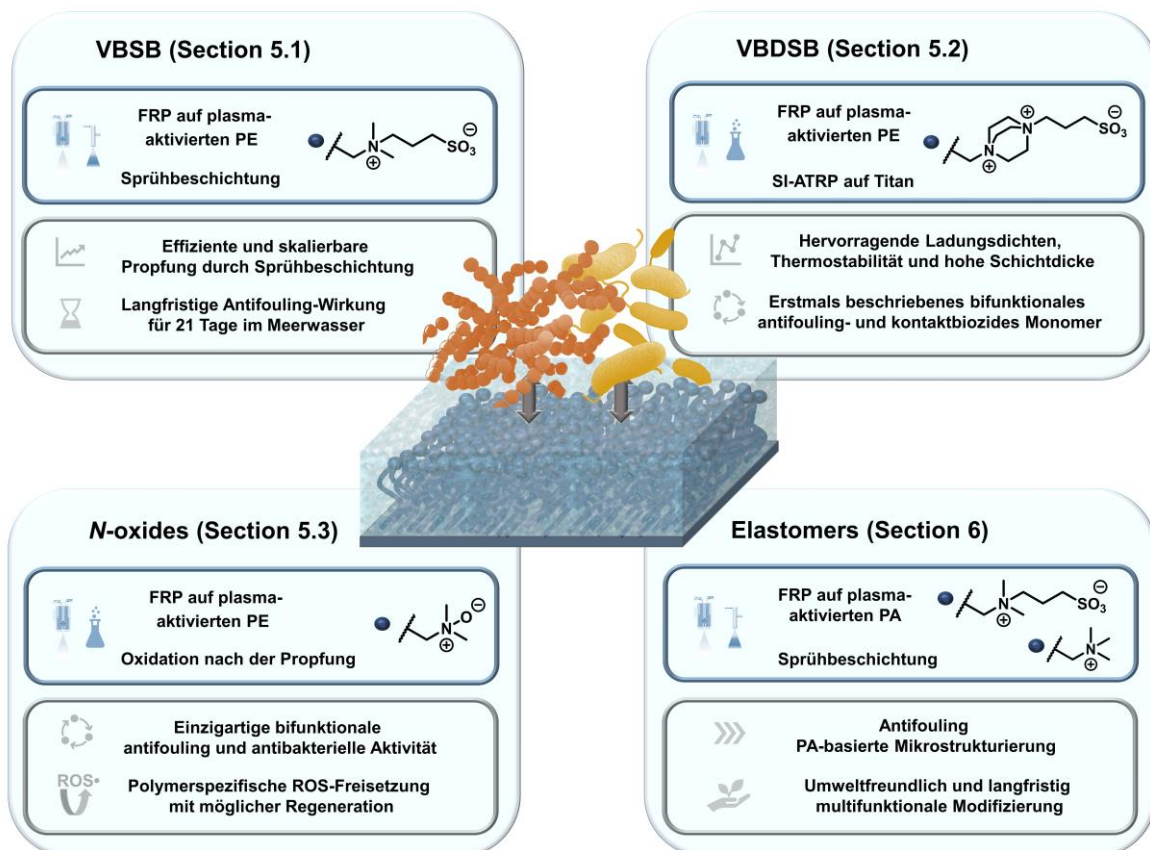


Abbildung 1: Zusammenfassende Übersicht der untersuchten Oberflächenmodifikationen mit der Beschreibung der genutzten Propfpolymerisation und der Darstellung der wichtigsten chemischen und biologischen Eigenschaften der charakterisierten Beschichtungen.

Einen ebenso neuartigen bifunktionellen Charakter zeigte die Oberflächenmodifizierung von PE mit polymeren *N*-oxiden. Diese wurden in jüngsten Studien als biomimetische zwitterionische Verbindungen mit geringen Proteinadsorptionen assoziiert. Die Immobilisierung polymerer *N*-oxide über eine *post-grafting* Oxidation auf plasmaaktiviertem PE lieferte hydrophile Oberflächen mit passiven Antifouling-Eigenschaften in Bakteriensuspensionen. Darüber hinaus wurde erstmalig in diesem Kontext eine antibakterielle Aktivität gegen Gram-negative und Gram-positive Bakterien, durch eine

Polymer-spezifische Freisetzung von reaktiven Sauerstoffspezies (ROS), beobachtet. Zudem wurde festgestellt, dass die bioaktiven *N*-oxid-Gruppen keinem Abbaumechanismus unterliegen, was auf einen nicht-limitierten, katalytischen bioziden Effekt hindeutete. Im Gegensatz zu anderen zwitterionischen Polymeren zeigen *N*-oxide damit eine einzigartige, antiadhäsive und antimikrobielle Wirkung.

Die skalierbare Sprühbeschichtung nach vorheriger Aktivierung mit Atmosphärendruck-Plasma fand zusätzlich eine erfolgreiche Anwendung in der Modifikation von Elastomeren im Kooperationsprojekt AFOUL („Entwicklung einer Antifouling-Gummimischung für Offshore-Unterwasseranwendungen“). Elastomer-basierte Schlauchsysteme, die für die Kühlung von Flüssiggas auf LNG Terminals genutzt werden, sind stark betroffen von marinem Biofouling. Diesem wird gegenwärtig mit umweltschädlicher Reinigung durch Hypochlorit entgegengewirkt. Polyamid-basierte Strukturen auf den genutzten Elastomeren führten zu einer initialen Topographie-bedingten Antifouling-Wirkung. Die darüber hinaus genutzte Propfpolymerisation bekannter kationischer und/oder zwitterionischer Polymere bestätigte langfristige Antifouling-Aktivität unter realen Seewasser-Bedingungen in einem maximalen Zeitraum von 9 Monaten. Diese synergistischen Modifizierungen prognostizieren eine Einsparung von 38.5 t des umweltschädlichen Hypochlorits pro Jahr sowie eine jährliche Reduktion der CO₂ Emissionen von 87 t.

2. Abstract

Interfering with the initial attachment processes of microorganisms to surfaces is a critical step in developing anti-adhesive (antifouling) and antibacterial material surfaces. In particular, the variation of polarity and charge on biofilm-associated surfaces enables the targeted modification of cell-surface interactions. The necessary chemical functionalization of the material surfaces, their analysis and microbiological evaluation are challenging. In addition, the interactions of microorganisms with the functionalized surfaces are insufficiently understood. The present work describes the synthesis and systematic investigation of charged polymer brushes on biofilm-relevant surfaces in this context.

The first work involved the immobilization of vinylbenzyl sulfobetaine (VBSB), a zwitterionic styrene derivative, on polyethylene (PE). The modification of the chemically inert PE was performed *via* atmospheric pressure plasma activation with subsequent spray coating, which is a scalable, industrially adaptable method compared to the originally used coating in solution. The resulting zwitterionic graft polymers showed layer thicknesses in the range of 50-100 nm, a charge density of $> 10^{16}$ accessible anionic sulfonate groups per cm^2 , and associated highly hydrophilic properties (water contact angle $< 10^\circ$). A novel photometric assay based on an ion exchange mechanism with crystal violet was developed and validated to determine the zwitterionic charge density. The elemental composition and presence of the VBSB polymer on PE were confirmed *via* XPS and FT-IR. The microbiological evaluation of the passive antifouling properties was confirmed in a bacterial adhesion test against Gram-positive bacteria (*S. aureus*). In addition, a long-term antifouling mechanism was observed in natural seawater over 21 days. This efficient and scalable protocol for producing zwitterionic polymer brushes was the basis for modifying marine elastomers (Section 6, non-cumulative part).

The verification of the anti-adhesive effectiveness of sulfobetaine groups and the proven contact-biocidal effect of quaternary ammonium groups provided the basis for developing the novel styrene monomer (VBDSB), which combines both of these functionalities. The surface-initiated polymerization of this monomer on titanium and polyethylene base material resulted in bifunctional polymer brushes with layer thicknesses of over 750 nm, confirmed by ToF-SIMS-SPM measurements. The chemical composition of the brush polymers was confirmed by XPS and FT-IR analyses. The surface charge, characterized by the zeta (ζ -) potential, was positive regardless of pH, and the number of solvent-accessible ammonium groups was $\sim 10^{16}$ N^+/cm^2 . This resulted in strong antibacterial activity against Gram-positive and Gram-negative bacteria. The confirmation of the bifunctional activity was finally completed by cell adhesion tests against Gram-positive and Gram-negative bacteria. The presentation, graft polymerization, and characterization of this novel monomer establish the new substance class

of polymeric "diammonium sulfonates" as the first such combination of active and passive mechanisms of action.

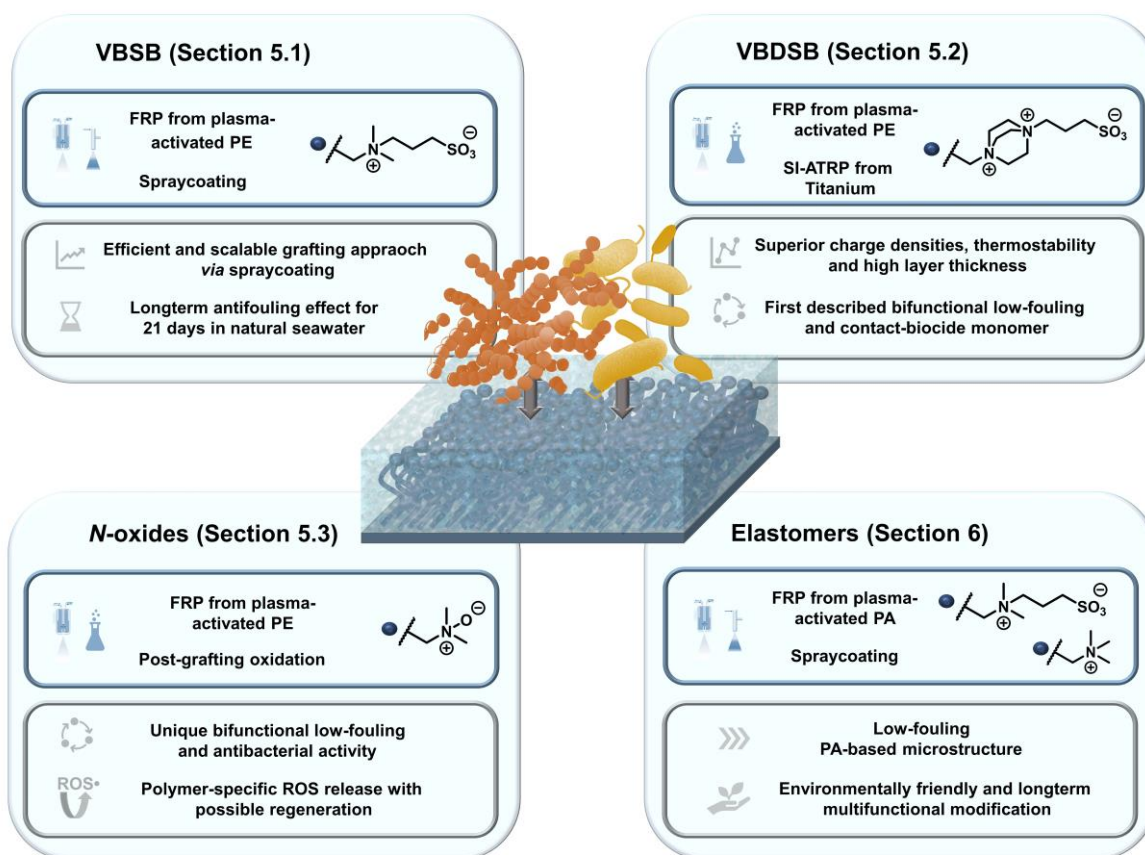


Figure 1: Summary of the investigated surface modifications, a description of the graft polymerization used, and a presentation of the most critical chemical and biological properties of the characterized coatings.

The surface modification of PE with polymeric *N*-oxides also led to materials with a novel bifunctional activity. In recent studies, polymeric *N*-oxides were associated with low protein adsorption, similar to other zwitterionic polymers. The immobilization of polymeric *N*-oxides via post-grafting oxidation on plasma-activated PE gave hydrophilic surfaces with passive antifouling properties in bacterial suspensions. Furthermore, antibacterial activity against Gram-negative and Gram-positive bacteria was observed for the first time in this context through polymer-specific release of reactive oxygen species (ROS). In addition, the bioactive *N*-oxide groups were found not to be subject to a degradation mechanism, indicating a non-limiting catalytic biocidal effect. In contrast to other zwitterionic polymers, *N*-oxides thus exhibit a unique anti-adhesive and antimicrobial effect.

After prior activation with atmospheric pressure plasma, the scalable spray coating was also successfully applied to modify elastomers in the AFOUL cooperation project ("Development of an antifouling rubber compound for offshore underwater applications"). Elastomer-based hose

systems used for cooling liquefied gas at LNG terminals are heavily affected by marine biofouling. This is currently counteracted by environmentally harmful cleaning with hypochlorite. Polyamide-based structures on the elastomers used led to an initial topography-related antifouling effect. In addition, the graft polymerization of known cationic and/or zwitterionic polymers confirmed long-term antifouling activity under natural seawater conditions over a maximum period of 9 months. These synergistic modifications predict a saving of 38.5 t of environmentally harmful hypochlorite per year and an annual reduction in CO₂ emissions of 87 t.

3. Introduction

3.1 Relevance of Biofouling

Microorganisms are invisible to the naked eye, yet they play a vital role in the earth's ecosystem. On the one hand, bacteria produce essential compounds for the earth's atmosphere and have a distinctive function in biogeochemistry. Moreover, they provide symbiotic exchange in vertebrates and invertebrates and contribute significantly to the maintenance of vital functions and metabolism.¹⁻³ On the other hand, they can act adversely by causing fatal systemic infections. Antibiotic-resistant bacteria, especially, pose a major challenge for humankind. Infections with resistant strains are associated with higher mortality rates and treatment costs compared to infections with antibiotic-susceptible bacteria.^{1, 4} This threat of resistant bacteria is worsened by a decreased number of new antibiotics available. In addition, the current widespread use of antibiotics contributes to the rise of resistant strains and less efficient treatment options against bacterial infections. Consequently, the World Health Organization (WHO) warns that a post-antibiotic era might be near.⁵

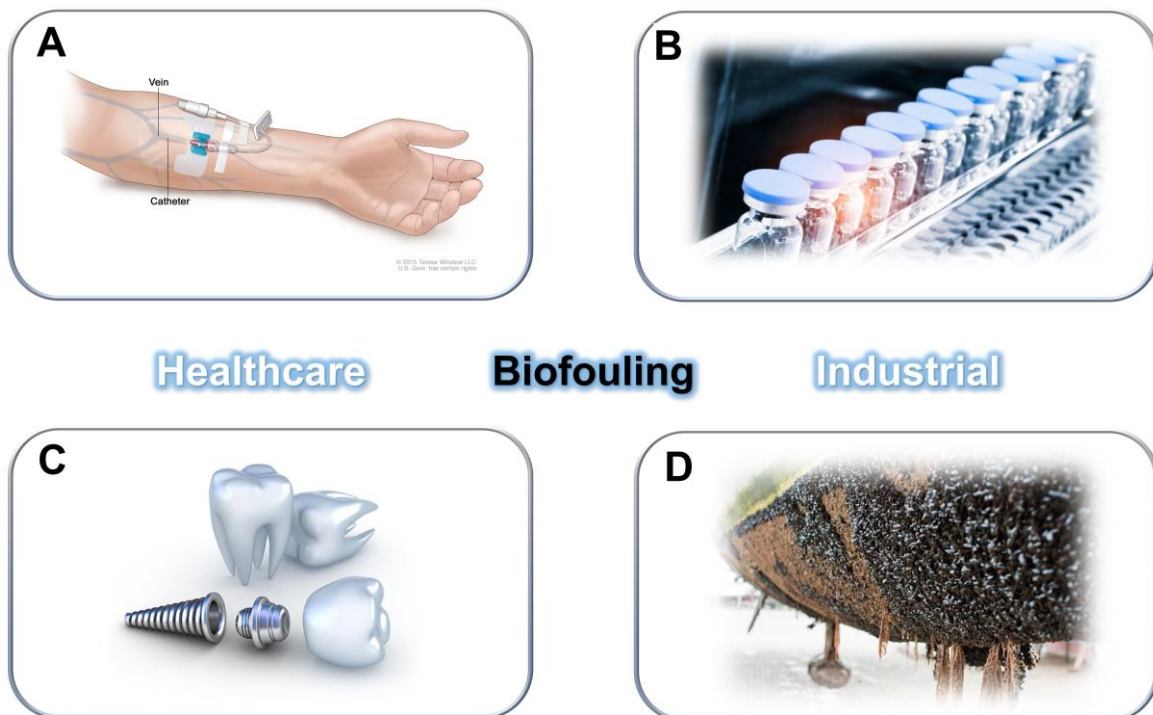


Figure 2: Examples of material surfaces typically affected by biofouling: Health-care-associated biofouling on catheters (A) or dental implants (C) related to severe infections and challenging antibiotic resistance.^{6, 7} Biofouling on pharmaceutical products (B) decreases product and patient safety. On marine applications such as ship hulls (D), biofouling's negative impact comes with severe economic and environmental harm.⁸⁻¹⁰

Moreover, microorganisms possess the ability to form aggregated colonies into biofilms, which can occur on any biotic or abiotic surface. This microbial assembly of biofilms is likewise ubiquitous and represents an evolutionarily essential process for the development of life on Earth, which still contributes to biogeochemical homeostasis today. Despite these natural advantages, biofilm formation on surfaces used for medical or industrial purposes can have serious consequences. On implants and medical devices (*e.g.*, catheters), the aggregation of opportunistic microorganisms can lead to severe systemic infections, which are associated with increased development of resistance and more difficult or even ineffective antibiotic therapy.^{6, 7} In healthcare-related manufacturing and processing, biofilms compromise disinfection methods. This contributes to an increase in biocide use and decreased product and customer safety.^{11, 12} In marine applications and drinking water processing, biofilm formation is the first step in the ensuing accumulation of higher organisms on surfaces. This so-called irreversible biofouling causes corrosion, high fuel consumption, or clogging.¹³ The control of irreversible biofouling is associated with increased use of disinfectants or complex and sometimes environmentally hazardous cleaning processes. As a result, both the presence and the prevention of biofouling lead to economic and ecological challenges. Thus, biofilms, biofilm-associated infections, and irreversible biofouling pose major challenges to healthcare and many industries.

3.1.1 Biofilm Formation

The aggregation and accumulation of bacteria in natural or artificial environments are driven by evolutionary causes. As one of the first viable life forms (~3.25 billion years ago), the assembly of single prokaryotic cells and lone colonies to a merged aggregate promoted bacterial fitness and selection pressure that allowed survival under challenging conditions.¹ This is essentially caused by the continuous and flexible adaptation of these prokaryotic aggregates to the surrounding environment and, thus, the reaction to harsh circumstances such as extreme temperatures, changing pH values, and exposure to UV light up to further ionizing irradiations.¹⁴ Biofilm formation is thus an essential and integral property that provides homeostasis for prokaryotic cells in any hostile or friendly media. Aggregation to a microbial community comes with a number of advantages for microorganisms, such as a change in physical appearance, modified intra- and intercellular signaling and communication, and an extracellular polymeric substance (EPS), which increases their resistance against external degrading influences. Due to continuous adaptations driven by interactions with the colonized surface and the surrounding media, the physio-chemical nature of each biofilm is highly individual regarding their three-dimensional shape, structure, and mechanical stability.¹⁴⁻¹⁷

A good model for the complex process of biofilm formation is the 5-step model, based on the surface colonization of *Pseudomonas aeruginosa*, one of the best-studied microorganisms on abiotic surfaces.^{18, 19} Briefly, the 5-step model (Figure 3 A-E) is a simplified description of the complex cross-interaction between the substrate (host), bacteria (colonizer) and the surrounding environment (media). It starts with the reversible attachment processes of microorganisms and biomolecules (step A). The formation of durable sessile populations and activation of specific regulons that induce the initial production of an EPS is described as the irreversible attachment (step B). The formation of the EPS, which contributes to 90% of the biofilm mass (consisting of polysaccharides, proteins, nucleic acids, lipids and mostly water), is a crucial process. EPS, as the extracellular polymeric scaffold of biofilms, exhibits the center for nutrient and energy conversion by simultaneously providing physical protection, thus maintaining biofilm homeostasis.^{14, 16} The ensuing maturation (steps C and D) is characterized by intercellular communication known as *quorum sensing*. It leads to an adaptation of the proteome and metabolome and a functional three-dimensional EPS-embedded community.²⁰ Regarding *quorum sensing*, the second messenger, cyclic di-guanylate (c-di-GMP), was identified as a key transducer for EPS production and maintenance. C-di-GMP transcriptomic levels can be correlated to the biofilm stages. The accumulation and production of the biofilm matrix are proportional to higher c-di-GMP levels. In contrast, biofilm dispersal is mainly associated with low c-di-GMP transcripts.^{20, 21} The last step in this model is the disaggregation and release of either single cells or biomolecules and toxins from the biofilm or clusters of the

biofilm matrix, which is further known as dispersion (step E). The released biomaterial of the biofilm matrix can further contaminate the surrounding environment or undergo novel attachment processes, completing the circle of biofilm formation. ^{3, 4, 22}

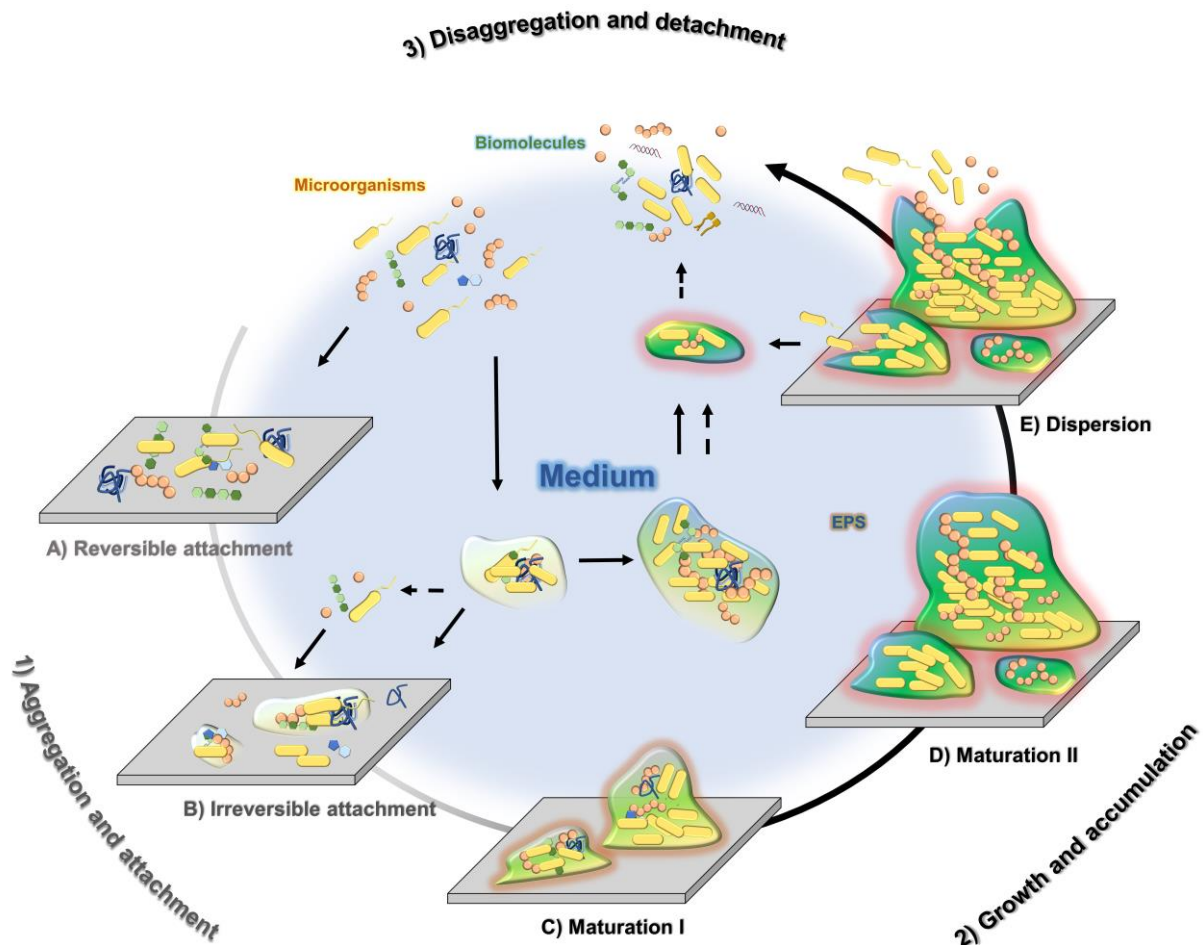


Figure 3: Dynamic process of biofilm formation in an open system. The three essential phases of biofilm development (1-3) are subdivided into five metaphases (A-E). The inner circle depicts biofilm formation in the media, while the surface-associated biofilms are on the continuous circular arrow. Intermittent arrows (—→) illustrate biofilm disaggregation, whereas aggregation is represented by continuous arrows (→).

The 5-step model originated from *P. aeruginosa* colonization displays an adaptable but limited scheme to describe biofilms.¹⁵ One of the main restricted aspects of this model is the generalization and drawback to one model pathogen (*P. aeruginosa*), implying homogenous colonization processes derived from *in vitro* assays that do not reflect real-life conditions. Native biofilms are often formed by a heterogeneous mixture of microorganisms and biomolecules (biomaterial) under fluid conditions involving nutrient and metabolic exchanges. Therefore, the complex interaction between the surrounding environment and the microorganisms' versatile adhesion mechanisms to the substrate's surface is neglected in the alleviated model. Thus, SAUER *et al.* generalized the 5-step model in which the initial steps are reconsidered and expanded by highlighting the heterogeneity of biomaterial and the complex dynamic interchange of the surrounding media on a micro- and macroscale.¹⁵ Herein, biofilm

formation is abstracted to a 3-step circular process¹⁵, which consists of 1) aggregation and attachment, 2) growth and accumulation and 3) disaggregation and detachment. The aggregation and attachment are determined by the microorganisms' species and the surface's nature. One major expansion in the initial adhesion context is the consideration of microorganisms into non-motile (mostly Gram-positive) and motile species (mostly Gram-negative). The latter are able to use transducing extracellular proteins (*e.g.*, *flagellum*, *fimbriae*, and *pili*) to identify surfaces and enable controlled settlement of cells on selected surfaces.¹⁹ Conversely, attachment of non-motile species primarily relies on gravitational forces, *i.e.*, shear forces, as high media fluency mitigates initial contact time.²³ Moreover, shear forces are also critical for non-motile species since mechanical impulses are known to activate surface-associated adhesion regulons, thus promoting surface settlement. A merged overview of both the 5-step surface-associated and the 3-step extended general biofilm process is given in Figure 3. The illustration contemplates biofilm development in more detail. The outer circle depicts surface-associated biofilm formation, considering biotic (*e.g.*, bones and tissues) or abiotic surfaces (*i.e.*, artificial materials) originating from the 5-step model (A-E). The inner circle depicts non-surface-associated biofilm formation and the possible interchange in dynamic and open biotopes between surface- and non-surface-related bacterial aggregations. Altogether, understanding initial attachment processes is critical for biofilm investigation. Accordingly, more profound insights into these processes can be used to derive targets for biofilm modulation. In experimental setups, it is crucial to consider motile and non-motile species in combination with applied shear forces.²³ This complexity of biofilm formation guides the planning, implementation, and interpretation of the microbiological assessment in this work.

3.1.2 Marine Biofouling

By far, the greatest challenge of surface-associated colonization is found in marine environments. This so-called marine biofouling follows similar initial principles to biofilm formation (section 3.1.1). However, marine biofouling is a more complex and the most difficult-to-address variant of surface settlement.^{24, 25} In this section, the definition and relevance of marine biofouling and its negative consequences will be discussed, followed by a critical summary of known strategies to prevent marine biofouling. This conclusively leads to the design of surfaces and modifications that will be explored in more detail in the following section (3.2).

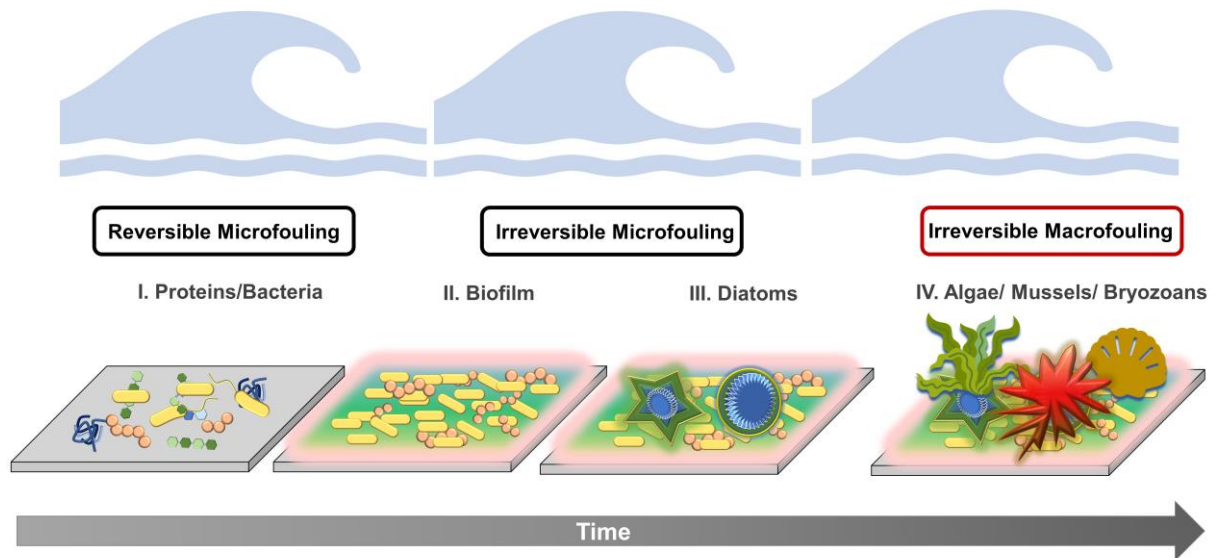


Figure 4: The four phases of biofouling in aquatic environments are categorized into micro- and macrofouling events. Marine biofouling starts from a conditioning biofilm, which depicts a connecting base for phytoplanktonic diatoms. Over time, marine organisms herein represented by algae, mussels, and bryozoans cause irreversible macrofouling.²⁶

Nearly any type of surface exposed to seawater is subject to direct colonization by microorganisms and higher organisms. Over 4000 marine species in aquatic ecosystems have been identified to be involved in marine biofouling. Each of these marine organisms possesses individual attachment properties. The dominating species involved in marine biofouling and their main fouling strategies are summarized in Table 1. The presence and attachment of aquatic species depend on environmental factors, such as the availability of vital resources and ecological niches with different climate conditions, level of nutrients, salinity, pH-value, and several other factors.^{25, 27} Definition-wise, four main phases of marine biofouling have been identified (Figure 4), that are not always strictly separated and may overlap in some cases. In summary, marine biofouling can be divided into microfouling and macrofouling, of which microfouling can occur either reversibly or irreversibly. As the main issue emerges the irreversible macrofouling. It involves the settlement of higher marine organisms (> 4000 species), whereas only 10 involved species of microorganisms (bacteria and diatoms) have been identified in the microfouling process.²⁸

Table 1: Overview of most commonly involved marine species in reversible microfouling and irreversible macrofouling events and breakdown of the major identified strategies for initial adhesion modified from QIU *et al.* ²⁸.

	Species	Fouling adhesion strategy ^{26, 29-31}
Microfouling (partially reversible)	Bacteria	Physicochemical interaction (section 3.2) <ul style="list-style-type: none"> • Coulomb forces, dipole-dipole-, hydrophobic-, specific-protein-interactions
	Diatoms	Interaction with biofilms and EPS: <ul style="list-style-type: none"> • Glycoproteins/ proteins • Enzymatic interactions
	Algae	Algal spores: <ul style="list-style-type: none"> • Spores-flagella interaction • Glycoproteins
Macrofouling (irreversible)	Bryozoan	Biofilm entity, density, and EPS interaction: <ul style="list-style-type: none"> • Mucopolysaccharides • Lectins and collagen-like proteins Extracellular matrix proteins
	Mussels/Barnacles	Cyprid and adult adhesion <i>via</i> catechol interaction: <ul style="list-style-type: none"> • Catechol-like 3,4-dihydroxy-phenylalanine (DOPA)-interactions • Glycoproteins/Scleroproteins

The continuous rise of globalization and marine mechanization since 1950 has catalyzed seaborne trade and the use of industrial marine applications. This evolution promoted the relevance and issue of marine biofouling, which can be viewed as a chain reaction with severe ecological and economic impacts.^{28, 32} The latter is primarily induced by the irreversible biofouling of higher organisms (*i.e.*, algae, bryozoans, mussels, and barnacles), which increases the friction coefficient due to enhanced surface roughness. This influences many other parameters, predominantly the energy needed to maintain the system's flow. Consequently, power and fuel consumption are escalating, with rising costs and emissions. The latter contributes significantly to environmental pollution by increasing the ejection of CO_x, NO_x, and SO_x gasses.³³ Adversely, fighting marine biofouling exhibits further environmental impact. The control of marine biofouling is always accompanied by an interference with a functional biotope. Considering the former solutions to prevent marine biofouling, which thrived by using toxic release coatings, the issue becomes particularly clear. Such releasing agents are known to be harmful to many aquatic species. Above all, the use of tributyltin-based

antifoulant coatings (TBT) and its derivatives was accompanied by severe genotoxicity and changes in biodiversity from 1970 until its global prohibition in 2008.^{24, 34} Yet, not only the application of toxic antifoulants demise biodiversity, also the relocation of non-native marine organisms as a consequence of vessel and shipment-associated biofouling expose critical impacts. This so-called biodiversity alteration induces severe changes in the respective ecosystems (Figure 5).^{13, 25}

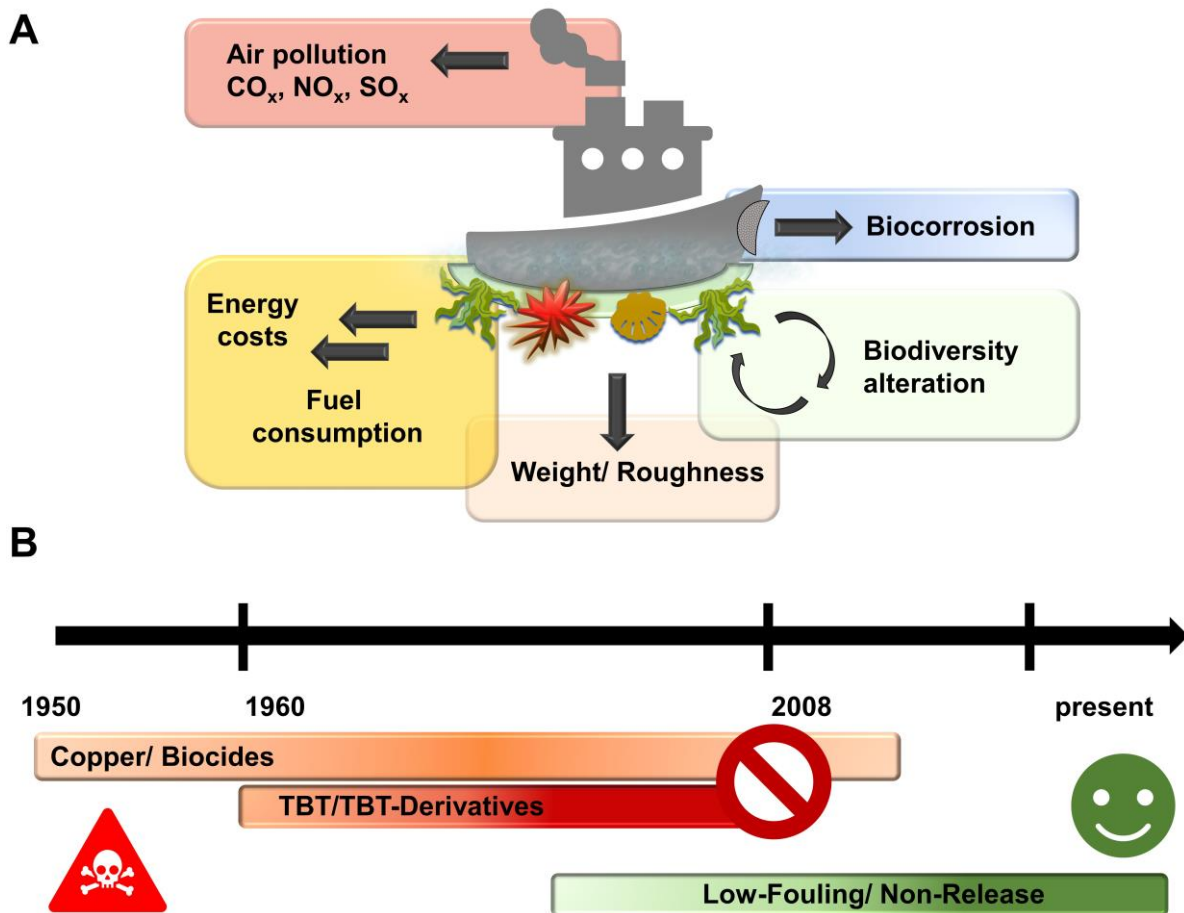


Figure 5: A: Negative impacts of marine biofouling.^{25, 28} Macrofouling increases weight and roughness, thereby enhancing fuel consumption and air pollution. Moreover, marine growth promotes biodiversity alteration by relocating non-native species and causes corrosive processes. **B:** Development of antifouling strategies from 1950 until the present.

Nowadays, the prevention of biofouling faces several difficulties that can be defined as follows: On the one hand, the requirements for antifoulants with respect to harmlessness are increasing as regulated in the Biocidal Product Regulation ((EU) No. 528/2012)).^{28, 35} On the other hand, the varying environmental conditions in which marine biofouling takes place challenge the development of broad-acting antifoulants. Accordingly, the excessive number of organisms involved in marine biofouling, each with its fouling characteristics, worsens the chance to develop wide-performing antifoulants. However, considering the comparably low number of

microorganisms involved in the initial steps of marine biofouling, the general academic *consensus* is thus based on intervention within these initial microbial attachment phases.²⁵ Modern solutions to prevent any kind of biofouling (not only marine biofouling) are based on environmental and economic compatibility. More precisely, these antifouling solutions have non-toxic, long-lasting, and preferentially non-release properties.³⁶ Consequently, current approaches deal with direct surface modifications in which all challenges are aimed to be widely addressed. For designing such surface modifications, a deep understanding of cell-surface interactions is required, which will be highlighted in the following sections.

3.2 Cell-Surface Interaction

The interaction of cells with surfaces is crucial for the formation of biofilms. Thus, many studies have deciphered fundamental principles for bacterial adhesion to surfaces: electrostatic effects (Coulomb forces), VAN DER WAALS attractions, and specific molecular interactions (Figure 6). These forces are not always clearly separable and often act synergistically during surface settlement.

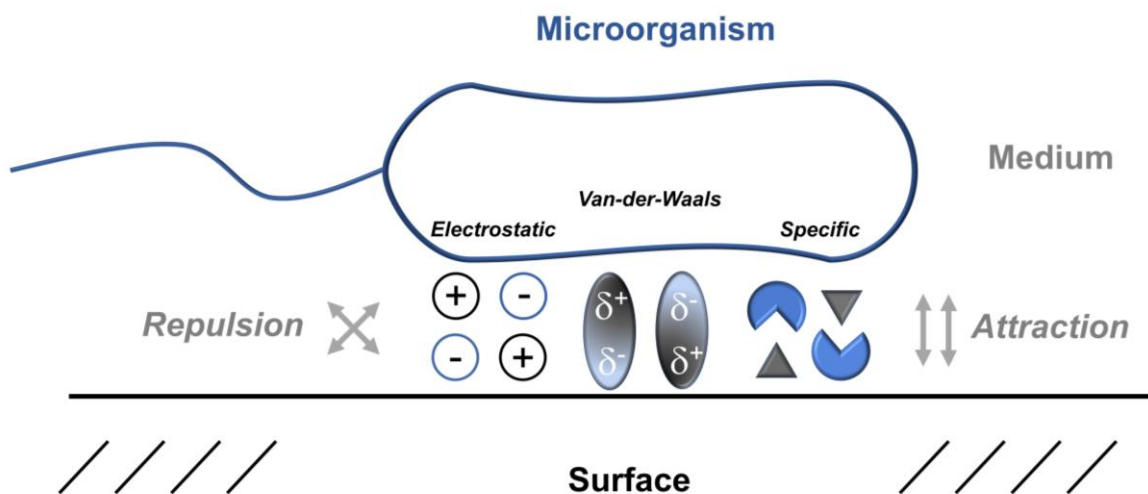


Figure 6: Overview of critical adhesive forces between bacteria and surfaces, modified from ZHENG *et al.*²³.

Electrostatic interaction generally depends on the structure of the electrochemical double layer of substrates and bacteria. These electrochemical double layers can be described by the surface zeta potential (ζ -potential). This potential of bacteria varies among different species but is generally negative.³⁷ Modulating the substrates ζ -potential can be achieved by introducing formal charges. For instance, conceivable modulation by the assembly of charged molecules at the interface affects bacterial adhesion. Attracting VAN DER WAALS forces likewise

contribute to bacterial adhesion at the interphase. These interactions strongly depend on the biochemical appearance as their manifestation relies on partial charges and induced dipoles.^{38, 23} Specific bindings are defined as all interactions based on specific protein- and specific molecular-signaling interactions. These interactions play a superior role in the attachment process and partially rely on the fundamental coulomb and dipole-dipole interaction. Most prominent specific connections are driven by *flagellum*, *pili*, or *fimbriae* interactions.³⁹ Likewise, bacterial surface sensing, including microbial surface components that recognize adhesive matrix molecules (MSCRAMMs) and acid-base interactions, are covered by this type of binding.³

Conclusively, identifying fundamental forces that determine bacterial surface attachment is crucial to ascertain potential targets for biofilm modulation. Derived from these principles, modifying the chemical integrity of the surface offers a potential strategy to interfere with said attraction forces and binding patterns. Furthermore, a detailed analysis of chemical composition and resulting physicochemical behavior supports the prediction, evaluation, and interpretation of biofilm formation and further biofouling processes.

A mathematical description of the adhesion process has been provided by the DLVO (developed by DEJARGUIN, LANDAU, VERWEY, and OVERBEEK) theory, originally derived from colloid systems (dispersed particles $< 5 \mu\text{m}$).^{40, 41} The DLVO-abstraction fundamentally describes energy contributions, which are needed to either attract or repel two sorts of condensed matter. This abstraction has been applied to bacterial surface adhesion (Figure 7).⁴² The DLVO function, combined with the previously described fundamental cell-surface connection pathways (Figure 6), highlights that repulsion and attraction are generally charge-driven interactions. In one respect, charges induce the electrostatic repulsion forces, contributing to bacterial rejection from the surface. These are described as double-layer repulsion (R_{DL}) and are accompanied by the rejection of the resultant electric fields, the born repulsion (R_B). Conversely, when speaking of bacterial adhesion, the initial and final surface approaches are driven by dipole-dipole attraction (A_{VdW}). As soon as these adhesive forces overcome the counteracting electric energy barrier, it results in the final adhesion of the cell to the surface (1st minimum). For inhibiting bacterial attachment to a surface, this energy barrier can thus be enhanced by increasing direct electrostatic repulsion (R_{DL}) and, subsequently, rejection of the bacteria by the induced electric fields (R_B).⁴²⁻⁴⁴ Increasing this energy barrier (depicted in Figure 7) is thus the key to developing antifouling surfaces. Accordingly, non-adhesive surface properties can be realized by installing charged and/or hydrophilic groups, which modulate the surface energy.

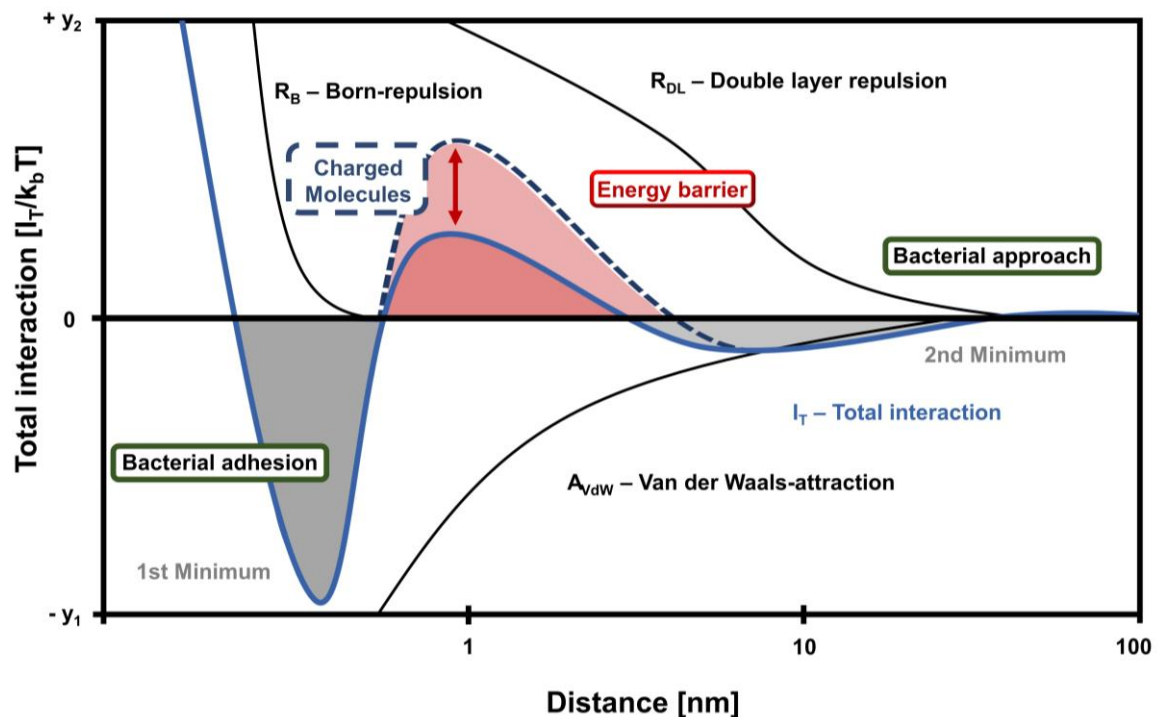


Figure 7: Simplified DLVO theory depicted as a function of involved repulsion (double layer and born repulsion) and attraction (VAN DER WAALS attraction) energies that contribute to the total interaction (blue line) and determine the achievement of bacterial approach (second minimum) and final bacterial adhesion to a substrate (1st minimum). The introduction of attractive or repulsive charges varies the amplitude of the energy barrier (intermittent blue line). This determines the thermodynamic bacterial adhesion at the interphase. Despite limitations, the function provides a mathematical illustration of the interaction mechanism of initial bacterial adhesion.^{40, 42}

However, the DLVO theory follows a mathematical model neglecting many properties of complex biological processes. Therefore, this theory does not cover all contributing influences, and each natural system should be interpreted individually. Other limitations, such as the size of the surface area, are also neglected.⁴⁴

3.2.1 Antifouling Strategies

Non-adhesive strategies for surface modification can be explained from a thermodynamic perspective, considering the concept of surface-free energy. Surface-free energy is defined as the energy that is either needed or released to create a new surface upon the surface of the original material. In other words, it is described as the energy difference between the original material surface and the covering foulants, e.g., bacteria or proteins. With respect to the laws of thermodynamics, systems tend to minimize their free energy. For example, materials with low surface energy ($WCA > 150^\circ$)⁴⁵ are already conditioned to a preferential thermodynamic state. It is, therefore, unfavorable to create a new film and enlarge its surface with adhering material such as bacteria or proteins. Common examples of materials with low surface

energies are fluorinated polymers or materials with specific topographical features (see 3.3.2). In contrast, surfaces with high surface energy ($WCA < 50^\circ$)⁴⁶ are usually generated by polar groups on the surface, such as zwitterions, polyethers, or polyalcohols. These groups form strong hydrogen bonds or dipole-dipole interactions with water. The resulting hydration layer minimizes the surface-free energy, increasing the energy barrier for other attaching foulants.⁴⁷ Steric repulsion induced by surface modifications can also contribute to antifouling activity. It may be achieved by assembling densely packed polymer brushes (e.g., OEG or PEG) on surfaces. As described in section 3.1.1, the bacterial biofilm relies on inter- and intracellular communication (*quorum sensing*) and has a unique proteome and metabolome. In addition to the above-mentioned chemical and physical antifouling strategies, initial biofilm formation stages can be inhibited with immobilized proteins modulating *quorum sensing* (QS) or other signaling mechanisms.^{48, 49}

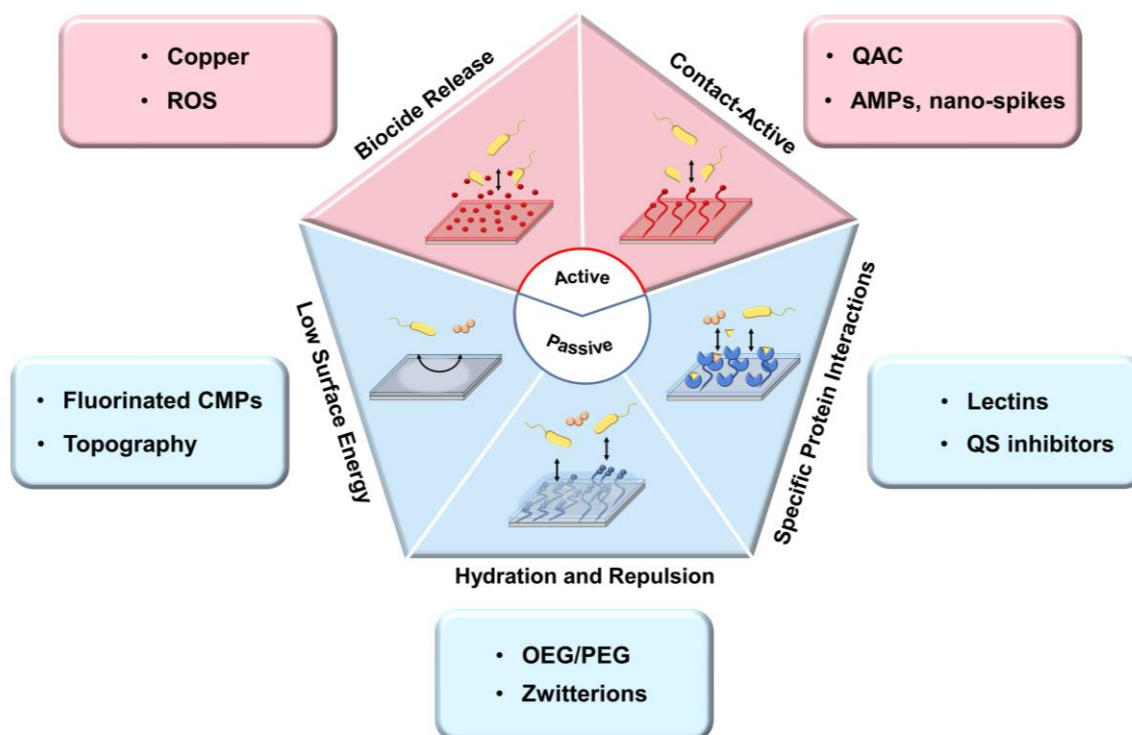


Figure 8: Antifouling strategies are divided into active approaches (red) that either degrade bacteria by release mechanism or exhibit degradation by contact through tethered antimicrobial agents or features. Non-adhesive antifouling (blue) is achieved by low or high surface energy and specific protein or signaling interactions.

Active antifouling strategies may either involve the release of an antibiotic or biocide or involve antimicrobial contact-activity. The latter may be achieved by installing positively charged polymers, such as quaternary ammonium compounds (QAC).⁵⁰⁻⁵² These polycations kill microorganisms upon contact, and the resulting materials are known as contact-biocides.⁵³

Other contact-active surface modifications involve antimicrobial peptides (AMPs)⁵⁴ or nanoscale topographic features like killing spikes (section 3.3.4).⁵⁵ The resulting materials have been demonstrated to prevent biofilm-associated infections of opportunistic pathogens in biomedical applications.⁵⁶ However, the polycationic surfaces lead to attractive electrostatic interactions with various biomolecules, and lysed biomaterial can, therefore, stick to the charged surface and may also be entrapped in non-charged nanopatterned structures. This process limits the efficacy of contact-biocide surfaces by blocking the contact-active functionality and forming a new proliferation ground for biofilm formation.⁵⁷ On the other hand, antimicrobial activity can be achieved by releasing antibiotic or toxic agents into the surrounding environment, thereby killing potential foulants. A noteworthy disadvantage of this release strategy is the negative impact of many released antibiotics and biocides on biotopes and their contribution to antibiotic resistance. Many novel release strategies are therefore based on biodegradable release agents such as bioactive peptides and enzymes with less impact on biodiversity and ecological homeostasis.⁵⁸

3.2.2 Surface-Initiated Graft Polymerization

There are several ways to transfer the previously discussed chemical and physical antifouling strategies to a material's surface. Many techniques are based on sol-gel-coatings,⁵⁹ nanotechnologies,⁶⁰ metal-ablative paints,^{61, 62} and chemical or physical modification of bulk materials.⁶³ Surface-initiated grafting of polymer brushes is a particularly attractive approach for chemically modifying material surfaces. This grafting technique allows the covalent connection of polymers to the surface without changing most bulk material properties.⁶⁴ Surface properties such as charge and hydrophilicity are determined by the choice of polymerizable monomer and polymerization technique. An overview of common graft polymerizations that have been employed for antifouling materials is given in the following sections.

3.2.2.1 Grafting Methods

In a broad sense, grafting is described as the immobilization of molecules on any surface. Graft polymerization involves, more specifically, the attachment of polymers to surfaces. In this case, the employed polymerization technique used for surface grafting strongly depends on the chemical composition and reactivity of the bulk material. Independent of the deployed grafting method, the immobilization of suitable molecules or macromolecules with chemically reactive surface functionalities is required. Such functionalization generates starting points, which

enable the covalent connection of the polymer brushes to the bulk material. However, physical and chemical surface activations can appear as diverse as synthesizing the desired polymer brushes. Derived from this premise, three main strategies to create polymer brushes are known as *grafting onto*, *grafting from*, and *grafting through* (Figure 9).

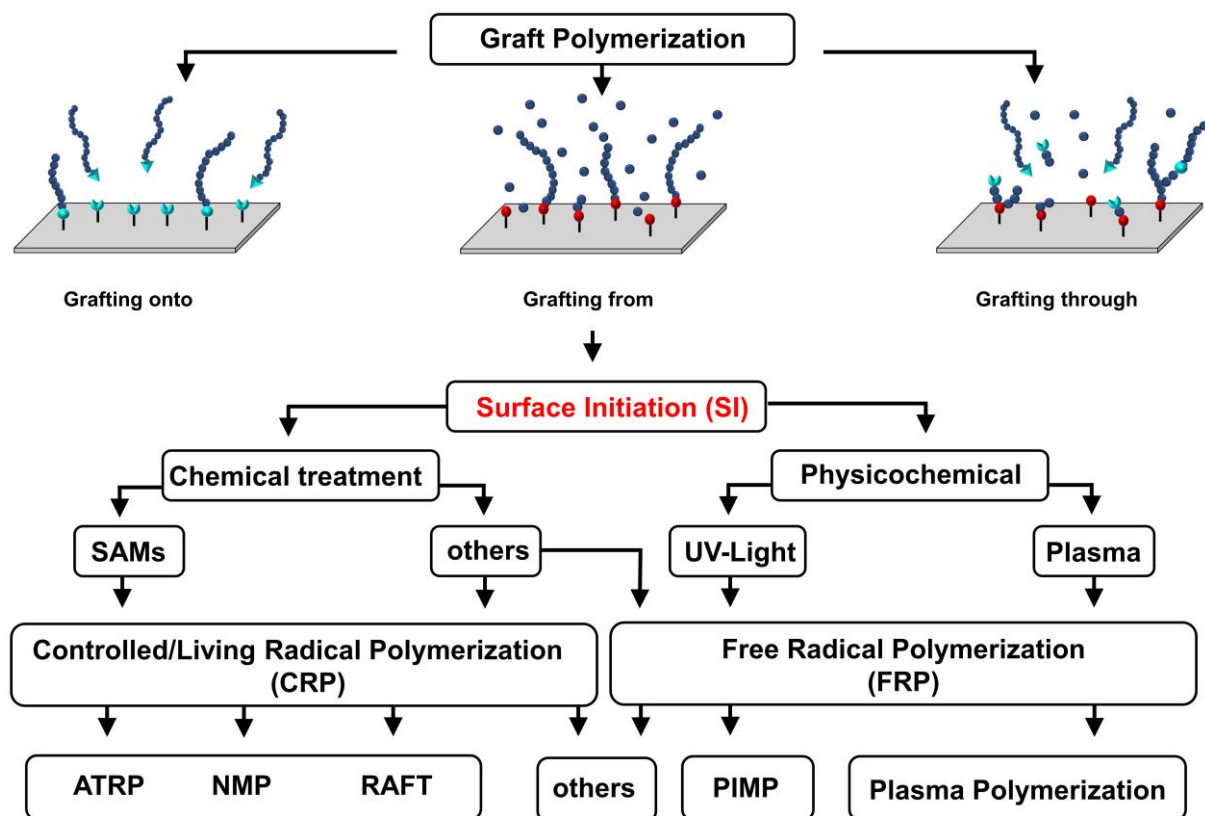


Figure 9: Principles of graft polymerizations focusing on the surface-initiated *grafting from* strategy.

The *grafting onto* approach involves reactions of pre-synthesized polymer chains with appropriate reactive groups on the substrate surface. An advantage of this strategy is the precise control of the molecular weight of the immobilized polymers prior to grafting, leading to well-defined polymer brushes.⁶⁵ A main disadvantage of this strategy is the insufficient grafting density and thickness of the resultant polymer brushes. Steric hindrance and repulsion of the chains during grafting limit the process.^{64, 65} Higher grafting densities can be generated with the *grafting from* approach. All grafting procedures rely on reactive functional groups on the surface and require thus the activation of otherwise inert base materials to allow chemical reactions like free or controlled/living radical polymerizations.⁶⁶ Common protocols for surface activation involve physico-chemical (*i.e.*, UV irradiation⁶⁷, plasma activation⁶⁸) or chemical pretreatments (*i.e.*, oxidizing or reducing agents). The latter is often followed by the immobilization of self-assembled monolayers (SAMs)⁶⁹, bearing initiator groups for *in situ* polymerization. The *grafting through* strategy combines elements of the *grafting from* and the *grafting onto* process. Briefly, surface-initiated anchor groups allow an *in-situ* polymerization

according to the *grafting from* approach. A subsequent grafting of added pre-synthesized polymers to the initial “*grafted from*” polymer chains leads to the final polymer brushes.⁶⁴

3.2.2.2 Controlled Radical Polymerizations

Because of the precise molecular architecture and homogeneity of the polymer brushes, the *grafting from* strategy has emerged as the method of choice for many antifouling materials. One associated polymerization technique is controlled/living radical polymerization (CRP), which precisely controls the polymer integrity regarding brush densities, thickness, dispersity, and chemical composition. Most CRP strategies involve the installation of linkers, mostly achieved by SAMs, which provide the covalent bond to the substrate's surface and the starting point for *grafting from* polymerization. CRP can be separated into various established synthetic approaches: Atom transfer radical polymerization (ATRP),⁷⁰ nitroxide mediated polymerization (NMP)⁷¹, and reversible addition-fragmentation chain transfer polymerization (RAFT).⁷²

ATRP is one of the best-studied SI-CRPs because of its applicability to a wide range of vinyl monomers.⁷²⁻⁷⁴ It is based on a halogenated initiator that provides the starting point for polymer growth (Figure 10). Additionally, a transition metal catalyst enables balanced propagation and termination, leading to precise control of the growing polymer brushes (Figure 11 A). RAFT polymerizations involve chain transfer agents (CTA or RAFT agents), mostly dithiocarbamates, dithioesters, or similar molecules. CTAs regulate the polymer brushes' chain length by establishing a dynamic equilibrium of initiation, propagation, and termination by reversible addition and fragmentation reactions.⁷⁵ In contrast, NMP involves a stable nitroxide radical that initiates and terminates respective polymer chains to obtain well-defined polymer brushes of low polydispersity.⁷⁶ The choice of the technique depends on the monomer and the desired properties of the resultant polymer brushes.

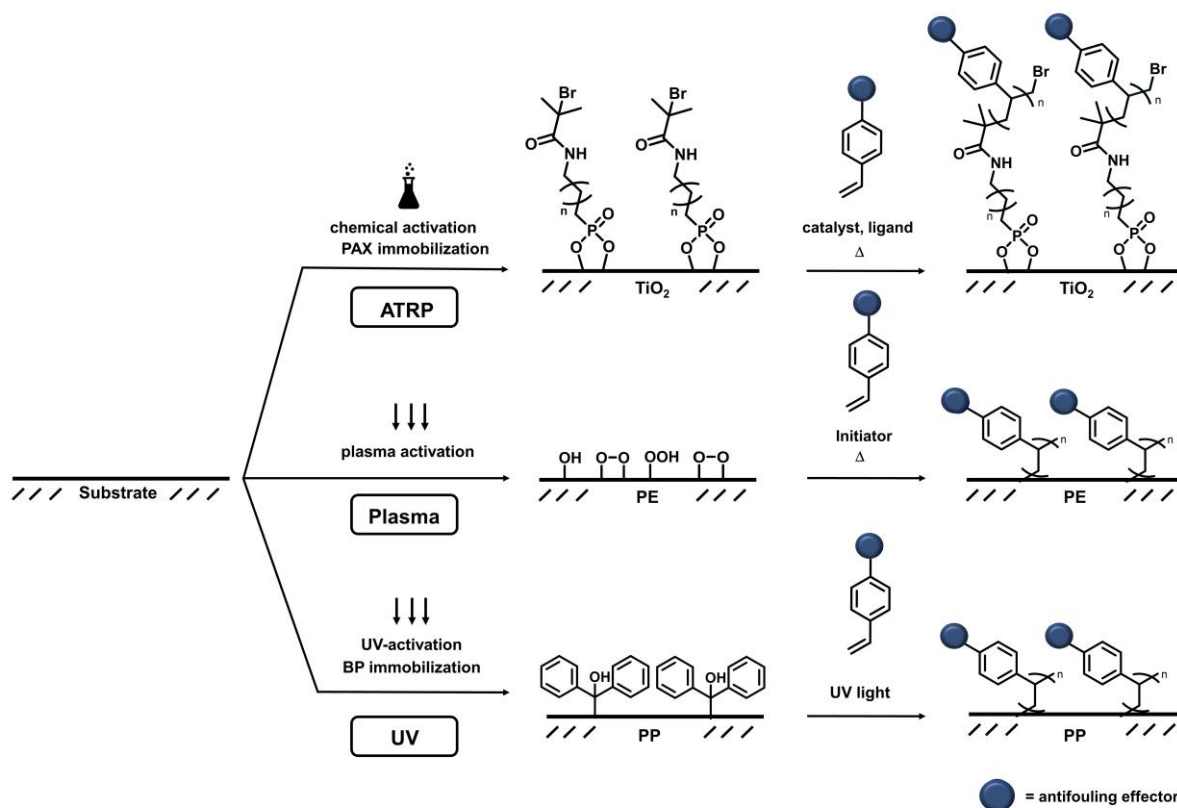


Figure 10: Exemplary routes for grafting a styrene derivative from a chemically inert surface. **SI-ATRP:** chemical surface activation with subsequent immobilization of phosphonic acid-derived bromine donor (PAX) on TiO_2 . Final grafting reaction in the presence of a catalyst and corresponding ligand to obtain controlled polymer brushes. **Plasma:** Atmospheric plasma activation of PE (mid-pathway) generates functional oxygen-containing groups, which enable free radical polymerization in the presence of a radical initiator and heat. **UV:** For PP-UV-grafting, immobilization of benzophenone (BP) is required as a consequence of UV irradiation and H-abstraction. In the second step, UV light initiates radical polymerization to the final graft polymers (lower pathway).

3.2.2.3 Free Radical Polymerizations

Free radical polymerization (FRP), or uncontrolled radical polymerization, is commonly used for the synthesis of a wide range of synthetic polymers with industrial applications. In contrast to CRP methods, FRP (*i.e.*, plasma polymerization) is often performed in alleviated procedures since no supporting catalysts or agents (*i.e.*, halogenated SAMs, CTAs) are implemented. Regarding surface activation, some bulk materials (*e.g.*, plastics) tend to have a less reactive surface than others (*e.g.*, metals and metal alloys) because of the lack of intrinsic functional groups. Therefore, using other initiations than SAMs and subsequent CRP, which would require harsh chemical treatments, is more advantageous environmentally and handling-wise. Accordingly, plasma treatment and UV-irradiation are mild and metal-free strategies to activate otherwise chemically inert surfaces (*e.g.*, PE or PP) for subsequent graft polymerizations. An overview of selected surface activations is given in Figure 10.

UV-mediated grafting means either free radical polymerization with prior immobilization of a photoinitiator (e.g., benzophenone) or surface-initiated photoiniferter-mediated-polymerization, called SI-PIMP. The latter is a hybrid form of controlled and free radical polymerization in terms of definition. Although the applied photoiniferter controls the initiation and termination of living chains, it does not provide reversible deactivation between living and dormant chains. Thus, no precise control of polymer weight and dispersity is given in SI-PIMP.⁷⁷ UV-mediated polymerization does not require high reaction temperatures. Therefore, UV-grafting is often associated with mild reaction conditions.⁷⁸

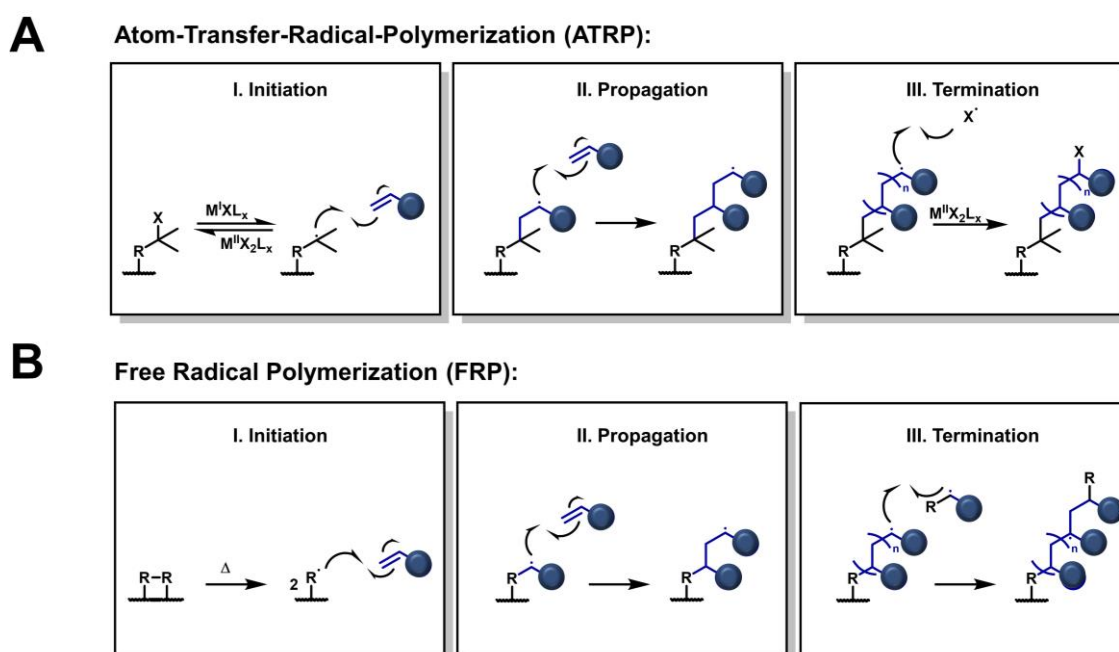


Figure 11: Reaction mechanism for Atom Transfer Radical Polymerization (ATRP) and Free Radical Polymerization (FRP). **A:** Mechanism of SI-ATRP. Initiation by the reaction of the alkyl halide by a transition metal complex ($M^I XL_x$) leads to the formation of surface-bound radicals. Chain propagation involves the reaction of surface-bound radicals with a double bond of the monomer. This is followed by the radical reaction of further monomers, leading to chain propagation. Termination occurs by radical recombination, such as halogenation, in the presence of the oxidized transition metal complex ($M^{II} X_2 L_x$). **B:** Thermal initiation generates two radicals that react with a monomer's double bond. Radical transfer to the further monomers leads to chain propagation. Recombination of two radicals leads to chain termination. For both techniques, other reactions like disproportionations may also be involved.

Besides UV-irradiation, plasma treatment is a particularly attractive method for surface activation because it allows the fast and linker-free functionalization of surfaces under environmentally friendly conditions. Plasma is an ionized gas that can be generated by applying energy such as heat or voltage to a defined process gas, resulting in a coexistence of ionized, neutral, and radical species.⁷⁹ The reactive particles attack various bulk materials and generate reactive functional groups on their surfaces. The process gas used for ionization and plasma generation determines the chemical composition of the reactive functionalities.

Especially the use of atmospheric air plasma has a high economic potential due to the efficient functionalization of bulk materials by ionizing ubiquitous atmospheric nitrogen and oxygen. The latter generates highly reactive oxygen-containing groups that serve as initiation points for free radical polymerization. An exemplary reaction mechanism for free radical polymerization is given in Figure 11 B.

3.3.3 Monomer Design

The structure of the graft polymer is dependent on the polymerization technique and the used monomer. The monomer is a critical component in the concept and defines the accessible polymerization chemistry and the properties of the final polymer. It consists of two essential units: a polymerizable group (typically a double bond) and an effector group. The effector group defines crucial properties of the final polymer, such as hydrophilicity, charge, solubility, and, thus, bioactivity. It can also impact the grafting density and the chemical or enzymatic stability of the polymer formed. In addition, chemical incompatibilities of the effector group with reagents or reaction conditions can restrict the accessible chemistry for polymerization.

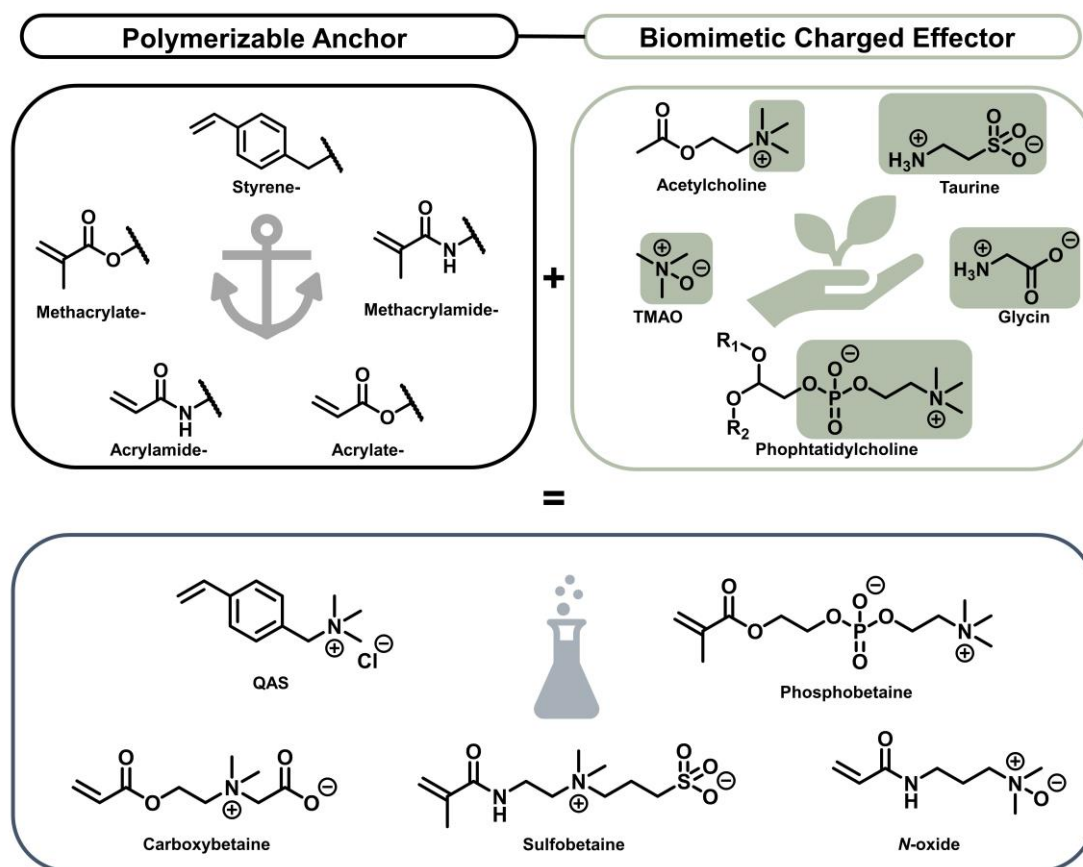


Figure 12: Biomimetic design principle for monomers used in this work for the *grafting-from* procedure.

Several aspects must be considered for the final structural selection of the monomer applied for graft polymerization. Monomers are typically used in large quantities, and a cost-effective, safe, scalable, and efficient synthesis is mandatory for later antifouling applications. In addition, the stability of the monomers and, consequently, of the polymers against high or low pH values, elevated temperature, redox processes, shear forces, and various other chemical, enzymatic, or physical impacts is important. Ideally, the polymerization of a monomer leads to a non-toxic polymer with enough stability for (long-term) biological application. Moreover, biodegradability can also be a decisive factor. Monomers need to be compatible with the applied polymerization techniques. For *in vivo* applications, a “stealth character” with good blood compatibility and a low immune response is crucial.

3.3.3.1 Polymer Backbone

The most common vinylic monomers used for graft polymerizations for antifouling applications are depicted in Figure 12. Most recent studies found that the bioactivity of the resulting polymer brushes is determined by the effector groups and is only slightly influenced by the backbone structure of the polymer. Therefore, the structure of the polymer backbone is primarily relevant for the physico-chemical stability of the polymer brushes.⁸⁰ Acrylates and methacrylates are the most extensively studied vinyl monomers. Their intrinsic reactivity is compatible with mild polymerization conditions and a variety of radical initiators. These properties make them applicable to multiple polymerization techniques. Moreover, ester or amide substructures are reasonably stable while being biodegradable at the same time.⁸¹ However, the chemical stability of polyacrylates or methacrylates and thermal decompositions can limit their application to certain polymerization techniques (*i.e.*, plasma- or UV-mediation) and compromise biological durability and stability.⁸¹⁻⁸³ An elevated stability of acrylates and acrylamides can be achieved by cross-linking.⁸⁴ Polystyrene backbones typically have higher stability than polyacrylates or methacrylates and are thus suited for long-term applications. Regarding free radical polymerization, styrene monomers tend to have a narrow control of the termination reaction due to their higher tendency for recombination. More importantly, polystyrene backbones are more stable against thermal or radiation-induced degradation, which enables the use of plasma or UV-mediated polymerization techniques.^{85, 86}

3.3.3.2 Effector Groups

The effector group plays a central role in designing suitable monomers for synthesizing polymer brushes with antifouling activity. As elaborated in the previous section (3.2), most antifouling surfaces are highly polar and often charged. Polycationic surfaces have contact-active properties (section 3.2.1) and can be prepared by the polymerization of quaternary ammonium compounds (QAC). Appropriate monomers bearing quaternary ammonium groups can be prepared in one step from halogenated precursors *via* MENSCHUTKIN-type substitutions (Figure 13 D and E). With diamine scaffolds (*i.e.*, DABCO), diammonium salts are accessible. QAS-based graft polymers are one of the most extensively studied for their contact-biocide behavior.⁸⁷ As a suggested mechanism of action, cationic surfaces attract small- or macromolecules by coulomb forces, thus destabilizing the outer membrane of microorganisms, leading to cell lysis.⁵¹ A significant disadvantage is the retention of dead and other anionic biomaterials on the positively polarized surface, which forms a potential nutrient base for biofilms.⁵⁷

To overcome the undesired attraction of biomaterial, effector groups that induce hydration and repulsion (see 3.2.1) enable so-called low-fouling and, most favorable, stealth properties. The latter is crucial for *in vivo* applications. In this context, the uncharged oligo-ethylene glycol (OEG) and poly-ethylene glycol (PEG) represented the gold standard for decades.^{36, 88} However, PEG derivatives often have limited stability in most biological systems due to their oxidative sensitivity.⁸⁹ Zwitterionic polymers are more stable analogs of OEG and PEG and have been shown to have excellent stealth properties.⁹⁰ One reason is the induced ionic solvation. Their ionic character enables the binding of water molecules upon electrostatic interactions, leading to more potent surface hydration than non-charged polymers (*i.e.*, OEG or PEG), which bind water *via* weaker hydrogen bonds.^{47, 91-93} The presence of H-bond acceptors only, high hydrophilicity, and neutral net charge were defined by WHITESIDE *et al.* as essential rules to ensure low-fouling activity.^{94, 95} To enhance hydration properties, the choice of appropriate cationic and anionic counterparts in zwitterionic polymers is vital.

Regarding cationic moieties, quaternary ammonium groups emerged as the most common functionality in the design of zwitterions.⁹⁶ Their chemical stability, non-toxic character, good biocompatibility (analogy to natural compounds such as choline), along with a high charge density make them superior to other cationic groups.^{90, 97, 98} The anionic counterpart and the separating carbon spacer also have an impact on hydration capacity, kosmotropic behavior, and steric repulsion.^{90, 99} In this context, four major anionic functionalities are used: Sulfates (SO_4^{2-}), sulfonates (SO_3^-), carboxylates- (CO_2^-) and phosphates (PO_4^{3-}). The selection of zwitterionic groups has often been guided by naturally occurring compounds. Examples can

be found in the amino acid taurine ($-\text{SO}_3^-$) and glycine ($-\text{CO}_2^-$) or the membrane component phosphatidylcholine ($-\text{PO}_3\text{R}^-$) (Figure 12).⁹⁰ Suitable monomers bearing zwitterions can be synthesized by straightforward nucleophilic substitutions or ring-opening alkylation (Figure 13 A and C).^{90, 100} Another example of zwitterionic functionalization, derived from the naturally occurring osmolyte trimethylamine *N*-oxide (TMAO), is polymeric trimethyl amine *N*-oxide (PTMAO). Polymeric *N*-oxides were first introduced by Marsh *et al.* in an antifouling context.¹⁰¹ The outstanding hydration ability and corresponding low protein adsorption are linked to the unique zwitterionic structure with no carbon spacer to separate anionic and cationic charge in the datively bonded *N*-oxide functionality.^{91, 102} The preparation of *N*-oxides can be achieved by oxidation of tertiary amines with organic (*i.e.*, MCPBA) or inorganic peroxides (*i.e.*, H_2O_2) and is thus readily scalable. Moreover, the use of PTMAO and its derivatives showed low complement activation and non-toxic behavior *in-* and *ex-vivo*, making *N*-oxide derivatives attractive for further research.^{91, 102}

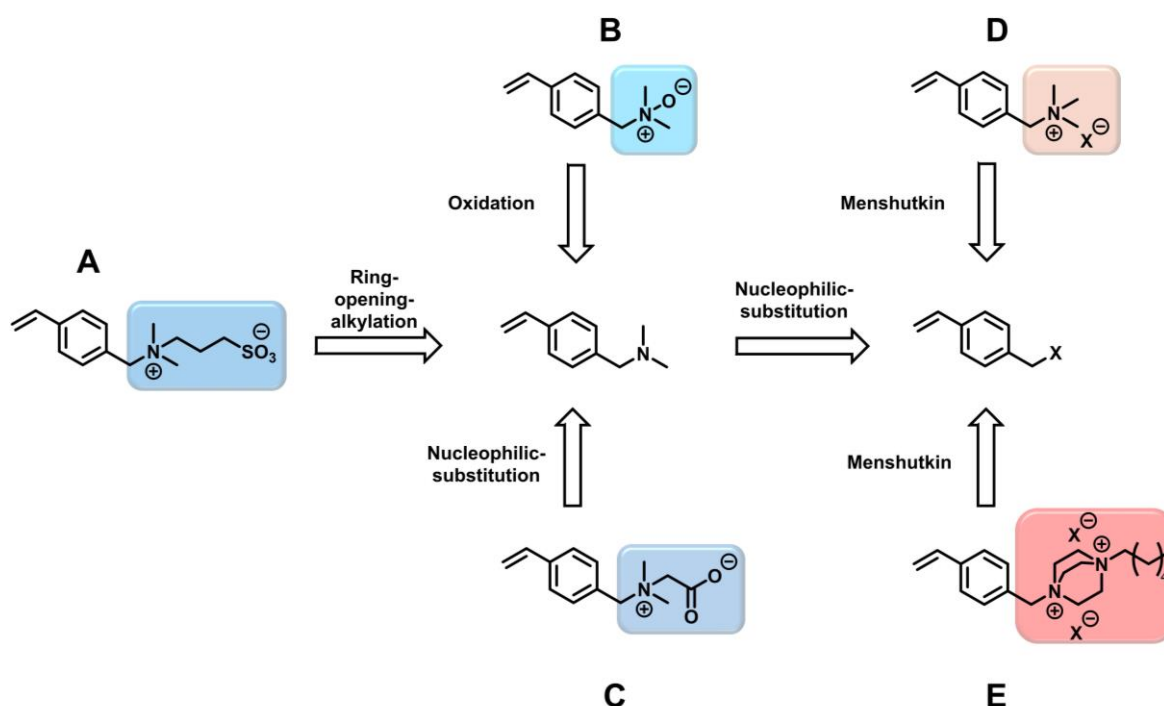


Figure 13: Retrosynthesis of selected styrene-based monomers. Zwitterions are depicted at their isoelectric point. **A:** Synthesis of zwitterionic sulfobetaine by ring opening alkylation.¹⁰³ **B:** Oxidation of tertiary amines to *N*-oxides.¹⁰⁴ **C:** Halogenated acetic acids can be used for nucleophilic substitution to generate carboxybetaines.¹⁰⁵ MENSCHUTKIN reactions enable the synthesis of quaternary ammonium salts (**D**) and diammonium salts (**E**).⁹⁷

In conclusion, charged monomers can be synthesized by combining the polymerizable unit with the effector group *via* scalable one- or two-step procedures. The effector group determines the resulting graft polymer's biological activity and physico-chemical properties. However, the properties of the monomer may differ significantly from those of the polymers. In brush layers, polymer chains have distinguished spatial distribution, leading to varying coulomb and dipole-

dipole interactions, neighboring group participations, and acid-base interactions. Stability, functionality, and compatibility with the applied grafting approach are thus crucial for the design and the choice of the monomer for graft polymerization and need to be evaluated for each monomer individually.

3.3.4 Surface Topography

Charged monomers and their corresponding graft polymers on surfaces generate high surface energies and are often associated with antifouling activity. As mentioned above, surfaces with low surface energy frequently possess self-cleaning properties and, therefore, exhibit likewise antifouling activity (Figure 8). In this context, micro- or nanostructured materials with unique surface topography have been particularly successful and can potentially be combined with other functional principles to provide multi-functional antifouling surfaces.

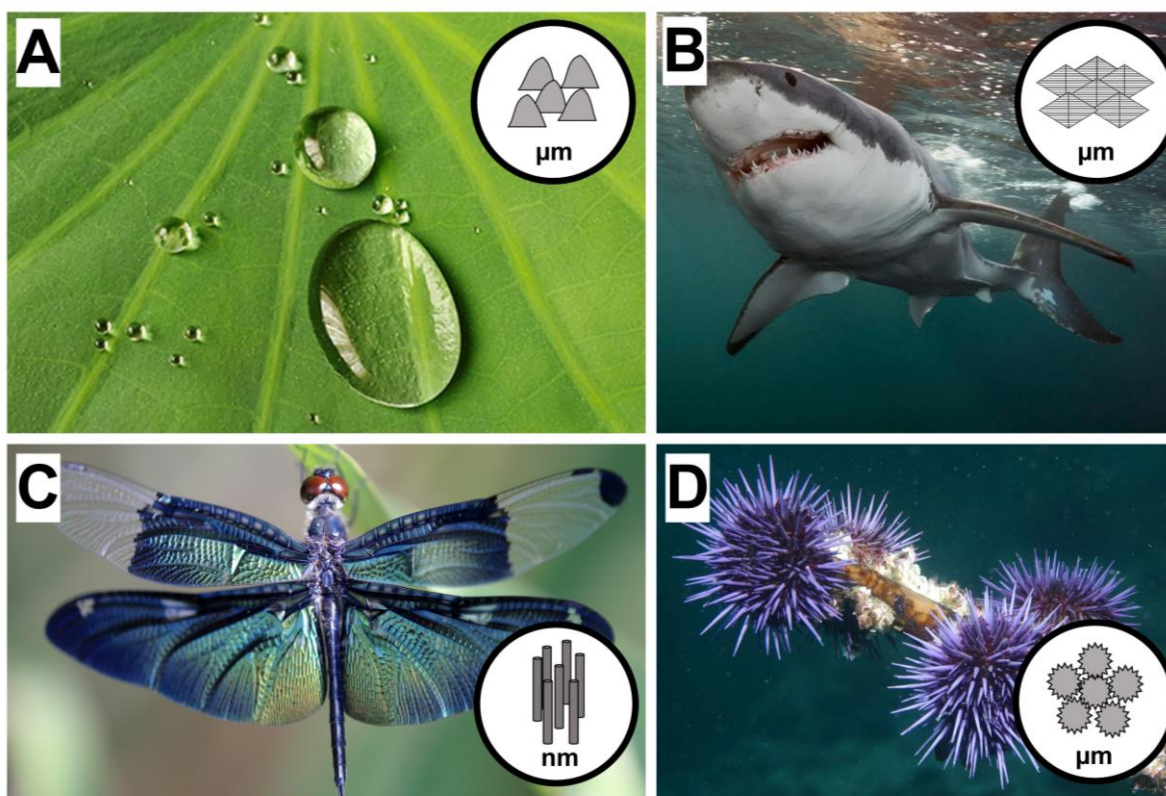


Figure 14: Naturally occurring antifouling surfaces and schematic illustrations of their appearance on a micro- or nanoscale modified from MAAN *et al.*¹⁰⁶ **A:** Lotus leaf with superhydrophobic and self-cleaning properties based on entrapped air in micropillars. **B:** The shark skin pattern causes low-fouling activity. **C:** Dragonfly wings exhibit nanopillars that kill bacteria upon contact. **D:** Sea urchins non-fouling surfaces by microroughness and microstructure.¹⁰⁷⁻¹¹⁰

Surface topography refers to surface engineering on a micro- or nanoscale, based on regular or irregular structures comprising a specific spatial spacing, size, and length. Due to the natural

occurrence of biofouling, nature has evolved numerous topographies that resist it. Therefore, many available and effective topographies are designed from biomimetic approaches. One of the most famous example is the microstructure of the lotus leaf (Figure 14 A), which induces anti-adhesive and self-cleaning properties, commonly known as the “Lotus-leaf-effect”.¹¹¹ Another example can be found in the microstructure of sea urchins (Figure 14 D). These species possess a visible, densely packed spiky surface, resistant against foulants of any size. Notable are structures of numerous marine organisms, such as the shark skin patterns, which exhibit their low-fouling maximum activity under movement, resulting in a shear force-associated antifouling effect (Figure 14 B).¹¹² By looking deeper into the physical interaction of a micro- or nanostructured surface with the surrounding environment, induced trapping of (dissolved) air plays a pivotal role. In such cases, the entrapped air generates a barrier between the liquid media and the solid substrate, which prevents suspended biomaterial from attachment. This principle, known as the CASSIE-BAXTER state, is illustrated in Figure 15 A.³⁸ The wettability of the surface depends on the induced CASSIE-BAXTER state and the chemical integrity of the material, or else, the availability of the contact area at the interface. The latter is crucial to assess bacterial adhesion. Contact areas larger than bacteria themselves are often linked to higher colonization since the implemented textures provide a scaffold and protection for microorganisms against external shear forces (Figure 15 C).^{38, 43}

In contrast, contact areas in the nanometer range provide reduced attachment sites for motile bacteria using surface-associated sensing to initiate surface attachment. Thus, reduced contact areas are correlated to reduced bacterial settlement (Figure 15 D). Likewise, degrading antifoulants are most likely constructed on the nanometer scale by introducing a spike-like structure that kills bacteria upon contact (Figure 15 B). Such a bioactive strategy occurs in the form of nanopillars presented on cicadas’ or dragonfly wings, which cause cell membrane deformation and subsequently killing of the bacteria (Figure 15 C).⁵⁵ Surface topography is linked to surface roughness, which is often described by the mean arithmetical roughness of a 2-dimensional line (R_a) and the mean arithmetical roughness of the 3-dimensional surface (S_a). Both parameters are used to indicate either enhanced or weakened bacterial adhesion.¹¹³ For example, various studies derived a threshold for bacterial adhesion of R_a in the range from 0.15 μm to 0.35 μm .¹¹⁴ However, other studies disproved the existence of such a threshold, leading to an overall contradictory field of research.²³ The existence of universal topographic patterns to prevent cell adhesion is thus debatable.

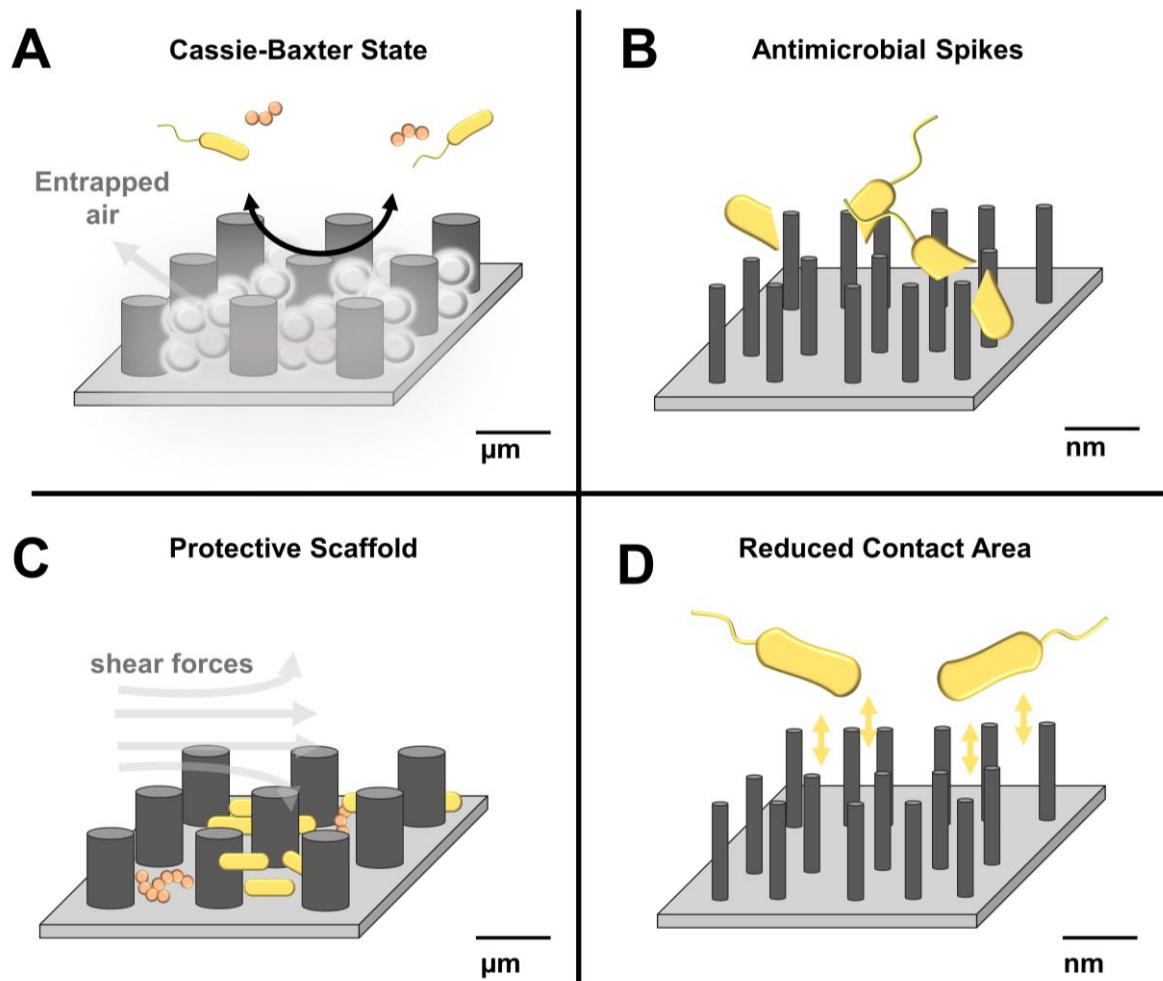


Figure 15: Topographic features on micro- and nanoscales.³⁶ **A:** Illustration of the CASSIE BAXTER state: Topography combined with super-hydrophobicity induces an anti-wetting state by entrapping air that reduces bacterial adhesion. **B:** Nanopillars can act as antimicrobial spikes by degrading prokaryotic cell membranes mechanically. **C:** Microstructures larger than bacterial cells provide a protective scaffold against mechanical forces. **D:** Bacterial surface sensing *via* chemotaxis transducing system prefers to adhere to contact areas that are larger than themselves. Thus, the reduced contact area is associated with lower bacterial attachment.

Since the described topographies are predominantly non-chemical antifoulants that do not directly affect or potentially contaminate biological ecosystems, this approach is defined as environmentally friendly.^{36, 115}

4. Aim of the Work

Biofouling is a ubiquitous issue impacting medical, pharmaceutical, and industrial areas. To overcome the associated overuse of antibiotics or biocides with severe consequences for humankind and the environment, direct surface modification represents an attractive strategy to interfere with initial biofouling processes.

A major aim of this thesis is, therefore, to provide new and efficient surface modifications of metals and plastics with antifouling or antibacterial activity. This work addresses three main objectives: 1. Optimization and extension of a plasma method for plastic modification and its application to graft polymerization on bulk materials. 2. Development of novel multifunctional antifouling surfaces by combining active and passive antifouling principles. 3. Synthesis and microbiological evaluation of antifouling surfaces composed of polymeric *N*-oxides. The anticipated workflow is given in Figure 16 and includes the synthesis of suitable monomers for radical polymerization based on styrene. Surface activation and graft polymerization should be optimized for each monomer, and the outcome should be thoroughly analyzed by a detailed surface analysis. The resulting materials are finally evaluated with different microbiological assays to confirm their bioactivity and decipher their mode of action.

The long-term efficiency of the materials in seawater is supposed to be investigated in the cooperation project, AFOUL, between the University of Hamburg and ContiTech Edelbüttler and Schneider GmbH (E+S). The latter project aimed for an environmentally friendly antifouling modification of the elastomer-based hose sections in seawater intake systems as a substitute for the present antifouling strategy based on hazardous hypochlorite cleaning.

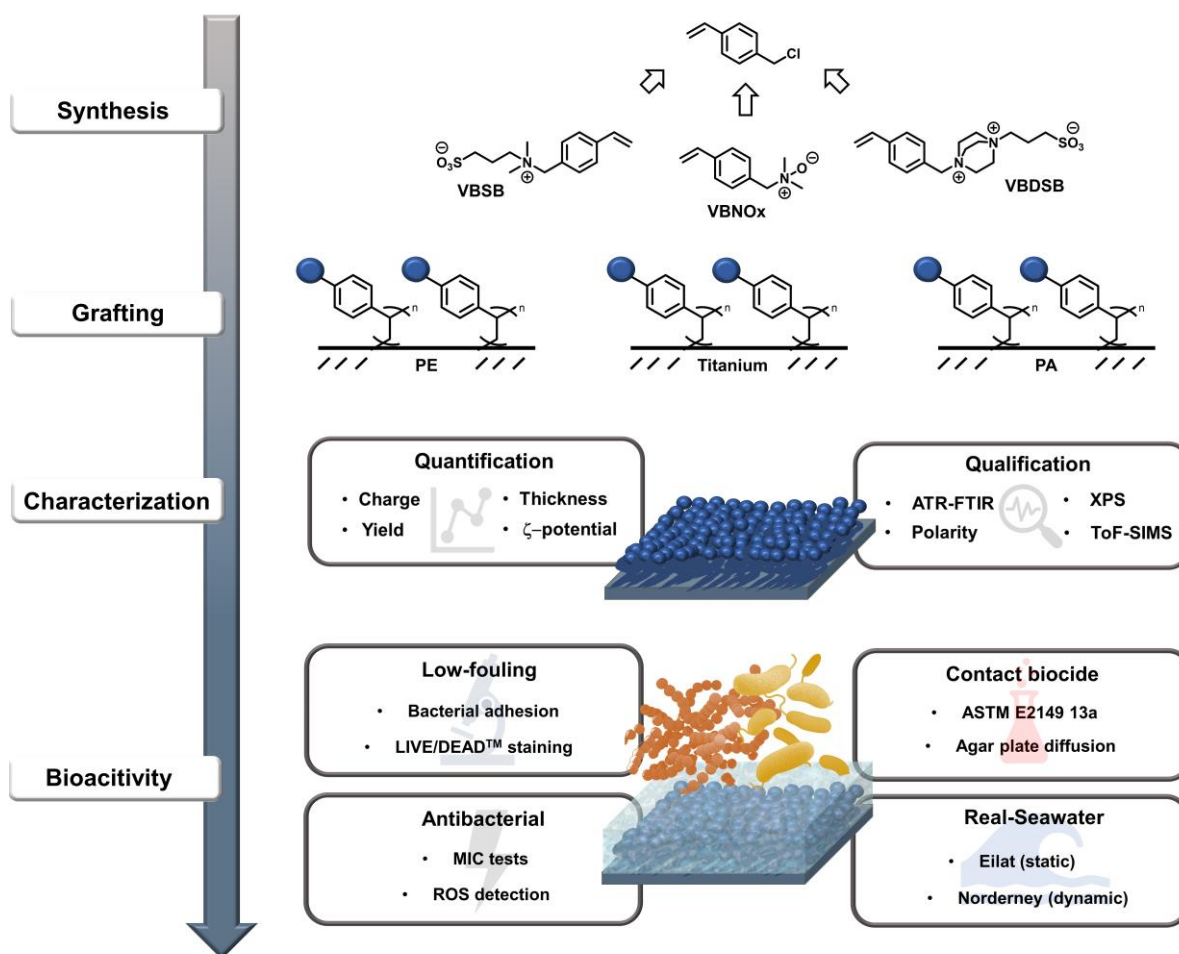


Figure 16: Schematic illustration of the workflow starting with the synthesis of monomers and their graft polymerization from different bulk materials. The resulting graft polymers are characterized with varying characterization techniques and finally tested for their bioactivity.

5. Results and Discussion (cumulative part)

5.1. Zwitterionic Surface Modification

The established modification of plastics included the generation of contact-biocidal graft polymers of QAS, mainly p-(VBTAC). The attraction of negatively charged cellular components emerged as a significant disadvantage of this contact-active mechanism. The subsequent accumulation of biomaterial on surfaces can generate new proliferation grounds for further biofouling. For long-term use, the contact-killing strategy is, therefore, less effective, which is why non-adhesive, low-fouling surface modifications provide a potential advantage. Previous studies on low-fouling surfaces generated by PEG modification revealed a disadvantageous sensitivity towards oxidative degradation. A novel approach to developing low-fouling surfaces involves transferring zwitterionic polymer brushes (section 3.3.3). Their superior hydration makes them attractive for application in surface design. Molecular simulations of the hydration-free energy have shown that sulfobetaine-based (SB) (-519.0 kJ/mol) and carboxybetaine-based (CB) (-404 kJ/mol) zwitterions are significantly more hydrated than OEG/PEG (-184 kJ/mol).¹¹⁶ SBs consist of one positive quaternary ammonium group and an anionic sulfonate ($R-SO_3^-$), while CBs hold an anionic carboxylate ($R-CO_2^-$) as countercharge. In direct comparison, CBs exhibit a sharper spatial distribution and more preferential dipole orientation of adsorbed water molecules. In contrast, the sulfonate moieties demonstrate a higher absolute number of adsorbed water molecules.^{90, 116} By additionally considering the lower pK_a value of sulfonates (1-2) compared to carboxylates (4-5), poly-SBs exhibit a widely applicable zwitterion with an overall neutral net charge over a wide pH range. Moreover, a flexible carbon spacer between negative and positive charge contributes to the zwitterionic performance by providing inter- and intramolecular interactions that enhance the thermostability and stimuli-responsive character of the resulting graft polymers. The latter encompasses enhanced low-fouling in media with elevated electrolyte concentrations.^{117, 118} Thus, their independent hydration towards the media's pH value, thermal stability, and high salt resistance make them attractive agents in a wide range of applications to combat initial biofilms. Based on these properties, poly-(SBs) have been reported as excellent antifouling agents in marine environments.¹¹⁹

To adapt these advantageous properties for a wide range of antifouling purposes, an extension of the established plasma modification process towards zwitterionic SB-based polymer brushes was developed. VBSB was obtained in a scalable two-step synthetic procedure, including a ring-opening alkylation of the corresponding styrene-based tertiary amine. As an extension, a more efficient and industrial scalable spray-coating method was developed, which reduced monomeric waste and enabled modification of larger PE surface areas compared to

the previously used method. Later, this framework provides the modification protocol for large elastomer specimens to modulate marine biofouling. However, the obtained zwitterionic polymer brushes grafted from polyethylene were characterized with respect to polarity, chemical integrity, and charge density. The latter was determined by a novel, colorimetric crystal violet dye assay, targeting solvent-accessible sulfonated groups, which was also used for further characterization of sulfonate-based modifications. For antifouling confirmation, the PE modifications were tested against clinically relevant *Staphylococcus aureus* and seawater containing foulants derived from the Baltic Sea in a marine environment.

Title: Zwitterionic surface modification of polyethylene *via* atmospheric plasma-induced polymerization of (vinylbenzyl-)sulfobetaine and evaluation of antifouling properties.

Authors: Burmeister, N., Vollstedt, C., Kröger, C., Friedrich, T., Scharnagl, N., Rohnke, M., Zorn, E., Wicha, S.G., Streit, W.R., Maison, W.

Type: Research article

Journal: Colloids and Surfaces B: Biointerfaces

Year: 2023

Volume: 224

Pages: 113195

DOI: 10.1016/j.colsurfb.2023.113195

Number of Pages: 11

Submitted: 18.11.2022

Accepted: 02.02.2023

Conceptualizing: Burmeister N., Vollstedt, C., Streit, W.R., Wicha, S.G, Maison, W.

Investigations: Burmeister, N., Vollstedt, C., Kröger, C., Friedrich, T., Scharnagl, N., Rohnke, M., Zorn, E.

Original Writing: Burmeister, N., Maison, W.

Review and Editing: Vollstedt, C., Kröger, C., Friedrich, T., Scharnagl, N., Rohnke, M., Zorn, E., Wicha, S.G., Streit, W.R.



Contents lists available at ScienceDirect

Colloids and Surfaces B: Biointerfaces

journal homepage: www.elsevier.com/locate/colsurfb

Zwitterionic surface modification of polyethylene via atmospheric plasma-induced polymerization of (vinylbenzyl)-sulfobetaine and evaluation of antifouling properties

Nils Burmeister^a, Christel Vollstedt^b, Cathrin Kröger^b, Timo Friedrich^a, Nico Scharnagl^c, Marcus Rohnke^d, Eilika Zorn^a, Sebastian G. Wicha^a, Wolfgang R. Streit^b, Wolfgang Maison^{a,*}

^a Universität Hamburg, Department of Chemistry, Bundesstrasse 45, 20146 Hamburg, Germany

^b Universität Hamburg, Department of Microbiology and Biotechnology, Ohnhorststrasse 18, 22609 Hamburg, Germany

^c Helmholtz-Zentrum Hereon GmbH, Institute of Surface Science, Max-Planck-Strasse 1, 21502 Geesthacht, Germany

^d Justus-Liebig-Universität Gießen, Institute of Physical Chemistry, Heinrich-Buff-Ring 17, 35392 Giessen, Germany

ARTICLE INFO

Keywords:
Antifouling
Polyethylene
Zwitterions
Sulfobetaines
Graft polymers

ABSTRACT

Zwitterionic polymer brushes were grafted from bulk polyethylene (PE) by air plasma activation of the PE surface followed by radical polymerization of the zwitterionic styrene derivative (vinylbenzyl)sulfobetaine (VBSB). Successful formation of dense poly-(VBSB)-brush layers was confirmed by goniometry, IR spectroscopy, XPS and ToF-SIMS analysis. The resulting zwitterionic layers are about 50–100 nm thick and cause extremely low contact angles of 10° (water) on the material. Correspondingly we determined a high density of $> 1.0 \times 10^{16}$ solvent accessible zwitterions/cm² (corresponding to 2.0×10^{-8} mol/cm²) by a UV-based ion-exchange assay with crystal violet. The elemental composition as determined by XPS and characteristic absorption bands in the IR spectra confirmed the presence of zwitterionic sulfobetaine polymer brushes. The antifouling properties of the resulting materials were evaluated in a bacterial adhesion test against gram-positive bacteria (*S. aureus*). We observed significantly reduced cellular adhesion of the zwitterionic material compared to pristine PE. These microbiological tests were complemented by tests in natural seawater. During a test period of 21 days, confocal microscopy revealed excellent antifouling properties and confirmed the operating antifouling mechanism. The procedure reported herein allows the efficient surface modification of bulk PE with zwitterionic sulfobetaine polymer brushes via a scalable approach. The resulting modified PE retains important properties of the bulk material and has excellent and durable antifouling properties.

1. Introduction

Once microorganisms adhere to surfaces and form sessile populations, the colonization process is enhanced by forming microbial biofilms which contribute to increased resistance and biological fitness [1–3]. As a result of population growth, cells can desorb from the biofilm and contaminate the surrounding environment, which has an impact on many areas such as medical treatments [4], pharmaceutical manufacturing [5], water purification [6], industrial packaging [7], marine technologies [8], and more.

Current commercial strategies to prevent biofilm formation on material surfaces are mostly based on leachable antimicrobial components in coatings and paintings with possible impact on the surrounding

environment often accompanied by increased bacterial resistance [9, 10]. The adhesion mechanisms of microorganisms are dependent on electrostatic, topographic and kinetic interactions at the material interface [7]. Modulation of biofilm growth can therefore also be achieved with non-release modifications such as microstructured [11] hydrophobic [12] or hydrophilic surfaces [13]. These surface modifications can be applied to various base materials [14] and lead to either contact-active antimicrobial activity [15,16], or repellent properties [17,18]. The latter can be achieved by topographical surface engineering on the nano- or microscale [11,12,19,20] or by chemical modification of material surfaces with hydrophilic [21] or hydrophobic groups [19,22]. In this field, (super) hydrophilic polymers with the ability to build a low fouling “water barrier” through electrostatic

* Corresponding author.

E-mail address: wolfgang.maison@uni-hamburg.de (W. Maison).

<https://doi.org/10.1016/j.colsurfb.2023.113195>

Received 18 November 2022; Received in revised form 31 January 2023; Accepted 2 February 2023

Available online 3 February 2023

0927-7765/© 2023 Elsevier B.V. All rights reserved.

interaction have attracted much attention and particularly zwitterionic polymers, such as poly(sulfobetaines) [23], poly(sulfobetaines) [24], poly(carboxybetaines) [25], poly(phosphobetaines) [26] and recently also poly(*N*-oxides) [27] have been applied to antifouling coatings [28, 29]. Poly(sulfobetaines) improve resistance to nonspecific protein binding and platelet adhesion [30,31] and do thus inhibit initial biofouling steps [13,17,32,33]. In addition, poly(sulfobetaines) have stimuli-responsive properties and thus ion-responsive antifouling effects [34,35]. Most studies of surface-immobilized zwitterionic polymers have been performed on glass, bulk metal or metal oxides [36], metal-based nanoparticles [37] and silicone [38]. Surface zwitterionization has also been applied to plastics by either “grafting to” or “grafting from” approaches [14,39]. While less studies in this field focus on zwitterionization of dense base materials, a majority address zwitterionization of materials with high surface area such as membranes or porous plastics [40–42,43]. The low number of examples for zwitterionization of bulk PE [26,44–46] and the limited associated biological data are remarkable because PE is the most widely used thermoplastic polymer with several favorable properties for applications in marine technology, medicine, the food industry and the pharmaceutical industry [7,47–49]. Antifoulant PE is therefore attractive for tubing, packaging and transport of water, food and pharmaceuticals, medical devices and any surface relevant to clinical hygiene. A common problem in this context is the difficult chemical activation of PE for surface modification which often requires harsh reaction conditions involving strong acids or oxidizing reagents, which can lead to damage of the bulk material. Hence, milder and non-toxic activation methods like UV-irradiation [50] or plasma treatment are advantageous [51–55]. The latter is particularly attractive for modification of large surface area and has been applied to the zwitterionization of membranes [40,56–58]. In previous studies, we have used a two-step procedure of atmospheric plasma activation and subsequent heat-induced radical polymerization for grafting cationic poly-(VBTA) brushes to bulk PE. The resulting materials have been shown to act as powerful contact biocides [16]. Herein we extend this approach to the synthesis of zwitterionic PE with a poly-(VBSB) layer. The resulting materials have been evaluated with respect to microbial adhesion of *S. aureus* and for long-term antifouling activity in natural seawater.

2. Materials and methods

2.1. Chemicals and materials

Additive-free polyethylene (LD-PE) foils with a thickness of 750 μm were purchased from Goodfellow and used as received. Vinylbenzylchloride (90%), dimethylamine solution (33% in ethanol), ammoniumperoxodisulfate (99%), crystal violet (Ph.Eur.), sodiumdodecylsulfate (Ph.Eur.) were purchased from Sigma-Aldrich. 1,3 propanesultone (99%) was purchased from Alfa-Aesar. Phosphate-buffered saline (PBS) with a final concentration of 137 mM NaCl, 10 mM phosphate, 2.7 mM KCl and a pH adjusted to 8.0 was prepared as a stock solution. All reagents were used without further purification. Crimp neck vials (N20, 10 mL volume) and crimp caps (N20, PTFE septum) for degassing were purchased from Macherey-Nagel GmbH (Düren, Germany). Airbrush (cup volume 600 mL) with an adjustable nozzle (1.4 mm) for grafting was purchased from Einhell (Landau, Germany).

2.2. Synthesis

The synthesis of VBSB and VBDMA followed a modified literature procedure [23,59].

2.2.1. *N,N*-dimethyl-1-(4-vinylbenzylamine) (VBDMA)

K_2CO_3 (1 eq, 176 mmol, 24.70 g) was added to a dimethylamine solution (33 wt%) in ethanol (7 eq, 1.24 mol, 221.14 mL). The resulting suspension was cooled to 0 °C and vinylbenzylchloride (1 eq, 176.91

mmol, 27.78 mL) was added dropwise within 30 min. The reaction mixture was stirred for 18 h at room temperature. All volatile components were removed under reduced pressure. The crude product was dissolved in 200 mL of EtOAc and 200 mL of H_2O . The two layers were separated and the aqueous layer was extracted 3 times with each 100 mL of EtOAc. The combined organic layers were dried over Mg_2SO_4 . Removal of the solvent under reduced pressure gave 26.29 g (163 mmol, 92%) of the title compound as an orange-red-colored oil.

^1H NMR (500 MHz, MeOD): δ [ppm] = 7.42 ($^3J_{\text{HH}}$ = 7.9 Hz, 2 H, 4-H, 7-H), 7.29 ($^3J_{\text{HH}}$ = 8.3 Hz, 2 H, 5-H, 6-H), 6.78 (dd, $^3J_{\text{HH}}$ = 10.8, 17.9 Hz, 1 H, 9-H), 5.79 (dd, $^2J_{\text{HH}}$ = 1.1, $^3J_{\text{HH}}$ = 17.9 Hz, 1 H, 10a-H), 5.23 (dd, $^2J_{\text{HH}}$ = 1.2, $^3J_{\text{HH}}$ = 10.8 Hz, 1 H, 10b-H), 3.47 (s, 2 H, 2-H), 2.25 (s, 6 H, 1-H).

^{13}C NMR (126 MHz, MeOD): δ [ppm] = 138.4 (C3), 138.3 (C9), 130.9 (C4, C7), 126.6 (C5, C6), 114.0 (C10) 64.6 (C2), 44.4 (C1).

2.2.2. 3-(Dimethyl(4-vinylbenzyl)ammonium)propane-1-sulfonate [(Vinylbenzyl)sulfobetaine (VBSB)]

1,3 propanesultone (1.5 eq, 139.54 mmol, 8.73 mL) was dissolved in 100 mL EtOAc at room temperature and VBDMA (1 eq, 93.02 mmol, 15.00 g) was added dropwise within 30 min. The reaction mixture was vigorously stirred at 50 °C for 20 h. The resultant precipitant was washed with ethyl acetate to obtain the colorless crude product. The crude product was crystallized from ethanol to obtain 23.16 g (81.73 mmol, 88%) of the title compound as a colorless solid.

^1H NMR (400 MHz, D_2O): δ [ppm] = 7.63 ($^3J_{\text{HH}}$ = 8.3 Hz, 2 H, 7-H, 9-H), 7.53 ($^3J_{\text{HH}}$ = 8.3 Hz, 2 H, 8-H, 10-H), 6.85 (dd, $^3J_{\text{HH}}$ = 11.1, 17.8 Hz, 1 H, 12-H), 5.96 (d, $^3J_{\text{HH}}$ = 17.8 Hz, 2 H, 13a-H), 5.44 (d, $^3J_{\text{HH}}$ = 11.1 Hz, 1 H, 13b-H), 4.52 (s, 1 H, 5-H), 3.46 (m, 2 H, H-3), 3.07 (m, 6 H, 4-H), 2.99 (t, $^3J_{\text{HH}}$ = 7.3 Hz, 2 H, 1-H), 2.34 (m, 2 H, 2-H).

^{13}C NMR (101 MHz, D_2O): δ [ppm] = 139.7 (C6), 137.1 (C13), 133.6 (C8, C10) 127.4 (C7, C9) 125.8 (C11), 116.3 (C12), 67.9 (C5) 61.3 (C3), 50.4 (C4) 44.0 (C1) 16.9 (C2).

2.3. Instrumental

2.3.1. Atmospheric air plasma

For plasma activation, an atmospheric air plasma system from Plasmamatreat GmbH (Steinhagen, Germany) was used. The atmospheric-pressure plasma was produced by a generator FG5001 with an applied working frequency of 21 kHz, generating a non-equilibrium discharge in a rotating jet nozzle RD1004 in combination with the stainless-steel tip No. 22826 for an expanded treatment width of approximately 22 mm. Additionally, the jet nozzle was connected to a Janome desktop robot type 2300 N for repetitious accuracy regarding treatment conditions. The process gas was dry and oil-free air at an input pressure of 5 bar in all experiments.

2.3.2. IR- and UV/vis spectroscopy

Infrared spectra were recorded from an attenuated total reflectance Fourier Transform infrared system (ATR-FTIR), model “IRAffinity-1S” from Shimadzu (Kyoto, Japan) using a “Quest” ATR accessory from Specac. The spectral range was set from 4000 cm^{-1} –400 cm^{-1} with a resolution of 0.5 cm^{-1} in absorbance mode and spectra were further processed with OriginPro 9 (2021) software. UV/vis spectra were obtained on a Genesys 10 S spectrophotometer from Thermo Scientific (Waltham, USA) using Visionlite software for analysis.

2.3.3. Contact angle measurements

Contact angle measurements were acquired with an OCA 20 goniometer from DataPhysics (Filderstadt, Germany) equipped with two automated dispensing units for different liquid probes, a high-speed video system with CCD-camera, measuring stage and halogen-lighting for static and dynamic contact angle measurements. For evaluation, independent triplicate measurements at three different points of the surface were done. Contact angles were measured with deionized water

using the static sessile drop method with a dispensing volume of 5 μL . The dispensing rate of the automatic syringe was set at 1 $\mu\text{L}/\text{min}$. The obtained angle was calculated with the OCA software.

2.3.4. NMR-spectroscopy

The measurements were performed in 5 mm O.D sample tubes using either a Bruker Avance I 500 MHz or Bruker Avance I 400 MHz (AV500 and AV400, Bruker, Ettlingen, Germany). The obtained spectra were processed with MestReNova x64 software. ^{13}C -spectra were recorded with ^1H -decoupling. Peak assignments were supported by 2D NMR experiments like ^1H , ^1H -COSY, ^1H , ^{13}C -HSQC and ^1H , ^{13}C -HMBC.

2.3.5. X-ray Photoelectron Spectroscopy (XPS) measurements

XPS measurements were performed using a KRATOS AXIS Ultra DLD (Kratos Analytical, Manchester, United Kingdom) equipped with a monochromatic Al K_{α} anode working at 15 kV (225 W). For the survey spectra, a pass energy of 160 eV was used while for the region spectra the pass energy was 20 eV. The investigated area was $700 \times 300 \mu\text{m}$. For all of the PE samples, charge neutralization was necessary. The evaluation and validation of the data were carried out with the software CASA-XPS version 2.3.24. Calibration of the spectra was done by adjusting the C1s signal to 284.5 eV. For deconvolution of the region files, background subtraction (U 2 Tougaard or Shirley) was performed before calculation.

2.3.6. Time of flight secondary ion mass spectrometry (ToF-SIMS) and scanning probe microscopy (SPM)

The modified polyethylene was exemplarily characterised in 3D by Time of Flight Secondary Ion Mass Spectrometry (ToF-SIMS). The analysis was carried out with a M6 Plus machine (IONTOF Company, Münster, Germany). Here a scanning probe microscope is included in the main vacuum chamber of the ToF-SIMS, which offers the possibility for correlation of topographic and mass spectrometric imaging data. For SIMS analysis 60 keV Bi_3^+ primary ions were used ($I = 0.05 \text{ pA}$ @ 200 μs cycle time). The Bi gun (nanoprobe 50) was operated in high-current bunched mode with a beam-defining aperture of 700 μm . For depth profiling the machine was operated in non-interlaced mode in combination with a 5 keV Ar_{2000}^+ sputter beam ($I = 1.328 \text{ nA}$). Low energetic electrons were used for charge compensation during the pause time of 1 s. An analysis area of $70 \times 70 \mu\text{m}^2$ (128×128 pixel) was chosen in the centre of the $200 \times 200 \mu\text{m}^2$ sputter area. Depth profiling was stopped at the interphase between coating and substrate. Before and after the measurement a scanning probe microscopy image of the analysis area was recorded in intermitted mode with 2048×128 pixels resolution as well as line scans in x and y direction with a scan length of 600 μm each. Data evaluation was carried out with Surface Lab software version 7.3 (IONTOF Company). Negative mass spectra were recorded and the achieved mass resolution was $m/\Delta m > 7.500$ (FWHM) @ $m/z = 65.04$ (C_5H_5).

2.3.7. Bacterial adhesion test

To investigate the bio-resistant properties of modified PE samples, we carried out a bacterial adhesion assay using a modified protocol from Khalil et al. [60]. All samples, pristine and treated PE foils, were sterilized in 90 vol% iPrOH and dried under laminar airflow (LAF) conditions before testing. The strain *Staphylococcus aureus* ATCC 29213 was cultured on Columbia agar overnight. The overnight culture was suspended and diluted in sterile saline solution (0.9%) to preserve a cell density of 10^4 colony-forming units per milliliter (CFU/mL). Triplicates of coated and non-coated PE foils (total surface area of each 0.8 cm^2) were placed in a 48-well plate and covered with 990 μL of Mueller Hinton Broth (MHB). 10 μL of the bacterial suspension was added to each sample to obtain a starting cell density of 10^2 CFU/mL. To track exponential bacterial growth and biofilm formation, substrates were incubated for 2, 6, 24 and 48 h at 37°C and were subsequently transferred each into 3 mL of sterile saline without stirring or shaking for 1

min solution as a cleaning step. Each foil was slightly pressed with the relevant side onto an agar plate (Columbia agar) and removed after 30 s. Transferred cells were incubated for 20 h at 37°C prior to cell counting. To evaluate bacterial growth and to exclude an antibacterial effect of the tested PE coupons, an aliquot of 100 μL was taken from each incubation experiment and analyzed with respect to bacterial growth in comparison to a positive control of MHB containing bacterial suspension without added PE coupon.

2.3.8. Biofilm adhesion in natural seawater

Pre-sterilized PE specimens with a total surface area of 0.8 cm^2 were immersed into 50 mL of natural seawater derived from the Baltic sea ($54^\circ 35' 14.50''\text{N}$, $10^\circ 17' 76.60''\text{E}$) and stored under gentle shaking (90 rpm) at 22°C . Sample foils were taken after 7, 14, and 21 days of incubation and rinsed with sterile PBS buffer prior to further analysis. Fluorescence imaging to examine biofilm formation on the sample PE foils was carried out using LIVE/DEAD™ BacLight™ Viability Kit [61]. Images were visualized via confocal laser scanning microscope LSM 800 with AiryScan from Zeiss (Jena, Germany) and edited with ZEN 2 (Blue Edition) software.

2.3.9. Modification of PE

PE foils with a thickness of 0.75 mm were rinsed with an isopropanol/water mixture of 70% (v/v) and dried for 15 min at 50°C prior to use. Plasma treatment of the PE foils was performed following the protocol of Kliewer et al. [16] The aqueous solution containing the VBSB monomer (20 wt%) and ammoniumperoxodisulfate (APS) as a radical initiator (1.0 wt%) was degassed with nitrogen for 20 min. The degassed aqueous solution of VBSB and APS was transferred into an airbrush and was vaporized at a distance of 5 cm under the pressure of a nitrogen stream of 2 bar onto the activated surface until a homogenous thin film was formed. The resulting samples were polymerized in a vacuum heater for 2 h at 85°C . After polymerization, the materials were washed three times for each 15 min with deionized water in an ultrasonic bath and dried for 20 min at 50°C prior to analysis.

2.3.10. Determination of grafting density by adsorption and desorption of crystal violet

For analysis of grafted polymer and determination of the charge density, an ion exchange assay in combination with UV/vis quantification was used. PE foils were rinsed with an isopropanol/water mixture of 70% (v/v) and stored in an ultrasonic bath for 10 min prior to use. PE foils were cut into squares of 1.0 cm^2 and were immersed into 1 wt% of aqueous crystal violet solution for 30 min on a shaker at 100 rpm at room temperature. PE foils were rinsed once with demin. water, transferred into 10 mL of demin. water and stored in an ultrasonic bath for 3×10 min with the renewal of the solvent in between to remove any residual non-bound dye. The PE foils were then treated with 10.0 mL of an aqueous 0.1 wt% sodium dodecyl sulfate solution for 30 min. The resulting solution containing the desorbed dye was analyzed by UV/vis spectroscopy at 590 nm. The resulting UV/vis absorbance was correlated to the concentration of desorbed crystal violet using the Beer-Lambert law:

$$c = \frac{A}{\epsilon \cdot l}$$

A: measured absorbance.

ϵ : extinction coefficient of crystal violet = $87000 \text{ M}^{-1}\text{cm}^{-1}$ [62].

l: optical path length [cm].

c: concentration of desorbed crystal violet [mol/L].

For calculation of the charge density, a blank value of pristine PE, treated under equivalent conditions was subtracted. Triplicate measurements of modified and pristine PE samples were performed.

2.3.11. Statistics

Statistics were performed using OriginPro 9 (2021) software. Data

are reported as mean value \pm standard deviation for continuous variables, or as a selective frequency for categorical variables. Pairwise comparison was performed to evaluate the bacterial adhesion test. A *p*-value of less than 0.05 was considered significant.

3. Results and discussion

The modification of polyethylene foils was performed in a two-step procedure, starting with the atmospheric air plasma activation of the PE foils. The plasma treatment is essential to install reactive functional groups on the PE surface which increase the wettability for aqueous monomer solutions and may serve as primer groups for covalent grafting of poly-(VBSB) by radical polymerization [63]. The latter was done with a plasma-spray coating protocol followed by thermal polymerization (Fig. 1). We used vinylbenzylsulfobetaine (VBSB) as a monomer and ammoniumperoxodisulfate (APS) as a radical initiator. In a previous study [16], we had obtained higher grafting yields for a cationic styrene derivative (VBTA) compared to methacrylate derivatives like METAC, which might have to do with less side reactions of the styrene derivative upon AIBN-initiated polymerization [64]. Assuming this to be roughly

comparable to VBSB polymerization, we therefore used the styrene derivative for zwitterionization again. An aqueous concentrated solution of VBSB and APS was sprayed under nitrogen pressure on the plasma-treated PE surface and the resulting film was polymerized at 85 °C for 2 h. Extensive washing under sonication gave the final modified PE films with grafted poly-(VBSB).

The effect of plasma activation and the subsequent polymerization protocol on surface polarity was followed by goniometry. Representative contact angles (water) are given in Fig. 1. The surface of pristine PE has a low polarity corresponding to a contact angle of approximately 100°. Plasma treatment increased the polarity of the surface significantly and decreased the contact angle to 40° reflecting the presence of polar functionalities. The following grafting (Fig. 1) of poly-(VBSB) to the plasma-activated PE surface by radical polymerization of VBSB led to a highly polar surface with a contact angle of about 10° after extensive washing of the surface with water and ultrasonication. In a control experiment, we checked the treatment of pristine PE (without plasma activation) with monomer VBSB under identical polymerization conditions and observed no immobilization of poly-(VBSB) on the PE surface as indicated by a high contact angle of approximately 100° after washing

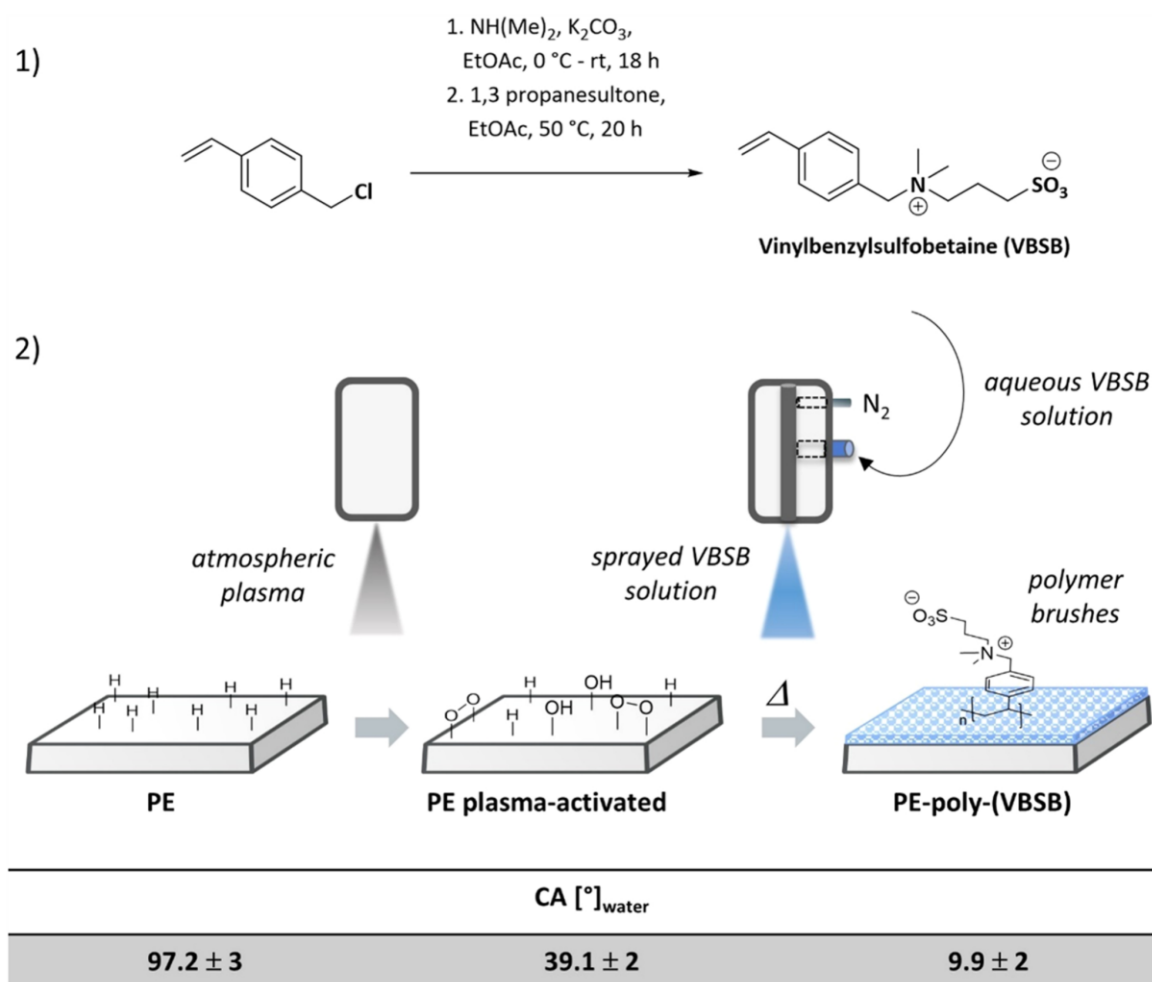


Fig. 1. 1) Synthesis of VBSB. 2) Schematic drawing of the two-step protocol for the synthesis of zwitterionic brushes on polyethylene foils including static contact angles of the surfaces with water for each step. Polymerization conditions for PE-poly-(VBSB): 20 wt% (vinylbenzyl)sulfobetaine (VBSB) in water with 1.0 wt% ammoniumperoxodisulfate (APS), 85 °C, 2 h. Subsequent washing: 3 \times 30 min with 70%water/ethanol mixture in an ultrasonic bath followed by drying at 50 °C. Contact angles (CA) are given as mean values of three independent measurements at different points of the surface.

(Fig. 1, SI). We have also screened a number of polymerization parameters, such as monomer concentration, radical initiator and temperature and checked the outcome via goniometry (Fig. 4.2, see also Fig. 1 and Table 1 in the SI). The conditions depicted in Fig. 1 lead to the lowest contact angle and thus presumably to the highest grafting efficiency.

ATR-FTIR spectra (Fig. 2) of poly-VBSB grafted PE showed characteristic stretching bands similar to the stretching bands of the VBSB-monomer spectra. For example, the S-O stretches at 1176 cm^{-1} and 1038 cm^{-1} are clearly visible as is a weak stretching band at 3032 cm^{-1} corresponding to the quaternary ammonium group of poly-(VBSB). The C-C and C-H stretching bands at 2916 cm^{-1} , 2846 cm^{-1} and 721 cm^{-1} belonging to the PE-backbone are observed in the spectra of pristine PE and PE-poly-(VBSB). The OH-stretching bands at 3200 cm^{-1} and 3500 cm^{-1} are associated with adsorbed water molecules in PE-(poly)-VBSB reflecting the strong hydration of the modified material that had been reported for other sulfobetains before [23,65].

XPS measurements support the changes in the elemental composition on the surface (Fig. 3). The peak at 401.9 eV in the N 1s spectra of PE-poly-(VBSB) depicted in Fig. 3.2 is most likely associated with the quaternary ammonium group. The second deconvoluted peak at 399.3 eV can be assigned to a second nitrogen species present in residual amounts. (Fig. 3.2) In the S2p region of the PE-poly-(VBSB) spectra a closely spaced spin-orbits components peak was detected (Fig. 3.2). The binding energy of 167.2 eV ($2p_{3/2}$) and 168.3 eV ($2p_{1/2}$) for sulfur can be assigned to the sulfonyl group ($\text{O}=\text{SO}_2$). The oxygen 1s spectra show a convoluted peak at 531.6 eV and indicate two oxygen species (Figs. 2–3, SI). We assigned the deconvoluted peak at 531.8 eV to the sulfonyl group. The second signal at 530.7 eV was attributed to adsorbed CO_2 or CO [66]. In contrast, the S2p spectra of pristine PE without detected spin splitting and respective binding energy of 168.2 eV show low residues of

sulfur species which most likely originated from manufacturing processes (Fig. 3.1). The fact that both surfaces show the same artifacts of fluorine (689.5 eV and 689.1 eV), can also be attributed to impurities due to manufacturing processes [67], packaging or plasma treatment [68] (Figs. 2–3, SI). Furthermore, Si 2p spectra with peaks at 102.1 eV and 102.5 eV might be derived from packaging material. Overall, the observed changes in atomic ratio and the shift in binding energies confirm the successful grafting of poly-(VBSB) on the PE surface [69].

A quantitative analysis of solvent-accessible zwitterions was performed by an adsorption assay using crystal violet. Similar assays have been reported for the characterization of polycationic surfaces with fluorescein as a negatively charged dye at neutral pH [70,71]. For the characterization of our zwitterionic surfaces we have found the cationic dye crystal violet to be advantageous. The method is based on the adsorption of crystal violet with a cationic counter ion for the anionic sulfonyl functions of poly-(VBSB) (Fig. 4.1). The process is most likely assisted by favorable cation- π -interactions of the dye and ammonium groups in poly-(VBSB) [72]. After washing, subsequent complete desorption of crystal violet with an aqueous solution of sodium-dodecyl-sulfate (0.1 wt%) allows the quantification of adsorbed crystal violet by determination of the UV/vis absorption at 590 nm . The reversible adsorption and the complete desorption process are also clearly visible by the violet color on poly-(VBSB)-PE after adsorption (Fig. 4.1 (d)) and in the desorption solution in Fig. 4.1 (b). Desorption is also accompanied by a complete loss of color of the test specimens. Pristine PE in contrast shows no adsorption of crystal violet and remains colorless after treatment with the dye (Fig. 4.1 (c)). The grafting density was estimated by assuming a 1:1 ratio of adsorbed crystal violet and accessible negative charge of sulfonyl-groups. The calculated charge densities correlate quite well with the high surface polarity, which is

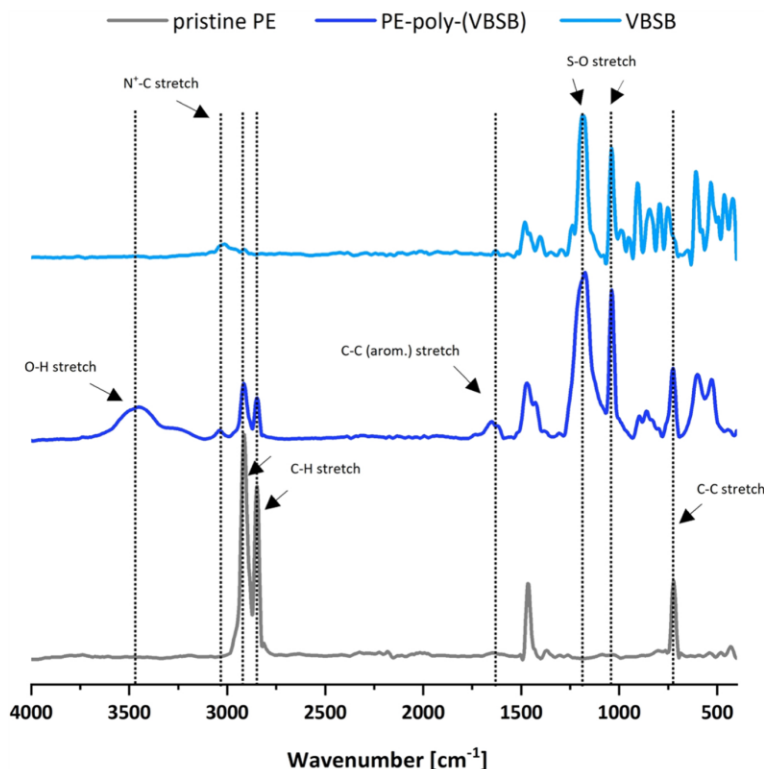


Fig. 2. ATR-FTIR spectra in absorbance mode of pristine PE, poly-(VBSB)-modified PE and VBSB monomer. Polymerization conditions for PE-poly-(VBSB): 20 wt% (vinylbenzyl)sulfobetaine (VBSB) in water with 1.0 wt% ammoniumperoxodisulfate (APS), $85\text{ }^{\circ}\text{C}$, 2 h. Subsequent washing: $3 \times 30\text{ min}$ with 70%water/ethanol mixture in an ultrasonic bath followed by drying at $50\text{ }^{\circ}\text{C}$.

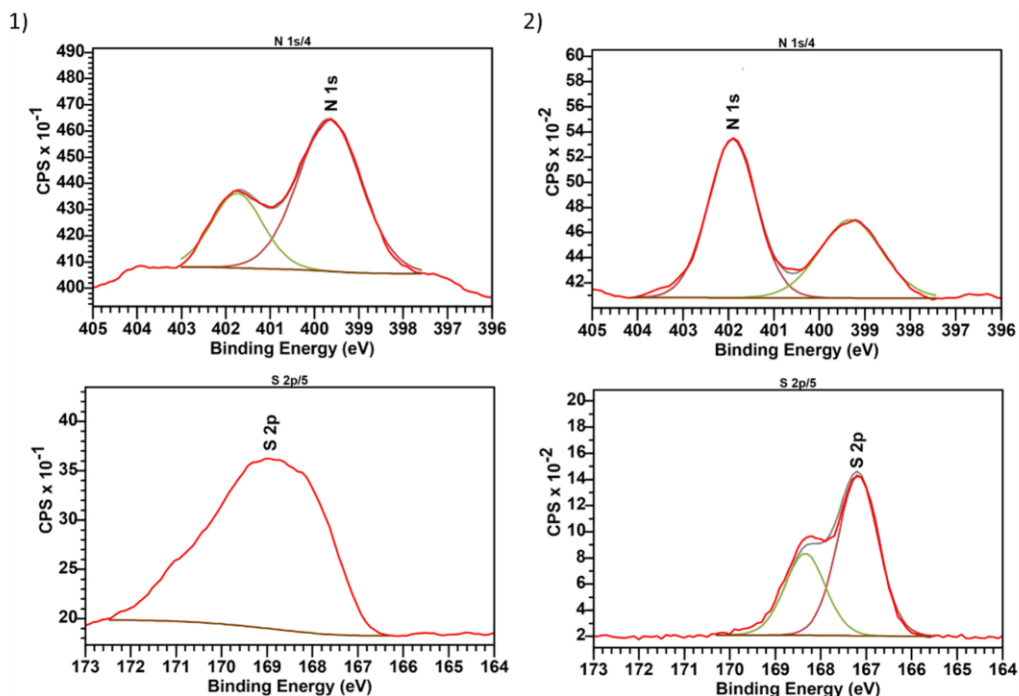


Fig. 3. XPS spectra of pristine PE (1) and poly-(VBSB) modified PE (2). 1) Deconvoluted N 1 s spectra, and S 2p region of pristine PE. 2) Deconvoluted N 1 s spectra and S 2p region with spin splitting from the XPS spectrum of modified PE-poly-(VBSB). Polymerization conditions for PE-poly-(VBSB): 20 wt% (vinylbenzyl)sulfobetaine (VBSB) in water with 1.0 wt% ammoniumperoxodisulfate (AP), 85 °C, 2 h. Subsequent washing: 3 × 30 min with 70%water/ethanol mixture in an ultrasonic bath followed by drying at 50 °C.

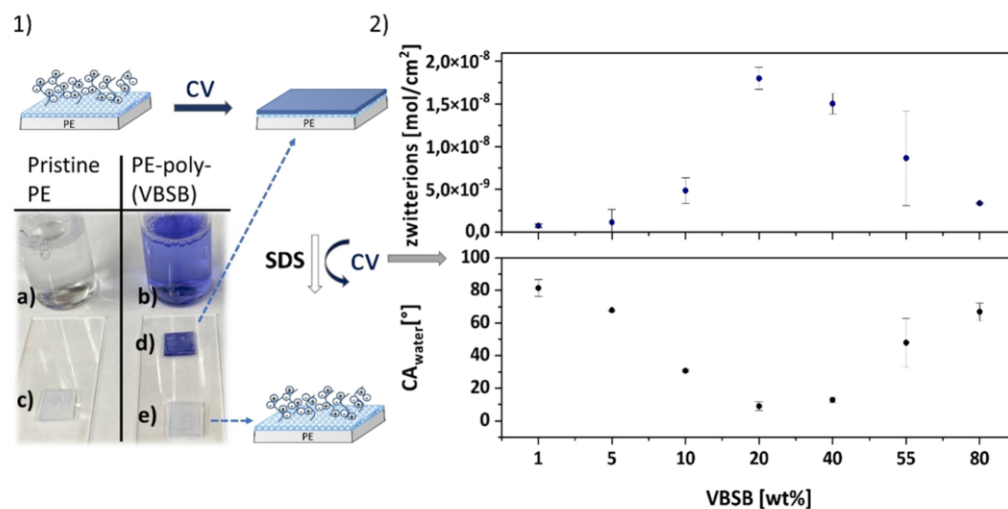


Fig. 4. Crystal violet (CV) adsorption assay: 1) Schematic drawing of CV adsorption assay. a) Desorption solution after SDS treatment of pristine PE, b) Desorption solution after SDS treatment of PE-poly-(VBSB), c) Pristine PE after treatment with CV, d) Modified PE foil after treatment with CV, e) Modified PE foil after SDS treatment. 2) Solvent-accessible zwitterions in mol/cm² as calculated from UV-absorbance of desorbed CV and corresponding contact angles (water) for graft polymerizations with different concentrations of (vinylbenzyl)sulfobetaine (VBSB) in water. Moles of zwitterions/cm² are given as mean values of three independent measurements (for calculation see Table 4, SI). Contact angles (CA) are given as mean values of three independent measurements at different points of the surface. Polymerization conditions for PE-poly-(VBSB): 20 wt% (vinylbenzyl)sulfobetaine (VBSB) in water with 1.0 wt% ammoniumperoxodisulfate (APS), 85 °C, 2 h. Subsequent washing: 3 × 30 min with 70%water/ethanol mixture in an ultrasonic bath followed by drying at 50 °C.

reflected by the low contact angle of modified PE (Fig. 4.2). We have used both parameters to follow the grafting efficiency of poly-(VBSB) at different concentrations of VBSB from 1 to 80 wt% (Fig. 4.2). The highest charge density and thus the highest grafting efficiency was observed at 20 wt% monomer concentration (Fig. 4.2). We assumed furthermore that a high grafting efficiency (and surface polarity) correlates to the antifouling efficiency of the material [73]. It is notable, that the observed number of accessible zwitterions is 2.0×10^{-8} mol/cm² (Fig. 4.2), corresponding to 10^{16} zwitterions/cm² (see also Table 4, SI). This value matches those determined for polycationic brushes on PE in an earlier study suggesting a similar grafting yield [16]. We have also investigated the impact of a crosslinking additive (divinylbenzene 0.2 wt%) on the polymerization of VBSB and found a decreased grafting density reflected by increased contact angles and lower charge densities compared to the non-crosslinked PE-poly-(VBSB) (Table 1, SI).

Moreover, modified PE-poly-(VBSB) was characterised by combined 3D mass spectrometric and scanning probe microscopy (SPM) analysis. Therefore, SPM images were taken before and after depth profiling with a time-of-flight secondary ion mass spectrometer (ToF-SIMS). Fig. 5(a) show correlated SIMS-SPM image of the (VBSB)-polymer coating in 3D. Due to the fact that the substrate roughness R_a is already in the 1–2.5 μm range, this topography is being transferred to the coating layer, which have a medium thickness of about 50–100 nm. Due to spacial inhomogeneities of the coating and the mentioned substrate roughness there is no clear interface detectable in the 2D depth profile plots (Fig. 5 (b)). However, the complete coating of the sample with poly-(VBSB) and thus a high density of polymer brushes is clearly assignable from the mass spectrometric data by SO_3^- fragments.

The chemical stability of the grafted polymer brushes is a critical parameter for the long-term antifouling efficiency of modified PE foils. We have tried to assess the stability by extensive Soxhlet extraction of PE-poly-(VBSB) with water and analyzed the surface changes via goniometry and mass loss (see Fig. 1 and Table 1 in the SI). In this context, it is notable that both the monomer VBSB and (non-immobilized) poly-(VBSB) have excellent water solubility. The measured contact angles remained low ($< 30^\circ$ (Fig. 1, SI)) within the first 6 h but increased to 45° C within 48 h of extraction. At the same time, we did not detect notable mass loss of non-covalently bound zwitterions (Table 2, SI). The observed decreased surface polarity is thus most likely not a

consequence of zwitterion release into solution. We assume that it is rather a consequence of thermal rearrangement processes within the bulk material [74,75]. This latter rearrangement phenomenon would most likely have no impact on most antifouling applications at much lower temperatures. We have tested this hypothesis with a long-term seawater treatment of PE-poly-(VBSB) at room temperature over three weeks and observed no significant change in surface polarity as reflected by a low contact angle (Table 3, SI). In consequence, we assume that poly-(VBSB) is covalently immobilized on our modified PE foils and confers non-fouling properties to the surface without leaching of zwitterions into the solution. This finding confirms our previous observations regarding covalent immobilization of polycationic polymers on PE [16].

The antifouling properties of poly-(VBSB)-PE foils were evaluated with a bacterial adhesion test according to a modified method by Khalil et al. [60]. Several different microbiological assays are available for the evaluation of the biological activities of modified artificial surfaces and materials [4,76]. Zwitterionic modifications presumably have no anti-bacterial potency but rather prevent the attachment of bacteria [30]. We selected therefore an adhesion experiment with *S. aureus* as the most appropriate experimental setup and adapted a protocol originally designed for the analysis of zwitterionic metal surfaces. *S. aureus* is a model pathogen frequently used for biofilm evaluation [77] as it is one of the most important biofilm-forming microbes on medical devices [78]. Furthermore, studies on bacterial cell walls also indicate a slightly lower negative zeta potential of *S. aureus* (-2 to -5 mV) [79] compared to many other microorganisms such as *E. coli* (-40 to -60 mV) [80] and *P. aeruginosa* (-9 mV) [79]. The zeta potential of zwitterionic sulfobetaine brushes has been reported to be negative (~ -40 mV), at least for methacrylate derivatives [13]. Therefore we assumed that *S. aureus* would be one of the most challenging model bacteria to simulate attachment processes [81]. Also, a comparative study investigating the attachment of *E. coli* and *S. aureus* species on different metal surfaces for implants revealed an overall more precise colonization tracking of *S. aureus* compared to *E. coli* on surfaces [82]. We used incubation times between 2 and 48 h to monitor bacterial adhesion. Briefly, poly-(VBSB)-PE foils and pristine PE foils were rinsed with water and sterilized prior to use. The initial bacterial concentration was 10^{12} CFU/mL in MHB and the incubation temperature was set at 37°C . The test samples were

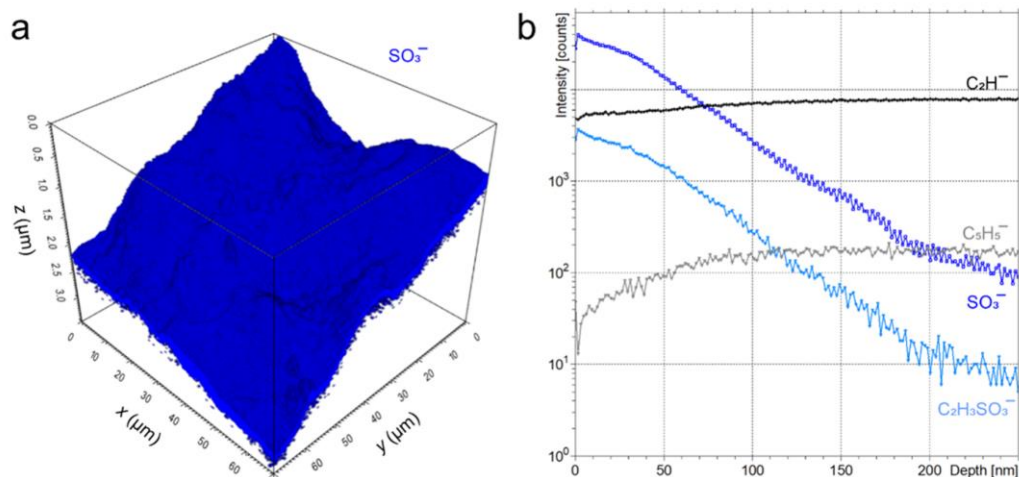


Fig. 5. Combined 3D ToF-SIMS and SPM analysis data of PE-poly-(VBSB). Figures a) shows the spacial distribution of the most intensive ion fragments, which represents the respective poly-(VBSB) coating layer. The 3D mass spectrometric data were correlated with SPM images taken before and after SIMS analysis. The classical SIMS depth profiles of the coating layers are depicted in b). In contrast to characteristic polyethylene mass fragments like C_2H^- and C_5H_5^- occurring in the whole polymer sample, specific S containing mass fragments are only detectable in the coating layer. SIMS analyses were carried out with Bi_3^+ ions for analysis in negative ion mode and Ar_{2000}^+ cluster ions for sputtering.

incubated with gentle shaking at 100 rpm to assure homogenous contact of the material with the bacterial suspension. After 2, 6, 24, and 48 h the test specimens were transferred into a sterilized saline solution for 1 min to desorb non-specifically attached bacteria. In contrast to most other bacterial adhesion tests [60,82,83], we decided to keep this cleaning step as short and as simple as possible to transfer all of the adherent microbes to agar plates in the subsequent step. The test specimens were finally printed carefully onto an agar plate (Columbia Agar), which was subsequently incubated at 37 °C for 20 h before colony counting.

Selected results shown in Fig. 6 clearly confirm the antifouling properties of poly-(VBSB)-PE foils. Unlike pristine PE, significantly fewer bacteria were transferred to the growth medium as shown in Fig. 6. The counted numbers of CFU are therefore dramatically reduced on poly-(VBSB)-PE foils compared to pristine PE (Fig. 6) at all measured time points between 2 and 48 h. Growth control experiments of the incubation solutions confirmed the pure antiadhesive function of our zwitterionic PE samples and excluded an antibacterial effect (Fig. 4, SI). We assume therefore that the low colony counts observed in the adhesion assay are a consequence of resistance to bacterial attachment rather than the antibacterial properties of the material.

PE-poly-(VBSB) and pristine PE were furthermore immersed in natural seawater to get a more realistic picture involving multispecies biofilm formation. In this case, the period of incubation was significantly longer (21 days), since biofilm formation in natural media and under simulated natural conditions proceeds slower compared to the laboratory conditions mentioned above [84]. Briefly, PE-poly-(VBSB) and pristine PE foils (0.5 cm²) were immersed in baltic seawater (54°35'14.50"N, 10°17'76.60"E) under dynamic conditions. Three separated samples were examined independently each after 7, 14 and 21 days of seawater incubation by applying LIVE/DEAD staining (LIVE-/DEAD™ BacLight™ Viability Kit) with subsequent fluorescence imaging by confocal microscopy (Fig. 5, SI). Notably, poly-(VBSB) modified PE

foils show a background fluorescence after LIVE/DEAD staining that is not visible on pristine PE foils (homogenous laminar light green color, Fig. 7(b)). This likely dye (SYTO™ 9)-induced fluorescence has been reported for zwitterionic derivatives [85,86] and is an additional confirmation of the presence of tethered poly-(VBSB) brushes on the PE surface. However, besides this autofluorescence no colonization of living microorganisms can be detected on poly-(VBSB)-PE foils confirming the bio-resistant properties of the zwitterionic material. Pristine PE foils in contrast are rapidly colonized and show a significant biofilm formation amounting to a film thickness of about 20–50 μm after 21 days (Fig. 7 (a)). Thus poly-(VBSB)-PE does efficiently prevent biofilm formation by various microorganisms present in natural seawater. It should also be noted, that the stability of the zwitterionic brushes leads to long-term efficiency, at least for the tested maximum period of 21 days. It is also interesting that images of poly-VBSB-PE do not show any significant red-colored artifacts, which would indicate lysed microorganisms, which again rules out an antibacterial effect of the zwitterionic material (Fig. 7(b), no dead microorganisms after 21 days). This comparison confirms the purely anti-adherent mechanism of poly-(VBSB)-PE.

4. Conclusion

We report an efficient and scalable two-step protocol for grafting zwitterionic polymer brushes from the surface of bulk PE. The protocol involves a mild atmospheric plasma activation and subsequent heat-induced film polymerization of VBSB, a sulfobetaine derivative of styrene. The latter step avoids plasma-induced polymer degradation and is economic with respect to monomer consumption. Successful grafting of poly-(VBSB) brushes from PE was reflected by extremely low contact angles with water (10°). ATR-FTIR spectroscopy and XPS analysis confirmed the presence of ammonium and sulfonate groups. A medium poly-(VBSB)-layer thickness of about 50–100 nm was determined by

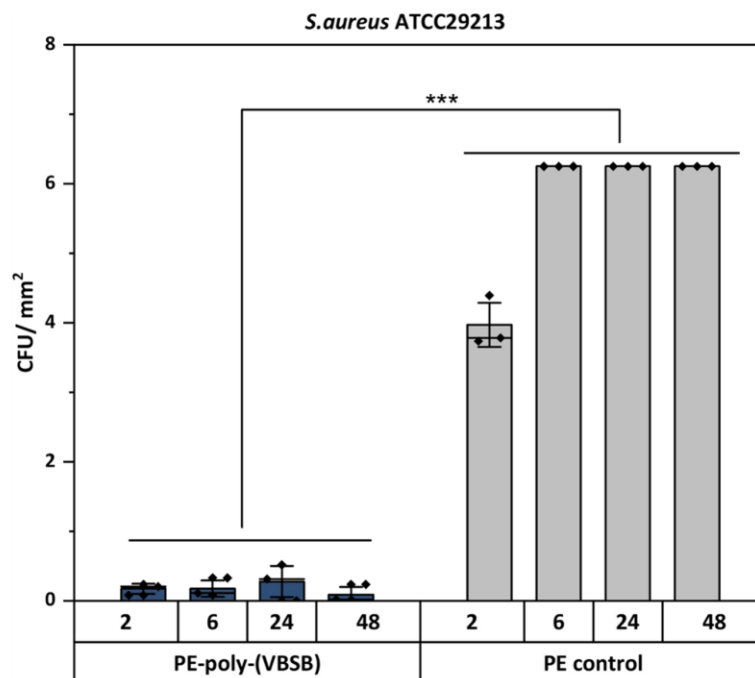


Fig. 6. Bacterial adhesion test: colony counts after 2, 6, 24 and 48 h incubation of PE-poly-VBSB and pristine PE with *S. aureus* ATCC29213. Polymerization conditions for PE-poly-(VBSB): 20 wt% (vinylbenzyl)sulfobetaine (VBSB) in water with 1.0 wt% ammoniumperoxodisulfate (APS), 85 °C, 2 h. Subsequent washing: 3 × 30 min with 70%water/ethanol mixture in an ultrasonic bath followed by drying at 50 °C. Statistical significance was determined via pairwise comparison $p < = 0.001$ ***).

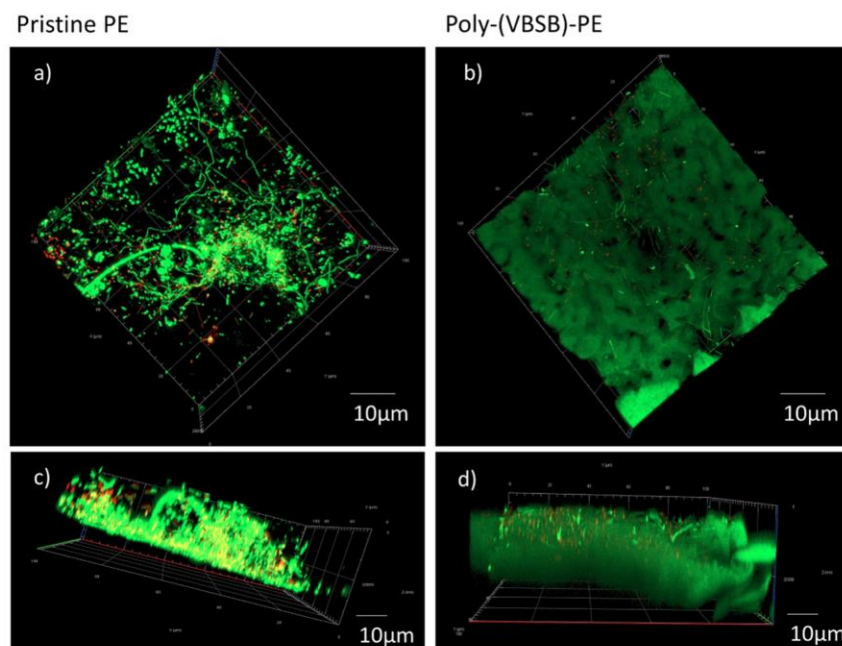


Fig. 7. Confocal fluorescence microscopy images of biofilm formation after 21 days of seawater incubation. Live/Dead staining: living microorganisms appear light green, dead microorganisms appear red; background autofluorescence of poly-VBSB brushes is visible as a laminar homogenous green layer, a) top view of pristine PE foil, b) top view of PE-poly-(VBSB) foils, c) front view of pristine PE-foil, d) front view of PE-poly-(VBSB) foil.

combined 3D ToF-SIMS and SPM analysis. In addition, a high surface charge density of 10^{16} zwitterions/cm² was estimated using a crystal violet adsorption assay, which together with the ToF-SIMS and SPM data indicates a high grafting density of zwitterionic polymers. A microbial adhesion test with *S. aureus* and a long-term incubation in natural seawater revealed efficient antifouling properties of poly-(VBSB)-PE. We attribute these findings to a purely anti-adherent and non-biocidal mechanism of the zwitterionic material. It is notable that the protocol used can be applied to bulk PE surfaces without changing intrinsic material properties such as color, strength and elasticity. The resulting polymer brushes are remarkably stable, at least for the longest test period used in this study (three weeks) and release no zwitterions into the solution. They are therefore interesting for applications in marine technology, medicine, the food industry and the pharmaceutical industry.

CRediT authorship contribution statement

Nils Burmeister: Writing – original manuscript, Conceptualization, Investigation. **Christel Vollstedt:** Conceptualization, Investigation. Writing – review – editing **Cathrin Kröger:** Investigation. **Timo Friedrich:** Investigation. **Nico Scharnagl:** Investigation. Writing – review & editing. **Marcus Rohnke:** Investigation. Writing – review & editing. **Eilika Zorn:** Investigation. **Sebastian Wicha:** Conceptualization. Writing – review & editing **Wolfgang R. Streit:** Supervision, Conceptualization, Resources. Writing – review & editing **Wolfgang Maison:** Supervision, Conceptualization, Resources. Writing – review & editing.

Supplementary materials

The following [supporting information](#) can be downloaded at: XXXXXX. Contact angles after polymerization and Soxhlet extraction; Investigation of polymerization with the crosslinking additive divinylbenzene (DVB); Weight loss after Soxhlet extraction (gravimetry);

Contact angles after bacterial adhesion tests and biofilm adhesion tests in natural seawater; XPS survey spectra; Determination of grafting density by adsorption and desorption of crystal violet; Gravimetric determination of pVBSB grafting yield; Bacterial adhesion assay – growth control; Biofilm adhesion in natural seawater; Synthetic procedures; NMR-spectra.

Declaration of Competing Interest

The authors declare that they have no known competing financial interests or personal relationships that could have appeared to influence the work reported in this paper.

Data Availability

Data will be made available on request.

Appendix A. Supporting information

Supplementary data associated with this article can be found in the online version at [doi:10.1016/j.colsurfb.2023.113195](https://doi.org/10.1016/j.colsurfb.2023.113195).

References

- [1] J.L. Green, A.J. Holmes, M. Westoby, I. Oliver, D. Briscoe, M. Dangerfield, M. Gillings, A.J. Beattie, Spatial scaling of microbial eukaryote diversity, *Nature* 432 (7018) (2004) 747–750.
- [2] B.M. Peyton, W.G. Characklis, Microbial biofilms and biofilm reactors, *Bioprocess Technol.* 20 (1995) 187–231.
- [3] G. O'Toole, H.B. Kaplan, R. Kolter, Biofilm formation as microbial development, *Annu. Rev. Microbiol.* 54 (1) (2000) 49–79.
- [4] S. Veerachamy, T. Yarlagadda, G. Manivasagam, P.K. Yarlagadda, Bacterial adherence and biofilm formation on medical implants: a review, *Proceedings of the Institution of Mechanical Engineers, Part H: J. Eng. Med.* 228 (10) (2014) 1083–1099.
- [5] P.S. Stewart, Prospects for anti-biofilm pharmaceutical, *Pharmaceuticals* 8 (3) (2015) 504–511.

- [6] K.C. Khulbe, C. Feng, T. Matsuura, The art of surface modification of synthetic polymeric membranes, *J. Appl. Polym. Sci.* 115 (2) (2010) 855–895.
- [7] E.A. Araújo, N.J. de Andrade, L.H.M. da Silva, A.F. de Carvalho, C.A. de Sá Silva, A.M. Ramos, Control of microbial adhesion as a strategy for food and bioprocess technology, *Food Bioprocess Technol.* 3 (3) (2010) 321–332.
- [8] M. Hakim, I. Utama, B. Nugroho, A. Yusim, M. Baithal, I. Suastika, Review of correlation between marine fouling and fuel consumption on a ship, *Proc. SENTA: 17th Conf. Mar. Technol.* (2017) 122–129.
- [9] A.M. Maan, A.H. Hofman, W.M. de Vos, M. Kamperman, Recent developments and practical feasibility of polymer-based antifouling coatings, *Adv. Funct. Mater.* 30 (32) (2020) 200936.
- [10] E. Almeida, T.C. Diamantino, O. de Sousa, Marine paints: the particular case of antifouling paints, *Prog. Org. Coat.* 59 (1) (2007) 2–20.
- [11] T. Sullivan, I. O'Callaghan, Recent developments in biomimetic antifouling materials: a review, *Biomimetics* 5 (4) (2020) 58.
- [12] J. Genzer, K. Efimenko, Recent developments in superhydrophobic surfaces and their relevance to marine fouling: a review, *Biofouling* 22 (5–6) (2006) 339–360.
- [13] S. Guo, D. Jańczewski, X. Zhu, R. Quintana, T. He, K.G. Neoh, Surface charge control for zwitterionic polymer brushes: tailoring surface properties to antifouling applications, *J. Colloid Interface Sci.* 452 (2015) 43–53.
- [14] D. Rana, T. Matsuura, Surface modifications for antifouling membranes, *Chem. Rev.* 110 (4) (2010) 2448–2471.
- [15] C.P. Gerba, Quaternary ammonium biocides: efficacy in application, *Appl. Environ. Microbiol.* 81 (2) (2015) 464–469.
- [16] S. Klierer, S.G. Wicha, A. Bröker, T. Naundorf, T. Catmadim, E.K. Oellingrath, M. Rohnke, W.R. Streit, C. Vollstedt, H. Kipphardt, Contact-active antibacterial polyethylene foils via atmospheric air plasma induced polymerisation of quaternary ammonium salts, *Colloids Surf. B. Biointerfaces* 186 (2020), 110679.
- [17] Z. Zhang, T. Chao, S. Chen, S. Jiang, Superlow fouling sulfobetaine and carboxybetaine polymers on glass slides, *Langmuir* 22 (24) (2006) 10072–10077.
- [18] C. Ventura, A.J. Guerin, O. El-Zubir, A.J. Ruiz-Sanchez, L.I. Dixon, K.J. Reynolds, M.L. Dale, J. Ferguson, A. Houlton, B.R. Horrocks, A.S. Clare, D.A. Fulton, Marine antifouling performance of polymer coatings incorporating zwitterions, *Biofouling* 33 (10) (2017) 892–903.
- [19] Y. Zhan, S. Yu, A. Amirfazli, A. Rahim Siddiqui, W. Li, Recent advances in antibacterial superhydrophobic coatings, *Adv. Eng. Mater.* 24 (4) (2022) 2101053.
- [20] C.M. Kirschner, A.B. Brennan, Bio-inspired antifouling strategies, *Annu. Rev. Mater. Res.* 42 (2012) 211–229.
- [21] K.J. Moses, S. Kim, M. Bilal, Y. Cohen, Tethered hydrophilic polymers layers on a polyamide surface, *J. Appl. Polym. Sci.* 135 (43) (2018) 46843.
- [22] X. Zhang, F. Shi, J. Niu, Y. Jiang, Z. Wang, Superhydrophobic surfaces: from structural control to functional application, *J. Mater. Chem.* 18 (6) (2008) 621–633.
- [23] R. Quintana, D. Jańczewski, V.A. Vasantha, S. Jana, S.S.C. Lee, F.J. Parra-Velandia, S. Guo, A. Parthiban, S.L.-M. Teo, G.J. Vancso, Sulfobetaine-based polymer brushes in marine environment: Is there an effect of the polymerizable group on the antifouling performance? *Colloids Surf. B. Biointerfaces* 120 (2014) 118–124.
- [24] J.F. Karthäuser, J. Koc, E. Schönemann, R. Wanka, N. Aldred, A.S. Clare, A. Rosenhahn, A. Laschewsky, Optimizing fouling resistance of poly(sulfobetaine)s through backbone and charge separation, *Adv. Mater. Interfaces* (2022).
- [25] W. Lin, J. Zhang, Z. Wang, S. Chen, Development of robust biocompatible silicone with high resistance to protein adsorption and bacterial adhesion, *Acta Biomater.* 7 (5) (2011) 2053–2059.
- [26] B. Yang, X. Duan, J. Huang, Ultrathin, biomimetic, superhydrophilic layers of cross-linked poly(phosphobetaine) on polyethylene by photografting, *Langmuir* 31 (3) (2015) 1120–1126.
- [27] B. Li, P. Jain, J. Ma, J.K. Smith, Z. Yuan, H.C. Hung, Y. He, X. Lin, K. Wu, J. Pfandtner, S. Jiang, Trimethylamine N-oxide-derived zwitterionic polymers: a new class of ultralow fouling bioinspired materials, *Sci. Adv.* 5 (6) (2019) eaaw9562.
- [28] M. Li, B. Zhuang, J. Yu, Functional zwitterionic polymers on surface: structures and applications, *Chem. Asian J.* 15 (14) (2020) 2060–2075.
- [29] S. Paschke, K. Lienkamp, Polyzwitterions: from surface properties and bioactivity profiles to biomedical applications, *ACS Appl. Polym. Mater.* 2 (2) (2020) 129–151.
- [30] J.B. Schlenoff, Zwitterion: coating surfaces with zwitterionic functionality to reduce nonspecific adsorption, *Langmuir* 30 (32) (2014) 9625–9636.
- [31] P.-S. Liu, Q. Chen, S.-S. Wu, J. Shen, S.-C. Lin, Surface modification of cellulose membranes with zwitterionic polymers for resistance to protein adsorption and platelet adhesion, *J. Membr. Sci.* 350 (1) (2010) 387–394.
- [32] Y. Zhang, Y. Liu, B. Ren, D. Zhang, S. Xie, Y. Chang, J. Yang, J. Wu, L. Xu, J. Zheng, Fundamentals and applications of zwitterionic antifouling polymers, *J. Phys. D: Appl. Phys.* 52 (40) (2019).
- [33] Q. Shao, S. Jiang, Molecular understanding and design of zwitterionic materials, *Adv. Mater.* 27 (1) (2015) 15–26.
- [34] B. Wu, L. Zhang, L. Huang, S. Xiao, Y. Yang, M. Zhong, J. Yang, Salt-Induced regenerative surface for bacteria killing and release, *Langmuir* 33 (28) (2017) 7160–7168.
- [35] Y. Fu, Y. Wang, L. Huang, S. Xiao, F. Chen, P. Fan, M. Zhong, J. Tan, J. Yang, Salt-responsive “killing and release” antibacterial surfaces of mixed polymer brushes, *Ind. Eng. Chem. Res.* 57 (27) (2018) 8938–8945.
- [36] A.B. Asha, Y. Chen, R. Narain, Bioinspired dopamine and zwitterionic polymers for non-fouling surface engineering, *Chem. Soc. Rev.* 50 (2021) 11668–11683.
- [37] X. Liu, H. Huang, G. Liu, W. Zhou, Y. Chen, Q. Jin, J. Ji, Multidentate zwitterionic chitosan oligosaccharide modified gold nanoparticles: stability, biocompatibility and cell interactions, *Nanoscale* 5 (9) (2013) 3982–3991.
- [38] Y. Qiao, X. Liu, Biocompatible coating, in: S. Hashmi, G.F. Batalha, C.J. Van Tyne, B. Yilbas (Eds.), *J. Mater. Process. Technol.*, Elsevier, Oxford, 2014, pp. 425–447.
- [39] A. Venault, Y. Chang, Designs of zwitterionic interfaces and membranes, *Langmuir* 35 (5) (2019) 1714–1726.
- [40] K. Akamatsu, W. Noto, H. Fukuzawa, A. Hara, S.-I. Nakao, Grafting of carboxybetaine polymers to polyethylene membranes via plasma graft polymerization to improve low-fouling properties and to tune the molecular weight cut-off, *Sep. Purif. Technol.* 204 (2018) 298–303.
- [41] T. Liu, D. Chen, Y. Cao, F. Yang, J. Chen, J. Kang, R. Xu, M. Xiang, Construction of a composite microporous polyethylene membrane with enhanced fouling resistance for water treatment, *J. Membr. Sci.* 618 (2021), 118679.
- [42] W. Zhai, H. Yu, H. Chen, L. Li, D. Li, Y. Zhang, T. He, Stable fouling resistance of polyethylene (PE) separator membrane via oxygen plasma plus zwitterion grafting, *Sep. Purif. Technol.* 293 (2022), 121091.
- [43] L. Song, J. Zhao, H. Yang, J. Jin, X. Li, P. Stagnaro, J. Yin, Biocompatibility of polypropylene non-woven fabric membrane via UV-induced graft polymerization of 2-acrylamido-2-methylpropane sulfonic acid, *Appl. Surf. Sci.* 258 (1) (2011) 425–430.
- [44] B. Shan, H. Yan, J. Shen, S. Lin, Ozone-induced grafting of a sulfoammonium zwitterionic polymer onto low-density polyethylene film for improving hemocompatibility, *J. Appl. Polym. Sci.* 101 (6) (2006) 3697–3703.
- [45] C.-M. Lim, J. Seo, H. Jang, J.-H. Seo, Optimizing grafting thickness of zwitterionic sulfobetaine polymer on cross-linked polyethylene surface to reduce friction coefficient, *Appl. Surf. Sci.* 452 (2018) 102–112.
- [46] D. Wang, X. Wu, L. Long, X. Yuan, Q. Zhang, S. Xue, S. Wen, C. Yan, J. Wang, W. Cong, Improved antifouling properties of photobioreactors by surface grafted sulfobetaine polymers, *Biofouling* 33 (10) (2017) 970–979.
- [47] A. Popelka, I. Novák, M. Lehochý, I. Chodák, J. Sedláčik, M. Gajtanska, M. Sedláčiková, A. Vesel, I. Junkar, A. Klejnová, M. Špírková, F. Bilek, Anti-bacterial treatment of polyethylene by cold plasma for medical purposes, *Molecules* 17 (1) (2012).
- [48] D. Jenke, Evaluation of the chemical compatibility of plastic contact materials and pharmaceutical products; safety considerations related to extractables and leachables, *J. Pharm. Sci.* 96 (10) (2007) 2566–2581.
- [49] M.J. Kasser, Regulation of UHMWPE biomaterials in total hip arthroplasty, *J. Biomed. Mater. Res. Part B Appl. Biomater.* 101B (3) (2013) 400–406.
- [50] K. Sadeghi, J. Seo, Photografting coating: an innovative approach to “non-migratory” active packaging, *Adv. Funct. Mater.* 31 (28) (2021) 2010759.
- [51] R. Davis, A. El-Shafei, P. Hauser, Use of atmospheric pressure plasma to confer durable water repellent functionality and antimicrobial functionality on cotton/polyester blend, *Surf. Coat. Technol.* 205 (20) (2011) 4791–4797.
- [52] R. Schwalm, UV coatings: basics, recent developments and new applications, Elsevier, 2006.
- [53] C. Oehr, M. Müller, B. Elkin, D. Hegemann, U. Vohrer, Plasma grafting — a method to obtain monofunctional surfaces, *Surf. Coat. Technol.* 116–119 (1999) 25–35.
- [54] F. Khelifa, S. Ershov, Y. Habibi, R. Snyders, P. Dubois, Free-radical-induced grafting from plasma polymer surfaces, *Chem. Rev.* 116 (6) (2016) 3975–4005.
- [55] M. Mazloumpour, P. Malshe, A. El-Shafei, P. Hauser, Conferring durable antimicrobial properties on nonwoven polypropylene via plasma-assisted graft polymerization of DADMAC, *Surf. Coat. Technol.* 224 (2013) 1–7.
- [56] Y. Chang, W.-J. Chang, Y.-J. Shih, T.-C. Wei, G.-H. Hsiue, Zwitterionic sulfobetaine-grafted poly(vinylidene fluoride) membrane with highly effective blood compatibility via atmospheric plasma-induced surface copolymerization, *ACS Appl. Mater. Interfaces* 3 (4) (2011) 1228–1237.
- [57] J. Zhao, L. Song, Q. Shi, S. Luan, J. Yin, Antibacterial and hemocompatibility switchable polypropylene nonwoven fabric membrane surface, *ACS Appl. Mater. Interfaces* 5 (11) (2013) 5260–5268.
- [58] A. Venault, T.-C. Wei, H.-L. Shih, C.-C. Yeh, A. Chinnathambi, S.A. Alharbi, S. Carretier, P. Aïmar, J.-Y. Lai, Y. Chang, Antifouling pseudo-zwitterionic poly(vinylidene fluoride) membranes with efficient mixed-charge surface grafting via glow dielectric barrier discharge plasma-induced copolymerization, *J. Membr. Sci.* 516 (2016) 13–25.
- [59] M. Dan, Y. Su, X. Xiao, S. Li, W. Zhang, A. New, Family of thermo-responsive polymers based on poly[N-(4-vinylbenzyl)-N,N-dialkylamine], *Macromolecules* 46 (8) (2013) 3137–3146.
- [60] F. Khalil, E. Franzmann, J. Ramcke, O. Dakischew, K.S. Lips, A. Reinhardt, P. Heisig, W. Maison, Biomimetic PEG-catecholates for stable antifouling coatings on metal surfaces: applications on TiO₂ and stainless steel, *Colloids Surf., B* 117 (2014) 185–192.
- [61] J.H. Priester, A.M. Horst, L.C. Van de Werfhorst, J.L. Saleta, L.A. Mertes, P. A. Holden, Enhanced visualization of microbial biofilms by staining and environmental scanning electron microscopy, *J. Microbiol. Methods* 68 (3) (2007) 577–587.
- [62] E.Q. Adams, L. Rosenstein, The color and ionization of crystal-violet, *J. Am. Chem. Soc.* 36 (7) (1914) 1452–1473.
- [63] V.M. Kochkodan, V.K. Sharma, Graft polymerization and plasma treatment of polymer membranes for fouling reduction: a review, *Journal of Environmental Science and Health, Part A* 47 (12) (2012) 1713–1727.
- [64] J.C. Bevington, H.W. Melville, R.P. Taylor, The termination reaction in radical polymerizations. Polymerizations of methyl methacrylate and styrene at 25°, *J. Polym. Sci.* 12 (1) (1954) 449–459.
- [65] S. Chen, L. Li, C. Zhao, J. Zheng, Surface hydration: principles and applications toward low-fouling/nonfouling biomaterials, *Polymer* 51 (23) (2010) 5283–5293.
- [66] J.T. Grant, Methods for quantitative analysis in XPS and AES, *Surf. Interface Anal.* 14 (6-7) (1989) 271–283.

N. Burmeister et al.

Colloids and Surfaces B: Biointerfaces 224 (2023) 113195

- [67] S. Ganesan, J. Hemanandh, K.S. Sridhar Raja, M. Purusothaman, Experimental investigation and characterization of HDPE & LDPE polymer composites, in: A. Arockiarajan, M. Duraiselvam, R. Raju (Eds.), *Advances in Industrial Automation and Smart Manufacturing*, Springer Singapore, Singapore, 2021, pp. 785–799.
- [68] R. Foerch, G. Beamson, D. Briggs, XPS valence band analysis of plasma-treated polymers, *Surf. Interface Anal.* 17 (12) (1991) 842–846.
- [69] J.L. Shi, E.T. Kang, K.G. Neoh, K.L. Tan, D.J. Liaw, Surface graft copolymerization of low density polyethylene films and its relevance to auto-adhesion, *Eur. Polym. J.* 34 (10) (1998) 1429–1434.
- [70] J.C. Tiller, C.-J. Liao, K. Lewis, A.M. Klivanov, Designing surfaces that kill bacteria on contact, *Proc. Natl. Acad. Sci.* 98 (11) (2001) 5981–5985.
- [71] H. Murata, R.R. Koepsel, K. Matyjaszewski, A.J. Russell, Permanent, non-leaching antibacterial surfaces—2: How high density cationic surfaces kill bacterial cells, *Biomaterials* 28 (32) (2007) 4870–4879.
- [72] L.R. Martins, L. Catone Soares, L.V. Alves Gurgel, L.F. Gil, Use of a new zwitterionic cellulose derivative for removal of crystal violet and orange II from aqueous solutions, *J. Hazard. Mater.* 424 (2022), 127401.
- [73] C. Leng, S. Sun, K. Zhang, S. Jiang, Z. Chen, Molecular level studies on interfacial hydration of zwitterionic and other antifouling polymers in situ, *Acta Biomater.* 40 (2016) 6–15.
- [74] M. Mortazavi, M. Nosonovsky, A model for diffusion-driven hydrophobic recovery in plasma treated polymers, *Appl. Surf. Sci.* 258 (18) (2012) 6876–6883.
- [75] C. Borcia, I.L. Punga, G. Borcia, Surface properties and hydrophobic recovery of polymers treated by atmospheric-pressure plasma, *Appl. Surf. Sci.* 317 (2014) 103–110.
- [76] M. van de Lagemaat, A. Grotenhuis, B. van de Belt-Gritter, S. Roest, T.J. Loontjens, H.J. Busscher, H.C. van der Mei, Y. Ren, Comparison of methods to evaluate bacterial contact-killing materials, *Acta Biomater.* 59 (2017) 139–147.
- [77] J. Begun, J.M. Gaiani, H. Rohde, D. Mack, S.B. Calderwood, F.M. Ausubel, C. D. Sifri, Staphylococcal biofilm exopolysaccharide protects against *Caenorhabditis elegans* immune defenses, *PLoS Pathog.* 3 (4) (2007), e57.
- [78] M.E. Davey, A. O'Toole, G. Microbial biofilms: from ecology to molecular genetics, *Microbiol. Mol. Biol. Rev.* 64 (4) (2000) 847–867.
- [79] G.M. Bruinsma, H.C. van der Mei, H.J. Busscher, Bacterial adhesion to surface hydrophilic and hydrophobic contact lenses, *Biomaterials* 22 (24) (2001) 3217–3224.
- [80] H. Schwegmann, A.J. Feitz, F.H. Frimmel, Influence of the zeta potential on the sorption and toxicity of iron oxide nanoparticles on *S. cerevisiae* and *E. coli*, *J. Colloid Interface Sci.* 347 (1) (2010) 43–48.
- [81] W.W. Wilson, M.M. Wade, S.C. Holman, F.R. Champlin, Status of methods for assessing bacterial cell surface charge properties based on zeta potential measurements, *J. Microbiol. Methods* 43 (3) (2001) 153–164.
- [82] M. Etxeberria, L. López-Jiménez, A. Merlos, T. Escuín, M. Viñas, Bacterial adhesion efficiency on implant abutments: a comparative study, *Int. Microbiol.* 16 (4) (2013) 235–242.
- [83] Z. Ma, J. Sun, X. Dong, D. Gan, W. Peng, Y. Li, W. Qian, P. Liu, J. Shen, Zwitterionic/active ester block polymers as multifunctional coatings for polyurethane-based substrates, *J. Mater. Chem. B* 10 (19) (2022) 3687–3695.
- [84] M. Toyofuku, T. Inaba, T. Kiyokawa, N. Obana, Y. Yawata, N. Nomura, Environmental factors that shape biofilm formation, *Biosci. Biotechnol. Biochem.* 80 (1) (2016) 7–12.
- [85] V. ArjunanãVasanthã, S.Z. Rahim, G. HanãJunyuan, S. ReddyãPuniredd, S. Lay-MingãTeo, Antibacterial, electrospun nanofibers of novel poly (sulfobetaine) and poly (sulfabetaïne) s, *J. Mater. Chem. B* 4 (15) (2016) 2731–2738.
- [86] Y. Xu, Q. Liu, X. Li, C. Wesdemiotis, Y. Pang, A zwitterionic squaraine dye with a large Stokes shift for in vivo and site-selective protein sensing, *Chem. Commun.* 48 (92) (2012) 11313–11315.

5.2 Combined Low-Fouling and Contact-Active Surface Modification

Since biofilm formation and, later on, biofouling involves many species with individual adhesion properties and growth patterns, multifunctional antifouling coatings have the most significant potential for success. The established protocol of KLEWER *et al.* provided cationic surfaces with strong contact-biocidal activity toward various clinically relevant microbial species. To avoid the attraction of unwanted negatively charged biomaterial, it was shown in the previous study that plasma polymerization could be used to generate zwitterionic surfaces that do not allow undesired accumulation of any biomaterial due to their low-fouling activity. However, such modification has no antibacterial properties.¹²⁰ In a clinical context, however, an antibacterial effect on opportunistic microorganisms is advantageous to avoid their spread and associated health hazards. Antibacterial surfaces killing microorganisms by contact can, therefore, help to prevent infections and, on the other hand, reduce the use of biocides and antibiotics. In consequence, they are valuable in avoiding the promotion of antibiotic resistance.^{56, 121}

To achieve non-adhesive and antibacterial activities, many attempts have been made to synthesize graft-co- or block-polymers bearing both zwitterionic low-fouling and cationic contact-biocide functionalities.^{122, 123} Previous studies on these mixed polymers have shown higher intra- and interchain coulomb attraction within the polymer brushes, which was often associated with higher thermostability, and other advantageous for long-time application.^{124, 125} A novel approach was developed in this section by combining two activity-principles in one monomer and its subsequent polymerization. This monomer carries a quaternary ammonium group and a sulfobetaine. It is readily available from DABCO in a scalable two-step procedure. The resulting 3-(4-(4-vinylbenzyl)-1,4-diazabicyclo[2.2.2]-octan-1,4-dium-1-yl)propane-1-sulfonate was obtained as a chloride salt (VBDSB). By grafting this novel compound from titanium and polyethylene substrates, the compatibility of this monomer was confirmed with SI-ATRP and plasma polymerization techniques. Significantly higher grafting yields of p-(VBDSB) were observed compared to similar polymers such as polycationic p-(VBTAC) or the polyzwitterionic p-(VBSB). We propose that strong inter- and intrachain attraction leads to an increase in layer thickness and superior thermostability. Finally, low-fouling and contact-biocide activity could be detected against various clinically relevant microorganisms. These observations confirmed the non-adhesive and antibacterial mechanism of the materials. Polymeric diammonium-sulfonates have thus been established as valuable new antifouling compounds with a dual mode of action.

Title: Low-Fouling and Antibacterial Polymer Brushes *via* Surface-Initiated Polymerization of a Mixed Zwitterionic and Cationic Monomer

Authors: Burmeister, N., Zorn, E., Preuss, L., Timm, D.T., Scharnagl, N., Wicha, S.G., Streit, W.R., Maison, W.

Type: Research Article, Journal Article

Journal: Langmuir

Year: 2023

Volume: 39

DOI: 10.1021/acs.langmuir.3c02657

Number of Pages: 13

Submitted: 07.09.2023

Accepted: 20.11.2023

Conceptualizing: Burmeister, N., Zorn, E., Maison, W.

Investigation: Burmeister, N., Zorn, E., Preuss, L., Timm, D.T., Scharnagl, N., Wicha, S.G., Streit, W.R., Maison, W.

Original Writing: Burmeister, N., Zorn, E., Maison, W.

Review and Editing: Burmeister, N., Zorn, E., Preuss, L., Timm, D.T., Scharnagl, N., Wicha, S.G., Streit, W.R., Maison, W.

LANGMUIR

pubs.acs.org/Langmuir

Article

Low-Fouling and Antibacterial Polymer Brushes via Surface-Initiated Polymerization of a Mixed Zwitterionic and Cationic Monomer

Nils Burmeister, Eilika Zorn, Lena Preuss, Donovan Timm, Nico Scharnagl, Marcus Rohnke, Sebastian G. Wicha, Wolfgang R. Streit, and Wolfgang Maisson*

Cite This: <https://doi.org/10.1021/acs.langmuir.3c02657>

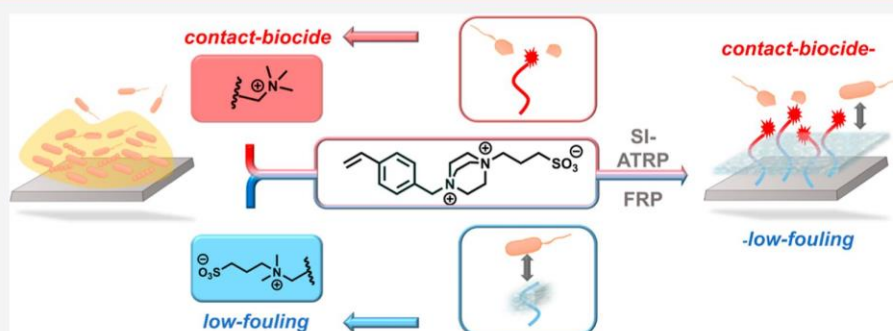
Read Online

ACCESS |

Metrics & More

Article Recommendations

Supporting Information



ABSTRACT: The use of surface-grafted polymer brushes with combined low-fouling and antibacterial functionality is an attractive strategy to fight biofilm formation. This report describes a new styrene derivative combining a quaternary ammonium group with a sulfobetaine group in one monomer. Surface-initiated polymerization of this monomer on titanium and a polyethylene (PE) base material gave bifunctional polymer brush layers. Grafting was achieved via surface-initiated atom transfer radical polymerization from titanium or heat-induced free-radical polymerization from plasma-activated PE. Both techniques gave charged polymer layers with a thickness of over 750 nm, as confirmed by ToF-SIMS-SPM measurements. The chemical composition of the brush polymers was confirmed by XPS and FT-IR analysis. The surface charge, characterized by the ζ potential, was positive at different pH values, and the number of solvent-accessible excess ammonium groups was found to be $\sim 10^{16}$ N^+/cm^2 . This led to strong antibacterial activity against Gram-positive and Gram-negative bacteria that was superior to a structurally related contact-active polymeric quaternary ammonium brush. In addition to this antibacterial activity, good low-fouling properties of the dual-function polymer brushes against Gram-positive and Gram-negative bacteria were found. This dual functionality is most likely due to the combination of antibacterial quaternary ammonium groups with antifouling sulfobetaines. The combination of bifunctional brush polymers with operationally simple polymerization techniques.

INTRODUCTION

Microbial biofilms are formed on almost any type of material exposed to biological media. They are of fundamental importance in nature and have implications for many industrial processes, the food and the health sector.¹ For in vivo applications, the adhesion of biomolecules to surfaces contributes to immunogenicity and low blood compatibility.² Microbial biofilms contribute to the development of resistance and increase the pathogenicity of microbes³ causing unwanted spread and/or infections in hospitals, the distribution of drinking water, on implants, food packaging, and other areas.^{4–6}

The chemical modification of base materials such as glass, plastics, and metals by surface-initiated graft polymerization is an efficient approach to prevent the formation of biofilms.⁷ The resulting brush layers have either antimicrobial (contact-

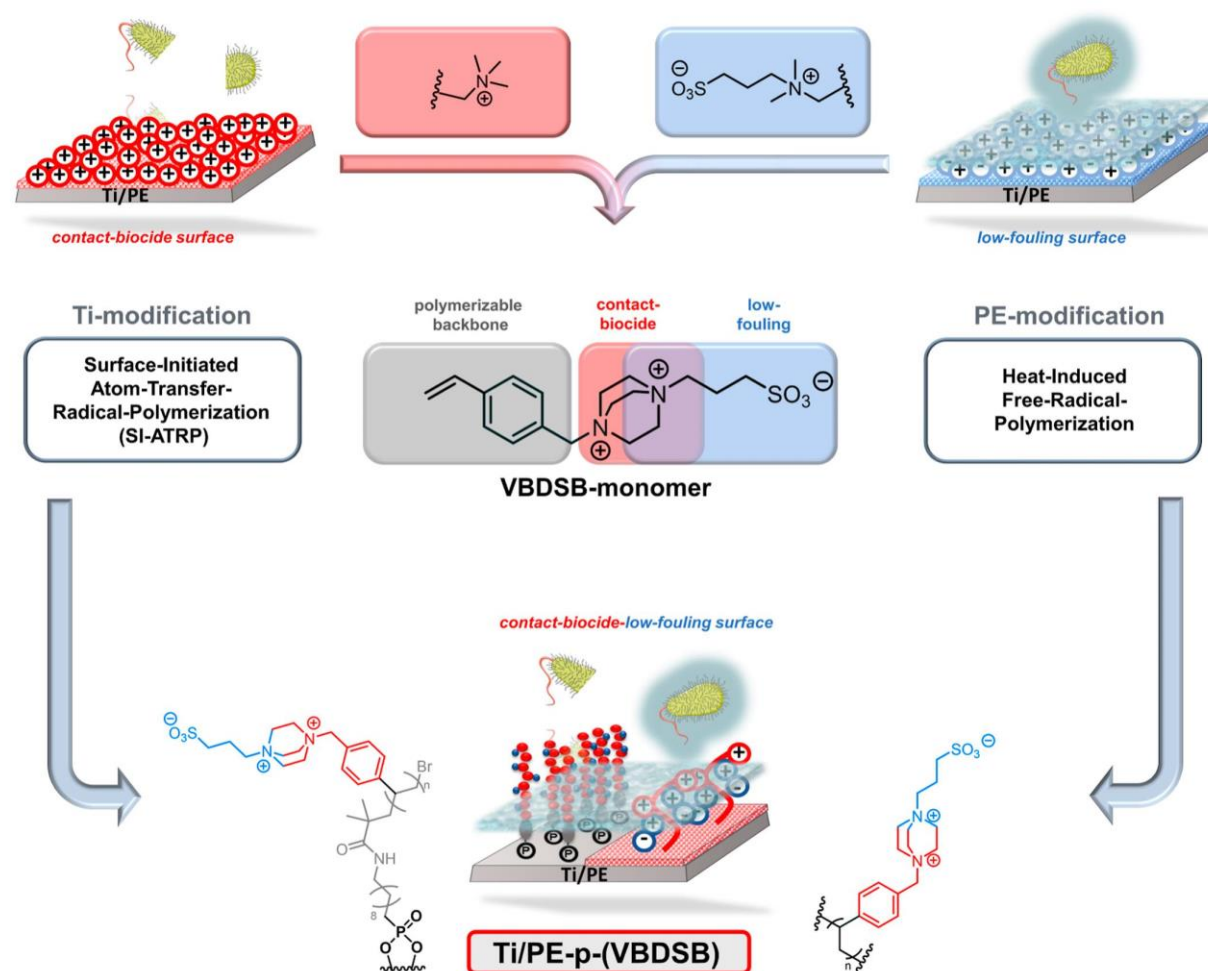
active) or antiadhesive (antifouling) properties, depending on their chemical composition. Contact-active materials are typically coated with positively charged polymers such as polymeric quaternary ammonium compounds with membrane disruptive properties.^{8,9} They have been shown to have strong antibacterial activity.¹⁰ However, the accumulation of bio-material by attractive charge interactions of the positively charged surfaces with negatively charged biomolecules or cell fragments causes a loss of function over time and can lead to

Received: September 7, 2023

Revised: November 20, 2023

Accepted: November 20, 2023

Scheme 1. Design Principle for the Styrene-Based Monomer VBDSB and the Following Graft Polymerizations from Polyethylene (PE) and Titanium Base Materials to Bifunctional Polymer Brush Layers with Contact-Activity and Low-Fouling Properties



an immune response and inflammation *in vivo*.^{11,12} Antifouling materials, on the other hand, are typically characterized by hydrophilic surfaces.^{13–15} The latter are often polymeric zwitterions composed of sulfobetaines, phosphobetaines, carboxybetaines, or *N*-oxides, leading to strong hydration barriers and thus antiadhesive properties for biomolecules and microorganisms.^{16–21} However, they lack antibacterial properties.²²

Many recent studies have therefore explored the combination of low-fouling and contact-active structures to bifunctional polymers, and efficient kill and release properties have been demonstrated for many of the resulting materials.^{23–26} The surface polymer layers in these studies have been assembled either by grafting of bifunctional random^{27,28} or block copolymers^{29–37} or by stepwise grafting of different homopolymers with contact-activity and low-fouling properties.^{23,24,38–40} Other combined-activity mechanisms for antibacterial materials involving contact-activity are also known, and several of these approaches are summarized in a recent review.⁴¹

We report herein a novel styrene-based monomer (VBDSB) containing a sulfobetaine and an additional quaternary ammonium moiety (Scheme 1). We used this monomer for surface-initiated polymerization from polyethylene (PE) and titanium. Both base materials are relevant for many applications in the health and food sector.^{42–44} With this study, we address the following major questions: (1) Are monomers with combined cations and zwitterions suitable for the synthesis of dense polymer brush layers by standard grafting-from procedures? (2) What are the properties of the resulting material surfaces with respect to polarity and surface charge? (3) Does the combination of a cation with a zwitterion in the monomer give a bifunctional polymer brush layer with contact-activity and antifouling properties against bacteria?

EXPERIMENTAL SECTION

Chemicals and Materials. All standard chemicals were purchased as reagent grade and used without further purification prior to use. Solvents were used as HPLC grade unless otherwise stated. Titanium coupons from pure titanium 3.7025 grade 1 (size: 20 mm × 10 mm × 1.0 mm) were purchased from Rocholl GmbH. ω -(α -Bromoisobutyramido)decylphosphonate (ADPA) was prepared ac-

cording to the protocol from Zorn et al.⁴⁵ Low-density polyethylene (LD-PE) foils with a thickness of 750 μm were purchased from Goodfellow and used as received. Phosphate-buffered saline (PBS) with a final concentration of 137 mM NaCl, 10 mM phosphate, 2.7 mM KCl, and a pH adjusted to 8.0 was prepared as a stock solution. Microorganisms *Staphylococcus aureus* (strain ATCC29213 and ATCC 25923), *Escherichia coli* (strain ATCC25922), and *Pseudomonas aeruginosa* (PA01) were purchased from American Type Culture Collection. Crimp neck vials (N20, 10 mL volume) and crimp caps (N20, PTFE septum) for degassing were purchased from Macherey-Nagel GmbH (Düren, Germany).

Synthesis. 1-(4-Vinylbenzyl)-1,4-diazabicyclo[2.2.2]octan-1-ium-chloride (VBDCI). 1,4-Diazabicyclo[2.2.2]octane (22.0 g, 196.1 mmol, 3.07 equiv) was dissolved in ethyl acetate (200 mL) and cooled to 0 °C. 4-Vinylbenzyl chloride (10.0 mL, 63.9 mmol, 1.00 equiv) was added dropwise. The solution was stirred at room temperature for 16 h. Filtration of the solid and washing with ethyl acetate (1 L) gave a light orange solid. Drying in vacuo gave the product as a light orange solid (14.65 g, 63.86 mmol, quant.). The product was stored at -18 °C for 2 months without decomposition.

¹H NMR (400 MHz, D₂O, δ): 7.64 (d, ³J_{H,H} = 8.3 Hz, 2H, 5-H, 7-H), 7.49 (d, ³J_{H,H} = 8.3 Hz, 2H, 4-H, 8-H), 6.86 (dd, ³J_{H,H} = 17.7 Hz, 11.0 Hz, 1H, 2-H), 5.97 (d, ³J_{H,H} = 17.7 Hz, ²J_{H,H} = 0.8 Hz, 1H, 1-Ha), 5.44 (d, ³J_{H,H} = 11.0 Hz, ²J_{H,H} = 0.8 Hz, 1H, 1-Hb), 4.49 (s, 1H, H-9), 3.47–3.44 (m, 6H, 10-H), 3.20–3.16 (m, 6H, 11-H). ¹³C {¹H} NMR (101 MHz, D₂O, δ): 139.7 (C3), 135.7 (C2), 133.4 (C4, C8), 126.8 (C5, C7), 125.3 (C6), 116.3 (C1), 68.0 (C9), 52.0 (C10), 44.2 (C11). HRMS (ESI⁺) *m/z*: [M + H]⁺ calcd for C₁₅H₂₁N₂⁺, 229.1705; found, 229.1698.

3-(4-(4-Vinylbenzyl)-1,4-diazabicyclo[2.2.2]octan-1,4-dium-1-yl)propane-1-sulfonate (VBDSB). 1-(4-Vinylbenzyl)-1,4-diazabicyclo[2.2.2]octan-1-ium chloride (10.0 g, 43.6 mmol, 1.00 equiv) was dissolved in 100 mL of MeCN, and 1,3-propane sultone (7.80 mL, 88.8 mmol, 2.04 equiv) was added dropwise. The solution was stirred at room temperature for 16 h. Filtration and washing with MeCN (500 mL) gave a colorless solid (13.21 g, 43.60 mmol, 86%). The product obtained was used for polymerization reactions, but it contained a mixture of chloride and 3-hydroxypropane-1-sulfonic acid as anionic counterions. For analytical purposes, an ion exchange chromatography (Dowex 1 \times 2, water) and freeze-drying gave the homogeneous chloride salt of the title compound as a colorless solid (4.78 g, 13.6 mmol, 32%). The product was stored at -18 °C for 2 months without decomposition.

¹H NMR (500 MHz, D₂O, δ): 7.67 (d, ³J_{H,H} = 8.3 Hz, 2H, 5-H, 7-H), 7.54 (d, ³J_{H,H} = 8.3 Hz, 2H, 4-H, 8-H), 6.88 (dd, ³J_{H,H} = 17.7 Hz, 11.0 Hz, 1H, 2-H), 6.00 (dd, ³J_{H,H} = 17.7 Hz, ²J_{H,H} = 0.8 Hz, 1H, 1-Ha), 5.48 (d, ³J_{H,H} = 11.0 Hz, ²J_{H,H} = 0.8 Hz, 1H, 1-Hb), 4.84 (s, 1H, H-9), 4.06 (s, 12H, 10, 11-H), 3.83–3.73 (m, 2H, 12-H), 3.03 (t, ³J_{H,H} = 7.2 Hz, 2H, 13-H), 2.36–2.24 (m, 2H, 14-H). ¹³C {¹H} NMR (101 MHz, D₂O, δ): 140.5 (C3), 135.6 (C2), 133.3 (C4, C8), 127.2 (C5, C7), 124.1 (C6), 116.8 (C1), 68.6 (C9), 63.3 (C12), 51.3 (C10), 50.7 (C11), 46.8 (C14), 17.8 (C13). HRMS (ESI⁺) *m/z*: [M + H]⁺ calcd for C₁₈H₂₇N₂O₃S⁺, 351.1737; found, 351.1728. IR $\tilde{\nu}$ (cm⁻¹): 3390 (OH), 3024 (CH), 2920 (NR₄⁺), 1624 (C = C), 1388 (S = O), 1176 (SO₃⁻), 1038 (SO₃⁻), 860 (CH).

METHODS

NMR Spectroscopy. ¹H-, ¹³C-, and ³¹P NMR measurements were carried out at room temperature in 5 mm o.d. sample tubes with a Bruker Avance III HD 400 MHz or Bruker Avance I HD 500 MHz spectrometer (AV400 and AV500, Bruker Biospin GmbH, Ettlingen, Germany). ¹H NMR spectra were calibrated against deuterated solvents. ¹³C NMR spectra were recorded with ¹H-broadband decoupling. Additionally, two-dimensional experiments (HSQC, H, H-COSY, and HMBC) were performed for peak assignment.

Mass Spectrometry. High-resolution mass spectra were measured with a MicroTOF-Q with an ESI source from Bruker Daltonik GmbH (Bremen, Germany).

Contact Angle Measurements. Water contact angles were obtained with an OCA 20 goniometer from DataPhysics (Filderstadt,

Germany). This goniometer is equipped with three automated dispensing units for different liquid probes, a highspeed video system with CCD camera, measuring stage, and halogen lighting for static and dynamic contact angle measurements. For evaluation, independent triplicate measurements at three different points on the surface of each test specimen were carried out. Advancing contact angles were measured with deionized water by using the static sessile drop method with a dispensing volume of 5 μL . The dispensing rate of the automatic syringe was set at 1 $\mu\text{L}/\text{min}$. The obtained angle was calculated with OCA software.

Electrokinetic ζ -Potential Measurements. The surface zeta potential (ζ -potential) was determined as the streaming potential using an electrokinetic analyzer Surpass (Anton Paar, Graz, Austria). The measurements were carried out using an adjustable gap cell in which two samples with a rectangular size of 1 cm \times 2 cm were clamped vis-à-vis with a micro slit of 110 μm in between. For each measurement, the starting conductivity of each measurement was set to 17 $\mu\text{S}/\text{m}$ with KCl as the electrolyte. The pH was adjusted from 9.5 to 2.5 stepwise with automatic pH titration by adding 0.05 M HCl. Presented values of ζ potentials were determined as mean value of four measurements for each pH step.

IR and UV/Vis Spectroscopy. Infrared spectra were recorded with an attenuated total reflectance Fourier Transform infrared (ATR-FTIR) system, model "IRAffinity-1S" from Shimadzu (Kyoto, Japan), using a "Quest" ATR accessory from Specac. The spectral range was set from 4000–400 cm⁻¹ with a resolution of 0.5 cm⁻¹ in the absorbance mode. The spectra were processed with OriginPro 9 (2021) software. UV/vis spectra were recorded on a Genesys 10S spectrophotometer from Thermo Scientific (Waltham, USA) using Visionlite software for analysis.

X-ray Photoelectron Spectroscopy (XPS). XPS measurements were performed using a KRATOS AXIS Ultra DLD (Kratos Analytical, Manchester, U.K.) equipped with a monochromatic Al K α anode working at 15 kV (225 W). For the survey spectra, a pass energy of 160 eV was used, while for the region spectra, the pass energy was 20 eV. The investigated area was 700 μm \times 300 μm . The evaluation and validation of the data were carried out with software CASA-XPS version 2.3.24. Calibration of the spectra was carried out by adjusting the C 1s signal to 284.5 eV. For deconvolution of the region files, background subtraction (U 2 Tougaard or Shirley) was performed before calculation.

Time-of-Flight Secondary Ion Mass Spectrometry (ToF-SIMS) and Scanning Probe Microscopy (SPM). 3D analysis of the coated samples was carried out with an M6 Plus machine (IONTOF GmbH, Münster, Germany). This type of time-of-flight secondary ion mass spectrometer (ToF-SIMS) is additionally equipped with a scanning probe microscope. The deposited polymers of both types of samples were analyzed in 3D by removal with a 5 keV Ar₃₀₀₀⁺ cluster beam ($I = 0.21$ nA). Therefore, each sample was analyzed with 60 keV Bi₃²⁺ ions in negative polarity on an area of 70 \times 70 μm^2 (128 \times 128 pixels, $I = 0.09$ pA at a cycle time of 200 μs , 700 μm LMIG aperture, spectrometry mode) alternating and centered to the Ar beam, which produced a 140 μm \times 140 μm sputter crater. After three analysis scans, two sputter scans were carried out followed by 2 s pause time for charge compensation with low energetic electrons. The achieved mass resolution was $m/\Delta m > 4.740$ fwhm for C₁₆N₂H₂₃SO₃⁻. For the calibration of the sputter time axes, further depth profiles of the coating only were carried out. Here, scanning probe microscopy (SPM) line scans were performed before and after depth profiling in the tapping mode to obtain the crater depths from the difference in the 2D topography profiles. The calculated erosion rates [PE-p-(VBDSB) 0.221 nm/s and Ti-p-(VBDSB) 1.489 nm/s] were used for calibration of the sputter time axes. For correlative 3D imaging, we carried out SPM imaging of the analyzed area before and after SIMS depth profiling and correlated the data. The complete data evaluation was carried out with Surface Lab 7.3 software (IONTOF GmbH, Münster, Germany).

The grafting yield was calculated from the estimated layer thickness from ToF-SIMS analysis with eq 1.

$$\sigma(\text{pVBDSB}) = d \times 1 \text{ cm}^2 \times \rho \quad (1)$$

with d = layer thickness estimated from ToF-SIMS analysis.

The density of the styrene polymer $\rho = 1.05 \text{ g/cm}^3$.

N^+ per cm^2 was calculated from the grafting yield with eq 2.

$$\frac{N^+}{\text{cm}^2} = \frac{\sigma(\text{pVBDSB}) \times N_A}{M(\text{VBDSB}) \times 10^4} \quad (2)$$

with $M(\text{VBDSB})$ = molecular weight of the monomer VBDSB 351.17 g/mol.

Thermogravimetric Analysis (TGA). Thermogravimetric analysis (TGA) was performed using a TGA 2 instrument (Mettler-Toledo GmbH, Gießen, Germany) using Alox crucibles. A temperature program with a ramp rate of 10 K/min (50–80 °C, 80 °C 10 min, 80–700 °C) was operated under a nitrogen atmosphere.

Atmospheric Air Plasma Activation of PE. For plasma activation, an atmospheric air plasma system from Plasmatec GmbH (Steinhagen, Germany) was used. The atmospheric-pressure plasma was produced by a generator FG5001 with an applied working frequency of 21 kHz, generating a nonequilibrium discharge in a rotating jet nozzle RD1004 in combination with the stainless-steel tip No. 22826 for an expanded treatment width of approximately 22 mm. Additionally, the jet nozzle was connected to a Janome desktop robot type 2300N for repetitious accuracy regarding the treatment conditions. The process gas was dry and oil-free air at an input pressure of 5 bar in all experiments.

PE Surface Modification via Free-Radical Polymerization.

PE foils with a thickness of 0.75 mm were rinsed with an isopropyl alcohol/water mixture of 70% (v/v) and dried for 15 min at 50 °C before use. Plasma treatment of the PE foils was performed at a distance of 6 mm between the plasma jet nozzle and the surface. The speed of the plasma jet nozzle was set at 110 mm/s. Samples were stored at room temperature in air for 8 min after plasma treatment. A solution of the appropriate polymerizable VBDSB (1.00 g, 2.85 mmol) and ammoniumperoxodisulfate as a free-radical initiator (0.11 mmol) in deionized water (2.5 mL) was purged with nitrogen for 10 min. Plasma-treated PE foils were placed in a degassed aqueous solution. The resulting reaction mixtures were purged with nitrogen for another 15 min and were subsequently polymerized for 2 h at 85 °C. After polymerization, the materials were treated with an EtOH/water mixture (70 vol %) for 15 min in an ultrasonic bath. The cleaning step was repeated three times with continuous renewing of the EtOH/water mixture (70 vol %). After washing, the resulting modified PE coupons were dried for 30 min in a nitrogen stream before use.

Immobilization of ADPA on Titanium Coupons. Titanium coupons (size: 20 × 10 × 1.0 mm) were immersed in acetone (10 mL), then MeOH (10 mL), and finally H₂O (10 mL) for 10 min each in an ultrasonic bath. Afterward the coupons were treated with piranha acid [H₂SO₄/H₂O₂ (3:1 V/V) *caution*: special care must be taken upon preparation of piranha acid; piranha solution reacts violently with organic materials]⁴⁶ for 1 h, rinsed with deionized water, and dried in vacuo.

The bifunctional phosphonic acid ADPA⁴⁵ (4 mg, 10 μmol) was dissolved in 10 mL of MeOH/H₂O [2:1 (V/V)]. The coupons were placed in the solution and heated to 80 °C for 3 days. Afterward, the coupons were immersed in MeOH (10 mL) three times for 10 min each with ultrasonication to remove noncovalently bound material.

SI-ATRP Polymerization. In a closed crimp neck vial with a septum for gas supply, CuBr (3 mg, 21 μmol), VBDSB (1.00 g, 2.85 mmol), and *N,N,N',N',N''*-pentamethyldiethylenetriamine (10 μL, 48 μmol) were dissolved in 4.0 mL of H₂O under nitrogen. Nitrogen was bubbled through the solution for 30 min before the titanium coupons with the immobilized phosphonic acid were added and nitrogen gas was bubbled through the solution for 5 min. The mixture was then heated to 70 °C under N₂. After 2 h, the titanium coupons were removed from the mixture and thoroughly rinsed with deionized water. The coupons were immersed in water (10 mL) three times and MeOH (10 mL) for 10 min each with ultrasonication to remove

noncovalently attached material. Afterward, the coupons were dried in a stream of nitrogen.

Chemical Structures. The following monomers (Figure 1) were graft polymerized according to the protocols outlined above and established procedures from our laboratory.^{45,47,48}

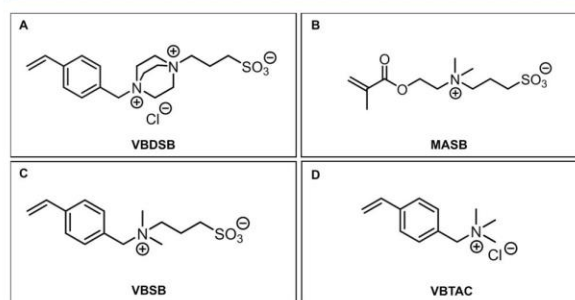


Figure 1. Molecular structures of monomers used for graft polymerizations. (A) 3-(4-(4-Vinylbenzyl)-1,4-diazabicyclo[2.2.2]octan-1,4-diium-1-yl)propane-1-sulfonate as a chloride salt (VBDSB). (B) 3-((2-(Methacryloyloxy)ethyl)dimethylammonio)propane-1-sulfonate (MASB). (C) 3-(Dimethyl(4-vinylbenzyl)ammonium)propane-1-sulfonate (VBSB). (D) Vinylbenzyl-trimethylammonium-chloride (VBTAC).

Determination of Charge Density. Solvent-accessible surface charges were determined by a slightly modified fluorescein assay developed by Tiller⁸ and Murata.⁴⁹ Titanium coupons with a total surface area of 4.6 cm² and PE foils with a modified surface area of 1.0 cm² were treated with 10.0 mL of a 1.0 wt % aqueous sodium fluorescein solution for 20 min under gentle shaking of the vessel. The test samples were removed and subsequently rinsed with deionized water. The test samples were then immersed in water (10 mL) for 10 min with ultrasonication to remove the residual fluorescein. This process was repeated three times. For desorption of the immobilized fluorescein, the test samples were treated with 9.0 mL of 0.1 wt % cetyltrimethylammonium chloride solution for 30 min with gentle shaking. After removal of the test samples, 1.0 mL of PBS buffer (0.1 M, pH 8.0) was added, and the absorbance of the resulting solution at 501 nm was measured. The concentration of desorbed fluorescein was calculated with an extinction coefficient of 77,000 M⁻¹·cm⁻¹. The absorption of a solution obtained by the same procedure from a nonmodified titanium coupon or nonmodified PE foil was subtracted as a blank value. All measurements were performed in triplicate. Assuming a 1:1 immobilization of the fluorescein/ammonium group, the concentration of fluorescein was correlated to the number of cationic charges on the coupons. The resulting UV/vis absorbance was correlated to the concentration of desorbed fluorescein using the Beer–Lambert law

$$c = \frac{A}{\epsilon \times l} \quad (3)$$

with A = measured absorbance, ϵ = extinction coefficient of fluorescein (77,000 1/M·cm), l = optical path length [cm], and c = concentration of desorbed fluorescein [mol/L].

Determination of Antimicrobial Activity (ASTM E2149-13a).

The antimicrobial evaluation was performed with a modified ASTM assay E21 49-13a.⁴⁷ All test samples were treated with 70 vol % isopropyl alcohol and dried at room temperature prior to testing. Test microorganisms [*S. aureus* ATCC 29213 (and 25,923) *E. coli* ATCC 25922, *P. aeruginosa* PA01] were grown on Columbia agar for 12 h and diluted to a concentration of an inoculum size of 10⁸ cfu/mL in 0.9 wt % NaCl. PE foils (surface area of 1.0 cm²) were treated with 2 mL of the diluted bacterial suspension (10⁵ cfu/mL) in a 24-well plate. Titanium coupons (surface area of 4.6 cm²) were treated with 4 mL of the diluted bacteria suspension (10⁵ cfu/mL) in a 5 mL falcon tube. Both, PE-p-(VBDSB), Ti-p-(VBDSB) and nonmodified PE and

Table 1. Selected Analytical Data for Polymer Brush Layers on Ti and PE as the Base Materials

sample	WCA ^a [deg]	charge density ^b [10 ¹⁵ N ⁺ /cm ²]	charge density ^c [10 ¹⁵ SO ₃ ⁻ /cm ²]	grafting yield ^d [μg/cm ²]	layer thickness ^e [nm]
Ti Ctrl	47.9 ± 10.1				
Ti-ADPA	76.1 ± 3.4				
Ti-p-(VBDSB)	44.5 ± 10.2	8.55 ± 3.4		78.8	750
Ti-p-(VBTAAC)	12.7 ± 1.9	14.2 ± 3.0		10.5	100
Ti-p-(VBSB)	35.5 ± 12.0		7.5 ± 0.9		
PE-Ctrl	98.5 ± 2.4				
PE-plasma	37.8 ± 2.6				
PE-p-(VBDSB)	38.5 ± 3.8	53.2 ± 5.9		157.5	1500
PE-p-(VBTAAC)	11.3 ± 3.3	18.9 ± 7.7		10.5	100
PE-p-(VBSB)	9.9 ± 2.0		108 ± 0.8	5.25	50–100

^aAdvancing water contact angles. Results are presented as mean value ± SD ($n \geq 3$). ^bSolvent-accessible ammonium groups determined via fluorescein assay. Results are presented as mean value ± SD ($n \geq 3$). ^cSolvent-accessible sulfonate groups determined via crystal violet assay. Results are presented as mean value ± SD ($n \geq 3$). ^dGrafting yield estimated from the layer thickness determined by ToF-SIMS-SPM analysis with eq 1. ^eLayer thickness estimated from the ToF-SIMS-SPM analysis.

titanium samples were incubated for 2 h under gentle shaking (120 rpm) at 37 °C. These conditions correspond to a challenge of 0.9×10^5 cfu/cm² titanium coupon and 2.0×10^5 cfu/cm² for PE coupons. After incubation, the bacteria solution and three dilutions of it were incubated on Columbia agar (100 μL of the incubation solution, 1:10 dilution, and 1:100 dilution) for 18 h at 37 °C. After incubation, colonies were counted, and log₁₀ reduction in a triplicate measurement was calculated using the following eq 4.

$$\text{bacterial log}_{10} \text{ reduction} = \log_{10} \left(\frac{N_0}{N} \right) \quad (4)$$

with N_0 = cfu (colony-forming units) before incubation and N = cfu (colony-forming units) after incubation.

Microbiological Assessment of Polymer Leaching. Test specimens of PE-p-(VBDSB) and PE-p-(VBTAAC) were incubated in 1980 μL of sterile saline solution for 2 h at 37 °C under gentle shaking. Afterward, test specimens were removed from the saline solution, and 20 μL of the bacterial suspension was added to obtain an initial concentration of 10^5 cfu/mL. The resulting solutions were again incubated for 2 h at 37 °C. 100 μL portion of the resulting solutions was aliquoted on Columbia Agar and incubated overnight. Log₁₀ reduction was calculated using eq 4. Values are presented as mean values ($n = 3$) ± SD.

Determination of Low-Fouling Activity (Bacterial Adhesion Test). All test samples were treated with 90 vol % iPrOH and dried under laminar airflow before testing. The bacterial strains (*S. aureus* ATCC29213, *E. coli* 25922, and *P. aeruginosa* PA01) were cultured separately for each assay on Columbia agar overnight. The overnight culture was suspended and diluted in sterile saline solution (0.9%) to preserve a cell density of 10^7 colony-forming units per milliliter (cfu/mL). PE-p-(VBDSB) and pristine PE test specimens (surface area: 1.0 cm²) were placed in a 24-well plate (one specimen per well) and covered with each 1980 μL of Mueller Hinton Broth (MHB). 20 μL of the bacterial suspension was added to each well to obtain a starting cell density of 10^5 cfu/mL. The procedure for Ti-p-(VBDSB) and nonmodified titanium (surface area: 4.6 cm²) was performed under equal conditions. The samples were incubated in bacterial solution for 24 h at 37 °C and were subsequently transferred into 3 mL of sterile saline solution without stirring or shaking for 10 min to remove loosely attached bacteria. Each foil was slightly pressed with the modified side onto an agar plate (Columbia agar) and removed after 30 s. Transferred cells were incubated for 20 h at 37 °C prior to cell counting. For evaluation, cell counts above 250 were set as too numerous to count (TNTC). An aliquot of 100 μL of supernatant was taken from each incubation experiment and analyzed with respect to bacterial growth in comparison to a positive control of MHB containing the initial bacterial suspension without added test specimens.

LIVE/DEAD Staining and Confocal Microscopy. Modified PE-p-(VBDSB), PE-p-(VBTAAC), PE-p-(MASB), and pristine PE speci-

mens with a surface area of 0.8 cm² were immersed in a six-well plate into 4 mL of *P. aeruginosa* PA01 (1.5×10^8 cfu/mL) in Luria–Bertani (LB) medium. The samples were incubated for 24 h at 37 °C under gentle shaking (100 rpm). After 24 h, test specimens were rinsed with PBS buffer shortly to detach loosely attached planktonic cells. Fluorescence imaging to examine biofilm formation on the test samples was supported by using the LIVE/DEAD BacLight Viability kit. Images were visualized via a confocal laser scanning microscope LSM 800 with AiryScan from Zeiss (Jena, Germany) and edited with ZEN 2 (Blue Edition) software.

Statistics. Statistics were performed using OriginPro 9 (2021) software. Data are reported as mean value ± standard deviation (SD) for continuous variables or as a selective frequency for categorical variables. Pairwise comparison via the Tukey test was performed to evaluate the antimicrobial test. A p -value of less than 0.05 was considered significant.

RESULTS AND DISCUSSION

Details for the synthesis of VBDSB can be found in the [Experimental Section](#) and the [Supporting Information](#). Briefly, diazabicyclooctane (DABCO) was monoalkylated with vinylbenzyl chloride. The resulting alkylated DABCO derivative was then treated with 1,3-propane sultone to give VBDSB. This operationally simple two-step procedure gave VBDSB in excellent overall yield and is easily scalable because the product and the intermediate are crystalline solids, and no chromatographic purification is needed. We picked DABCO as a diamine scaffold because it is readily available, and DABCO-derived cationic polymers have previously been shown to have good contact-activity against Gram-positive and Gram-negative bacteria.^{50–52}

For the graft polymerization of VBDSB from titanium and PE, we used two established polymerization protocols. Polymer brush layers on titanium coupons were prepared by surface-initiated atom transfer radical polymerization (SI-ATRP).⁴⁵ The two-step procedure involved the covalent immobilization of a bifunctional phosphonic acid containing a bromoisobutryl group that can serve as an initiator for SI-ATRP. Subsequent radical polymerization with the monomer VBDSB was performed with Cu(I)-catalysis and gave a dense p-(VBDSB) brush layer on the titanium surface. The corresponding graft polymerization from LD-PE was achieved in a two-step procedure using atmospheric air plasma activation of PE foils and subsequent heat-induced free-radical polymerization of the VBDSB-monomer to give PE-p-(VBDSB).⁴⁷ Both protocols, SI-ATRP on Ti and the two-step protocol for PE, have been used before for the preparation

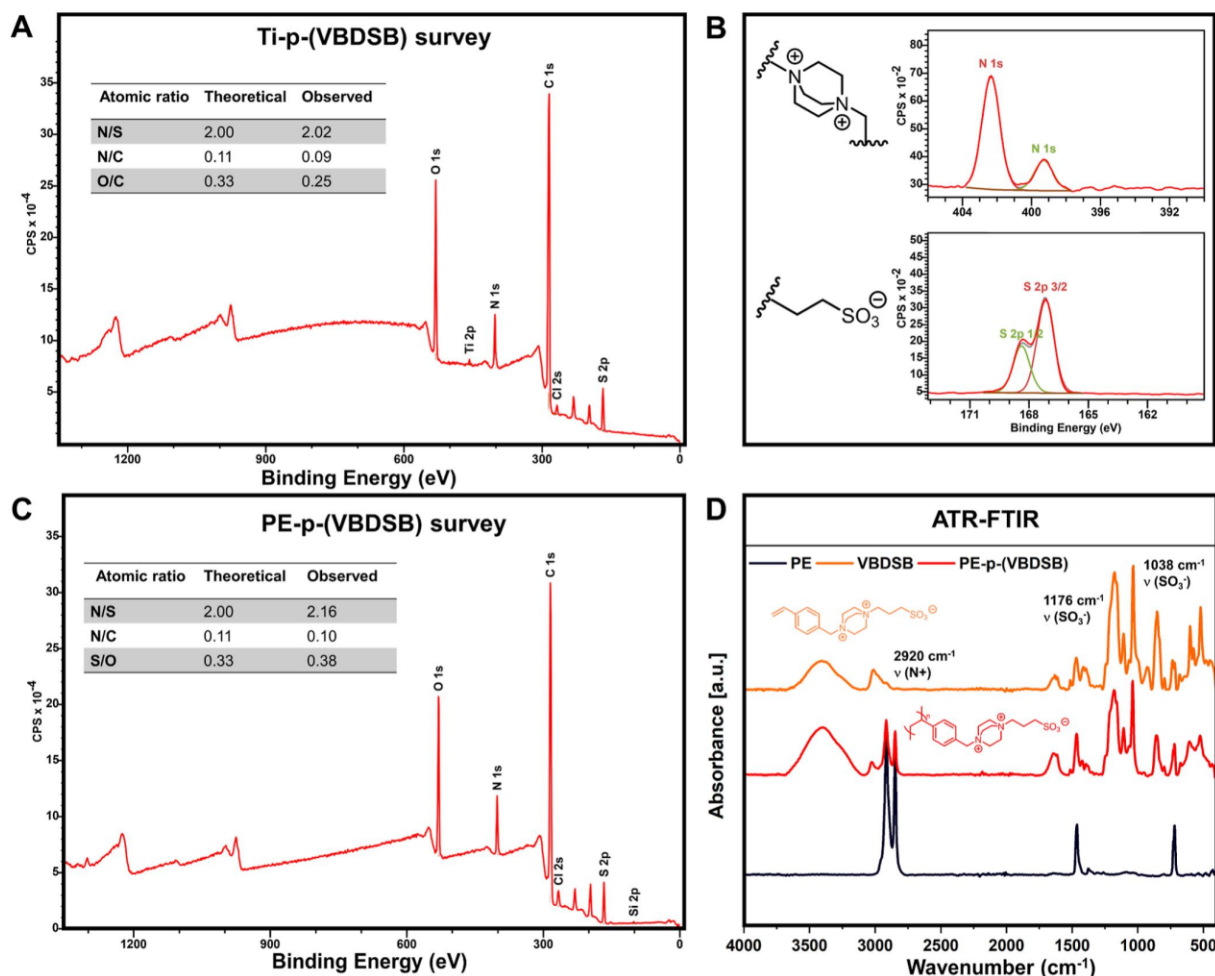


Figure 2. Selected XP and ATR-FTIR spectra of the p-(VBDSB) brush layers. (A) XP survey spectra of Ti-p-(VBDSB) with calculated atomic ratios. (B) Deconvoluted N 1s and S 2p regions of Ti-p-(VBDSB). (C) XP survey spectra of PE-p-(VBDSB) were recorded with calculated atomic ratios. XPS survey spectra of PE-p-(VBDSB) with calculated atomic ratios. Deconvoluted N 1s and S 2p regions for PE-p-(VBDSB) and further O 2p and C 1s regions for both Ti-p-(VBDSB) and PE-p-(VBDSB) are available in the Supporting Information (Figures S5 and S6). (D) ATR-FTIR spectra of PE-p-(VBDSB) compared to the VBDSB monomer and a pristine PE sample.

of polycationic and zwitterionic polymer brush layers on Ti and PE, and the details may be found in the corresponding publications.^{45,47,48} A part of the analytical data for PE-p-(VBDSB) and Ti-p-(VBDSB) are shown in Table 1. Also included are data for the corresponding cationic (VBTAC) and zwitterionic (VBSB) polymer brushes on Ti and PE prepared with the same protocols. The successful polymerization of VBDSB on both PE and titanium samples was reflected by a decrease in water contact angles [45° for Ti-p-(VBDSB) and 39° for PE-p-(VBDSB)] compared to the pristine base materials. It is notable that the corresponding cationic p-(VBTAC) and the zwitterionic p-(VBSB) brushes have significantly lower water contact angles of about $15\text{--}20^\circ$. The relatively high contact angles observed for Ti-p-(VBDSB) and PE-p-(VBDSB) suggest the formation of dense polymer brushes with high thickness. It has been previously reported that surface contact angles of zwitterionic brush layers depend strongly on layer thickness.⁵³ Thick brush layers lead to strong charge interactions in the polymer and thus have significantly increased contact angles with water. A similar effect seems to

operate in p-(VBDSB) brush layers, which were formed with a layer thickness of ~ 750 nm (grafting yield = $78.8 \mu\text{g}/\text{cm}^2$) on Ti and ~ 1500 nm (grafting yield = $157.5 \mu\text{g}/\text{cm}^2$) on PE (Table 1). These values are significantly higher than those observed for the corresponding cationic p-(VBTAC) (layer thickness ~ 100 nm, grafting yield = $10.5 \mu\text{g}/\text{cm}^2$) and the zwitterionic p-(VBSB) (layer thickness $\sim 50\text{--}100$ nm, grafting yield = $5.25 \mu\text{g}/\text{cm}^2$) brushes, although all polymer brushes were prepared using the same protocols for SI-ATRP from Ti and free-radical polymerization from PE. This increase in grafting yield and brush layer thickness for VBDSB polymerization is counterintuitive. The accumulation of charges in VBDSB might be expected to lead to an increase in charge repulsion (compared to cationic VBTAC and zwitterionic VBSB monomers) and therefore a decrease in polymerization efficiency. However, the opposite is the case, which finds precedence in reports on radical polymerizations of polycationic acrylate and methacrylate derivatives.⁵⁴ The authors compared the radical polymerization of monomers with either one or two ammonium groups and found a dramatic

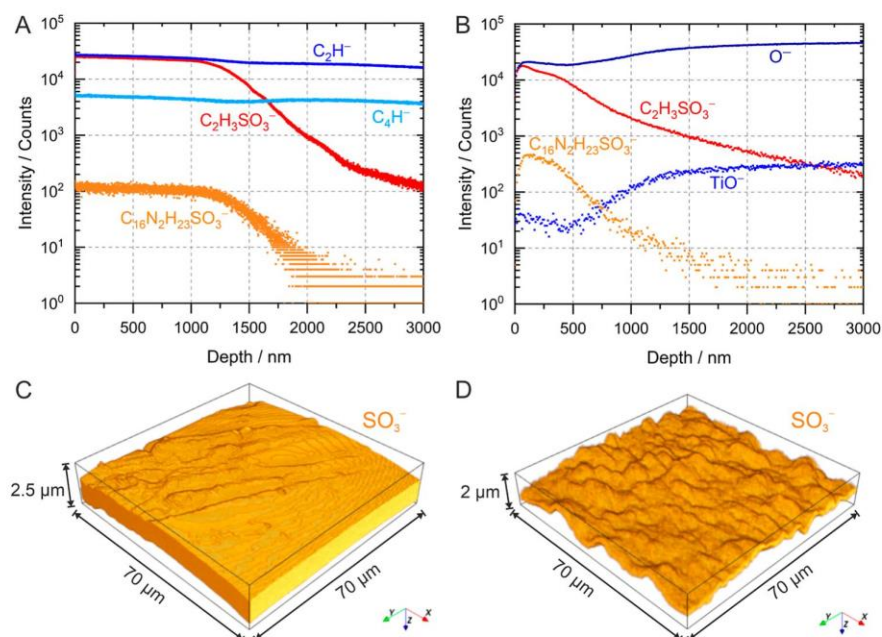


Figure 3. ToF-SIMS depth profiles of (A) PE-p-(VBDSB) and (B) Ti-p-(VBDSB). SIMS analyses were performed with Bi₃²⁺ ions in the negative-ion mode. To determine polymer thickness, an Ar₃₀₀₀⁺ cluster beam was applied for sputter removal between the analysis scans. In (C) PE-p-(VBDSB) and (D) Ti-p-(VBDSB) correlated SPM and mass spectrometric 3D data of the coating layers are shown. Due to good count statistics, the SO₃⁻ signal was selected as representative mass fragment for the polymer brush layer.

autoacceleration for the polymerization of a monomer containing two neighboring ammonium groups, which they attributed to an enhancement of the viscosity as a consequence of reduced ionic strength due to counterion condensation upon monomer to polymer transformation. Similar processes might be operating in VBDSB polymerizations, explaining the extremely thick brush layers formed. A contribution of noncovalently attached polymer to the overall p-(VBDSB) layer cannot be completely excluded, but it is unlikely at this point. The analysis of the stability of the grafted p-(VBDSB) layer by Soxhlet extraction with water for 2 h revealed almost constant water contact angles of PE-p-(VBDSB) before and after extraction and no measurable loss of polymer (see Table S1). It is notable that the nongrafted polymer itself (prepared by polymerization in solution) has a low solubility in water [maximum solubility of p-(VBDSB) ~100 mg/L]. The presence of noncovalently bound but hardly soluble polymer on PE-p-(VBDSB) and Ti-p-(VBDSB) is thus possible. However, it does not leach in measurable quantities into an aqueous solution. In this context, it is notable that noncovalent antibacterial coatings have been successfully explored before.⁵⁵

The solvent-accessible charge density is an important parameter for the contact-biocide activity. The number of solvent-accessible ammonium ions in polycationic brush layers is typically estimated by a fluorescein adsorption assay.⁸ Charge densities of 8.55×10^{15} N⁺/cm² for Ti-p-(VBDSB) and of 53.2×10^{15} N⁺/cm² for PE-p-(VBDSB) were observed. Both values are similar to previously measured charge densities for p-(VBTAC) brush layers and are clearly above the proposed antibacterial threshold of 5×10^{15} N⁺/cm² for contact-biocides.⁴⁹ A similar absorption assay can be used for the quantification of sulfobetaine groups of zwitterionic polymer brushes using the cationic dye crystal violet.⁴⁷ This assay revealed 7.5×10^{15} N⁺/cm² for Ti-p-(VBSB) and $108 \times$

10^{15} N⁺/cm² for PE-p-(VBSB). However, due to the added positive charge in VBDSB resulting presumably in electrostatic repulsion between the cationic dye crystal violet and the p-(VBDSB) brushes, no significant adsorption of dye was detected. The method is thus not suitable for the quantification of zwitterions in p-(VBDSB) brushes.

It is also notable that p-(VBDSB) has an improved thermostability compared to that of the purely cationic homologue p-(VBTAC) as determined by thermogravimetric measurements (Figure S1 in the SI). High thermal stabilities of ammonium groups in zwitterionic polymers have also been found by other authors.^{56,57} TGA of p-(VBDSB) brush layers revealed a thermostability of the material up to ~300 °C. In contrast, p-(VBTAC) dequaternizes at much lower temperatures around 200 °C like other polymeric ammonium salts (Figure S1). This increased thermostability of p-(VBDSB) is an important property from a practical point of view, for example, for steam sterilization (typically performed at 200–250 °C) or alternative high-temperature processing of materials bearing p-(VBDSB) graft polymers.

The successful grafting of p-(VBDSB) on Ti and PE was verified by ATR-FTIR, XPS, and ToF-SIMS measurements. Selected results are depicted in Figures 2 and 3. The ATR-FTIR-spectra of PE-p-(VBDSB) depicted in Figure 2D confirm the identity of the p-(VBDSB) brush. Characteristic bands can be assigned to the –SO₃ stretching vibration at 1038 and at 1176 cm⁻¹ and the stretching vibration of the quaternary ammonium functionality at 2920 cm⁻¹.^{58,59} Aromatic C–H stretching vibrations of the styrene backbone are visible at 3028 cm⁻¹.

Moreover, successful grafting of VBDSB from both base materials was confirmed *via* XPS. Figure 2A,C shows almost identical survey spectra of Ti-p-(VBDSB) and PE-p-(VBDSB). Both reveal an excellent fit of the expected with the XPS-

derived atomic ratios. The observed fit in the N/S atomic ratio on both materials confirms the integrity of the polymer on the surface. The high-resolution spectra for Ti-p-(VBDSB) are shown in Figure 2B and reveal a characteristic N 1s peak at 402.3 eV assigned to the quaternary ammonium groups.^{60,61} An additional N 1s peak at 399.29 eV was assigned to polymer-entrapped residual N₂, which was not removed in vacuo. The S 2p was deconvoluted into two peaks at 168.4 and 167.2 eV which were assigned to the characteristic S 2p_{1/2} and S 2p_{3/2} spin splitting associated with the sulfonates. Missing bromine peaks in the XP spectra (binding energies ~190 eV) after ATRP on Ti-p-(VBDSB) might be due to the detection limit of the system or to the fact that the living chain ends may not be located in the measured area or that only dead chains of the polymerization are presented.⁶² More high-resolution spectra for both materials Ti-p-(VBDSB) and PE-p-(VBDSB) are given in the Supporting Information (Figures S5–S8).

For the 3D characterization of the two coating types, we carried out imaging mass spectrometry in combination with SPM. Figure 3A,B shows depth profiles of the coated samples. The VBDSB layers are in both cases represented by characteristic mass fragments C₁₆N₂H₂₃SO₃⁻ and C₂H₃SO⁻. The thickness of the grafted polymer [Ti-p-(VBDSB)] is about 750 nm. In contrast, the polymer layer on the PE substrate [PE-p-(VBDSB)] is two times thicker (about 1500 nm). The erosion rate, which we calculated from the depth profiling data (see experimental), is about seven times lower, which indicates greater hardness of the PE-p-(VBDSB) sample. In Figure 3C,D, the correlated SPM-SIMS data sets are shown. The data reveal clearly dense polymer brush layers on top of the samples. The surface of PE-p-(VBDSB) is quite flat, whereas Ti-p-(VBDSB) has a rough surface, originating from the underlying rough titanium base material. In both cases, the SO₃⁻ fragment was chosen for visualization due to its high secondary ion count rate, resulting in a good image quality.

The surface charge of PE-p-(VBDSB) and Ti-p-(VBDSB) was evaluated with ζ -potential measurements at different pH values and compared to the results of pristine PE and titanium (Figure 4). Polycationic materials PE-p-(VBTAC) and Ti-p-(VBTAC) and polyzwitterionic materials PE-p-(MASB) and Ti-p-(VBSB) were also included. For both pristine base materials (PE and Ti), a highly negative surface charge is obtained at alkaline and neutral pH values (gray curve, Figure 4A,B) due to the adsorption of hydroxide anions, whereas at acidic pH values of 4 and lower, the surface potentials change to slightly positive values.⁶³ The zeta potential is positive over all measured pH values, as expected, for the polycationic materials PE-p-(VBTAC) and Ti-p-(VBTAC) (pink curves, Figure 4A,B). For comparison, measurements for the zwitterionic materials PE-p-(MASB) and Ti-p-(VBSB) (blue curve, Figure 4A) are also depicted. They show the surface charge for a typical sulfobetaine polymer brush layer, which is known to have a neutral to slightly negative surface potential over the whole pH range tested due to the low pK_a value of the sulfonic acids.²⁷ The mixed cationic/zwitterionic surface modifications p-(VBDSB) (red curves, Figure 4A,B) are similar to the purely cationic surface modifications p-(VBTAC) and also have a positive surface charge over the complete pH-range tested. This confirms the excess positive charge imposed by the diammonium sulfonate monomer units. This result is also in line with the results of the dye adsorption assays mentioned above. No adsorption was detected after treatment of p-(VBDSB) layers with the positively charged dye

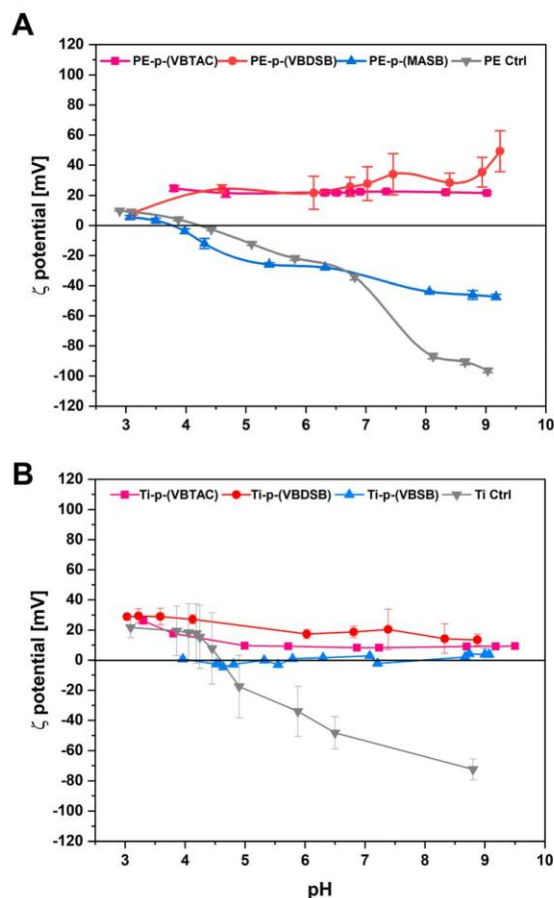


Figure 4. (A) Zeta-potential measurements of PE-brush polymers [PE-p-(VBDSB) in red, PE-p-(VBTAC) in pink, and PE-p-(MASB) in blue] compared to pristine PE (in gray). (B) Zeta-potential measurements of Ti-brush polymers [Ti-p-(VBDSB) in red, Ti-p-(VBTAC) in pink, and Ti-p-(VBSB) in blue] compared to nonmodified titanium (in gray). Results are presented as mean values ($n = 4$) \pm SD.

crystal violet most likely due to electrostatic repulsion on the positively charged surfaces.

Several microbiological methods are available for the evaluation of the antimicrobial activity of contact-killing materials.⁶⁴ However, it is hard to prove the antimicrobial mechanism of these materials.⁶⁵ The antimicrobial activity of PE-p-(VBDSB) was evaluated using a standard assay for antimicrobial materials (ASTM E1249 E13a) and compared to the activity of PE-p-(VBTAC), a known polycationic material with good contact-activity.⁴⁸ Briefly, all test specimen coupons were challenged with the appropriate bacteria (10^5 cfu/mL) for 2 h under gentle shaking (120 rpm) at 37 °C in sterile saline solution. These conditions correspond to a challenge of 0.9×10^5 cfu per cm² titanium coupon and 2.0×10^5 cfu per cm² for PE coupons. An equivalent of the solution and two dilutions (100 μ L of the incubation solution, 1:10 dilution, and 1:100 dilution) were transferred to Columbia agar and incubated for 18 h at 37 °C, and colonies were counted. Both materials and pristine PE were exposed to Gram-negative *E. coli* ATCC 25922 and Gram-positive *S. aureus* ATCC29213. Selected results of this assay are depicted as log₁₀ reductions in

Figure 5 (see Table S2 for further results). The antibacterial activity of PE-p-(VBDSB) with a \log_{10} reduction of 3.5 ± 0.1

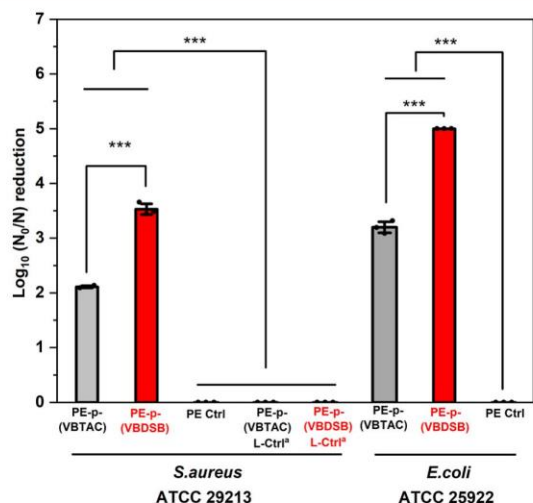


Figure 5. Results of the modified ASTM E2149 13a assay for determination of the antibacterial activity of the PE-modified sample PE-p-(VBDSB) and PE-p-(VBTAC) against Gram-positive *S. aureus* ATCC 29213 and Gram-negative *E. coli* ATCC 25922. \log_{10} reductions in bacterial growth were calculated, as described in the Experimental Section. Results are presented as mean value ($n \geq 3$) \pm SD. Statistical significance was determined via pairwise comparison using the Tukey-Test $p \leq 0.001$ (***). ^(a)Antimicrobial activity of leaching solutions (L-Ctrl) was determined after removal of the test specimen [PE-p-(VBDSB)] from the solution, as described in the Experimental Section.

for *S. aureus* and 5.0 ± 0.0 for *E. coli* is significantly higher than that of PE-p-(VBTAC) (2.1 ± 0.1 for *S. aureus* and 3.2 ± 0.2 for *E. coli*), confirming the antibacterial effect of the overall positively charged p-VBDSB layer. A reason for the higher activity of the mixed cationic/zwitterionic p-(VBDSB) compared to the purely cationic p-(VBTAC) might be the slightly higher surface potential of the p-VBDSB layer, leading to a stronger attraction of the bacterial outer membranes. Considering the surface potential of *E. coli* (-40 to -60 mV)⁶⁶ and *S. aureus* (-2 to -5 mV),⁶⁷ the more positive surface potential for p-(VBDSB) layers [$+35$ mV (PE) and $+18$ mV (Ti)] compared to p-(VBTAC) layers [$+22$ mV (PE) and $+8$ mV (Ti)] might also explain the higher activity against *E. coli*. Another factor to consider is the number of solvent-accessible cationic charges, which is extremely high for PE-p-(VBDSB) compared to all other materials tested. As mentioned above, it is hard to prove a contact-active mechanism experimentally. The observed activities may also be explained with a release of antibacterial and noncovalently attached polymers into solution.⁶⁸ However, additional experimental evidence supports the contact-activity of the investigated materials: (1) leaching of polymer into solution upon a 2 h Soxhlet extraction was not observed (Table S1). (2) An Agar plate diffusion test revealed no zone of inhibition for the materials tested (see Figure S9). (3) The leaching solution of PE-p-(VBDSB) showed no antimicrobial activity after removal of the test specimens (Figure 5, L-Ctrl). (4) The nongrafted polymer p-(VBDSB) had no antimicrobial activity up to the solubility limit of p-(VBDSB) in water when tested against *S. aureus*

ATCC 29213 and *E. coli* ATCC 25922 (both $\text{MIC}_{90} > 78.75$ $\mu\text{g/mL}$).

The antibacterial activity is supported by LIVE/DEAD staining and confocal fluorescence imaging (Figure 6). The mixed cationic/zwitterionic PE-p-(VBDSB), cationic PE-p-(VBTAC), zwitterionic PE-p-(MASB), and pristine PE were incubated with *P. aeruginosa* (1.5×10^8 cfu/mL), a Gram-negative pathogen with high clinical relevance and excellent ability to form biofilms.^{69,70} LIVE/DEAD staining and confocal fluorescence imaging after 24 h of incubation revealed a high number of living cells (green) on the surface of pristine PE, reflecting normal biofilm formation by *P. aeruginosa*. In contrast, mostly dead cells (red) were observed on cationic PE-p-(VBTAC), confirming its contact-activity. A low number of live cells was observed on zwitterionic PE-p-(MASB). The latter confirms the low-fouling ability of p-(MASB) and shows therefore significantly less bacterial cell adhesion compared to pristine PE. The mixed cationic/zwitterionic p-(VBDSB) leads also to slightly reduced adhesion of bacteria and a non-homogeneous accumulation of dead cells confirming the combined dual activity. It should be noted that a laminar background autofluorescence is visible in Figure 6A. It is most likely associated with the nonspecific adsorption of SYTO 9 in combination with the high layer thickness of the p-(VBDSB) polymer coating compared to p-(VBTAC) and p-(MASB). Such (SYTO 9 induced) autofluorescence has been detected in previous studies too.^{47,71,72}

An additional bacterial adhesion test was performed to further evaluate the antifouling properties of p-(VBDSB) brush layers following an established protocol.⁴⁷ Briefly, test specimens were incubated with bacteria (10^5 cfu/mL) in MHB to allow exponential bacterial growth and stored under gentle shaking for 24 h. After incubation, the test specimens were dipped into sterile saline solution to desorb loosely attached planktonic cells. Subsequently, the test specimens were placed on an agar plate (Columbia Agar) for 30 s, and the plates were then incubated for 20 h, followed by cell counting. Selected results for titanium are presented in Figure 7. The low number of adhering bacteria on Ti-p-(VBDSB) confirms a significant antifouling effect of the mixed cationic/zwitterionic material for Gram-positive and Gram-negative bacteria. Similar antifouling properties were found for PE-p-(VBDSB) (Table S3). These findings support the results of LIVE/DEAD staining with subsequent confocal microscopy (Figure 6).

CONCLUSIONS

A new styrene-based monomer VBDSB has been synthesized in two steps via sequential alkylation of cyclic diamine DABCO. VBDSB contains a sulfobetaine and an additional quaternary ammonium group. It is thus to the best of our knowledge the first example for a monomer combining a cationic and a zwitterionic moiety. The graft polymerization of VBDSB from PE base material was performed via plasma activation and subsequent heat-induced free-radical polymerization, whereas on titanium base material, an SI-ATRP protocol was used with a bromoisobutyryl containing phosphonic acid as an initiator. The obtained grafting yields were significantly higher than those obtained with similar monomers bearing only a cationic ammonium group (VBTAC) or a zwitterionic sulfobetaine (VBSB). We attribute the improved polymerization properties of VBDSB to autoacceleration of the polymerization caused by the high charge density. This phenomenon has been described for

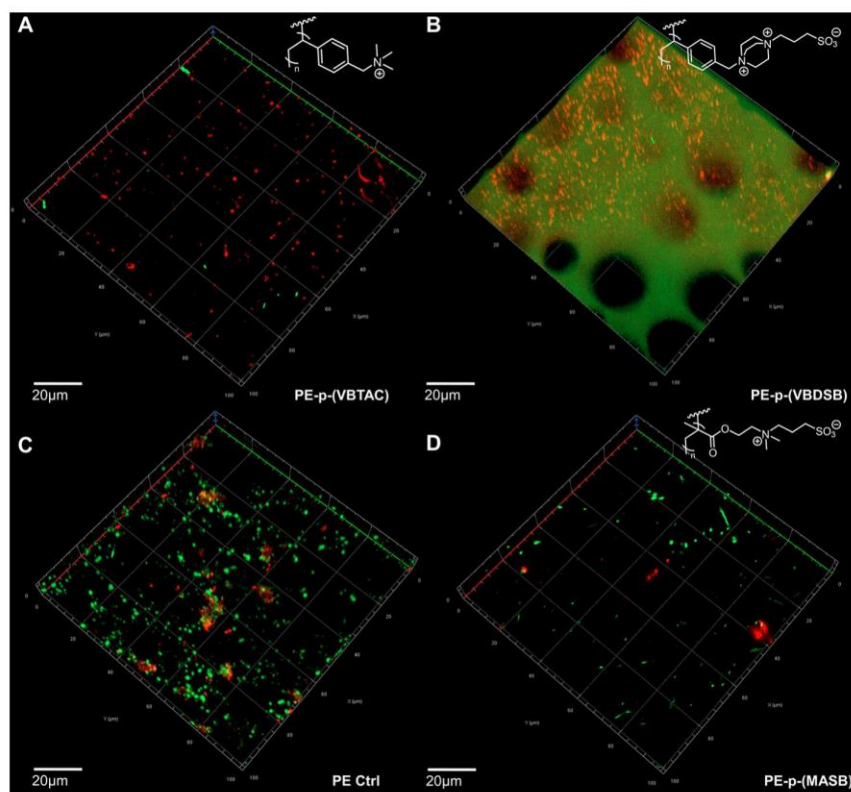


Figure 6. Confocal fluorescence images after LIVE/DEAD staining. (C) CSF image: Images were taken 24 h after the incubation of test specimens with *P. aeruginosa* PA01 in LB media. Live cells appear green, dead cells appear red. (A) Image of bacteria on contact-biocide PE-p-(VBTAC). (B) Image of bacteria on PE-p-(VBDSB). Note the background autofluorescence of the polymer brush. (C) Image of bacteria on a PE control (PE Ctrl). (D) Image of bacteria on zwitterionic PE-p-(MASB).

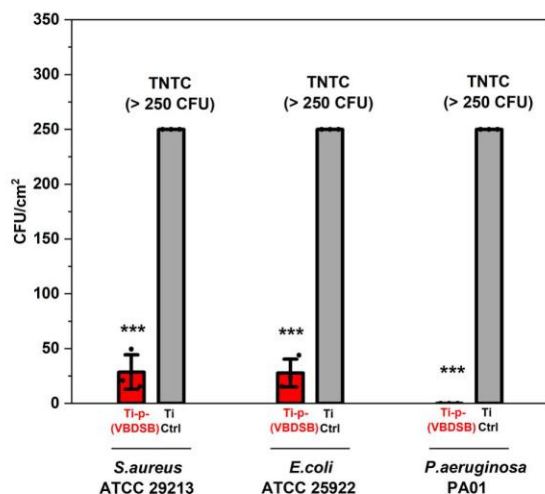


Figure 7. Results of the bacterial adhesion assay of Ti-p-(VBDSB) against Gram-positive *S. aureus* ATCC 29213 and Gram-negative *E. coli* ATCC 25922 and *P. aeruginosa* PA01. Results are presented as mean value ($n \geq 3$) \pm SD. Cell counts above 250 were denoted as TNTC. Statistical significance was determined via pairwise comparison using the Tukey-Test $p \leq 0.001$ (***).

dicationic monomers before.⁵⁴ However, a contribution of noncovalently attached polymer to the overall p-(VBDSB)

layer cannot be completely excluded at this point. Graft polymerizations gave p-(VBDSB) brush layers with a thickness of 750 nm on Ti and 1500 nm on PE. The resulting surfaces have relatively high-water contact angles of $\sim 40^\circ$, reflecting strong charge interactions in the thick brush layers and a positive zeta potential over a broad pH range caused by the net positive charge of VBDSB. The p-VBDSB brush layers are furthermore characterized by a good thermostability up to 300 °C, as measured by TGA. Thermostability is an important material property from a practical point of view, for example, for steam sterilization. Other contact-active brush layers are limited by dequaternizations typically occurring at temperatures around 200 °C, which is not compatible with high-temperature sterilization protocols.

Charge densities of $8.55 \times 10^{15} \text{ N}^+/\text{cm}^2$ for Ti-p-(VBDSB) and of $53.2 \times 10^{15} \text{ N}^+/\text{cm}^2$ for PE-p-(VBDSB) were observed. Both values are similar to previously measured charge densities for p-(VBTAC) brush layers and are clearly above the proposed antibacterial threshold of $5 \times 10^{15} \text{ N}^+/\text{cm}^2$ for contact-biocides.⁴⁹ In consequence, good antibacterial properties against Gram-negative and Gram-positive bacteria were observed for p-(VBDSB) brush layers on Ti and PE. The reductions in bacterial growth observed for the mixed cationic/zwitterionic p-(VBDSB) brushes were superior or similar to those obtained for purely cationic p-(VBTAC) brushes for most pathogens tested. In addition, a strong antifouling effect was observed for the mixed cationic/zwitterionic p-(VBDSB) brushes, comparable to that of purely zwitterionic p-(VBSB)

brushes. Our microbiological results clearly confirm the initially proposed dual functionality of p-(VBDSB) polymer brushes with both contact-activity and antifouling properties.

■ ASSOCIATED CONTENT

Supporting Information

The Supporting Information is available free of charge at <https://pubs.acs.org/doi/10.1021/acs.langmuir.3c02657>.

TGA measurements of modified TiO₂ nanoparticles and PE samples; ATR-FTIR measurements of TiO₂-p-(VBDSB); fluorescein and crystal violet assay for charge density determination; stability test (Soxhlet extraction); XPS analysis of pristine Ti and PE and deconvoluted regions of Ti/PE-p-(VBDSB); results of the ASTM assay E2149-13a; results of the bacterial adhesion assay; and NMR spectra of VBD and VBDSB (PDF)

■ AUTHOR INFORMATION

Corresponding Author

Wolfgang Maison – Department of Chemistry, Universität Hamburg, 20146 Hamburg, Germany; orcid.org/0000-0003-2793-5722; Email: wolfgang.maison@uni-hamburg.de

Authors

Nils Burmeister – Department of Chemistry, Universität Hamburg, 20146 Hamburg, Germany

Eilika Zorn – Department of Chemistry, Universität Hamburg, 20146 Hamburg, Germany

Lena Preuss – Department of Microbiology and Biotechnology, Universität Hamburg, 22609 Hamburg, Germany

Donovan Timm – Department of Chemistry, Universität Hamburg, 20146 Hamburg, Germany

Nico Scharnagl – Helmholtz-Zentrum Hereon GmbH, Institute of Surface Science, 21502 Geesthacht, Germany; orcid.org/0000-0002-5511-625X

Marcus Rohnke – Justus-Liebig-Universität Gießen, Institute of Physical Chemistry, 35392 Giessen, Germany; orcid.org/0000-0002-8867-950X

Sebastian G. Wicha – Department of Chemistry, Universität Hamburg, 20146 Hamburg, Germany

Wolfgang R. Streit – Department of Microbiology and Biotechnology, Universität Hamburg, 22609 Hamburg, Germany

Complete contact information is available at: <https://pubs.acs.org/doi/10.1021/acs.langmuir.3c02657>

Author Contributions

N.B. and E.Z. contributed equally to this paper. The manuscript was written through contributions of all authors. All authors have given approval to the final version of the manuscript. N.B., E.Z., and W.M. were responsible for conceptualization. N.B., E.Z., N.S., and M.R. were responsible for methodology. N. B., E.Z., L.P., D.T., N.S., and M.R. were responsible for investigation. S.G.W., W.R.S., and W.M. were responsible for supervision. N.B., E.Z., and W.M. were responsible for writing the original draft. N.B., E.Z., L.P., N.S., M.R., S.G.W., W.R.S., and W.M. were responsible for writing, review, and editing.

Funding

M.R. thanks the BMBF for funding the SIMS-SPM machine under grant no. 03XP0427.

Notes

The authors declare no competing financial interest.

■ ACKNOWLEDGMENTS

Proof reading of the manuscript by Antje Wagner is acknowledged. Prof. Dr. Mathias Ernst (Hamburg University of Technology, TUHH) provided access to instruments for surface zeta potential measurements.

■ REFERENCES

- Hall-Stoodley, L.; Costerton, J. W.; Stoodley, P. Bacterial biofilms: from the natural environment to infectious diseases. *Nat. Rev. Microbiol.* **2004**, *2* (2), 95–108.
- Wang, Y. X.; Robertson, J. L.; Spillman Jr, W. B.; Claus, R. O. Effects of the chemical structure and the surface properties of polymeric biomaterials on their biocompatibility. *Pharm. Res.* **2004**, *21* (8), 1362–1373.
- Flemming, H. C.; Wingender, J.; Szewzyk, U.; Steinberg, P.; Rice, S. A.; Kjelleberg, S. Biofilms: an emergent form of bacterial life. *Nat. Rev. Microbiol.* **2016**, *14* (9), 563–575.
- Galie, S.; Garcia-Gutierrez, C.; Miguelez, E. M.; Villar, C. J.; Lombo, F. Biofilms in the Food Industry: Health Aspects and Control Methods. *Front. Microbiol.* **2018**, *9*, 898.
- Percival, S. L.; Suleman, L.; Vuotto, C.; Donelli, G. Healthcare-associated infections, medical devices and biofilms: risk, tolerance and control. *J. Med. Microbiol.* **2015**, *64* (4), 323–334.
- Zhou, W.; Li, W.; Chen, J.; Zhou, Y.; Wei, Z.; Gong, L. Microbial diversity in full-scale water supply systems through sequencing technology: a review. *RSC Adv.* **2021**, *11* (41), 25484–25496.
- Li, W.; Thian, E. S.; Wang, M.; Wang, Z.; Ren, L. Surface Design for Antibacterial Materials: From Fundamentals to Advanced Strategies. *Adv. Sci.* **2021**, *8* (19), No. e2100368.
- Tiller, J. C.; Liao, C. J.; Lewis, K.; Klibanov, A. M. Designing surfaces that kill bacteria on contact. *Proc. Natl. Acad. Sci. U.S.A.* **2001**, *98* (11), 5981–5985.
- Kaur, R.; Liu, S. Antibacterial surface design - Contact kill. *Prog. Surf. Sci.* **2016**, *91* (3), 136–153.
- Alfei, S.; Schito, A. M. Positively Charged Polymers as Promising Devices against Multidrug Resistant Gram-Negative Bacteria: A Review. *Polymers* **2020**, *12* (5), 1195.
- Cheng, G.; Xue, H.; Zhang, Z.; Chen, S.; Jiang, S. A switchable biocompatible polymer surface with self-sterilizing and nonfouling capabilities. *Angew. Chem., Int. Ed. Engl.* **2008**, *47* (46), 8831–8834.
- Asri, L. A. T. W.; Crismaru, M.; Roest, S.; Chen, Y.; Ivashenko, O.; Rudolf, P.; Tiller, J. C.; van der Mei, H. C.; Loontjens, T. J. A.; Busscher, H. J. A Shape-Adaptive, Antibacterial-Coating of Immobilized Quaternary-Ammonium Compounds Tethered on Hyperbranched Polyurea and its Mechanism of Action. *Adv. Funct. Mater.* **2014**, *24* (3), 346–355.
- Chapman, R. G.; Ostuni, E.; Takayama, S.; Holmlin, R. E.; Yan, L.; Whitesides, G. M. Surveying for surfaces that resist the adsorption of proteins. *J. Am. Chem. Soc.* **2000**, *122* (34), 8303–8304.
- Banerjee, I.; Pangule, R. C.; Kane, R. S. Antifouling coatings: recent developments in the design of surfaces that prevent fouling by proteins, bacteria, and marine organisms. *Adv. Mater.* **2011**, *23* (6), 690–718.
- Khalil, F.; Franzmann, E.; Ramcke, J.; Dakischew, O.; Lips, K. S.; Reinhardt, A.; Heisig, P.; Maison, W. Biomimetic PEG-catecholates for stable antifouling coatings on metal surfaces: applications on TiO₂ and stainless steel. *Colloids Surf., B* **2014**, *117*, 185–192.
- Paschke, S.; Lienkamp, K. Polyzwitterions: From Surface Properties and Bioactivity Profiles to Biomedical Applications. *ACS Appl. Polym. Mater.* **2020**, *2* (2), 129–151.
- Li, M.; Zhuang, B.; Yu, J. Functional Zwitterionic Polymers on Surface: Structures and Applications. *Chem.—Asian J.* **2020**, *15* (14), 2060–2075.

- (52) Herman, J. L.; Wang, Y.; Lilly, E. A.; Lallier, T. E.; Peters, B. M.; Hamdan, S.; Xu, X.; Fidel, P. L.; Noverr, M. C. Synthesis, Antifungal Activity, and Biocompatibility of Novel 1,4-Diazabicyclo[2.2.2]Octane (DABCO) Compounds and DABCO-Containing Denture Base Resins. *Antimicrob. Agents Chemother.* **2017**, *61* (4), 10.
- (53) Cheng, N.; Brown, A. A.; Azzaroni, O.; Huck, W. T. S. Thickness-Dependent Properties of Polyzwitterionic Brushes. *Macromolecules* **2008**, *41* (17), 6317–6321.
- (54) Ahmadloo, H.; Losada, R.; Wandrey, C. Effect of Very High Charge Density and Monomer Constitution on the Synthesis and Properties of Cationic Polyelectrolytes. *Polymers* **2016**, *8* (6), 234.
- (55) Bieser, A. M.; Thomann, Y.; Tiller, J. C. Contact-Active Antimicrobial and Potentially Self-Polishing Coatings Based on Cellulose. *Macromol. Biosci.* **2011**, *11* (1), 111–121.
- (56) Favresse, P.; Laschewsky, A. Synthesis and investigation of new amphiphilic poly(carbobetaine)s made from diallylammonium monomers. *Polymer* **2001**, *42* (7), 2755–2766.
- (57) Wu, T.; Beyer, F. L.; Brown, R. H.; Moore, R. B.; Long, T. E. Influence of Zwitterions on Thermomechanical Properties and Morphology of Acrylic Copolymers: Implications for Electroactive Applications. *Macromolecules* **2011**, *44* (20), 8056–8063.
- (58) Chang, Y.; Chang, W.-J.; Shih, Y.-J.; Wei, T.-C.; Hsiue, G.-H. Zwitterionic Sulfobetaine-Grafted Poly(vinylidene fluoride) Membrane with Highly Effective Blood Compatibility via Atmospheric Plasma-Induced Surface Copolymerization. *ACS Appl. Mater. Interfaces* **2011**, *3* (4), 1228–1237.
- (59) Quintana, R.; Jańczewski, D.; Vasantha, V. A.; Jana, S.; Lee, S. C.; Parra-Velandia, F. J.; Guo, S.; Parthiban, A.; Teo, S. L.-M.; Vancso, G. J. Sulfobetaine-based polymer brushes in marine environment: Is there an effect of the polymerizable group on the antifouling performance? *Colloids Surf., B* **2014**, *120*, 118–124.
- (60) Demirci, S.; Caykara, T. High density cationic polymer brushes from combined “click chemistry” and RAFT-mediated polymerization. *J. Polym. Sci., Part A: Polym. Chem.* **2012**, *50* (15), 2999–3007.
- (61) Shan, B.; Yan, H.; Shen, J.; Lin, S. Ozone-induced grafting of a sulfoammonium zwitterionic polymer onto low-density polyethylene film for improving hemocompatibility. *J. Appl. Polym. Sci.* **2006**, *101* (6), 3697–3703.
- (62) Liu, P.-S.; Chen, Q.; Wu, S.-S.; Shen, J.; Lin, S.-C. Surface modification of cellulose membranes with zwitterionic polymers for resistance to protein adsorption and platelet adhesion. *J. Membr. Sci.* **2010**, *350* (1–2), 387–394.
- (63) Zangi, R.; Engberts, J. B. F. N. Physisorption of Hydroxide Ions from Aqueous Solution to a Hydrophobic Surface. *J. Am. Chem. Soc.* **2005**, *127* (7), 2272–2276.
- (64) van de Lagemaat, M.; Grotenhuis, A.; van de Belt-Gritter, B.; Roest, S.; Loontjens, T. J. A.; Busscher, H. J.; van der Mei, H. C.; Ren, Y. Comparison of methods to evaluate bacterial contact-killing materials. *Acta Biomater.* **2017**, *59*, 139–147.
- (65) Fik, C. P.; Konieczny, S.; Pashley, D. H.; Waschinski, C. J.; Ladisch, R. S.; Salz, U.; Bock, T.; Tiller, J. C. Telechelic Poly(2-oxazoline)s with a Biocidal and a Polymerizable Terminal as Collagenase Inhibiting Additive for Long-Term Active Antimicrobial Dental Materials. *Macromol. Biosci.* **2014**, *14* (11), 1569–1579.
- (66) Schwegmann, H.; Feitz, A. J.; Frimmel, F. H. Influence of the zeta potential on the sorption and toxicity of iron oxide nanoparticles on *S. cerevisiae* and *E. coli*. *J. Colloid Interface Sci.* **2010**, *347* (1), 43–48.
- (67) Bruinsma, G. M.; van der Mei, H. C.; Busscher, H. J. Bacterial adhesion to surface hydrophilic and hydrophobic contact lenses. *Biomaterials* **2001**, *22* (24), 3217–3224.
- (68) Ho, C. H.; Odermatt, E. K.; Berndt, I.; Tiller, J. C. Long-term active antimicrobial coatings for surgical sutures based on silver nanoparticles and hyperbranched polylysine. *J. Biomater. Sci. Polym. Ed.* **2013**, *24* (13), 1589–1600.
- (69) Stover, C. K.; Pham, X. Q.; Erwin, A. L.; Mizoguchi, S. D.; Warrenner, P.; Hickey, M. J.; Brinkman, F. S. L.; Hufnagle, W. O.; Kowalik, D. J.; Lagrou, M.; et al. Complete genome sequence of *Pseudomonas aeruginosa* PAO1, an opportunistic pathogen. *Nature* **2000**, *406* (6799), 959–964.
- (70) Miryala, S. K.; Anbarasu, A.; Ramaiah, S. Systems biology studies in *Pseudomonas aeruginosa* PAO1 to understand their role in biofilm formation and multidrug efflux pumps. *Microb. Pathog.* **2019**, *136*, 103668.
- (71) Vasantha, V. A.; Zainul Rahim, S. Z.; Jayaraman, S.; Junyuan, G. H.; Puniredd, S. R.; Ramakrishna, S.; Teo, S. L. M.; Parthiban, A. Antibacterial, electrospun nanofibers of novel poly (sulfobetaine) and poly (sulfobetaine) s. *J. Mater. Chem. B* **2016**, *4* (15), 2731–2738.
- (72) Xu, Y.; Liu, Q.; Li, X.; Wesdemiotis, C.; Pang, Y. A zwitterionic squaraine dye with a large Stokes shift for in vivo and site-selective protein sensing. *Chem. Commun.* **2012**, *48* (92), 11313–11315.

5.3 Polymeric *N*-oxides for the Modulation of Biofilms

Combining different antifouling activity principles is often advantageous to avoid biofilm formation. As presented in the previous section, a combination of contact-biocide and low-fouling activities has been realized by developing a new monomer suitable for graft polymerization on various bulk materials. This approach also established a new class of antifouling substances, the polymeric diammonium-sulfonates, which enable the local killing of bacteria to reduce infection risks with a concurrent non-adhesive (low-fouling) nature. Yet, the degradation of surrounding bacteria by surface modification is even more desirable to suppress the spread of bacteria in a clinical context but also in industrial settings.

In this section, polymeric *N*-oxide brushes on PE are investigated for their potential as antifouling compounds. Surface modifications with *N*-oxides for antifouling purposes were first described by MARSH et al. The *N*-oxide functionality is a unique form of a zwitterion due to its semi-polar N^+-O^- bond.¹⁰¹ It gained attention as an antifouling and stealth agent due to the shortest possible charge separation by only one sigma bond. A consensus in zwitterionic research for antifouling purposes is that the negative correlation between charge separation and hydration ability makes *N*-oxides an almost perfect low-fouling effector.¹⁰² Besides the antifouling behavior, other *N*-oxides are versatile compounds for synthetic purposes (*i.e.*, NMO-mediated oxidation) or as part of synthetic routes (*e.g.*, MEISENHEIMER rearrangement¹²⁶, POLONOVSKI reaction¹²⁷, COPE elimination¹²⁸, *etc.*). More importantly, some structures bearing *N*-oxides exhibit antimicrobial and antitumor activity in the right chemical environment, making the N^+-O^- functionality an attractive pharmacophore in drug design and drug conjugation. Most recently, polymeric *N*-oxides were reported to show remarkable electrochemical properties along with redox activity, which strongly differs from their monomeric counterpart. This might indicate further reactivity beyond their stealth appearance when applied *in vivo* or *in vitro*. A protocol was established for grafting styrene-based, methacrylate-based, and methacrylamide-based polymeric *N*-oxides from a PE substrate. The resulting polymer brushes were fully characterized regarding their chemical and physical integrity. The modified substrates exhibited excellent low-fouling activity against clinically and industrially relevant Gram-positive and Gram-negative species. In addition, an unexpected antibacterial activity was detected during the microbiological investigations. The latter was identified as a unique property of polymeric *N*-oxides. The underlying mechanism of action is most likely based on radical generation, which was elaborated by DPPH radical scavenging. Further EPR spectroscopy revealed reactive oxygen species ($\bullet OH$ or $\bullet O^{2-}$) to be involved in this antimicrobial action. Repetitive use of the polymeric *N*-oxide substrates indicates that polymeric *N*-oxides might contribute catalytically to the generation of ROS since no degradation or byproducts were experimentally observed. This bifunctional activity, which degrades microorganisms not

only by contact but in the surrounding environment, permits a superior combined approach compared to the described modification in section 5.2. An additional advantage of polymeric *N*-oxides is their easy synthesis *via* amine oxidation. *N*-oxides combine several desirable properties for antifouling materials and might have game-changing potential for managing bacteria in clinical and industrial settings. However, they also have intrinsic reactivity, which might compromise *in vivo* applications.

Title: Surface Grafted *N*-Oxides have Low-Fouling and Antibacterial Properties

Authors: Burmeister, N., Zorn, E., Farooq, A., Preuss, L., Vollstedt C., Friedrich, T. Mantel, T., Scharnagl, N., Rohnke, M., Ernst, M. Wicha, S.G., Streit, W.R., Maison, W.

Type: Research Article, Journal Article

Journal: Advanced Materials Interfaces

Year: 2023

Volume: 10

DOI: <https://doi.org/10.1002/admi.202300505>

Number of Pages: 13

Submitted: 15.06.2023

Accepted: 30.08.2023

Conceptualizing: Burmeister N., Streit, W.R., Wicha, S.G, Maison, W.

Investigation: Burmeister, N., Zorn, E., Farooq, A., Preuss, L., Friedrich, T., Scharnagl, N., Rohnke M.

Original Writing: Burmeister, N., Maison, W.

Review and Editing: Zorn, E., Farooq, A., Preuss, L., Vollstedt C., Friedrich, T. Mantel, T., Scharnagl, N., Rohnke, M., Ernst, M. Wicha, S.G., Streit, W.R.

RESEARCH ARTICLE

Surface Grafted N-Oxides have Low-Fouling and Antibacterial Properties

Nils Burmeister, Eilika Zorn, Aneeq Farooq, Lena Preuss, Christel Vollstedt, Timo Friedrich, Tomi Mantel, Nico Scharnagl, Marcus Rohnke, Mathias Ernst, Sebastian G. Wicha, Wolfgang R. Streit, and Wolfgang Maison*

Low-fouling materials are often generated by surface zwitterionization with polymers. In this context, poly-N-oxides have recently attracted considerable attention as biomimetic stealth coatings with low protein adsorption. Herein, this study reports that poly-N-oxides can be grafted from plasma-activated plastic base materials. The resulting hydrophilic surfaces have low-fouling properties in bacterial suspensions and suppress the formation of biofilms. Moreover, efficient antibacterial activity against Gram-negative and Gram-positive bacteria caused by release of reactive oxygen species is observed. The latter effect is specific for polymeric N-oxides and is most likely triggered by a reductive activation of the N-oxide functionality in the presence of bacteria. In contrast to other zwitterionic polymers, N-oxides combine thus low-fouling (stealth) properties with antibacterial activity. The bioactive N-oxide groups can be regenerated after use by common oxidative disinfectants. Poly-N-oxides are thus attractive antibacterial coatings for many base materials with a unique combined mechanism of action.

causing unwanted spread and/or infections in hospitals, implants, food packaging, the distribution of drinking water and other areas.^[4] Low-fouling (also antifouling or stealth) surfaces are designed to prevent the attachment of biomolecules and microorganisms.^[5] Low-fouling surface properties come typically with good biocompatibility of materials. This allows in vivo applications without platelet activation or the initiation of the foreign body recognition system.^[6] Biocompatibility is thus often linked to low-fouling, although the two concepts are not synonymous. However, there is a strong overlap in the technology used to implement them. Surface zwitterionization, often achieved by grafting polymeric zwitterions, is a particularly successful method in this context.^[7]

The resulting polymer layers are strongly hydrated and they install a protective water layer at the material/solution interface.^[8] Zwitterions fit therefore the requirements defined by Whitesides for low-fouling applications.^[9]

Three major classes of zwitterions have been used frequently for low-fouling applications: phosphobetaines $-\text{OPO}_3^-(\text{CH}_2)_n\text{N}^+\text{Me}_3$,^[10] carboxybetaines $-\text{N}^+(\text{CH}_2)_n\text{CO}_2^-$,^[11] and sulfobetaines $-\text{N}^+(\text{CH}_2)_n\text{SO}_3^-$.^[12] It has been demonstrated that the hydration properties of these polymers depend on the alkyl spacer $-(\text{CH}_2)_n-$ between the anionic (acidic) and the

1. Introduction

Almost all materials are rapidly covered by biomolecules and microorganisms when exposed to biological media. This so-called biofilm formation is of fundamental importance in nature and has implications for many industrial processes and the health sector.^[1] For in vivo applications, the adhesion of biomolecules to surfaces contributes to immunogenicity and low blood compatibility.^[2] Microbial biofilms enhance the development of resistance and increased pathogenicity of microbes.^[3]

N. Burmeister, E. Zorn, A. Farooq, T. Friedrich, S. G. Wicha, W. Maison
 Department of Chemistry
 Universität Hamburg
 Bundesstrasse 45, 20146 Hamburg, Germany
 E-mail: wolfgang.maison@uni-hamburg.de

L. Preuss, C. Vollstedt, W. R. Streit
 Department of Microbiology and Biotechnology
 Universität Hamburg
 Ohnhorststrasse 18, 22609 Hamburg, Germany
 T. Mantel, M. Ernst
 Institute of Water Resources and Water Supply
 Technische Universität Hamburg
 Denickestraße 17, 21073 Hamburg, Germany
 N. Scharnagl
 Institute of Surface Science
 Helmholtz-Zentrum Hereon GmbH
 Max-Planck-Strasse 1, 21502 Geesthacht, Germany
 M. Rohnke
 Institute of Physical Chemistry and Center for Materials Research
 Justus-Liebig-University Giessen
 Heinrich-Buff-Ring 17, 35392 Giessen, Germany

 The ORCID identification number(s) for the author(s) of this article can be found under <https://doi.org/10.1002/admi.202300505>

© 2023 The Authors. Advanced Materials Interfaces published by Wiley-VCH GmbH. This is an open access article under the terms of the Creative Commons Attribution License, which permits use, distribution and reproduction in any medium, provided the original work is properly cited.

DOI: 10.1002/admi.202300505

cationic ammonium group (other cations besides ammonium groups have also been used but are less common). A short alkyl spacer was found to be advantageous for optimal low-fouling properties in most studies.^[13] Recently, Jiang et al. introduced consequently polymeric *N*-oxides $-N^+-O^-$ as low-fouling and biocompatible polymers.^[14] With only one sigma bond, *N*-oxides contain the smallest possible spacer to separate the charges in a zwitterion. In addition, *N*-oxides have several desirable properties for low-fouling applications. They are easy to prepare by oxidation of tertiary amines^[15] and they have a dative N^+-O^- bond with extremely high charge separation compared to homologue P^+-O^- or S^+-O^- bonds. Consequently, *N*-oxides have high dipole moments of 4–5 D^[16] and form strong hydrogen bonds with water.^[17] This makes *N*-oxides powerful kosmotropes,^[18] a property used technically, for example as kinetic hydrate inhibitors to avoid the formation of gas clathrates in gas or oil production.^[19] The same properties are also used in nature for example with trimethylammoniumoxide (TMAO), a natural *N*-oxide found in seawater fish (and also in humans).^[20,21] TMAO stabilizes proteins by counteracting protein-denaturing compounds (eg. chaotropes like urea) or denaturing forces like heat and pressure. It is also notable that *N*-oxides of alkaloids are non-toxic derivatives of their toxic membrane-permeable parent amines used for vesicle storage in plants and insects.^[22] With the transfer of these properties to a polymeric *N*-oxide (PTMAO), Jiang et al. demonstrated that zwitterionization of surfaces with PTMAO leads to extremely low levels of blood protein adsorption and reduced fibroblast adhesion. It was also shown that protein conjugates of PTMAO were invisible to immune recognition in mice. These interesting findings trigger the question: Are polymeric *N*-oxides also efficient low-fouling reagents to prevent the formation of microbial biofilms on surfaces? Several other questions come to mind, when considering the fundamental differences of *N*-oxides compared to other zwitterions. In addition to the (favorable) properties mentioned above, *N*-oxides contain a weak $N-O$ bond and are chemically reactive compounds.^[23] This is reflected by their common use as oxidants and intermediates in organic synthesis^[24] as well as biosynthesis.^[25] Several *N*-oxides of low molecular weight are biologically active and have been explored as drugs.^[22c,26] Reductive metabolism by microorganisms or in hypoxic tissue triggers their biological activity as antibiotics or cytotoxic compounds for chemotherapy.^[27] Polymeric *N*-oxides are used as oxidants in organic synthesis,^[24c] as cathode interlayer materials in organic solar cells^[28] and have been found to be active against silicosis.^[29] The chemical reactivity as well as the antibacterial and cytotoxic properties of many *N*-oxides raises questions about additional biological activities of polymeric *N*-oxides beyond their stealth properties.^[30]

The most important questions addressed by this study are thus: 1. Do polymeric *N*-oxides on surfaces have antifouling properties for microorganisms? 2. How durable are their effects given their relatively high chemical reactivity? 3. Do polymeric *N*-oxides have other biological effects besides their stealth properties? 4. Are the biological effects of polymeric *N*-oxides different from those of their small molecule analogues? In this report, we use grafted polymeric *N*-oxides on polyethylene (PE) as a base material to address the questions above.

2. Results

2.1. Surface Grafting of Poly-*N*-Oxides to Polyethylene

Covalent zwitterionization of PE with polymeric *N*-Oxides was performed via a three-step procedure (Figure 1). Briefly, the chemically unreactive PE surface was activated through an atmospheric plasma treatment. The resulting reactive functionalities serve as anchor points for heat-induced graft polymerization of a suitable precursor of the methacrylate- or vinylbenzyl-type (either VBDMA, MADMA or MAADMA) to form the corresponding polymer brushes (poly-VBDMA, poly-MADMA or poly-MAADMA). These two initial steps followed an established procedure for surface modification of PE from our lab.^[31] Final zwitterionization of the polymer brushes was achieved by post-grafting oxidation with H_2O_2 . An alternative direct polymerization of monomeric *N*-oxides of the methacrylate- or vinylbenzyl-type (as described for the syntheses of other polymeric *N*-oxides)^[14] was not an option here because the *N*-oxide moieties were found to be not compatible with the heat-induced polymerization protocol employed. Successful grafting and subsequent oxidation were reflected by extremely low static contact angles $\theta = 10-30^\circ$ with water for the resulting materials PE-poly-(VBNOx), PE-poly-(MAANOx) an PE-poly-(MANOx) (Table 1). In addition, the presence of poly-*N*-oxides was confirmed by combined 3D mass spectrometric and scanning probe microscopy (SPM) analysis by a variety of characteristic nitrogen and oxygen-containing organic mass fragments such as CN^- and CNO^- (Figure 2). SPM images taken before and after depth profiling with a time-of-flight secondary ion mass spectrometer (ToF-SIMS) revealed a surface roughness R_a of 1–2.5 μm and a brushlayer thickness of $\approx 50-100$ nm.

The successful immobilization of polymeric *N*-oxides on PE was also verified by ATR-FTIR spectroscopy and X-ray photoelectron spectroscopy (XPS) analysis. Exemplary data is depicted in Figure 3 (see Figure S1, Supporting Information for IR-spectra of other materials). The FTIR-spectra of PE-poly-(VBNOx) in Figure 3a reveal the characteristic $N-O$ vibration at 933 cm^{-1} , which is also visible in the monomer (VBNOx) spectrum. These characteristic $N-O$ bands are also observed for the other zwitterionic materials PE-poly-(MANOx) and PE-poly-(MAANOx), along with carbonyl bands from the polymethacrylate and polymethacrylamide backbones (spectra not shown, see Figure S1, Supporting Information). For full characterization of the grafting process, we performed XPS measurements of pristine PE, plasma activated PE and modified poly-(*N*-oxide)-PE (see SI for additional spectra). The spectra revealed the presence of peroxides on the PE surface after plasma activation with a dominant peak at 532.4 eV in the O1s spectra (Figures S3 and S4, Supporting Information). The atomic ratios of N/C was 0.07 which is similar to the theoretical value of 0.09 and indicates successful radical polymerization and subsequent oxidation to PE-poly-(VBNOx) (Figure S5, Supporting Information). Slight deviation of the theoretical atomic ratios of N/O and O/C can be explained by impurities, probably associated to polymer entrapped carbon monoxide and/or water. The deconvoluted peak at 402.6 eV in the N1s spectra was assigned to the quaternary ammonium group in the $N-O$ bond which is also reflected by a peak at 531.0 eV in the O1s spectra (Figure 3b). Both, N1s and

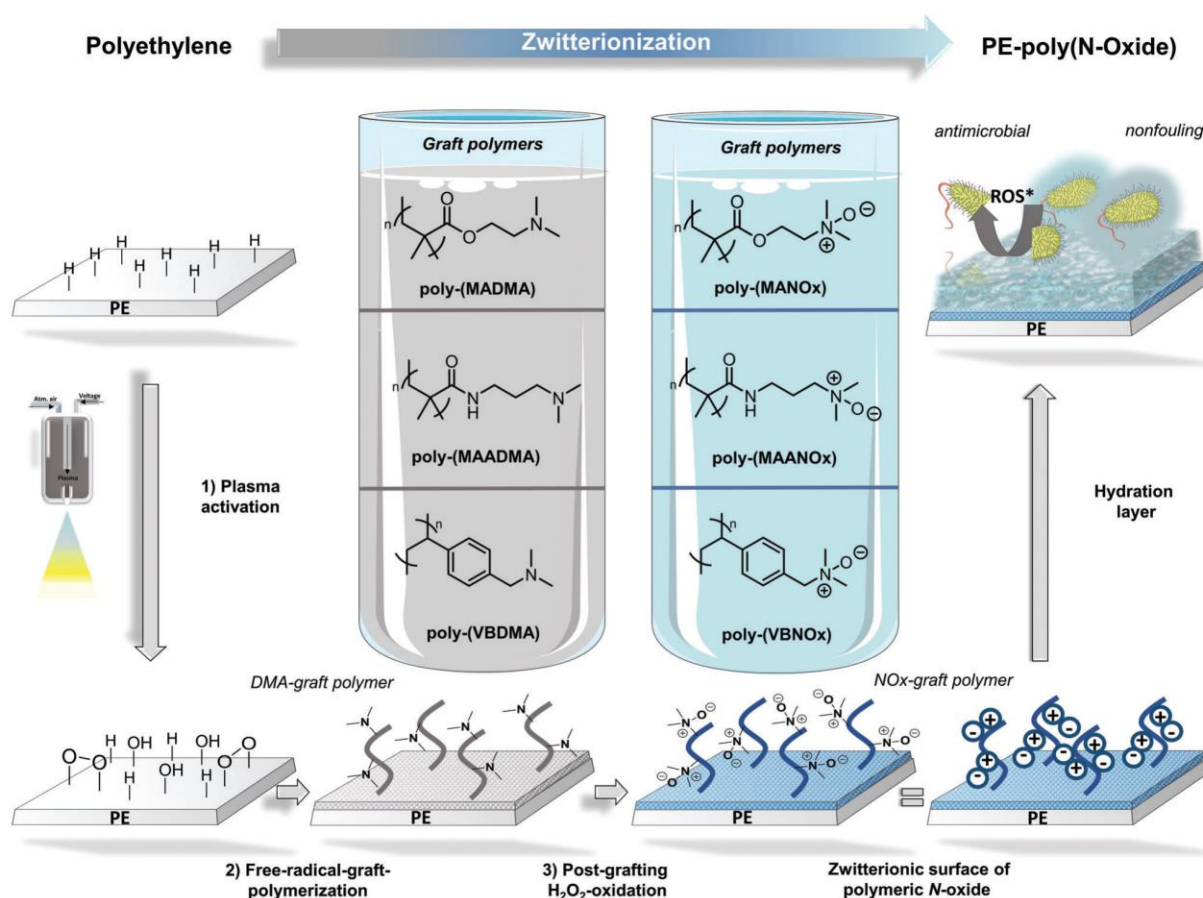


Figure 1. Surface grafting of *N*-oxides to PE foils. 1) Plasma activation of otherwise inert PE, 2) heat-induced radical polymerization, 3) post-grafting zwitterionization of the polymer brushes by oxidation of tertiary amines to *N*-oxides with H₂O₂.

O1s binding energies are consistent with previous reports on polymeric *N*-oxides. N1s spectra indicate good conversion of tertiary amines to the corresponding *N*-oxides by H₂O₂-treatment for 72 h. However, the signal at 399.3 eV can be assigned to residual tertiary amines. Furthermore, a detailed deconvolution of N1s spectra reveals an additional small signal at 400.3 eV, which is also detectable in the survey spectra of pristine PE (Figures S2, S5, and S6, Supporting Information). These minor impurities are due to non-identified nitrogen species on the surface.

2.2. Microbiological Assessment of Low-Fouling Activity

The low-fouling activity of PE with three different grafted *N*-oxides was tested with a bacterial adhesion assay and a LIVE/DEAD staining.^[31b,32] *Staphylococcus aureus* (Gram-positive, strain ATCC29213) was used as a model pathogen. It is a clinically relevant pathogen responsible for many health care related infections.^[33] In addition, *Vibrio campbellii* (previously classified as *Vibrio harveyi*) (Gram-negative, strain BB120) was used as a second model organism because it is a major

Table 1. Polymerization conditions and water contact angles (WCA) for grafted polymers on PE.

Entry	Monomer [wt%]	AIBN [wt%]	PE-poly-(XXDMA), WCA [°] ^{a)}	PE-poly-(XXNOx), WCA [°] ^{a)}
1	–	–	–	pristine PE, 95.2 ± 1.6
2	VBDMA, 40	1.0	PE-poly-(VBDMA), 9.9 ± 1.4	PE-poly-(VBNOx), 9.9 ± 1.4
3	MADMA, 20	0.1	PE-poly-(MADMA), 19.8 ± 2.	PE-poly-(MANOx), 19.8 ± 2.3
4	MAADMA, 40	0.1	PE-poly-(MAADMA) 29.4 ± 1.9	PE-poly-(MAANOx) 29.4 ± 1.9

^{a)} Advancing WCA were measured with deionized water using the static sessile drop method and are given as mean value ± SD of at least three independent samples.

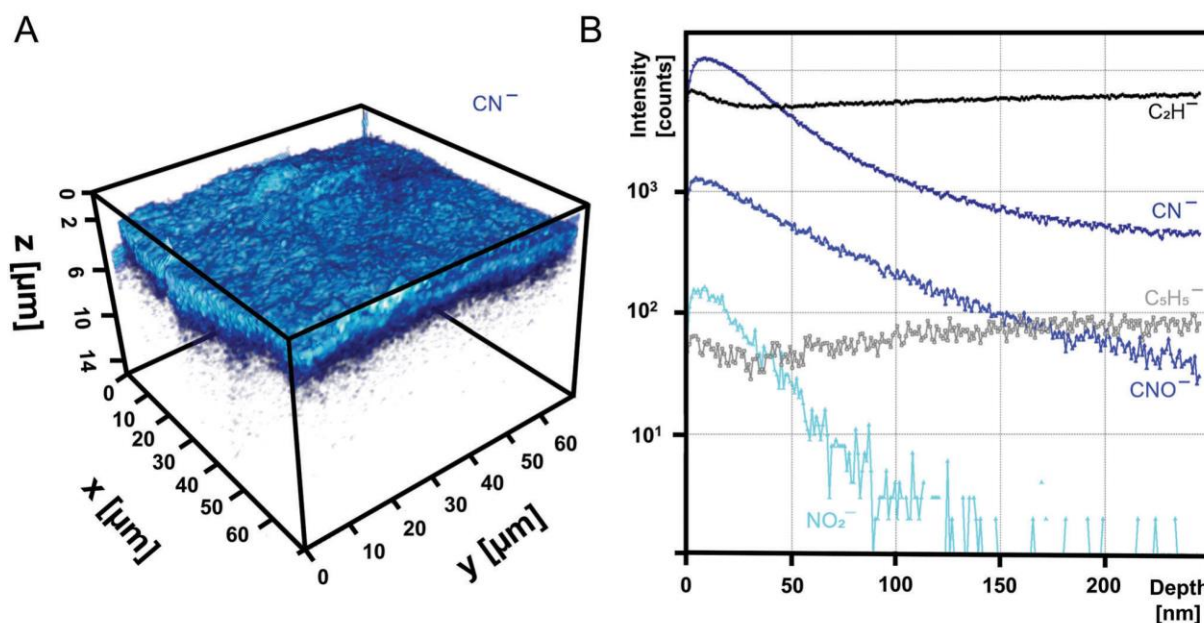


Figure 2. Combined 3D ToF-SIMS and SPM imaging analysis of PE-poly-(VBNOx). A) Correlative SPM/SIMS-3D image of the poly-(VBNOx) coating layer with the spatial distribution of CN^- as the most intensive ion on top of the substrate. Shades of blue correspond to signal intensity of CN^- . B) ToF-SIMS depth profile of PE-poly-(VBNOx) with poly-(VBNOx)-specific nitrogen containing mass fragments CN^- , CNO^- , and NO_2^- and characteristic PE fragments C_2H^- and C_5H_5^- . SIMS analysis was performed in negative ion mode with Bi_3^+ ions. Depth profiling was carried out using Ar^+_{2000} cluster ions for sputtering.

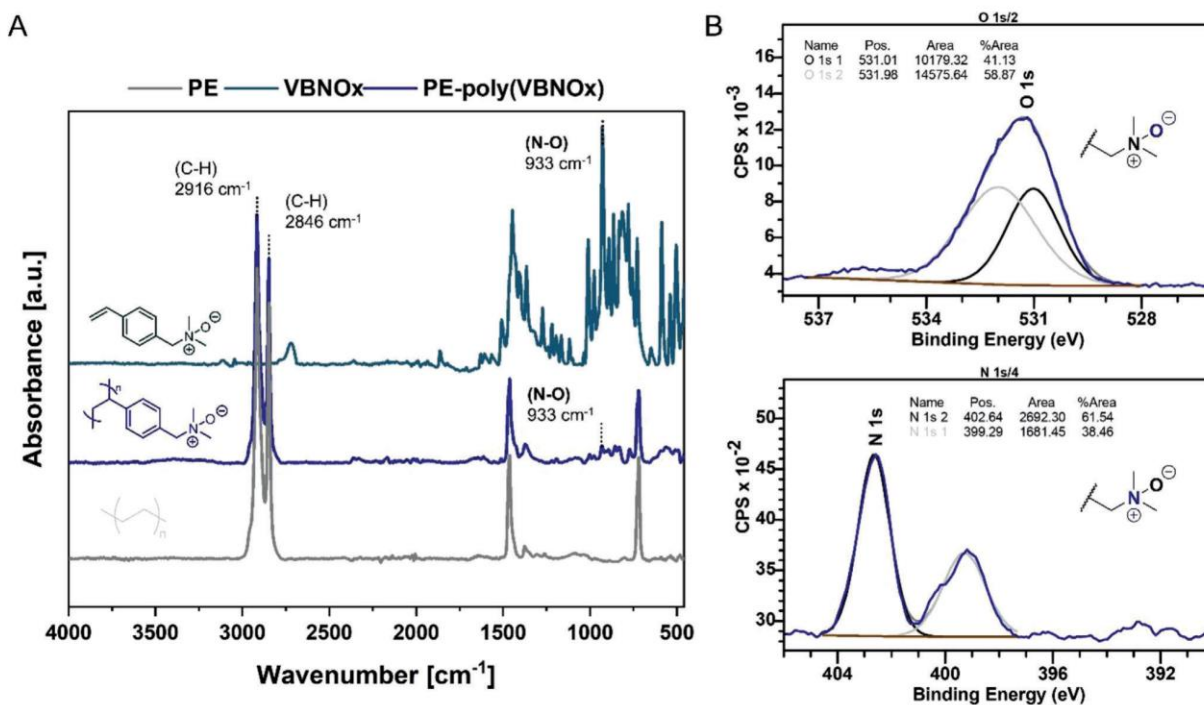


Figure 3. Characterization of PE-poly-(VBNOx) by ATR-FTIR and XPS. A) ATR-FTIR spectra in absorbance mode of pristine PE, PE-poly-(VBNOx), and VBNOx monomer for comparison. B) Deconvoluted regions of O 1s and N 1s XPS spectra of PE-poly-(VBNOx). Survey spectra of pristine PE, plasma activated PE and PE-poly-(VBNOx) are available in the supporting material.

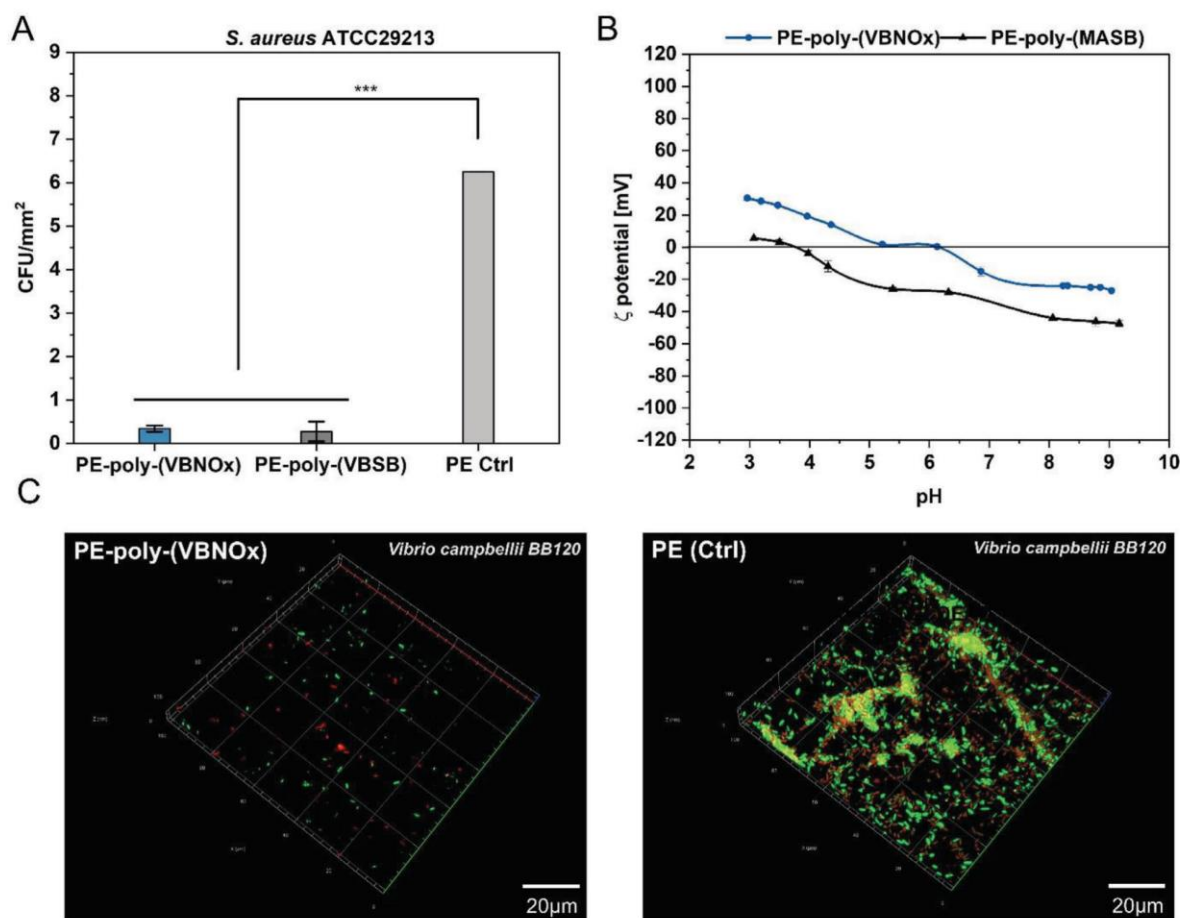


Figure 4. Microbiological assessment of low-fouling surfaces. A) Bacterial adhesion assay with *S. aureus* (strain ATCC29213): Colony counts after incubation of PE-poly-(VBNOx), PE-poly-(VBSB) and pristine PE as control (Ctrl) with *S. aureus* (initial concentration: 10^5 CFU mL⁻¹ in MHB) for 24 h. Statistical significance was determined via pairwise comparison (Tukey test) $p \leq 0.001$ (***). B) Zeta potential measurement of PE-poly-(VBNOx) and PE-poly-(MASB) at pH 3–9. C) Biofilm adhesion: confocal microscopy of PE-poly-(VBNOx) (left) and PE (right) after 24 h incubation with *V. campbellii* (strain BB120) in artificial seawater, followed by LIVE/DEAD™ staining. Live bacteria appear light green, dead bacteria red. The images indicate representative areas within static biofilms.

contributor to the marine microbiome and has also been identified as a potential pathogen in coastal water. Moreover, *V. campbellii* forms rapidly biofilms on plastic substrates (particularly on PE) accompanied with high antibiotic resistance.^[34] Briefly, sterilized test specimens (size: 1.0 cm²) were fully immersed in a bacterial suspension (10^2 – 10^5 CFU mL⁻¹) and stored with gentle shaking ensuring complete contact of the materials with the inoculum. After 24 h, samples were transferred into a sterile saline solution to desorb loosely attached microbes. Growth controls of each media were collected at this point to verify presence and concentration of living bacteria. Finally, test specimens were printed carefully onto an agar plate (Columbia Agar) and were subsequently incubated at 37 °C for 20 h before colony counting. Pristine PE specimens were used as controls. In addition, a poly-sulfobetaine grafted zwitterionic PE sample (PE-poly-(VBSB)) with known excellent low-fouling properties was used for comparison.^[31b] The results shown in **Figure 4a** reveal a low-fouling effect of the grafted polymeric *N*-oxide on

PE (PE-poly-(VBNOx)), comparable to the corresponding polymeric sulfobetaine control material (PE-poly-(VBSB)). A second adhesion assay was performed with the marine organism *V. campbellii* in artificial seawater, followed by confocal microscopy after a LIVE/DEAD staining (LIVE-/DEAD BacLight Viability Kit). The resulting images after incubation confirmed the low-fouling activity of PE-poly-(VBNOx) and show almost no adhering live bacteria (green fluorescence) on PE-poly-(VBNOx) after 24 h immersion in seawater whereas pristine PE was rapidly colonized by bacteria (**Figure 4c**). Polymeric *N*-oxides like poly-(VBNOx) have thus excellent low-fouling activity against the here tested Gram-negative and Gram-positive bacteria and are competitive with established zwitterionic materials such as polysulfobetaines. *N*-oxides (pKa \approx 4–5) have significantly higher pKa values than sulfonic acids in sulfobetaines (pKa \approx 1–2). The zeta potential of zwitterionic materials bearing sulfobetaines is thus strongly negative in a broad pH range.^[35] In contrast, the analysis of poly-*N*-oxide materials like PE-poly-(VBNOx) revealed

only slightly negative to neutral zeta potentials at biologically most relevant pH values of 5–8.^[36] Neutral surface zeta potentials were previously found to be ideal for optimal low-fouling performance.^[35]

2.3. Antibacterial Activity of Poly-(*N*-Oxides)

The observed low-fouling activity of polymeric *N*-oxides against bacteria has not been described before. However, it is not surprising, given the reported low protein fouling of these materials.^[14,36] It was notable though, that a dramatic antimicrobial effect was observed in the growth controls of the adhesion assays. When bacterial solutions were exposed to PE-poly-(VBNOx) almost all bacteria were immediately killed. This was a striking contrast to growth controls of pristine PE and also sulfobetaine PE-poly-(VBSB). Both did not reveal any antibacterial effect. The antimicrobial activity of three different *N*-oxides was therefore confirmed by a quantitative analysis according to ASTM E2149-13a, a common assay to evaluate antimicrobial materials.^[37] We selected *S. aureus* (Gram-positive, strain ATCC29213) and *E. coli* (Gram-negative, strain ATCC25922) for the assay. Briefly, sterilized PE test specimens were immersed with bacterial solutions of 10^5 CFU mL⁻¹ at 37 °C. After incubation for 2 h, the resulting solutions were aliquoted in *log* levels ranging from 10^5 – 10^2 CFU mL⁻¹ onto Columbia agar and were subsequently incubated for 17 h before colony counting. Results are depicted in **Figure 5** and reveal a remarkable antimicrobial effect of the poly-*N*-oxide-grafted materials for both Gram-positive *S. aureus* and Gram-negative *E. coli*.

The antimicrobial effect was confirmed for all three polymeric *N*-oxides tested and is thus not dependent of the polymer backbone structure. However, the methacrylamide-derivative PE-poly-(MAANOx) showed a lower antimicrobial effect than both other *N*-oxides. This might indicate an effect of the alkyl-spacer length or the linking functionality (amide vs ester) of the polymerizable group on antibacterial activity. Either a release of antimicrobial compounds from the material or a contact-active mechanism might explain the observed antibacterial effect. The latter would be principally possible due to the high p*K*_a value of *N*-oxides. This might cause protonation under slightly acidic conditions created by colonizing bacteria. Significant protonation of PE-poly-(VBNOx) starts at pH values lower than 4, leaving a positively charged and thus possibly contact-active surface, as evident from the zeta potential measurements in **Figure 4B**. However, such low pH values have only been reported locally in biofilms.^[38] We have not detected any biofilm formation or adhesion of bacteria to the *N*-oxide test specimens in our adhesion assays making contact activity unlikely. Further evidence for a release mechanism came from an agar plate diffusion test (DIN EN ISO 20645:2002-02) with *S. aureus* and *E. coli*. An inhibition zone around the poly-*N*-oxide test specimen was clearly visible supporting leaching of antimicrobial compounds (**Figure S7**, Supporting Information). Release of residual H₂O₂ from the oxidative preparation of *N*-oxide polymer brushes was excluded through inspection of the XPS spectra and via a horseradish peroxidase assay (**Figure S10**, Supporting Information)^[39] This assay is sensitive to H₂O₂-concentrations in the micromolar range which is or-

ders of magnitudes lower than the MIC of H₂O₂ for *S. aureus* (MIC = 0.27–0.66 mM) and *E. coli* (MIC = 1.33–2.66 mM).^[40]

As mentioned in the introduction, some *N*-oxides have been reported to have antimicrobial or cytotoxic properties. These compounds are typically benzotriazine dioxides or phenazine dioxides of low molecular weight. A prototype is tirapazamine (TPZ, MW = 178 g mol⁻¹), an experimental anticancer drug and antibiotic. The mode of action of TPZ involves most likely a reductive activation leading to the formation of cytotoxic hydroxyl radicals by cleavage of a N–O bond.^[27] The latter homolytic bond cleavage is not surprising because the bond dissociation energies of *N*-oxides are known to be relatively low.^[23] However, the formation of reactive oxygen species from *N*-oxides under physiological conditions has been reported for a limited set of compounds only but not for polymeric *N*-oxides.^[27] The formation of radical species from grafted polymeric *N*-oxides was tested with DPPH*, a stable radical commonly used as a radical scavenger. The DPPH*-radical has an absorption maximum at 520 nm and the loss of absorption intensity at this wavelength can be correlated to the formation of radical adducts.^[41] Treatment of PE-poly-(VBNOx) with DPPH* at 37 °C lead to significant scavenging of DPPH* after 2 h and almost complete DPPH* consumption after 24 h (**Figure 6a**). In contrast, the corresponding monomeric *N*-oxide VBNOx leads to only minor consumption of DPPH* after 24 h suggesting that only polymeric *N*-oxides generate potentially antibacterial radical species under physiological conditions. The identity of the generated radicals was analyzed by electron paramagnetic resonance (EPR)-spectroscopy after treatment of PE-poly-(VBNOx) with DMPO as a spin trap. The resulting EPR spectra show the presence of a radical trapped by DMPO (**Figure 6b**). The analysis of respective hyperfine coupling constants ($a_N = 15.9$ G and $a^{\beta}_H = 4.1$ G) revealed an oxygen-centered radical, either a hydroxyl-radical (OH*) or a superoxide-radical (O^{2-*})^[42] and is a clear indication of released reactive oxygen species (ROS-formation). Again, generation of ROS species was found to be specific for the grafted polymeric *N*-oxides but was not observed for the monomeric *N*-oxide (VBNOx) (**Figure 6**). In consequence, no antibacterial activity of VBNOx was detected and we determined minimal inhibitory concentrations (MIC) of VBNOx > 1024 μg mL⁻¹ for *E. coli* and *S. aureus* (**Table S1**, Supporting Information).

The release of ROS from polymeric *N*-oxides triggered questions regarding the fate of the material and the durability of the observed antibacterial effect. Specimens of PE-poly-(VBNOx) were therefore repeatedly exposed to bacteria according to ASTM E2149-13a. **Figure 7** shows the results of these experiments. They reveal a retained activity of the material after repeated use with no measurable loss in function. The antibacterial activity after repeated use is not dependent on intermediate purification and treatment of the test specimens before the next incubation experiment. Intermediate treatment of PE-poly-(VBNOx) with three different disinfection reagents (NaOCl, H₂O₂ and *i*PrOH/*o*PrOH/*e*tOH (BacillolAF)) lead to identical antibacterial activity of the material. Activity is also retained if no disinfection is performed between incubations. However, the transfer of residual bacteria leads to a significantly higher (>10⁵ CFU mL⁻¹) initial concentration of bacteria in the test solutions after repeated incubation. The resulting high inoculum leads to a slight

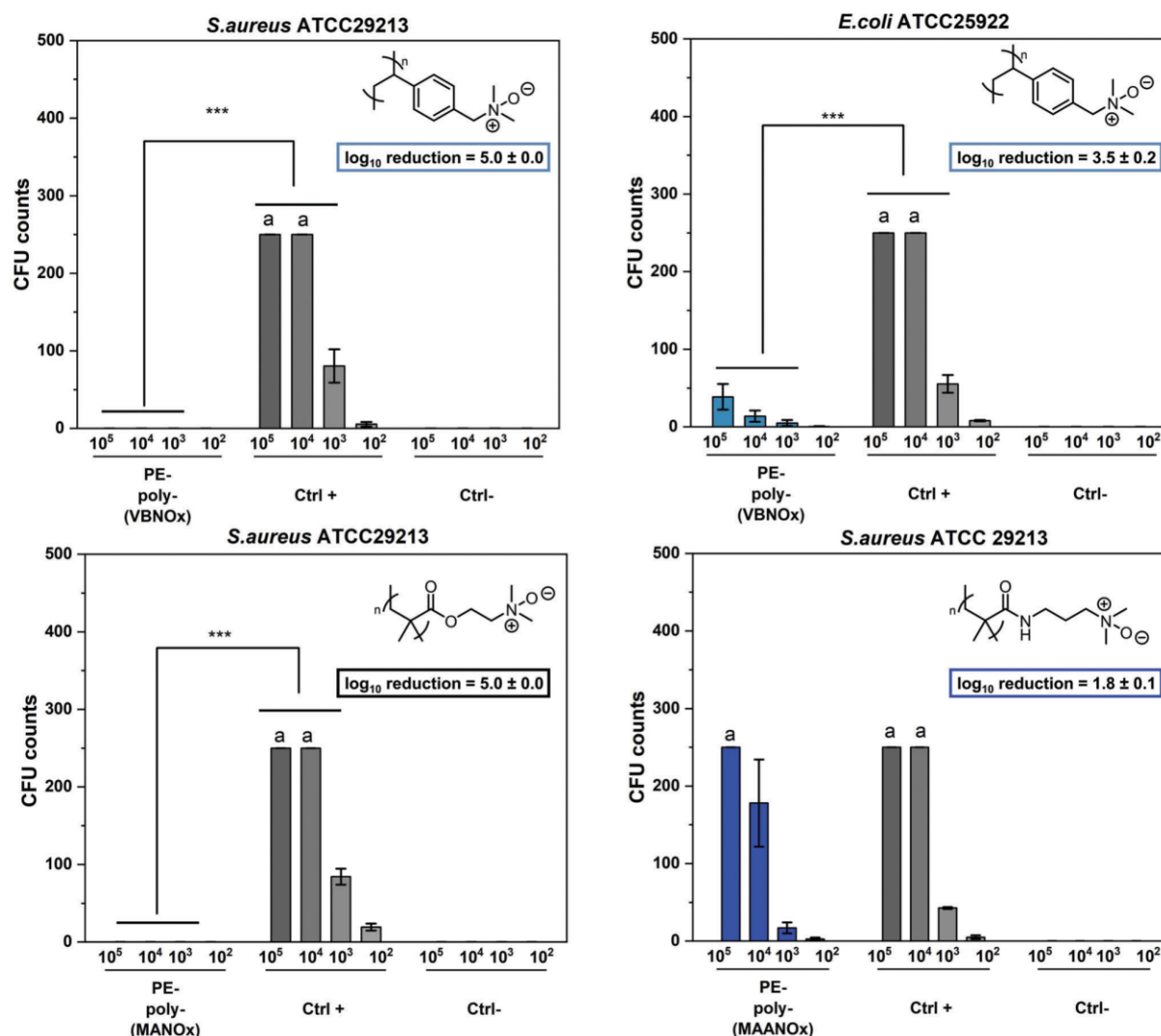


Figure 5. Antibacterial activity of three different grafted polymeric *N*-oxides on PE measured by ASTM E2149-13a. Colony counts after incubation of PE test specimens with bacterial suspensions at different dilutions (10^5 – 10^2 CFU mL⁻¹) for 2 h. Each experiment was performed in triplicate, pristine PE (Ctrl +) and pure saline (Ctrl -) were used in control experiments. Colony counts above 250 were set as “too numerous to count” (TNTC) (a). Log₁₀ reduction was calculated as described in the experimental. Statistical significance was determined via pairwise comparison (Tukey test) $p \leq 0.001$ (***), $p \leq 0.01$ (**).

increase of surviving bacteria after the repeated 2 h exposure to the PE-poly-(VBNOx) specimen. Analysis of the test specimens after repeated exposure to microorganisms revealed identical chemical and physical properties of the material. It is notable that we observed no degradation of the grafted polymeric *N*-oxides. Chemical degradation processes of the grafted polymeric *N*-oxides can lead to the formation of hydroxylamines and carbonyl groups, although these conversions are typically observed at higher temperatures than our test conditions.^[15,24a] We did not find any evidence for these functional groups and in addition, the contact angle and the zeta potential of the materials remained constant after threefold use (Figure S13, Supporting Information). The release of ROS

from polymeric *N*-oxides at room temperature is most likely a consequence of a reductive activation of the *N*-oxide in the presence of microorganisms. It might thus follow the same mechanisms reported for cytotoxic activation of some *N*-oxides in hypoxic tumor tissue.^[26a,b,27,43]

3. Discussion

Three different polymeric *N*-oxides were successfully grafted to PE as a base material. We have used an established two-step protocol involving atmospheric plasma activation of PE and subsequent heat-induced graft polymerization of methacrylate,

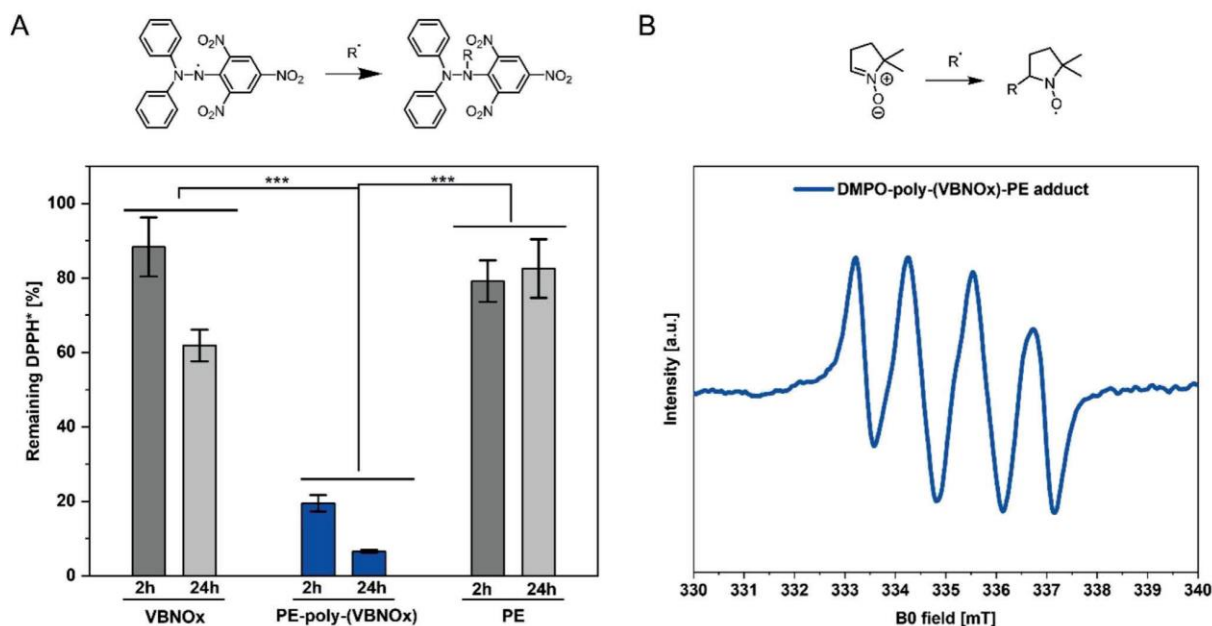


Figure 6. Evaluation of ROS formation from PE-poly-(VBNOx). A) DPPH radical scavenging and remaining DPPH-radical after exposure to VBNOx ($1024 \mu\text{g mL}^{-1}$), PE-poly-(VBNOx) (surface area: 1 cm^2), and pristine PE (surface area: 1 cm^2) at 37°C in MeOH. B) EPR spectra after treatment of DMPO with a PE-poly-(VBNOx) specimen (surface area: 1 cm^2). Control experiments were performed with pristine PE + DMPO and PE-poly-(VBNOx) without DMPO, data available in the supplementary material (Figure S12, Supporting Information). Statistical significance was determined via pairwise comparison (Tukey test) $p \leq 0.001$ (***).

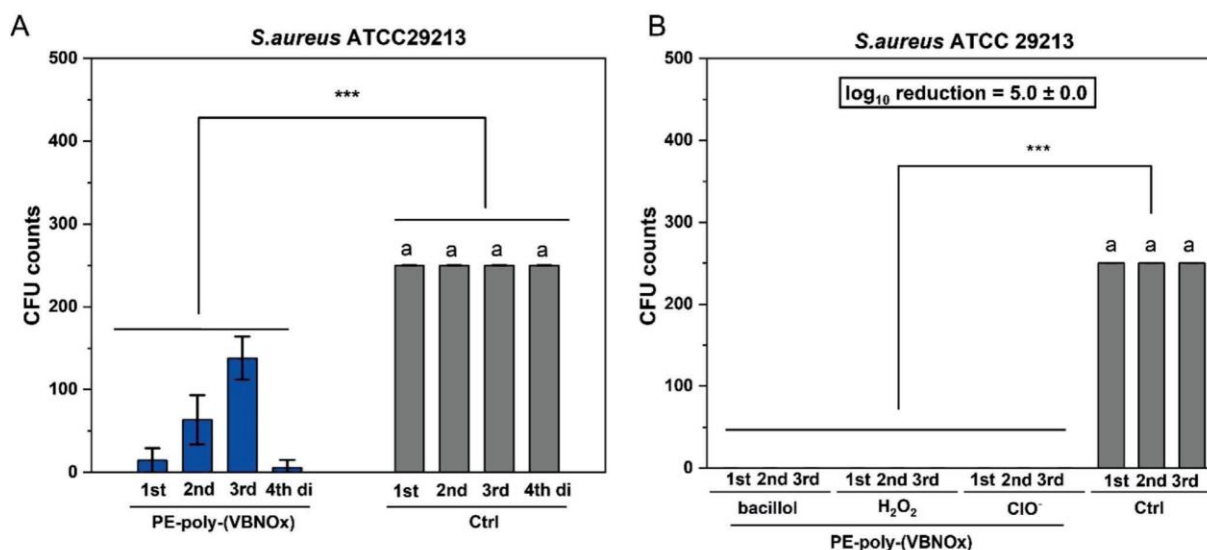


Figure 7. A) Repeated use of pristine PE (Ctrl) and PE-poly-(VBNOx) specimens (surface area: each 1.0 cm^2) in an antibacterial assay following ASTM E2149-13a. The test specimens were exposed to the incubation solutions without intermediate disinfection three times (1st, 2nd, 3rd). An additional fourth exposure was performed after H_2O_2 disinfection (4th di). B) Repeated antibacterial assay (ASTM E2149-13a with *S. aureus*) for pristine PE and PE-poly-(VBNOx) specimens (surface area: each 1.0 cm^2). The test specimens were exposed to new incubation solutions (10^5 CFU mL^{-1}) after intermediate disinfection (BacillolAF: *i*PrOH/*Pr*OH/EtOH, aqueous H_2O_2 (30% v/v) and aqueous NaOCl (12% v/v)) three times (1st, 2nd, 3rd). Bars represent mean values \pm SD of three independent measurements. Colony counts above 250 were set as "too numerous to count" (TNTC) (a). Statistical significance was determined via pairwise comparison (Tukey test) $p \leq 0.001$ (***).

methacrylamide and vinylbenzene monomers. The process generates covalently linked dense polymer brushes of polymeric tertiary amines. These were oxidized with H_2O_2 to the target polymeric *N*-oxides in a final step. The resulting materials were characterized by IR, XPS and ToF-SIMS confirming the complete conversion of tertiary amine groups to the corresponding *N*-oxides. We found a brush layer thickness of $\approx 50\text{--}100$ nm for the grafted polymeric *N*-oxides. The surfaces are characterized by extremely low static contact angles $\theta = 10\text{--}30^\circ$ with water and almost neutral zeta potentials in the pH range from 5–7 for PE-poly-(VBNOx), PE-poly-(MAANOx) and PE-poly-(MANOx). The latter parameter distinguishes grafted poly-*N*-oxides from other poly-zwitterions such as sulfobetaines which have negative zeta potentials at pH values as low as 4, reflecting the higher acidity of sulfonic acids ($\text{p}K_{\text{a}} \approx 1\text{--}2$) compared to *N*-oxides ($\text{p}K_{\text{a}} \approx 4\text{--}5$).

The whole process of *N*-oxide grafting described herein is scalable and uses readily available starting materials. It should also be applicable to many other plastics besides PE as a base material. However, the heat-induced graft polymerization is not compatible with monomers containing *N*-oxides because these are intrinsically unstable at higher temperatures. This is a notable difference to other grafting procedures such as copper catalyzed surface-initiated atom transfer radical polymerization (SI-ATRP), which has been shown to be compatible with *N*-oxide monomers.^[14] The low water contact angles and the almost neutral zeta potentials of all three grafted poly-*N*-oxides (PE-poly-(VBNOx), PE-poly-(MAANOx) and PE-poly-(MANOx)) are ideal parameters for low-fouling surfaces. These stealth properties of poly-*N*-oxides have been shown to prevent protein adhesion before.^[14,36,44] It was therefore not surprising that we also observed good low-fouling properties in bacterial adhesion tests against *S. aureus*, an important pathogen for health care related infections and *V. campbellii*, a marine microorganism.

However, beside the confirmation of a low-fouling effect for poly-*N*-oxides, the growth controls of these adhesion experiments revealed clear antibacterial properties. These were confirmed in standard ASTM assays with Gram-negative and Gram-positive bacteria. We attribute these antibacterial properties to the generation and release of radicals, which we confirmed at 37 °C via DPPH as a radical scavenger. The resulting EPR spectra of DMPO-radical adducts revealed the generation of ROS from poly-*N*-oxide surfaces. Other possible reasons for the antibacterial properties of poly-*N*-oxides such as contact-activity through protonation of *N*-oxides or release of residual (antibacterial) H_2O_2 are unlikely. A release mechanism is clearly supported by an inhibition zone around the PE-poly-*N*-oxide specimens which would not be observed for a contact-active material. Release of residual H_2O_2 was excluded via a sensitive HRP-assay. The generation of ROS from *N*-oxides under physiological conditions has been reported for a limited set of aromatic *N*-oxides of low molecular weight only. It has been reported that the release of ROS from drugs containing *N*-oxide groups (e.g., tirapazamine) is triggered in hypoxic tumor tissue or in the presence of bacteria by reductive activation. In this context it is remarkable that we found the generation of ROS to be an exclusive feature of poly-*N*-oxides (PE-poly-(VBNOx), PE-poly-(MAANOx) and PE-poly-(MANOx)) and it was not observed in close analogues of low molecular weight such as VBNOx, MANOx or MAANOx. The latter compounds did not show any ROS formation and did also not have appreciable levels

of antibacterial activity (MICs > 1024 $\mu\text{g mL}^{-1}$ against *E. coli* and *S. aureus*).

We propose that the formation of ROS from poly-*N*-oxides follows a similar mechanism as tirapazamine and derivatives. Further evidence for this hypothesis comes from a recent report of Gao and coworkers.^[43a] In this study, polymeric *N*-oxides were used as selective drug carriers for hypoxic tumor tissue (see also^[45]) due to their bioreduction by CYP450-enzymes. We suspect that a similar reductive conversion of poly-*N*-oxides occurs in the presence of microorganisms leading to ROS release and thus antibacterial activity. In contrast to the most common chemical *N*-oxide degradation mechanisms mentioned above, this bioreductive pathway reduces PE-poly-(VBNOx), PE-poly-(MAANOx) and PE-poly-(MANOx) back to the corresponding polymeric tertiary amines PE-poly-(VBDMA), PE-poly-(MAADMA) and PE-poly-(MADMA). The *N*-oxides could then be regenerated from these polyamines explaining the constant antibacterial effects of polymeric *N*-oxides even after repeated exposure to bacteria. This reoxidation step might be mediated by oxidative disinfectants like NaOCl and H_2O_2 . Remarkably, we noted no loss of antibacterial activity for repeated use of poly-*N*-oxides even without oxidative intermediate treatment (disinfection with BacilloLAF) or even without intermediate disinfection. These latter findings might suggest self-replenishing properties of poly-*N*-oxides, presumably mediated by molecular oxygen either in solution or in air. Both the release of ROS (and thus antibacterial activity) and the reoxidation of the material are clearly special properties of the polymeric *N*-oxide because neither significant ROS production nor antibacterial activity was observed with the corresponding monomeric *N*-oxides of low molecular weight. These special properties might be caused by the close assembly of multiple *N*-oxide functionalities and thus a neighbor group effect in the polymer. Similar effects have been proposed to operate in charge transfer from polymeric *N*-oxides used in intermolecular *n*- or *p*-doping processes in optoelectronic devices.^[28a,46] Neighbor group effects of polar groups have also been proposed to accelerate oxidations of tertiary amines of low molecular weight.^[47]

4. Conclusion

Our studies reveal that grafted polymeric *N*-oxides are attractive low-fouling coatings for plastic base materials and might thus find application in many fields related to bacterial biofilm formation. In contrast to other zwitterionic polymers poly-*N*-oxides do not only generate stealth surfaces upon grafting but have unique antibacterial properties caused by the release of ROS. Poly-*N*-oxides combine thus low-fouling properties with the release of antibacterial compounds in a rather simple polymer. In addition, the biologically active *N*-oxide functionality can easily be regenerated upon oxidation with common disinfectants. Even without added oxidants, we noted antibacterial activity of poly-*N*-oxides upon repeated challenge of our materials with bacteria. However, whether this effect is caused by *N*-oxide regeneration or the large reservoir of *N*-oxide functionalities on the surface needs to be confirmed in future studies. The combined low-fouling and antibacterial mode of action enables applications requiring the eradication of bacteria. If ROS formation limits in vivo applications of poly-*N*-oxides needs to be determined in future studies. However, current in vivo data do not support toxic effects of poly-*N*-

oxides,^[14,43a,b,45,48] which is plausible assuming that ROS release is only triggered in hypoxic tumor tissue or in the presence of bacteria.

5. Experimental Section

Chemicals and Materials: Polyethylene (LD-PE) with a thickness of 750 μm was purchased from Goodfellow and was used as received. Vinylbenzylchloride (90 %), dimethylamine solution (33 % in ethanol), azo-bis-(isobutyronitrile) (AIBN) (98 %), hydrogen-peroxide solution (30 % v/v in water), (2-dimethylaminoethyl) methacrylate (99 %), N-[3-dimethylamino-propyl]-methacrylamide (99 %), 2,2-diphenyl-1-picrylhydrazyl (DPPH), 5,5-dimethyl-1-pyrrolin-N-oxide (DMPO), horseradish peroxidase (250 units per mg), pyrogallol (99 %) were purchased from Sigma-Aldrich. Microorganisms *S.aureus* (strain ATCC29213), *E.coli* (strain ATCC29522) and *Vibrio campbellii* (strain BB120 also known as strain ATCC-BAA-1116) were purchased from American Type Culture Collection. All reagents were used without further purification. Crimp neck vials (N20, 10 mL volume) and crimp caps (N20, PTFE septum) for degassing were purchased from Macherey-Nagel GmbH (Düren, Germany).

Atmospheric Air Plasma: For plasma activation, an atmospheric air plasma system from Plasmamatreat GmbH (Steinhagen, Germany) was used. The atmospheric-pressure plasma was produced by a generator FG5001 with an applied working frequency of 21 kHz, generating a non-equilibrium discharge in a rotating jet nozzle RD1004 in combination with the stainless-steel tip No. 22826 for an expanded treatment width of ≈ 22 mm. Additionally, the jet nozzle was connected to a Janome desktop robot type 2300N for repetitious accuracy regarding treatment conditions. The process gas was dry and oil-free air at an input pressure of 5 bar in all experiments.

IR- and UV/Vis Spectroscopy: Infrared spectra were recorded with an attenuated total reflectance Fourier Transform infrared system (ATR-FTIR), model "IRAffinity-1S" from Shimadzu (Kyoto, Japan) using a "Quest" ATR accessory from Specac. The spectral range was set at 4000 cm^{-1} – 400 cm^{-1} with a resolution of 0.5 cm^{-1} in absorbance mode and spectra were processed with OriginPro 9 (2021) software. UV/vis spectra were obtained on a Genesys 10S spectrophotometer from Thermo Scientific (Waltham, USA) using Visionlite software for analysis.

Contact Angle Measurements: Contact angles were acquired with an OCA 20 goniometer from DataPhysics (Filderstadt, Germany) equipped with two automated dispensing units for different liquid probes, a high-speed video system with CCD-camera, measuring stage and halogen-lighting for static and dynamic contact angle measurements. For evaluation, independent triplicate measurements at three different points of the surface were done. Advancing contact angles were measured with deionized water using the static sessile drop method with a dispensing volume of $5\ \mu\text{L}$. The dispensing rate of the automatic syringe was set at $1\ \mu\text{L min}^{-1}$. The obtained angle was calculated with the OCA software.

Electrokinetic ζ -Potential Measurements: The surface zeta potential (ζ -potential) was determined as streaming potential using an electrokinetic analyzer Surpass (Anton Paar, Graz, Austria). The measurements were carried out using an adjustable gap cell in which two samples with a rectangular size of $1\text{ cm} \times 2\text{ cm}$ were clamped vis-à-vis with a micro slit of $110\ \mu\text{m}$ in between. For each measurement, the starting conductivity was set to $17\ \mu\text{S m}^{-1}$ with KCl as electrolyte. The pH was adjusted from 9.5–2.5 stepwise with automatic pH titration by adding $0.05\ \text{M HCl}$. Presented values of ζ potentials were determined as mean value of four measurements for each pH step.

Nuclear Magnetic Resonance (NMR) Spectroscopy: The measurements were performed in 5 mm o.d. sample tubes using either a Bruker Avance 600, 500, or 400 MHz (AV600, AV500 and AV400, Bruker, Ettlingen, Germany). The obtained spectra were processed with MestReNova x64 software. ^{13}C -spectra were recorded with ^1H -decoupling. Peak assignments were supported by 2D NMR experiments like ^1H , ^1H -COSY, ^1H , ^{13}C -HSQC and ^1H , ^{13}C -HMBC.

Time of Flight Secondary Ion Mass Spectrometry (ToF-SIMS) and Scanning Probe Microscopy (SPM): The analysis was carried out with an M6 Plus

machine (IONTOF Company, Münster, Germany). Here a scanning probe microscope is included in the main vacuum chamber of the ToF-SIMS, which offers the possibility for correlation of topographic and mass spectrometric imaging data. For SIMS analysis $60\ \text{keV Bi}_3^{++}$ primary ions were used ($I = 0.05\ \text{pA}$ at $200\ \mu\text{s}$ cycle time). The Bi gun (nanoprobe 50) was operated in high-current bunched mode with a beam-defining aperture of $700\ \mu\text{m}$. For depth profiling, the machine was operated in a non-interlaced mode in combination with a $5\ \text{keV Ar}_{2000}^+$ sputter beam ($I = 1.328\ \text{nA}$). Low energetic electrons were used for charge compensation during the pause time of 1 s. An analysis area of $70 \times 70\ \mu\text{m}^2$ (128×128 pixels) was chosen in the centre of the $200 \times 200\ \mu\text{m}^2$ sputter area. Depth profiling was stopped at the interface between coating and substrate. Before and after the measurement a scanning probe microscopy image of the analysis area was recorded in intermitted mode with 2048×128 pixels resolution as well as line scans in x and y directions with a scan length of $600\ \mu\text{m}$ each. Data evaluation was carried out with Surface Lab software version 7.3 (IONTOF Company). Negative mass spectra were recorded and the achieved mass resolution was $m/Dm > 7.500$ (FWHM) at $m/z = 65.04$ (C_5H_5^-).

X-Ray Photoelectron Spectroscopy (XPS): XPS measurements were performed using a KRATOS AXIS Ultra DLD (Kratos Analytical, Manchester, United Kingdom) equipped with a monochromatic Al K_{α} anode working at 15 kV (225 W). For the survey spectra, a pass energy of 160 eV was used while for the region spectra, the pass energy was 20 eV. The investigated area was $700 \times 300\ \mu\text{m}^2$. For all of the PE samples, charge neutralization was necessary. The evaluation and validation of the data were carried out with the software CASA-XPS version 2.3.24. The spectra were calibrated by adjusting the C1s signal to 284.5 eV. For deconvolution of the region files, background subtraction (U 2 Tougaard or Shirley) was performed before calculation.

Electron Paramagnetic Resonance (EPR) Spectroscopy: EPR spectroscopy was performed on a Magnetech Miniscope MS400 X-band benchtop spectrometer (9.30–9.55 GHz). The samples were measured in 4 mm quartz glass EPR tubes at RT and 77K. 5,5-Dimethyl-1-pyrrolin-N-oxide (DMPO, 100 mm in either MeOH or benzene) was used as a spin trap to detect short-living radicals. Data evaluation was performed using "ESR-MPlot & Analyze" software. The final examination of recorded EPR spectra was carried out using OriginPro 9.0 software.

DPPH-Radical Detection Assay: The assay was performed according to a modified literature procedure.^[49] A 2,2-diphenyl-1-picrylhydrazyl (DPPH, $10^{-4}\ \text{M}$) stock solution in MeOH and benzene was prepared. A volume of 2 mL DPPH stock solution was added to each test sample. Reactions were carried out for 2 and 24 h at $37\ ^\circ\text{C}$ (and $70\ ^\circ\text{C}$) without stirring. For determination of remaining DPPH-radical, absorptions ($A_{520\text{nm}}$) of sample solutions and DPPH* stock solution were measured via UV/vis spectroscopy at 520 nm. Background absorption of the pure solvent was subtracted. The concentration of remaining DPPH-radical after sample exposition was determined according to Equation 1:

$$\text{Remaining [DPPH}^*] (\%) = \frac{A_{520\text{nm}}(\text{sample}) - A_{520\text{nm}}(\text{solvent})}{A_{520\text{nm}}(\text{DPPH stock}) - A_{520\text{nm}}(\text{solvent})} \times 100 \quad (1)$$

Horseradish Peroxidase (HRP) Assay for Hydrogen Peroxide Detection: Horseradish-peroxidase ($0.2\ \text{mg mL}^{-1}$) and pyrogallol ($2.5\ \text{mg mL}^{-1}$) were dissolved in a PBS solution (pH adjusted to 8.0). Grafted-poly-N-oxide samples were added and incubated for 5 min at $25\ ^\circ\text{C}$ under gentle shaking. For validation, a positive control with added hydrogen peroxide ($0.1\ \text{mM}$) and a negative control without hydrogen peroxide were evaluated under the same conditions. Absorptions ($A_{420\text{nm}}$) of test samples were measured via UV/vis spectroscopy at 420 nm. A blank value of PBS solution was subtracted. Residual enzymatic activity was determined relatively to the H_2O_2 -containing positive control using equation 2:

$$\text{Relative HRP activity (\%)} = \frac{A_{420\text{nm}}(\text{sample}) - A_{420\text{nm}}(\text{solvent})}{A_{420\text{nm}}(\text{positive control}) - A_{420\text{nm}}(\text{solvent})} \times 100 \quad (2)$$

Determination of Antibacterial Activity (ASTM E2149-13a): A modified ASTM assay E2149-13a was performed for evaluation of antimicrobial activity. All test samples were sterilized with iPrOH/water mixture (90 vol %)

and subsequently dried under laminar airflow (LAF) prior to testing. The bacterial strains *Staphylococcus aureus* (strain ATCC 29213) and *Escherichia coli* (strain ATCC 25922) were cultured on Columbia agar overnight. The overnight culture was suspended and diluted in sterile saline solution (0.9 %) to preserve a cell density of 1.5×10^8 (OD = 0.5) and diluted to a final concentration of 10^5 colony-forming units per milliliter (CFU mL⁻¹). Zwitterionized and pristine PE test specimens (surface area: 1.0 cm²) were placed in a 24-well plate (one specimen per well) and covered with 2.0 mL of the respective bacterial suspension (10^5 CFU mL⁻¹). The incubation was carried out at 37 °C under air for 2 h. Afterwards, the incubated solutions and three subsequent dilutions were incubated on Columbia Agar (100 µL of 10^5 , 10^4 , 10^3 and 10^2 CFU mL⁻¹) for 17 h at 37 °C, prior to cell counting. Colony counts above 250 CFU were set as “too numerous to count” (TNTC). Each experiment was performed as a triplicate. The log₁₀ reduction for each assay was calculated using following equation 3:

$$\log_{10} \text{ reduction} = \log \left(\frac{\text{colony forming units (CFU) before exposure}}{\text{colony forming units (CFU) after exposure}} \right) \quad (3)$$

Determination of Low-Fouling Activity (Adhesion Test): All test samples were treated with 90-vol % iPrOH and dried under laminar airflow (LAF) before testing. The strain *Staphylococcus aureus* (strain ATCC 29213) was cultured on Columbia agar overnight. The overnight culture was suspended and diluted in sterile saline solution (0.9 %) to preserve a cell density of 10^4 colony-forming units per milliliter (CFU mL⁻¹). Zwitterionized and pristine PE test specimens (surface area: 1.0 cm²) were placed in a 24-well plate (one specimen per well) and covered with each 1980 µL of Mueller Hinton Broth (MHB). 20 µL of the bacterial suspension was added to each well to obtain a starting cell density of 10^2 CFU mL⁻¹. The samples were incubated in bacterial solution for 24 h at 37 °C and were subsequently transferred into 3 mL of sterile saline solution without stirring or shaking for 10 min to remove loosely attached bacteria. Each foil was slightly pressed with the modified side onto an agar plate (Columbia agar) and removed after 30 s. Transferred cells were incubated for 20 h at 37 °C prior to cell counting. An aliquot of 100 µL supernatant was taken from each incubation experiment and analyzed with respect to bacterial growth in comparison to a positive control of MHB containing the initial bacterial suspension without added test specimens.

LIVE/DEAD Staining and Confocal Microscopy: Modified poly-*N*-oxide-PE and pristine PE specimens with a surface area of 0.8 cm² were immersed in a 6 well plate into 4 mL of *Vibrio campbellii* (strain BB120, OD_{600nm} 0.05) in artificial seawater. The samples were incubated 24 h at 28 °C under gentle shaking (100 rpm) to simulate natural growth conditions. After 24 h test specimens were rinsed with PBS buffer shortly to detach loosely attached planktonic cells. Fluorescence imaging to examine biofilm formation on the test samples was carried out using the LIVE/DEAD BacLight Viability Kit. Images were visualized via confocal laser scanning microscope LSM 800 with AiryScan from Zeiss (Jena, Germany) and edited with ZEN 2 (Blue Edition) software.

Agar Diffusion Plate Test: DIN EN ISO 20645: Leaching of antibacterial components from the poly-*N*-oxide-specimens was evaluated following DIN EN ISO 20645:2002-02 (agar-diffusion assay). Briefly, test specimens were placed with the poly-*N*-oxide-grafted surface facing downwards in a two-layer agar plate (Columbia agar). The top agar layer was previously covered with 200 µL of 1.5×10^8 CFU mL⁻¹ of either *S. aureus* (strain ATCC29213) or *E. coli* (strain ATCC25922) suspension. Plates were incubated for 20 h at 37 °C. The plates were then assessed for the development of an inhibition zone surrounding the test specimen.

Determination of Minimum Inhibitory Concentration (MIC): The minimum inhibitory concentration (MIC) of VBNOx, MANOx and MAANOx against *S. aureus* (strain ATCC29213) and *E. coli* (strain ATCC25922) was determined by the microdilution method (Methods for Dilution Antimicrobial Susceptibility Tests for Bacteria That Grow Aerobically; Approved Standard—Ninth Edition. CLSI document M07-A9. Wayne, PA: Clinical and Laboratory Standards Institute; 2012) and compared to the MICs of (vinyl benzyl)-trimethylammonium chloride (VBTAC) and benzalkoniumchloride (BAC). Tests were performed under air at 37 °C for 20 h. The MIC was defined as the minimum concentration to achieve transparent solu-

tions in the wells. As an upper limit, a concentration of 1024 µg mL⁻¹ of the test compounds was used.

Zwitterionization of PE-Foils with Grafted Poly-*N*-Oxides: PE foils with a thickness of 0.75 mm were rinsed with an isopropanol/water mixture of 70% (v/v) and dried for 15 min at 50 °C prior to use. Plasma treatment of the PE foils was performed at a distance of 6 mm between the plasma jet nozzle and the surface. The speed of the plasma jet nozzle was set at 110 mm s⁻¹. Samples were stored at room temperature under air for 8 min after plasma treatment. In a typical experiment, a solution of the appropriate polymerizable tertiary amine (VBDMMA, MADMA or MAADMA) (20 or 40 wt%) and 2,2'-Azobis(isobutyronitrile) (AIBN) as a free radical initiator (0.1 wt% or 1.0 wt%) in EtOAc was purged with nitrogen for 10 min. Plasma-treated PE foils were placed in the degassed solution containing the appropriate polymerizable tertiary amine and AIBN. The resulting reaction mixtures were purged with nitrogen for another 15 min and were subsequently polymerized for 2 h at 85 °C. After polymerization, the materials were treated with a EtOH/water mixture (70vol%) for 15 min with ultrasonication three times and dried for 30 min at room temperature. The resulting specimens were subsequently treated with an aqueous solution of hydrogen peroxide (30% w/w) for 72 h at room temperature under rapid shaking (150 rpm). Residual hydrogen peroxide was destroyed by immersion of the specimens into NaOH solution (1.0 mol L⁻¹) for 24 h at room temperature under gentle shaking. The resulting specimens were washed three times with EtOH/water mixture (70vol%) for each 15 min in an ultrasonic bath and dried for 30 min in a nitrogen stream and were stored before use at room temperature under nitrogen atmosphere.

Statistical Analysis: Statistics were performed using OriginPro 9 (2021) software. Data are reported as mean value ± standard deviation for continuous variables, or as a selective frequency for categorical variables, unless otherwise described. A pairwise comparison of the Tukey test was performed to determine statistical significance. A *p*-value of less than 0.05 (*) was considered significant.

Supporting Information

Supporting Information is available from the Wiley Online Library or from the author.

Acknowledgements

This work was supported by the University of Hamburg. Open access funding enabled and organized by Projekt DEAL.

Conflict of Interest

The authors declare no conflict of interest.

Data Availability Statement

The data that support the findings of this study are available in the supplementary material of this article.

Keywords

antibacterial materials, antifouling, *N*-oxides, reactive oxygen species, zwitterions

Received: June 15, 2023

Revised: July 25, 2023

Published online:

- [1] L. Hall-Stoodley, J. W. Costerton, P. Stoodley, *Nat. Rev. Microbiol.* **2004**, *2*, 95.
- [2] Y. X. Wang, J. L. Robertson, W. B. Spillman, R. O. Claus, *Pharm. Res.* **2004**, *21*, 1362.
- [3] H. C. Flemming, J. Wingender, U. Szewzyk, P. Steinberg, S. A. Rice, S. Kjelleberg, *Nat. Rev. Microbiol.* **2016**, *14*, 563.
- [4] a) S. Galie, C. Garcia-Gutierrez, E. M. Miguez, C. J. Villar, F. Lombo, *Front. Microbiol.* **2018**, *9*, 898; b) S. L. Percival, L. Suleman, C. Vuotto, G. Donelli, *J. Med. Microbiol.* **2015**, *64*, 323; c) W. Zhou, W. Li, J. Chen, Y. Zhou, Z. Wei, L. Gong, *RSC Adv.* **2021**, *11*, 25484.
- [5] a) I. Banerjee, R. C. Pangule, R. S. Kane, *Adv. Mater.* **2011**, *23*, 690; b) D. Rana, T. Matsuura, *Chem. Rev.* **2010**, *110*, 2448; c) A. M. C. Maan, A. H. Hofman, W. M. Vos, M. Kamperman, *Adv. Funct. Mater.* **2020**, *30*, 2000936; d) S. Zheng, M. Bawazir, A. Dhall, H. E. Kim, L. He, J. Heo, G. Hwang, *Front Bioeng Biotechnol* **2021**, *9*, 643722.
- [6] M.-C. Sin, S.-H. Chen, Y. Chang, *Polym. J.* **2014**, *46*, 436.
- [7] a) A. Venault, Y. Chang, *Langmuir* **2019**, *35*, 1714; b) J. B. Schlenoff, *Langmuir* **2014**, *30*, 9625; c) Y. Chang, *J. Polym. Res.* **2022**, *29*, 286; d) Q. Li, C. Wen, J. Yang, X. Zhou, Y. Zhu, J. Zheng, G. Cheng, J. Bai, T. Xu, J. Ji, S. Jiang, L. Zhang, P. Zhang, *Chem. Rev.* **2022**, *122*, 17073; e) S. Paschke, K. Lienkamp, *ACS Applied Polymer Materials* **2020**, *2*, 129.
- [8] Q. Shao, S. Jiang, *J. Phys. Chem. B* **2014**, *118*, 7630.
- [9] R. G. Chapman, E. Ostuni, S. Takayama, R. E. Holmlin, L. Yan, G. M. Whitesides, *J. Am. Chem. Soc.* **2000**, *122*, 8303.
- [10] a) S. Hiranphinyophat, Y. Iwasaki, *Sci. Technol. Adv. Mater.* **2021**, *22*, 301; b) K. Ishihara, N. P. Ziats, B. P. Tierney, N. Nakabayashi, J. M. Anderson, *J. Biomed. Mater. Res.* **1991**, *25*, 1397.
- [11] B. Cao, Q. Tang, G. Cheng, *J. Biomater. Sci., Polym. Ed.* **2014**, *25*, 1502.
- [12] a) A. B. Lowe, M. Vamvakaki, M. A. Wassall, L. Wong, N. C. Billingham, S. P. Armes, A. W. Lloyd, *J. Biomed Mater Res* **2000**, *52*, 88; b) C. Viklund, K. Irgum, *Macromolecules* **2000**, *33*, 2539; c) Y. Zhang, Y. Liu, B. Ren, D. Zhang, S. Xie, Y. Chang, J. Yang, J. Wu, L. Xu, J. Zheng, *J. Phys. D: Appl. Phys.* **2019**, *52*, 403001.
- [13] a) Q. Shao, S. Jiang, *J. Phys. Chem. B* **2013**, *117*, 1357; b) H. Du, X. Qian, *J. Comput. Chem.* **2016**, *37*, 877; c) C. Y. Chiu, Y. Chang, T. H. Liu, Y. N. Chou, T. J. Yen, *J. Mater. Chem. B* **2021**, *9*, 8437; d) S. Abraham, A. So, L. D. Unsworth, *Biomacromolecules* **2011**, *12*, 3567; e) Y. Higaki, J. Nishida, A. Takenaka, R. Yoshimatsu, M. Kobayashi, A. Takahara, *Polym. J.* **2015**, *47*, 811; f) J. F. Karthäuser, J. Koc, E. Schönemann, R. Wanka, N. Aldred, A. S. Clare, A. Rosenhahn, A. Laschewsky, *Advanced Materials Interfaces* **2022**, *9*, 2200677.
- [14] B. Li, P. Jain, J. Ma, J. K. Smith, Z. Yuan, H. C. Hung, Y. He, X. Lin, K. Wu, J. Pfaendtner, S. Jiang, *Sci. Adv.* **2019**, *5*, 9562.
- [15] I. O'Neil, *Sci. Synth.* **2009**, *40*, 860.
- [16] E. P. Linton, *J. Am. Chem. Soc.* **1940**, *62*, 1945.
- [17] J. Hunger, N. Ottosson, K. Mazur, M. Bonn, H. J. Bakker, *Phys. Chem. Chem. Phys.* **2015**, *17*, 298.
- [18] Q. Zou, B. J. Bennion, V. Daggett, K. P. Murphy, *J. Am. Chem. Soc.* **2002**, *124*, 1192.
- [19] Q. Zhang, M. A. Kelland, H. Frey, J. Blankenburg, L. Limmer, *Energy Fuels* **2020**, *34*, 6298.
- [20] J. Zhen, Z. Zhou, M. He, H. X. Han, E. H. Lv, P. B. Wen, X. Liu, Y. T. Wang, X. C. Cai, J. Q. Tian, M. Y. Zhang, L. Xiao, X. X. Kang, *Front. Endocrinol. (Lausanne)* **2023**, *14*, 1085041.
- [21] a) A. Rani, A. Jayaraj, B. Jayaram, V. Pannuru, *Sci. Rep.* **2016**, *6*, 23656; b) Y. T. Liao, A. C. Manson, M. R. DeLyser, W. G. Noid, P. S. Cremer, *Proc. Natl. Acad. Sci. USA* **2017**, *114*, 2479; c) T. C. Gluick, S. Yadav, *J. Am. Chem. Soc.* **2003**, *125*, 4418.
- [22] a) R. Lindigkeit, A. Biller, M. Buch, H. M. Schiebel, M. Bopppe, T. Hartmann, *Eur. J. Biochem.* **1997**, *245*, 626; b) T. Hartmann, G. Toppel, *Phytochemistry* **1987**, *26*, 1639; c) V. M. Dembitsky, T. A. Glorizova, V. V. Porokov, *Phytomedicine* **2015**, *22*, 183.
- [23] R. D. Bach, H. B. Schlegel, *J. Phys. Chem. A* **2021**, *125*, 5014.
- [24] a) D. Bernier, U. K. Wefelscheid, S. Woodward, *Org. Prep. Proced. Int.* **2009**, *41*, 173; b) A. Petrosyan, R. Hauptmann, J. Pospech, *Eur. J. Org. Chem.* **2018**, *2018*, 5237; c) A. M. Bauer, E. E. Ramey, K. G. Oberle, G. A. Fata, C. D. Hutchison, C. R. Turlington, *Tetrahedron Lett.* **2019**, *60*, 151193.
- [25] D. Yan, K. Wang, S. Bai, B. Liu, J. Bai, X. Qi, Y. Hu, *J. Am. Chem. Soc.* **2022**, *144*, 4269.
- [26] a) G. Cheng, B. Li, C. Wang, H. Zhang, G. Liang, Z. Weng, H. Hao, X. Wang, Z. Liu, M. Dai, Y. Wang, Z. Yuan, *PLoS One* **2015**, *10*, 0136450; b) Z. Shah, R. Mahbuba, B. Turcotte, *FEMS Microbiol. Lett.* **2013**, *347*, 61; c) C. Avendaño, J. C. Menéndez, in *Medicinal Chemistry of Anticancer Drugs*, (Eds.: C. Avendaño, J. C. Menéndez), Elsevier, Amsterdam **2008**, p. 93; d) S. E. Walsh, J. Y. Maillard, A. D. Russell, C. E. Catrenich, D. L. Charbonneau, R. G. Bartolo, *J. Appl. Microbiol.* **2003**, *94*, 240; e) P. Wardman, K. I. Priyadarsini, M. F. Dennis, S. A. Everett, M. A. Naylor, K. B. Patel, I. J. Stratford, M. R. L. Stratford, M. Tracy, *Br. J. Cancer* **1996**, *74*, 70.
- [27] X. Shen, K. S. Gates, *Chem. Res. Toxicol.* **2019**, *32*, 348.
- [28] a) M. Lv, Y. Li, X. Wei, Y. Xu, Z. Ge, X. Chen, *ACS Appl. Energy Mater.* **2019**, *2*, 2238; b) A. C. Griffin, A. M. Bhatti, G. A. Howell, *MRS Online Proc. Libr.* **1987**, *109*, 115.
- [29] a) H. W. Schlipkötter, A. Brockhaus, *Klin. Wochenschr.* **1961**, *39*, 1182; b) N. G. Puchkova, A. V. Nekrasov, Y. F. Razvodovskii, B. S. El'tsefon, *Polymer Science U.S.S.R.* **1980**, *22*, 1407.
- [30] N. Zhang, K. Cheng, J. Zhang, N. Li, X. Yang, Z. Wang, *J. Membr. Sci.* **2022**, *660*, 120829.
- [31] a) S. Kliewer, S. G. Wicha, A. Broker, T. Naundorf, T. Catmadim, E. K. Oellingrath, M. Rohnke, W. R. Streit, C. Vollstedt, H. Kipphardt, W. Maison, *Colloids Surf., B* **2020**, *186*, 110679; b) N. Burmeister, C. Vollstedt, C. Kröger, T. Friedrich, N. Scharnagl, M. Rohnke, E. Zorn, S. G. Wicha, W. R. Streit, W. Maison, *Colloids Surf., B* **2023**, *224*, 113195.
- [32] F. Khalil, E. Franzmann, J. Ramcke, O. Dakischew, K. S. Lips, A. Reinhardt, P. Heisig, W. Maison, *Colloids Surf., B* **2014**, *117*, 185.
- [33] G. L. Archer, *Clin. Infect. Dis.* **1998**, *26*, 1179.
- [34] a) I. Karunasagar, S. K. Otta, I. Karunasagar, *Aquaculture* **1996**, *140*, 241; b) C. M. Waters, B. L. Bassler, *Genes Dev.* **2006**, *20*, 2754.
- [35] S. Guo, D. Jańczewski, X. Zhu, R. Quintana, T. He, K. G. Neoh, *J. Colloid Interface Sci.* **2015**, *452*, 43.
- [36] C. Zhang, J. Zhou, X. Ye, Z. Li, Y. Wang, *Macromolecules* **2021**, *54*, 4236.
- [37] M. van de Lagemaat, A. Grotenhuis, B. van de Belt-Gritter, S. Roest, T. J. A. Loontjens, H. J. Busscher, H. C. van der Mei, Y. Ren, *Acta Biomater.* **2017**, *59*, 139.
- [38] H.-C. Flemming, J. Wingender, *Nat. Rev. Microbiol.* **2010**, *8*, 623.
- [39] Z. Temoçin, M. Yiğitoğlu, *Bioprocess Biosyst. Eng.* **2009**, *32*, 467.
- [40] Y. S. Raval, L. Flurin, A. Mohamed, K. E. Greenwood-Quaintance, H. Beyenal, R. Patel, *Antimicrob. Agents Chemother.* **2021**, *65*, 01966.
- [41] O. P. Sharma, T. K. Bhat, *Food Chem.* **2009**, *113*, 1202.
- [42] J. P. Gotham, R. Li, T. E. Tipple, J. R. Lancaster, T. Liu, Q. Li, *Free Radical Biology and Medicine* **2020**, *154*, 84.
- [43] a) L. Zhang, J. Sun, W. Huang, S. Zhang, X. Deng, W. Gao, *J. Am. Chem. Soc.* **2023**, *145*, 1707; b) J. Jin, P. Yuan, W. Yu, J. Lin, A. Xu, X. Xu, J. Lou, T. Yu, C. Qian, B. Liu, J. Song, L. Li, Y. Piao, T. Xie, Y. Shen, H. Tao, J. Tang, *ACS Nano* **2022**, *16*, 10327; c) H. Zhang, C.-H. Huang, *Environ. Sci. Technol.* **2005**, *39*, 593.
- [44] H. Huang, C. Zhang, R. Crisci, T. Lu, H. C. Hung, M. S. J. Sajib, P. Sarker, J. Ma, T. Wei, S. Jiang, Z. Chen, *J. Am. Chem. Soc.* **2021**, *143*, 16786.

- [45] W. Fan, Q. Wei, J. Xiang, Y. Tang, Q. Zhou, Y. Geng, Y. Liu, R. Sun, L. Xu, G. Wang, Y. Piao, S. Shao, Z. Zhou, J. Tang, T. Xie, Z. Li, Y. Shen, *Adv. Mater.* **2022**, *34*, 2109189.
- [46] X. Guan, K. Zhang, F. Huang, G. C. Bazan, Y. Cao, *Adv. Funct. Mater.* **2012**, *22*, 2846.
- [47] A. L. J. Beckwith, P. H. Eichinger, B. A. Mooney, R. H. Prager, *Aust. J. Chem.* **1983**, *36*, 719.
- [48] P. F. Holt, *Br. J. Ind. Med.* **1971**, *28*, 72.
- [49] M. Suzuki, A. Kishida, H. Iwata, Y. Ikada, *Macromolecules* **1986**, *19*, 1804.

6. Modification of Elastomers (not contributing to the cumulative part)

6.1 Charged Polymers Grafted from Elastomers for Offshore Applications

Nils Burmeister^a, Fabrizio Pagnanelli^b, Wolfgang Maison^a

^aUniversität Hamburg, Department of Chemistry, Bundesstrasse 45, 20146 Hamburg, Germany

^cContinental AG, ContiTech Deutschland GmbH, Hannoversche Strasse, 21079 Hamburg, Germany

As highlighted in section 3.1.2, marine biofouling is the most challenging process to modulate due to the wide variety of species involved and the changing environmental conditions. However, in its initial steps, marine biofouling is principally identical to other non-marine biofouling processes. Although marine biofouling involves as many species as no other, the initial microbial attachment only relies on 10 identified species. Thus, interfering with initial microbial adhesion is a crucial target for interference with marine biofouling. Since combinational antifouling properties are most likely more efficient, we identified a surface with initial non-adhesive ability due to a polyamide 6.6 (PA 6.6) surface modification with topographic features and thoroughly characterized the microstructure, which is responsible for the low surface energy. For further modification, we used atmospheric plasma activation, which is known to be adaptable to PA 6.6 substrates, which was followed by the upscaled *grafting from* approach *via* spray coating (developed and optimized in section 5.1). As polymer brushes, we grafted contact-active (p-VBTAC), non-adhesive p-(VBSB), and a combined active-non-adhesive-acting copolymer (p-(VBTAC-co-VBSB)) from these PA surfaces. The resulting graft polymers, along with the specific microstructure, were evaluated under laboratory conditions and in real-life seawater assays in a static and dynamic experimental setting. The following studies and results were obtained from April 2020 - October 2022 during the cooperation project “Development of an antifouling rubber compound for offshore underwater application” with the acronym “AFOUL” between the University of Hamburg, ContiTech and Edelbüttler and Schneider GmbH (E+S). The results were summarized in the patent application 2022P02354 DE (HACT).

6.1.1 Introduction

Seawater intake systems (SWIs), produced and applied by Continental AG, are a fundamental component in producing liquified natural gas (LNG). The primary use of seawater intake systems is found on FPSO/FLNG (floating production storage and offloading unit floating liquified natural gas) vessels for the initial stage of the gas liquefaction cooling process (Figure 17 A). SWIs are made out of rubber-based hose sections, with a length of approximately 11 meters, which are connected by PA 6.6-based flanges to reach the desired total length of 30-200 m. Regarding their use in marine environments, hose sections are constructed with a 20-30-year lifespan by considering all weather, flow, and wave conditions.

A significant issue in the application of SWIs is marine biofouling, which appears on nearly any submerged material, as explained in section 3.1.2. In this context, marine biofouling adds further complexity. Previous experiences have demonstrated that, after approximately six months, the system's total mass increases by 150%. Thus, biofouling contributes significantly to the total weight and a rise of the friction coefficient up to values from 2-4.¹²⁹, resulting in significant increases in power and energy consumption with subsequent CO₂ emission or systemic failure in the worst case. To overcome marine encrusting, a current approach is based on a cleaning process *via* hypochlorite. This toxic and environmentally hazardous compound is electrolytically generated directly on the respective FPSO/FLNG vessel units. Based on the EMA report Q2 2019 ¹²⁹, approximately 3600 tons of hypochlorite were used for purging and discharged into the seawater after use. This antifouling method severely impacts biodiversity, resulting in severe environmental damage, and is comparable to former antifouling TBT-release coatings.

The illustrated hazardous impact highlights the urgent need for an alternative to overcome marine biofouling and reduce environmental damage. Henceforth, we aimed to modify the base material directly by adapting established protocols, *i.e.*, plasma activation with subsequent graft polymerization to obtain covalently bound antifouling coatings. As a desired antifouling strategy, graft polymerization of cationic, zwitterionic, and a mixture of both charged monomers was considered. Another critical contribution provided the implementation of an antifouling topography. Specific texture features in the PA surface exhibit intrinsic non-adhesive ability, which offers the opportunity to generate multi-functional antifouling surfaces when combined with graft polymerization protocols.

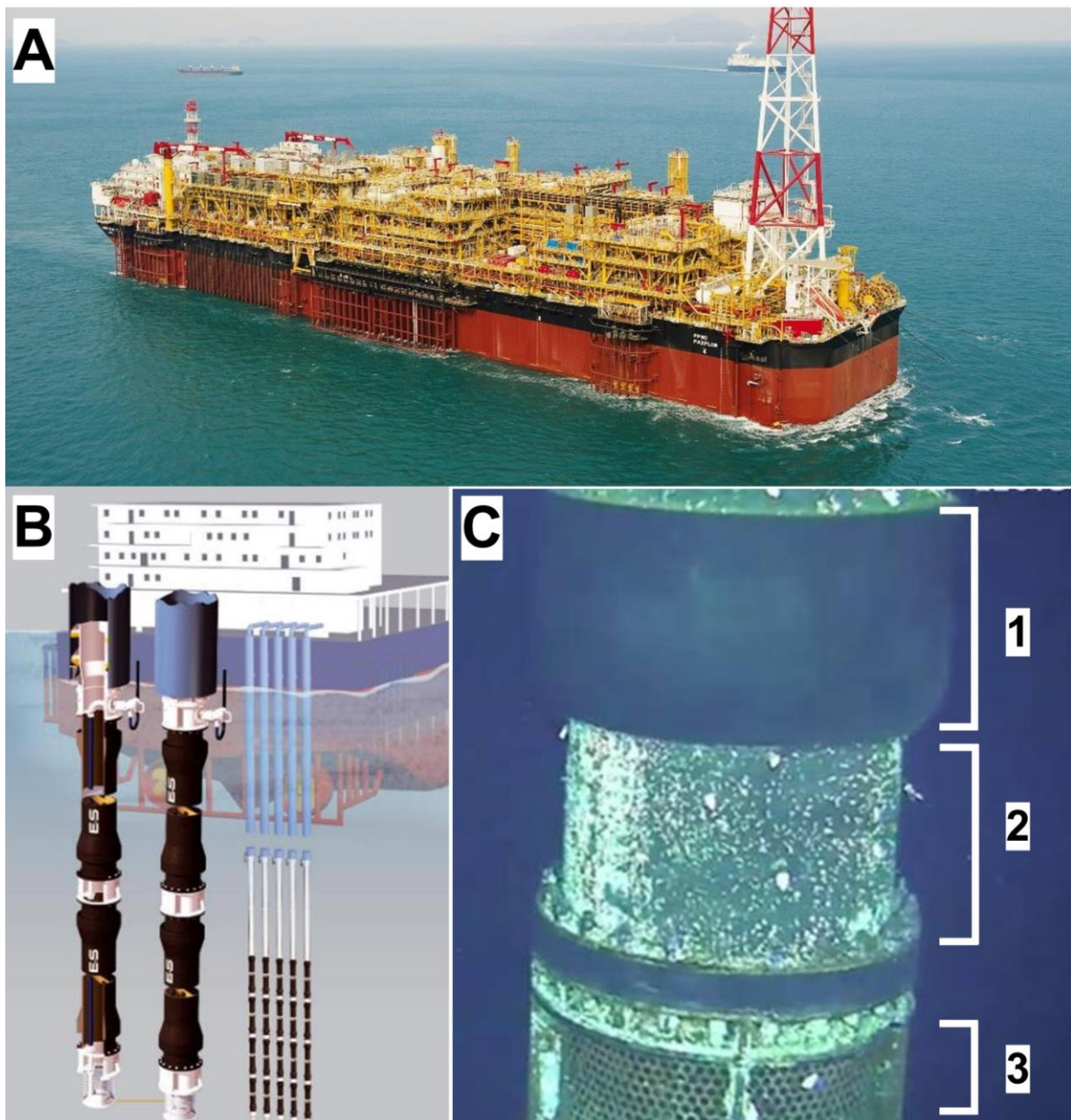


Figure 17: **A:** Image of a Floating Production Storage and Offloading Unit (FPSO) for producing liquified natural gas (LNG). **B:** Schematic illustration of the double-lined seawater intake system (SWI) for the cooling process manufactured by Continental AG and Edelbüttler and Schneider (E+S) GmbH. Image of a hose section during application in seawater **(C)** with the representation of the compositions of the different materials indicating different growth patterns: 1) polyamide 6.6 based-textile flange for connection. 2) rubber base KTL material. 3) Anchoring unit out of steel.¹²⁹

6.1.2 Materials and Methods

All standard chemicals were purchased as reagent grade and used without further purification prior to use. Solvents were used in HPLC grade unless otherwise stated. Rubber samples were provided from ContiTech and E+S GmbH and were cut into the desired size for each experimental setup described in the following sections. Phosphate-buffered saline (PBS) with a final concentration of 137 mM NaCl, 10 mM phosphate, 2.7 mM KCl and a pH adjusted to 8.0 was prepared as a stock solution. Microorganisms *Staphylococcus aureus* (strain ATCC29213) was purchased from the American Type Culture Collection. Crimp neck vials (N20, 10 mL volume) and crimp caps (N20, PTFE septum) for degassing were purchased from Macherey-Nagel GmbH (Düren, Germany). An airbrush (cup volume 600 mL) with an adjustable nozzle (1.4 mm) for grafting was purchased from Einhell (Landau, Germany).

Contact angle measurements

Water contact angles were obtained with an OCA 20 goniometer from DataPhysics (Filderstadt, Germany). This goniometer is equipped with three automated dispensing units for different liquid probes, a highspeed video system with a CCD camera, a measuring stage, and halogen lighting for static and dynamic contact angle measurements. For evaluation, independent triplicate measurements were done at three different points on the surface of each test specimen. Advancing contact angles were measured with deionized water using the static sessile drop method with a dispensing volume of 5 μL . The dispensing rate of the automatic syringe was set at 1 $\mu\text{L}/\text{min}$. The obtained angle was calculated with the OCA software.

Atmospheric air plasma activation

An atmospheric air plasma system from Plasmatreat GmbH (Steinhagen, Germany) was used for plasma activation. The atmospheric-pressure plasma was produced by a generator FG5001 with an applied working frequency of 21 kHz, generating a non-equilibrium discharge in a rotating jet nozzle RD1004 in combination with the stainless-steel tip No. 22826 for an expanded treatment width of approximately 22 mm. Additionally, the jet nozzle was connected to a Janome desktop robot type 2300N for repetitious accuracy regarding treatment conditions. The process gas was dry and oil-free air at an input pressure of 5 bar in all experiments.

Laser scanning microscopy

The surface analysis of the PU beams was carried out using a Keyence laser scanning microscope. The system is equipped with a VK-X250K controller and a VK-X260K microscope. The image acquisition of the plastic surface was performed with a laser of 408 nm wavelength (violet laser) using the VK acquisition module software. The Multi-File Analyzer software was used for data analysis.

Rubber surface modification *via* free radical polymerization

Rubber ((T+) KTL: natural rubber/styrene-butadiene polymer (NR/SBR)) samples that were coated with a polyamide 6.6 tape and a thickness of 2.0 mm were rinsed with an isopropanol/water mixture of 70 vol% and dried for 15 min at 50 °C before use. Plasma treatment was performed at a distance of 4 mm between the plasma jet nozzle and the surface. The speed of the plasma jet nozzle was set at 110 mm/s. Samples were stored at room temperature under air for 8 min after plasma treatment. A solution of the appropriate polymerizable monomer (20-40 wt%) and ammoniumperoxodisulfate (APS) or 2,2-azobisisobutyronitrile (AIBN) as a free radical initiator (1.0 wt%) and divinyl benzene (DVB) as a cross-linker (0.12 wt%) in deionized water (5.0 mL) was purged with nitrogen for 10 min. The degassed aqueous reaction mixture was transferred into an airbrush and vaporized at a distance of 5 cm under a nitrogen stream of 2 bar pressure onto the plasma-treated rubber samples until a homogenous thin film was formed. This procedure was repeated three times. The resulting rubber samples were subsequently polymerized for 2 h at 85 °C in a vacuum heater. After polymerization, the materials were placed in an EtOH/water mixture (70 vol%) for 1 h. The cleaning step was repeated three times with continuous renewing of the EtOH/water mixture (70 vol%). After washing, the resulting modified rubber samples were dried and stored at room temperature.

Synthesis of T+ p-(VBNOx) *via* free radical polymerization

Rubber ((T+) KTL: natural rubber/styrene-butadiene polymer (NR/SBR)) samples that were coated with a polyamide 6.6 tape and a thickness of 2.0 mm were rinsed with an isopropanol/water mixture of 70 vol% and dried for 15 min at 50 °C before use. Plasma treatment was performed at a distance of 4 mm between the plasma jet nozzle and the surface. The speed of the plasma jet nozzle was set at 110 mm/s. Samples were stored at room temperature under air for 8 min after plasma treatment. A solution of VBDMA as a polymerizable monomer (40 wt%) and 2,2-azobisisobutyronitrile (AIBN) as a free radical initiator (1.0 wt%) in deionized water (5.0 mL) was purged with nitrogen for 10 min. Plasma-

treated T+ were placed in the degassed aqueous solution. The resulting reaction mixtures were purged with nitrogen for another 15 min and were subsequently polymerized for 2 h at 85 °C. The resulting specimens were subsequently treated with an aqueous hydrogen peroxide solution (30% w/w) for 72 h at room temperature under rapid shaking (150 rpm). Residual hydrogen peroxide was decomposed by immersion of the specimens into NaOH solution (1.0 mol/L) for 24 h at room temperature under gentle shaking. The finally obtained T+-p-(VBNOx) samples were washed three times with EtOH/water mixture (70 vol%) for each 15 min in an ultrasonic bath and dried for 30 min in a nitrogen stream and were stored before use at room temperature under nitrogen atmosphere.

Synthesis of T+ p-(VBDSB) via free radical polymerization

Rubber ((T+) KTL: natural rubber/styrene-butadiene polymer (NR/SBR)) samples that were coated with a polyamide 6.6 tape and a thickness of 2.0 mm were rinsed with an isopropanol/water mixture of 70% (v/v) and dried for 15 min at 50 °C before use. The speed of the plasma jet nozzle was set at 110 mm/s. Samples were stored at room temperature under air for 8 min after plasma treatment. A solution of the appropriate polymerizable VBDSB (1.00 g, 2.85 mmol) and ammonium persulfate (APS) as a free radical initiator (0.11 mmol) in deionized water (2.5 mL) was purged with nitrogen for 10 min. Plasma-treated T+ were placed in the degassed aqueous solution. The resulting reaction mixtures were purged with nitrogen for another 15 min and were subsequently polymerized for 2 hours at 85 °C. After polymerization, the materials were treated with an EtOH/water mixture (70 vol%) for 15 min in an ultrasonic bath. The cleaning step was repeated three times with continuous renewing of the EtOH/water mixture (70 vol%). After washing, the resulting modified T+ p-(VBDSB) samples were dried for 30 min in a nitrogen stream before use.

Determination of antimicrobial activity (ASTM E2149-13a)

The antimicrobial evaluation was performed with a modified ASTM assay E21 49-13a.¹³⁰ All test samples were treated with 70 vol% isopropyl alcohol and dried at room temperature prior to testing. Test microorganisms (*Staphylococcus aureus* ATCC 29213) were grown on Columbia agar for 12 h and diluted to a concentration of an inoculum size of 10^5 CFU/mL in 0.9 wt% NaCl. Rubber samples (surface area of 2.0 cm²) were treated with 5 mL of the diluted bacterial suspension (10^5 CFU/mL) in 5 mL falcon tubes. The respective suspensions with the rubber samples were incubated for two hours under gentle shaking (120 rpm) at 37 °C. After incubation, the bacteria solution and three dilutions were incubated on Columbia agar (100 μ L

of the incubation solution, 1:10 and 1:100 dilution) for 18 h at 37 °C. After incubation, colonies were counted, and \log_{10} reduction in a triplicate measurement was calculated using equation 1.

$$\text{Bacterial log}_{10} \text{ reduction} = \log_{10} \left(\frac{N_0}{N} \right) \text{ (Equation 1)}$$

With N_0 = CFU (colony forming units) before incubation and N = CFU (colony forming units) after incubation.

Determination of low-fouling activity (bacterial adhesion test)

Before testing, all test samples were treated with 90 vol% iPrOH and dried under laminar airflow (LAF). The bacterial strain (*S. aureus* ATCC29213) was cultured separately for each assay on Columbia agar overnight. The overnight culture was suspended and diluted in sterile saline solution (0.9%) to preserve a cell density of 10^7 colony-forming units per milliliter (CFU/mL). Modified rubber samples and control specimens (surface area: 1.0 cm²) were placed in a 24-well plate (one specimen per well) and covered with each 1980 μ L of Mueller Hinton Broth (MHB). 20 μ L of the bacterial suspension was added to each well to obtain a starting cell density of 10^5 CFU/mL. The samples were incubated in bacterial solution for 24 h at 37 °C. They were subsequently transferred into 3 mL of sterile saline solution without stirring or shaking for 10 min to remove loosely attached bacteria. Each foil was slightly pressed with the modified side onto an agar plate (Columbia agar) and removed after 30 s. Transferred cells were incubated for 20 h at 37 °C prior to cell counting. Cell counts above 250 were set for evaluation as too numerous to count (TNTC). An aliquot of 100 μ L supernatant was taken from each incubation experiment and analyzed for bacterial growth compared to a positive control of MHB containing the initial bacterial suspension without added test specimens.

LIVE/DEAD staining and confocal microscopy

Pre-sterilized rubber samples with a total surface area of 0.8 cm² were immersed into 50 mL of natural seawater derived from the Baltic Sea (54°35'14.50"N, 10°17'76.60"E) and stored under gentle shaking (90 rpm) at 22 °C. Sample foils were taken after 21 days of incubation and rinsed with sterile PBS buffer prior to further analysis. Fluorescence imaging to examine biofilm formation on the modified rubber specimens, including controls, was carried out using LIVE/DEAD™ BacLight™ Viability Kit ¹³¹. Images were visualized *via* confocal laser scanning microscope LSM 800 with AiryScan from Zeiss (Jena, Germany) and edited with ZEN 2 (Blue Edition) software.

Real-life seawater tests under static conditions

The seawater test under static conditions was conducted in cooperation with Dr. Brill partner at the Dr. Brill partner station in Eilat, Israel (29°30'15.0"N 34°55'10.0"). This station is a component of "The Interuniversity Institute for Marine Sciences", which belongs to "The Hebrew University of Jerusalem" on the Red Sea. The plates with a rectangular size of 10 cm x 10 cm and a thickness of 2 mm containing both test and reference specimens were mounted on a grid on site. The reference plates were set up, while the test plates included an untreated rubber plate (KTL base material), which was used as a positive reference for evaluation. One rubber material coated with Hempel's foul release coating, "SilicOne" (PR SilicOne L & PR SilicOne R), was also used as a negative reference. All the test plates were tested according to the 'Standard Method for Testing Antifouling Panels in Shallow Submergence' outlined in ASTM D 3623-78a (2020) 132 at a depth of 4 m before being positioned before the pier. The samples were exposed for a total of 275 days (9 months) from the 14th of December 2021 until the 15th of September 2022.

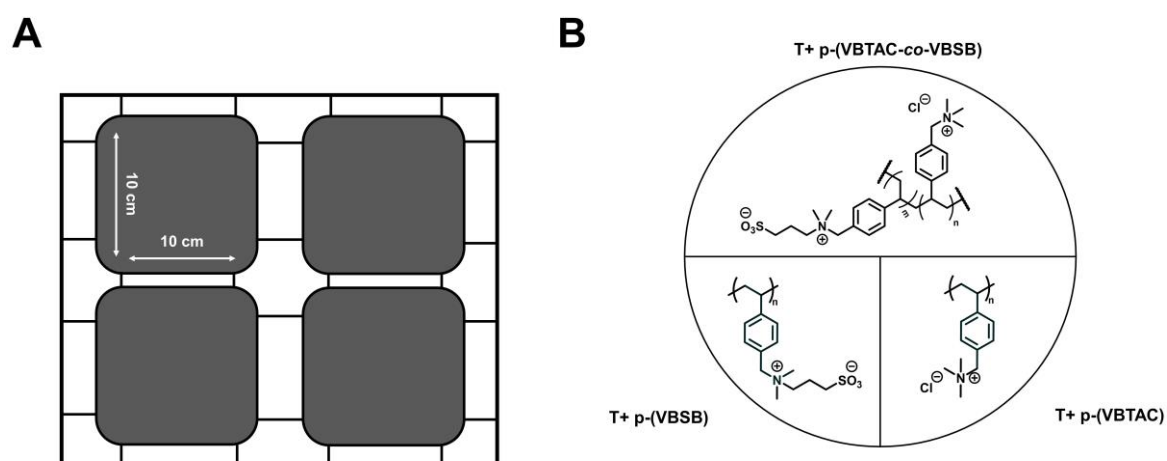


Figure 18: **A** illustrates the static seawater test rig and the respective installation of the test plates with a rectangular size of 10 cm x 10 cm. **B**: Chemical structures of the polymer brushes grafted from the rubber base material with a polyamide 6.6 wrapping tape on the surface.

Real-life seawater test under dynamic conditions

The seawater test under dynamic conditions was conducted in cooperation with Dr. Brill partner in Norderney, Germany (53°42'01.9" N 7°10'05.8" E). The size of the test plates was adapted to the RotoMarin® test rig and can be seen in Figure 19. For control purposes, one test plate was assessed with Hempel's SilicOne® serving as the negative control (Ctrl-), and an untreated Polyvinylchloride (PVC) plate was used as the positive control (Ctrl+).

The Institute for Antifouling and Biocorrosion has produced the RotoMarin® test rig to perform simulated dynamic field tests.^{132, 133} The respective test system considers different speed and

shear forces depicted in Figure 19. The approach is established on the ASTM D4939 - 89 (Reapproved 2020) - Standard Test Method for Biofouling and Fluid Shear Forces in Natural Seawater¹³³, which intends to expose marine antifouling coating to said forces. The plates were exposed for 62 days from the 10th of August until the 11th of October in 2022.

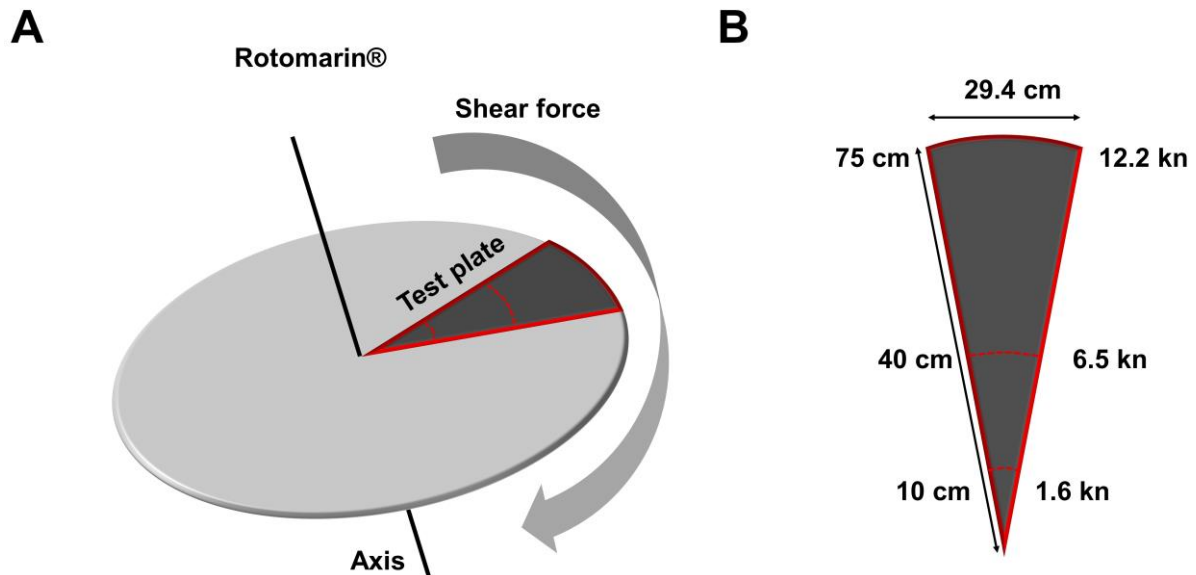


Figure 19: **A:** Scheme of the RotoMarin® test rig submerged into seawater at Norderney, Germany. **B:** Depiction of respective values of shear forces applied to the test plates and the rectangular size of the coated and non-coated test plates.

Statistics

Statistics were performed using OriginPro 9 (2021) software. Data are reported as mean value \pm standard deviation (SD) for continuous variables or as a selective frequency for categorical variables. A pairwise comparison *via* the Tukey test was performed to evaluate the antimicrobial test. A p-value of less than 0.05 was considered significant.

6.1.3 Results and Discussion

6.1.3.1 Characterization

Initial inspections of the seawater intake systems (SWIs) revealed areas that appear to be less affected by marine growth (Figure 17, part 1). The composition of these areas consists of rubber-based elastomers vulcanized with a polyamide 6.6 (PA 6.6)- based wrapping tape on the surface. This wrapping tape depicts a polymer composite of hexamethylenediamine and adipic acid (Figure 20 F). Based on the growth patterns associated with different material compositions, the characterization of the PA 6.6 modified elastomer indicated a specific topography with possible antifouling ability that was considered for further investigations. By determining the surface polarity through contact angle measurements of the PA 6.6 modified elastomer ($177.8 \pm 1.3^\circ$) compared to the base rubber KTL (natural rubber/styrene-butadiene polymer (NR/SBR)) material ($116.0 \pm 4.6^\circ$), we observed superhydrophobic properties (Table 2). Further investigations *via* laser scanning microscopy revealed a unique uniform roughness and 3-dimensional structure of the polyamide surface. The structure is defined as a concave pattern by regularly spaced concave lobes at 90 μm intervals, with a length of 520 μm , measured from the center of the lobes' two highest points (at 284.9 μm). The total height difference was 344.7 μm (Figure 20 B-F). The mean 2-dimensional line roughness (R_a) was found to be 96.8 μm , and the measured 3-dimensional surface roughness (S_a) was 78.0 μm (Table 2), overall indicating microstructured surface.

Table 2: Polymerization conditions and selected physicochemical properties for the respective polymer brushes.

Material	Monomer XX conc. [wt%]	RI YY conc. [wt%]	DVB conc. [wt%]	WCA [$^\circ$] ^{c)}	R_a [μm] ^{d)}	S_a [μm] ^{e)}
T+ ^{a)}		-	-	177.8 ± 1.3	96.8	78.0
T+ p-(VBSB)	10 VBSB	1.0	0.12	37.7 ± 4.1	96.1	74.0
T+ p-(VBTAC)	40 VBTAC	1.0	0.12	28.9 ± 5.5	91.7	71.1
T+ p-(VBTAC-co-VBSB)	10 VBTAC/ 10 VBSB	1.0	-	78.3 ± 27.8	97.6	77.9
Pristine rubber ^{b)}	-	-	-	116 ± 4.6	3.4	2.6

^{a)} Rubber base material with added topography *via* PA 6.6. ^{b)} pristine rubber with neither PA 6.6 nor any graft-polymer modification. ^{c)} Advancing water contact angles ($n \geq 6$) are presented as mean value \pm SD ^{d)} average 2-dimensional roughness of the surface ^{e)} Average 3-dimensional roughness of the surface determined by laser scanning microscopy.

According to previous reports, PA 6.6 is compatible with plasma activation protocols and applicable for plasma-mediated graft polymerization.¹³⁴ Since scalable plasma polymerization

was established *via* spray-coating (section 5.1), we adapted this approach by using comparable reaction conditions to those we used for polyethylene surfaces. Based on the antifouling evidence of our latest studies¹³⁵⁻¹³⁷, we decided to graft polymerize cationic p-(VBTAC) as a known contact-biocidal agent, zwitterionic p-(VBSB), as low-fouling sulfobetaine-derivative and a combination of both, cationic and zwitterionic p-(VBTAC-co-VBSB), from the PA 6.6 surfaces. An illustration of the framework and the resulting polymer brushes is given in Figure 20 A.

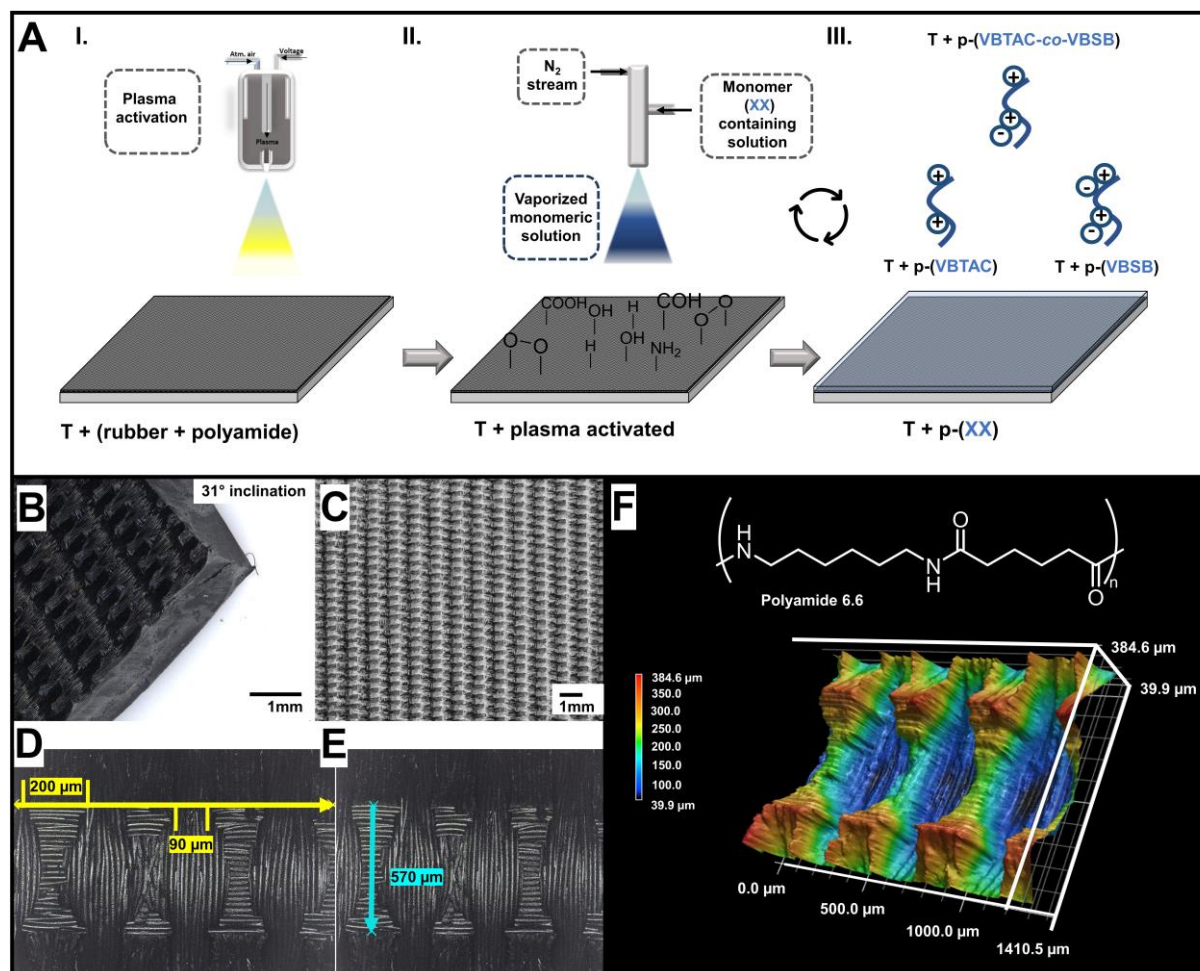


Figure 20: A: Scheme of plasma graft polymerization procedure on PA 6.6 vulcanized rubber and the resulting graft polymer brushes. B-F: Laser scanning microscopy of the PA 6.6 surface inducing superhydrophobic properties. B: Overview of the rubber-modified sample depicting a merged material due to vulcanization processes of the rubber bulk material with PA 6.6. C: Overview of the regular microstructure pattern. Microscale measurement of the relevant spacing between the concave invaginations (90 μm) and the size of the salient units (200 μm). E: Length between the salient units' two highest points (570 μm) creating the structured pattern. F: Three-dimensional illustration with an included heat map of the PA 6.6 texture.

In contrast to previous procedures, we repeated the transfer of the monomeric solution *via* airbrush, including plasma exposure, three times. Such repetition is a standard procedure for plasma-mediated grafting from polymerization, which induces initial polymerization reactions and an initial cross-linking reaction due to the plasma exposure, thus correlating to higher

grafting yield and stability.¹³⁸ To confirm successful grafting, we monitored the polarity of the surface by advancing water contact angle measurement. We detected a significant decrease of the initial superhydrophobic surface of $\sim 178^\circ$ to values in the range of $30\text{--}80^\circ$, indicating accomplished modification of the PA surface. The initial monomeric concentrations, as well as resulting water contact angles after polymerization, are given in Table 2. For the copolymer of p-(VBTAC-co-VBSB), a 1:1 distribution *via* NMR was detected, confirming the presence of both zwitterionic and cationic structures (Figure 21 D). Another important factor in the development of long-term functional polymer brushes is thermostability. For method validation, the respective polymers must withstand temperatures higher than 100°C to be compatible with the repetition of plasma exposure.¹³⁸ For further practical uses, temperatures in the $285\text{--}305^\circ\text{C}$ range are only considered during sterilization processes and can be neglected to interpret the described seawater application. We, therefore, determined the initial thermostability of the respective homopolymers *via* thermogravimetric measurements (TGA) (Figure 21 A-C). Results imply high thermal resistance up to 300°C , where typically eliminations of the quaternary ammonium group appear.¹³⁹

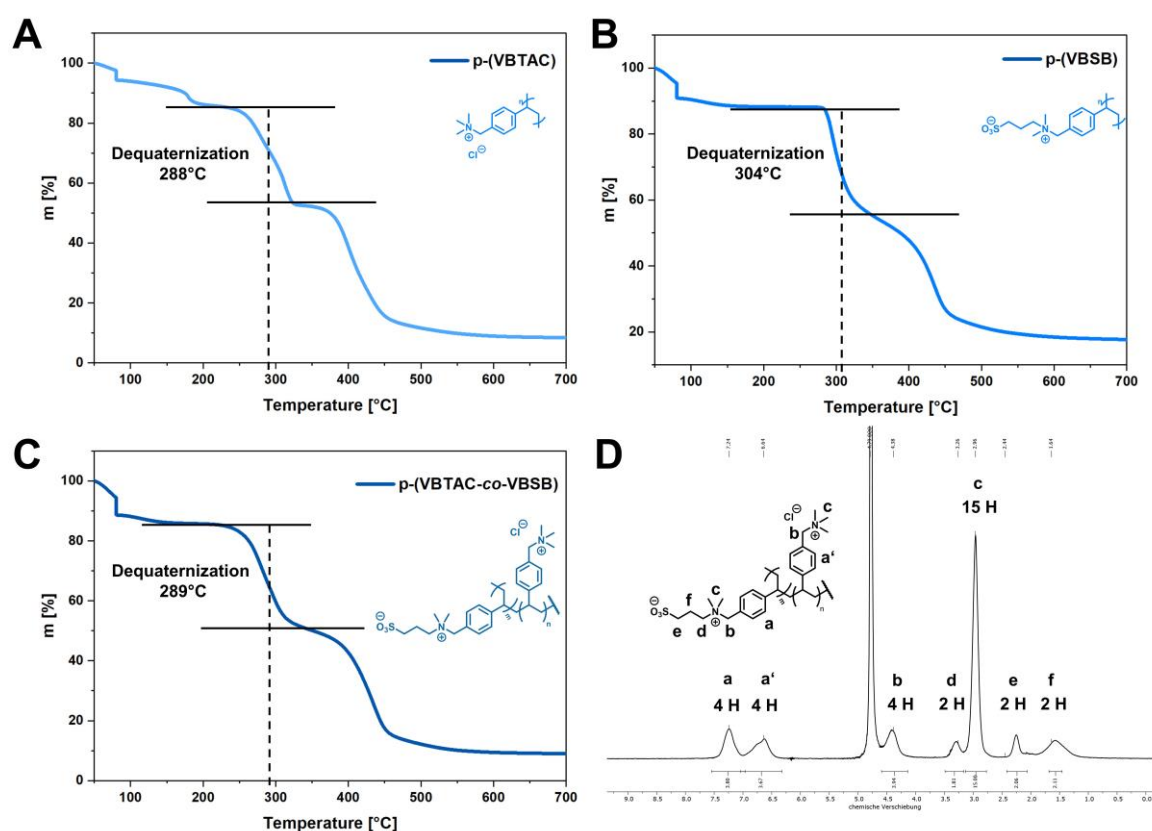


Figure 21: Thermogravimetric measurements of the homopolymers of **A:** p-(VBTAC), **B:** p-(VBSB) and **C:** p-(VBTAC-co-VBSB). The dequaternization step of the ammonium group is outlined and used as a reference for comparison. **D:** The ^1H NMR spectrum, recorded in D_2O at 400 MHz, indicates a 1:1 polymerization resulting in an equal distribution of VBTAC and VBSB monomeric units

Notably, the highest thermostability was detected for the zwitterionic p-(VBSB) homopolymer, likely associated with enhanced inter- and intrachain interaction.

6.1.3.2 Microbiological Assessment

Several studies of topographic features on micrometer scales indicate low surface wettability and low surface energy, resulting in anti-adherent surface properties. In the case of submerged materials, the so-called CASSIE-BAXTER state directs low-fouling abilities by entrapping air within the micropatterns. This physical state creates an energetic barrier for microorganisms to attach (Figure 15 A). Conversely, microstructure depicts a physical scaffold that protects microorganisms and biomaterial to resist mechanical stress, such as shear forces. The latter includes the tendency of bacteria to attach to spatial structures that are generally larger than themselves, allowing interfacial attachment interactions (Figure 22 C).³⁶ Both counteracting mechanisms of interactions are reflected in the bacterial adhesion assay, which was used to determine low-fouling effects. Results indicate a lower microbial adhesion (CFU/cm²) after 24 hours (Table 3) than pristine rubber without microstructure. In contrast, a modest low-fouling effect of T+ was observed compared to the materials with additional graft polymer (T+(p-XX)). The latter suggests a superior antifouling effect due to a combination of microstructure with polymer brushes.

Table 3: Results of the microbiological evaluation under laboratory conditions.

Material	Log ₁₀ reduction ^{c)}	Bacterial adhesion [CFU/cm ²] ^{d)}
T+ ^{a)}	0.0 ± 0.0	194 ± 11
T+ p-(VBSB)	0.0 ± 0.0	152 ± 36
T+ p-(VBTAC)	4.0 ± 0.1***	Not applied
T+ p-(VBTAC-co-VBSB)	3.2 ± 0.3***	84 ± 30***
Pristine rubber ^{b)}	0.0 ± 0.0	> 250 (TNTC) ^{e)}

^{a)} Rubber base material with added topography *via* a PA 6.6 texture. ^{b)} Pristine rubber with neither added topography *via* a PA 6.6 wrapping tape nor graft polymer. ^{c)} Log₁₀ reduction values for the antimicrobial determination *via* ASTM E2149-13a. Values are presented as mean values ± SD (n ≥ 3). Log₁₀ reduction was calculated as described in the materials and method section. ^{d)} Results of the bacterial adhesion assay presented as mean value ± SD in the units of CFU/cm². ^{e)} Values above 250 colony counts were set as too numerous to count (TNTC). Statistical significance was determined *via* pairwise comparison using the Tukey-Test p ≤ 0.001 (***).

In this context, laser scanning microscopy of the resulting graft polymers (p-VBTAC, p-(VBSB) and p-(VBTAC-co-VBSB) from polyamide surfaces indicate similar parameters for 2- and 3-dimensional surface roughness compared to the non-grafted polyamide reference (T+). This observation reveals the maintained microstructure and preservation of the intrinsic low-fouling

property. The results of the bacterial adhesion assay of the zwitterionic p-(VBSB) confirmed enhanced anti-adhesive properties. Even lower cell counts were detected for the combined graft-polymer p-(VBTAC-co-VBSB), indicating a synergistic effect by combining cationic and zwitterionic polymer on a micro-structured surface modification. The antibacterial activity was measured using the ASTM E2149-13a, a standard assay for antibacterial materials.¹³⁰ Results presented as \log_{10} reduction are given in Table 3. As a known contact-biocide agent, the cationic p-(VBTAC) showed excellent bacterial eradication against *Staphylococcus aureus*, a standard pathogen for clinical and industrial biofilm formation.¹⁴⁰ The combined modification p-(VBTAC-co-VBSB) depicts a \log_{10} reduction of 3.2 ± 0.3 , indicating a reasonable antimicrobial effect for industrial application.¹³⁰

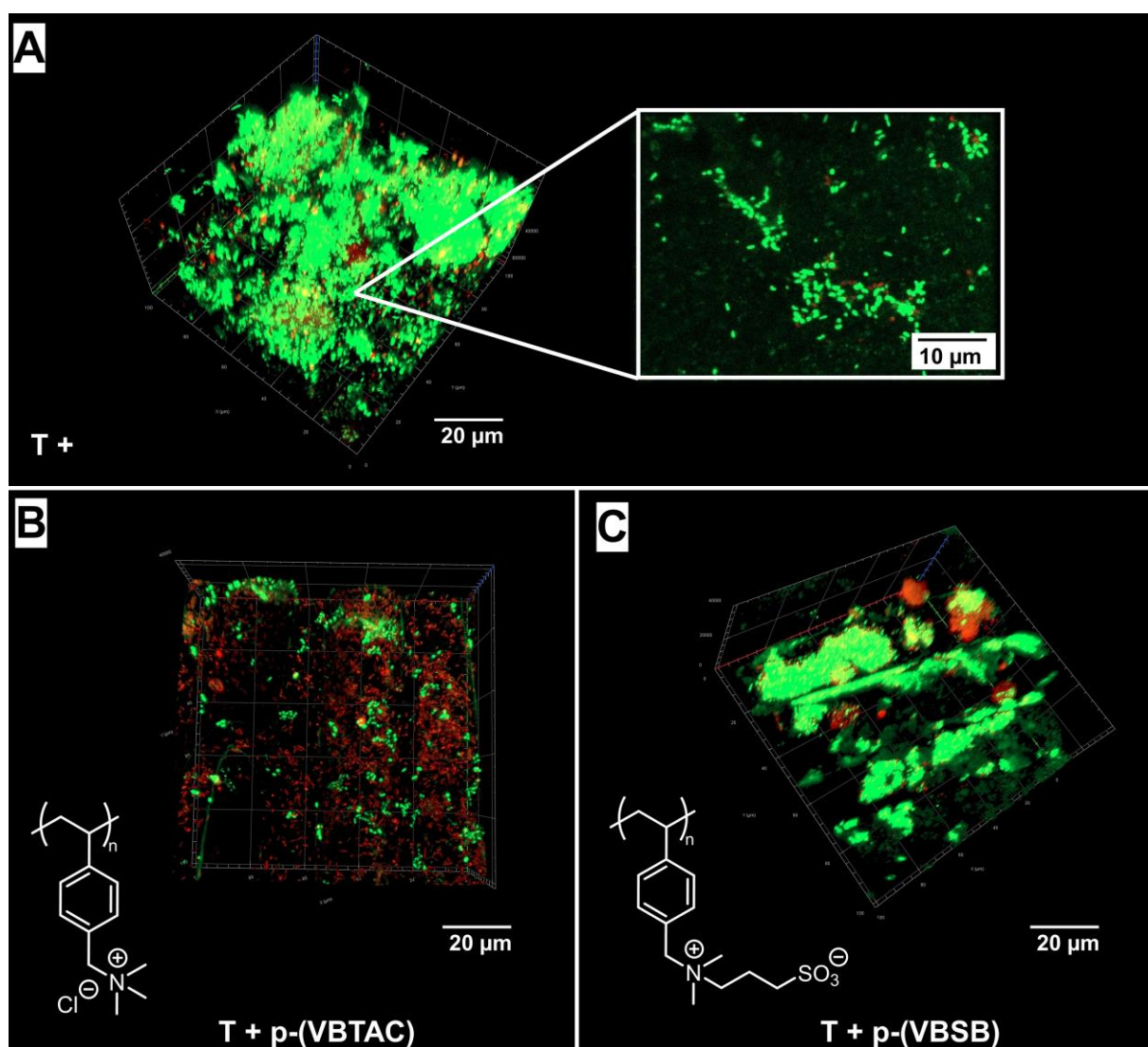


Figure 22: Biofilm imaging after 21 days past incubation in seawater. **A:** Rubber with PA 6.6 surface (T+). **B:** Cationic contact-biocide modification grafted from the PA surface (T+p-(VBTAC)). **C:** Zwitterionic SB was grafted from the PA surface (T+p-(VBSB)) for low-fouling modulation. Imaging was carried out by LIVE/DEAD™ staining with subsequent confocal microscopy. Living bacteria appear light green, and dead cells appear red.

Furthermore, we investigated the antifouling behavior of the grafted polymers in marine environments. Samples of T+ and grafted T+-p-(VBTAC) and T+-p-(VBSB) with a rectangular size of 0.8 cm² were incubated in samples of Baltic seawater (54°35'14.50"N, 10°17'76.60"E) at 22 °C for 21 days followed by LIVE/DEAD™ staining and confocal imaging. T+-p-(VBTAC) depicts high amounts of dead cells (Figure 22 B), which correlates with the previously observed contact-biocidal activity (Table 3). The zwitterionic modification (T+ p-(VBSB)) shows areas without accumulation of microorganisms, implying less biofilm formation than T+, which displays the highest percentage of visible biofilm after 21 days. Detailed imaging shows smaller *coccus*-like microorganisms. We hypothesize that the pure topography in the micrometer range provides the mentioned physical protection for non-motile microorganisms such as *Staphylococci* since their attachment and accumulation are predominantly based on sedimentation.²³ To confirm such a hypothesis, future analysis of biofilm-related transcriptomes would be crucial.

6.1.3.3 Seawater Assays

The microbiological assessment of the modifications, low-fouling, and antibacterial properties under controlled laboratory conditions provides a selective experimental setup for further testing under seawater conditions. This is evident from the division of the marine biofouling process into chronological phases initiated by microbial biofilm formation (Figure 25 A).²⁵ Further attachment and integration of marine diatoms to microbial biofilms form the upper limit of microfouling and, simultaneously, the transition between reversible microfouling and irreversible macrofouling as the final phase of marine biofouling. For final seawater testing, we exploit two different experimental setups and locations. The latter was chosen to cover a high number of biofouling-involved species and multiple environmental parameters such as pH value, salinity, and temperature fluctuations. Static and dynamic conditions were selected since the respective graft polymers partially rely on shear forces such as the passive low-fouling p-(VBSB) and p-(VBTAC-co-VBSB) modifications.

Primarily, the static seawater test was performed in Eilat, Israel, from December 2021 until October 2022, with an average temperature of 21-30 °C and a salinity of around 4.1‰, exhibiting a marine macrofauna dominated by bryozoans, tubeworms, and (green) algae.¹⁴¹ Briefly, test specimens with an overall size of 10 cm² were submerged for 9 months at a sea depth of 4 m. For experimental validation, a positive control of pristine KTL-rubber (Ctrl+) and a negative control (Ctrl-) of rubber dyed with a commercially available antifouling paint ("SilicOne" by HEMPEL©). Each month, biofouling samples were taken and analyzed for marine coverage according to ASTM D 6990-20 (Standard Practice for Evaluating Biofouling

Resistance and Physical Performance of Marine Coating Systems) protocol.¹³² The overall fouling was determined each month as a sum of the percentages of the involved organisms and algae. The overall results of each month are illustrated in Figure 23. All modifications exhibit significantly lower fouling rates than pristine KTL rubber after 9 months. Especially the combination of cationic and zwitterionic functionalities (T+ p-(VBTAC-co-VBSB)) reveals an overall excellent fouling rate of only 19%, similar to the commercially available antifouling coating “SilicOne” by HEMPEL© (Ctrl -) (15%). The modest antifouling quality of both zwitterionic T+-p-(VBSB) and non-grafted but micro-structured T+ can be explained by missing shear forces, which both modifications rely on. The cationic T+-p-(VBTAC) might indicate micro- and macrofouling events due to dead material attachment due to the positively charged surfaces. The latter is often associated with higher biomaterial attachment and is also claimed to be a general disadvantage of contact-active cationic modifications.⁵⁷ (section 3.2.1).

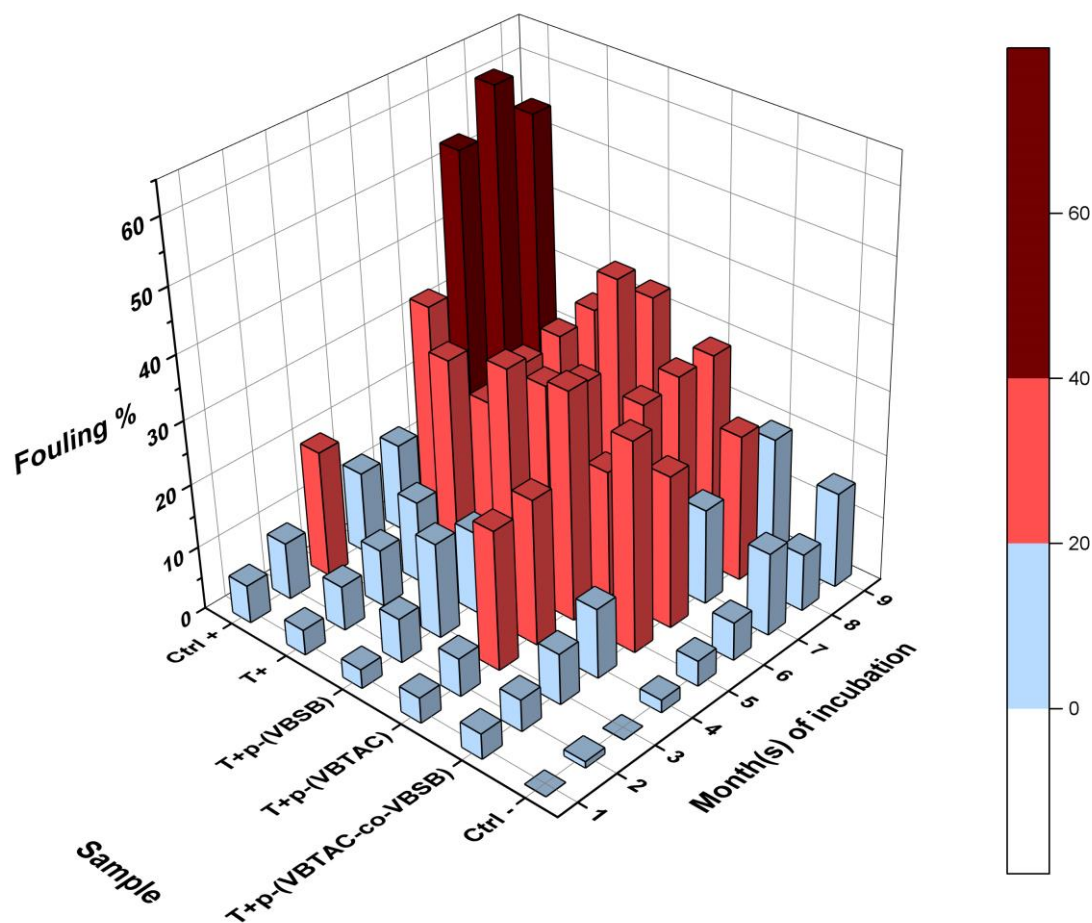


Figure 23: Overall results of the static seawater test with a total duration of 9 months of seawater exposure in Eilat, Israel. In the static experiment, a negative control (Ctrl-; SilicOne” by HEMPEL©) with known antifouling properties shows comparable overall fouling (15%) to the developed modification T+ p-(VBTAC-co-VBSB) (19%). Additional unmodified elastomer (pristine rubber KTL-base material) was used as a positive control (Ctrl +), depicting the overall highest fouling rate of ~60%.

For evaluation of macrofouling patterns, all test plates were analyzed regarding eight different species that are mainly involved in marine biofouling, e.g., barnacles, oysters, tubeworms, bryozoans, hydroids, tunicates, amphipods, sponges and algae.²⁸ The detailed growth analysis illustrated as fouling rates (%) within 9 months of incubation are given in Figure 24. Results demonstrate different patterns of macrofouling for all tested materials, including positive and negative control. These differences are most likely attributed to each surface's different chemical compositions and microstructures enabling selective biofilm formation resulting from particular cell-surface interactions (as highlighted in section 3.2), leading to such individual marine macro-colonization (section 3.1.2).

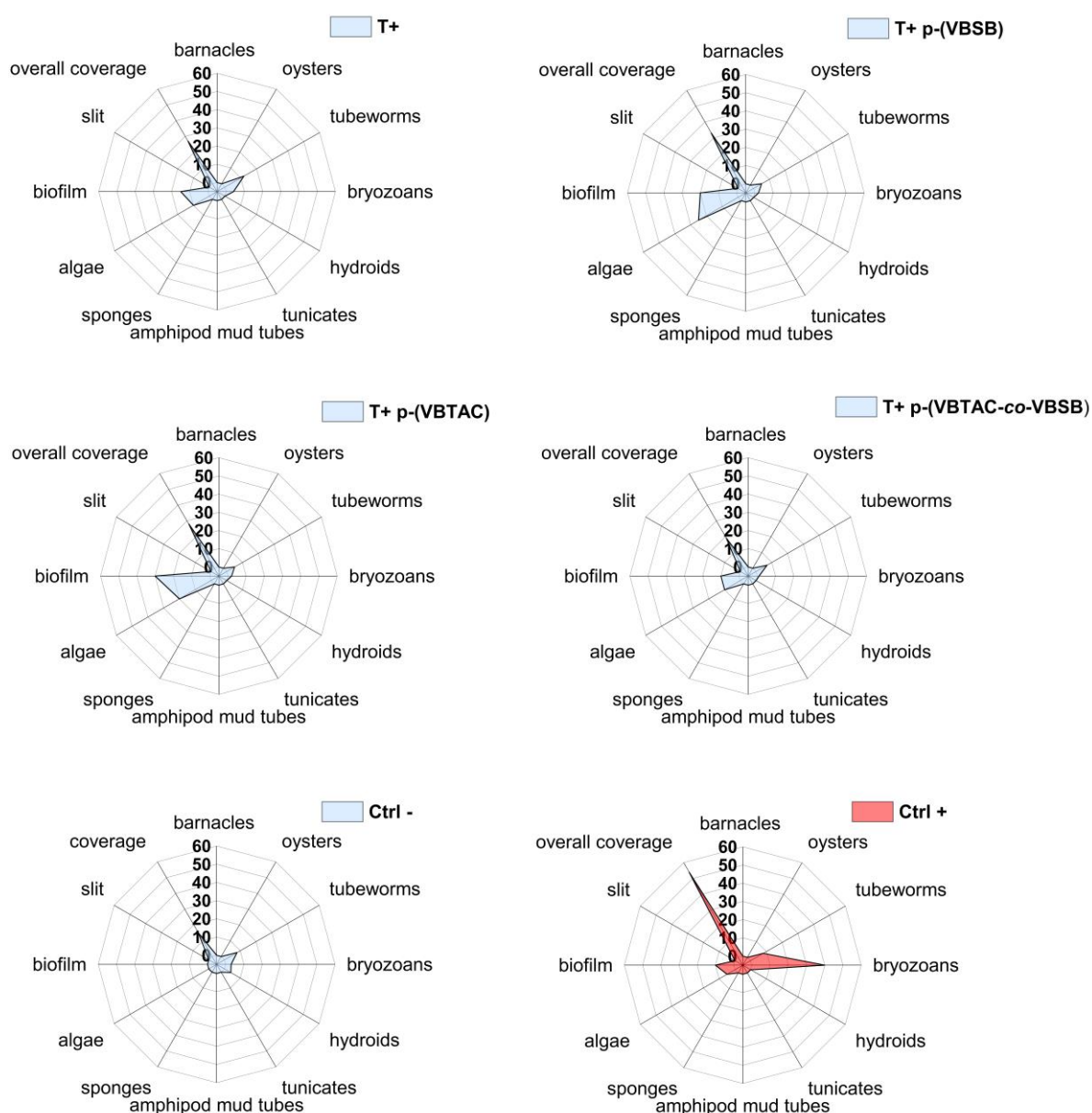


Figure 24: The breakdown of the organisms involved in overall biofouling for the respective graft polymers of the elastomers and the corresponding controls after 9 months of incubation.

However, the T+p(VBTAC-co-VBSB) modified elastomer depicts low coverage of all enumerated marine species, similar to the positive control, confirming a long-term antifouling effect. These results are in line with the previously reported laboratory assessments. Notably, biofilm coverage (Figure 24) for T+(VBTAC) of 30% and T+(VBSB) of 20% are significantly higher than the combined graft-polymer of T+(VBTAC-co-VBSB) (10%), which again indicates the previously reported synergistic effect. Furthermore, the identification of critical organisms that are responsible for macrofouling events is essential for the evaluation of the seawater assays. In most studies, the coverage of bryozoans is considered an organism of interest to determine the quality of the applied antifouling specimens since their encrusting is associated with strong biofilm formation (section 3.1.2 Table 1). In addition, bryozoans are linked to severe bio-corrosive processes¹⁴² and are one of the dominating fouling species³⁰ that impair the friction coefficient and thus power and energy consumption in marine applications.^{25, 27, 28}

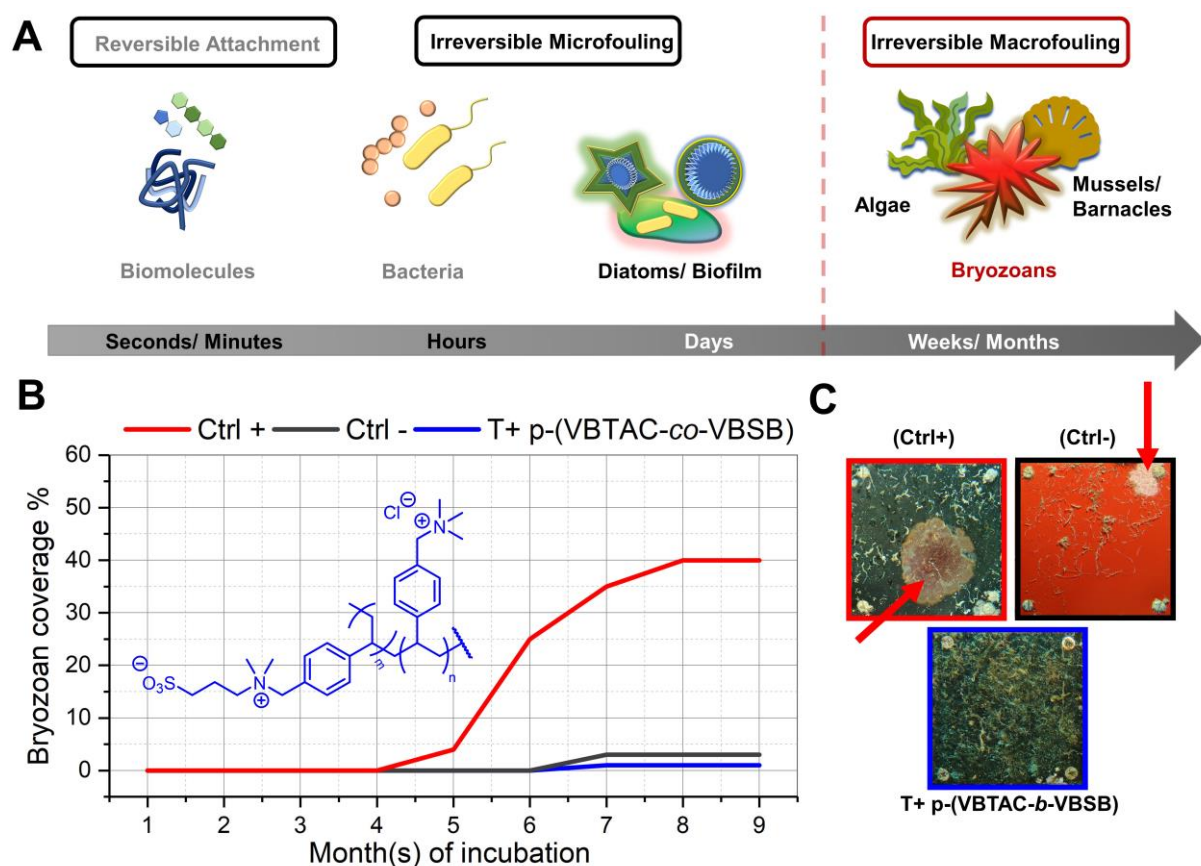


Figure 25: **A:** Overview of the timescale of the irreversible macrofouling events in a marine environment. **B:** Monthly recorded bryozoan coverage for KTL-based rubber (Ctrl +), Antifouling paint "SilicOne" (Ctrl -), and modified T+p-(VBTAC-co-VBSB) elastomer as an indicator for irreversible macrofouling and potential strong biofilm formation. Images of the respective bryozoan encrusting are depicted by red arrows (**C**).

For the overall performance of T+ (p-VBTAC-co-VBSB), the bryozoan coverage within 9 months reaches a value of only 1%, which is significantly lower than the non-modified rubber (40%), used as the positive control (Ctrl+). Most notably, slightly higher bryozoan encrusting

(3%) was detected for the applied negative control (Ctrl-) in comparison to the modified T+ p-(VBTAC-co-VBSB).

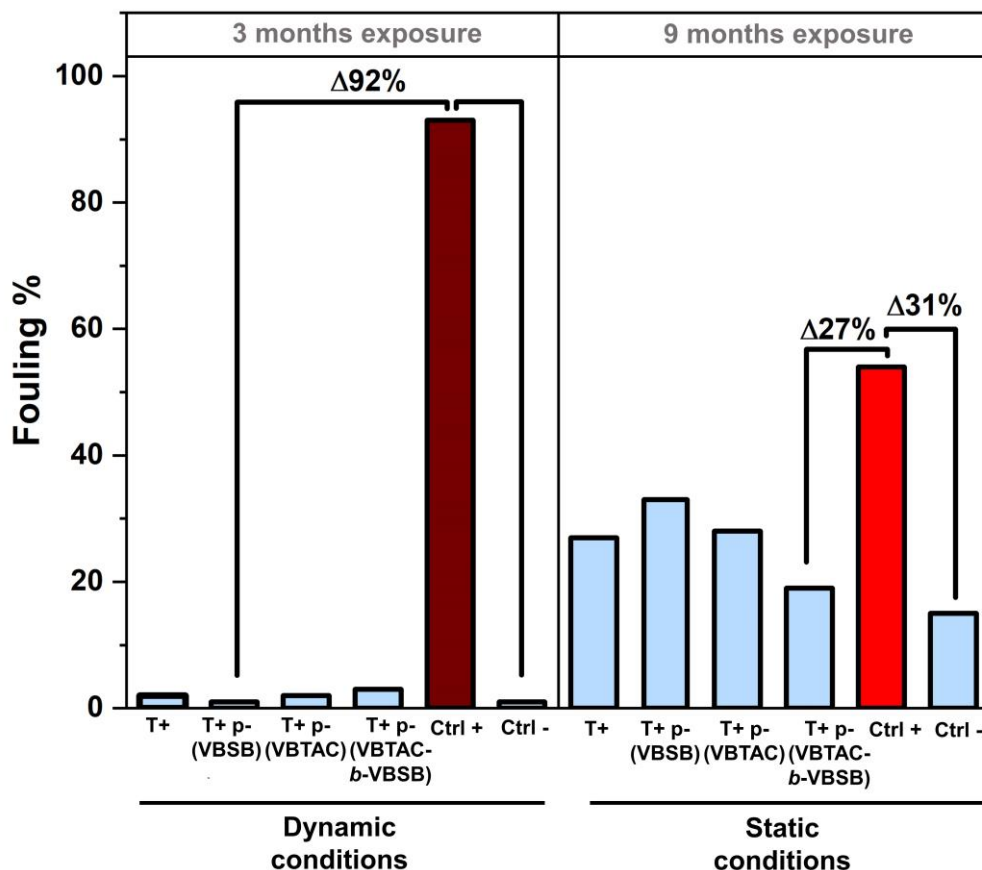


Figure 26: Final results of both seawater tests under dynamic conditions (**left side**) and static conditions (**right side**). Under applied shear forces of 0.82 m/s, the passive-acting zwitterionic T+ p-(VBSB) material shows a fouling resistance of 99%, equal to the negative control. It is 92% more effective than the applied positive control (PVC). Static measurement of T+ (p-VBTAC-co-VBSB) reveals a value of 27% more effectiveness than the non-modified rubber.

A dynamic seawater assay was performed in Norderney, Germany, to evaluate the antifouling efficacy of the modified rubber surfaces. To ensure constant shear forces, all test plates, including the negative (“SilicOne” by HEMPEL ©) and positive controls, in this case, made from polyvinyl chloride (PVC), were placed in the RotoMarin© device, a standard method for testing antifouling properties. The applied shear forces were set to 0.82 m/s. The overall exposure time was set to 3 months due to time restrictions of the project. Within these 3 months, the marine fouling was inspected according to standard protocol ASTM D 6990-20. The final results of the fouling coverage (in %) (Figure 26) depict an excellent performance of T+ p-(VBSB) (1%), the zwitterionic modification, whose antifouling effect in marine biotopes has been confirmed in previous studies (section 5.1). The additive effect is likely due to the maintained topography, which exhibits intrinsic low-fouling ability and thus enhances the

passive antifouling performance reflected in the bacterial adhesion assays (Table 3). However, all modified elastomer compounds performed significantly better than the applied PVC (Ctrl+). Furthermore, the modified elastomers showed no significant difference from the applied negative control (“SilicOne” manufactured by HEMPEL®), which confirms the high antifouling capacity of all modifications independent from the used location.

6.1.3.4 Environmental Impact

To finalize the efficacy of the rubber modifications as a sustainable and bio-friendly alternative for the current seawater intake system cleaning *via* hypochlorite, the overall savings regarding hypochlorite and carbon dioxide (CO₂) emissions were calculated prospectively (Table 4).

Table 4: Prospective calculations on savings

Elastomer	Hypochlorite per FPSO or FLNG [t]	CO₂ Emissions ^{b)} [t]
Pristine Rubber (KTL)	57.8 ^{a)}	-
T+ p-(VBTAC-co-VBSB)	19.6	-
Savings per year	38.2	87
Savings per term [25 years]	955	10 819

^{a)} Quantities of hypochlorite consumption per FPSO/FLNG according to manufacturer’s data. The calculation is based on a typical SWI system of two lines. ^{b)} Prospective CO₂ emissions as a consequence of increased friction coefficient; thus, power and energy consumption are calculated per SWI system.

The calculations are based on the antifouling efficiency of T+ p-(VBTAC-co-VBSB) as the best-performing coating during the static and long-term seawater evaluation by depicting an efficacy of 80%, thus leading to a saving of hypochlorite of 38.2 tons per year and a reduction of CO₂-emission up to 87 tons/year as a consequence of the reduced friction coefficient due to lower marine biofouling. These prospective savings highlight the environmentally friendly and economic opportunity provided by the herein-presented synergistic development of a low-fouling microstructure combined with plasma-mediated graft polymerization of charged monomers.

6.1.3.5 Outlook

As highly effective bifunctional polymer brushes, VBDSB (section 5.2) and *N*-oxides (section 5.3) are attractive future modifications in this context. A first attempt of grafting VBDSB or VBNOx from PA on elastomer materials indicated the successful installation of the bifunctional

graft polymers. Moreover, ASTM E2149-13a assays confirmed the contact-biocide activity of such modifications, making it an attractive future application. Selected results of the modification process and bioactivity are summarized in Table 5.

Table 5: Novel modifications of elastomers and determined bioactivity as prospective SWIs-applications to fight marine biofouling.

Material	Monomer XX conc. [wt%]	WCA [°] ^{b)}	Log ₁₀ reduction ^{c)}
T+ p-(VBDSB) ^{a)}	VBDSB 20	23.1 ± 7.6 ***	3.2 ± 0.2 ***
T+ p-(VBNOx) ^{a)}	VBNOx 40	30.7 ± 9.0 ***	5.0 ± 0.0 ***
Pristine rubber ^{d)}	-	116 ± 4.6	0.0 ± 0.0

^{a)} The plasma graft modification protocol was adapted for PA 6.6 surfaces as described in the experimental section 9.2. ^{b)} Advancing water contact angles ($n \geq 6$). presented as mean value \pm SD. ^{c)} Log₁₀ reduction values for the antimicrobial determination *via* ASTM E2149 13a. Values are presented as mean values \pm SD ($n \geq 3$). Log₁₀ reduction was calculated as described in the experimental sections. ^{d)} Pristine rubber with neither added topography *via* a PA 6.6 wrapping tape nor any coating. Statistical significance was determined *via* pairwise comparison using the Tukey-Test $p \leq 0.001$ (***).

6.1.4 Conclusion

The studies provide an applicable plasma-mediated graft polymerization from polyamide 6.6 modified rubber surfaces. We could confirm that the polyamide 6.6 rubber modification (T+) shows an intrinsic low-fouling effect due to continuous regular topography in a micrometer range, which induces superhydrophobic and, thus, low surface energy. Graft polymerization from polyamide 6.6 resulted in charged polymer brushes of cationic p-(VBTAC), zwitterionic p-(VBSB), and a combination of both p-(VBTAC-co-VBSB). The latter provided a partial synergistic effect with respect to low-fouling and contact-biocide activity, which was confirmed by microbiological tests under controlled conditions. Moreover, these combined modifications show excellent long-term antifouling effects under static and dynamic conditions comparable to commercially available biocide-free coatings used as positive controls. As a future application to sweater intake systems, prospective calculations reveal a saving of hypochlorite waste up to 38.5 t per year and a reduction of 87 t CO₂ emission, making these modifications a considerable environmentally friendly alternative to reduce marine biofouling without burdening the surrounding ecosystem.

6.1.5 Acknowledgements

Prof. Dr. Sebastian G. Wicha (University of Hamburg, Department of Chemistry) provided access to the S2 laboratory and equipment for microbiological evaluation. Prof. Dr. Wolfgang R. Streit, Cathrin Kröger, and Lena Preuss (University of Hamburg, Department of Microbiology and Biotechnology) performed LIVE/DEAD™ staining and confocal microscopy imaging as a part of the microbiological assessment.

7. Discussion - Critical Summary and Outlook

Intervening with the initial attachment processes of biomaterial and microorganisms can be realized by modulating surface polarity, thus minimizing the surface's bioadhesive properties. A sustainable approach is the graft polymerization of charged monomers, which can be applied to various bulk materials. To develop effective and sustainable modifications, a framework of suitable synthetic, analytical, and microbiological methodology needed to be established in all studies of this work. To design efficient antifouling solutions, it was crucial to identify and combine different antifouling-activity principles. In addition, specific modifications (*i.e.*, polymeric *N*-oxides) revealed surprising properties that partially counteracted the originally reported findings of previous studies.

The following section highlights the connection of the studies with a focus on methodology. The second section explores the effects of different graft polymerization techniques on the resulting charged graft polymer brushes and their influence on microbial colonization patterns. Both sections try to shed light on the peculiar interactions of chemically modified materials and microorganisms. A third and closing section summarizes how these studies might improve the future development of new antifouling solutions.

7.1 Methodology

Biofilms are heterogeneous and structurally complex. Their prevention requires, therefore, broad-acting antifouling strategies. Commonly, these strategies involve a combination of antifouling principles. The required chemical protocols for graft polymerization on different base materials were established in the first project of this thesis with the preparation of zwitterionic PE surfaces. Examples include the improved grafting procedure with plasma-activation of PE and subsequent graft polymerization with spray-coating. Both allow the scalable formation of high-density polymer brushes on different base materials. In addition, essential methods for the surface analytics of charged polymer brushes were developed, such as the crystal-violet-based colorimetric assay for the analysis of solvent-accessible charges, a key parameter for the biological activity of many charged polymer brushes. This method also provided the basis for further dye-based assays, such as the acid fuchsin dye assay for the quantification of surface-grafted *N*-oxides.¹⁴³ Particularly important was the development of suitable microbiological assays, such as the bacterial adhesion assay, which were necessary to decipher the activity principles of the different polymer brushes. The use of a reproducible assay for microbiological evaluation allowed a valid comparison of bioactivities of the herein synthesized charged polymer brushes.

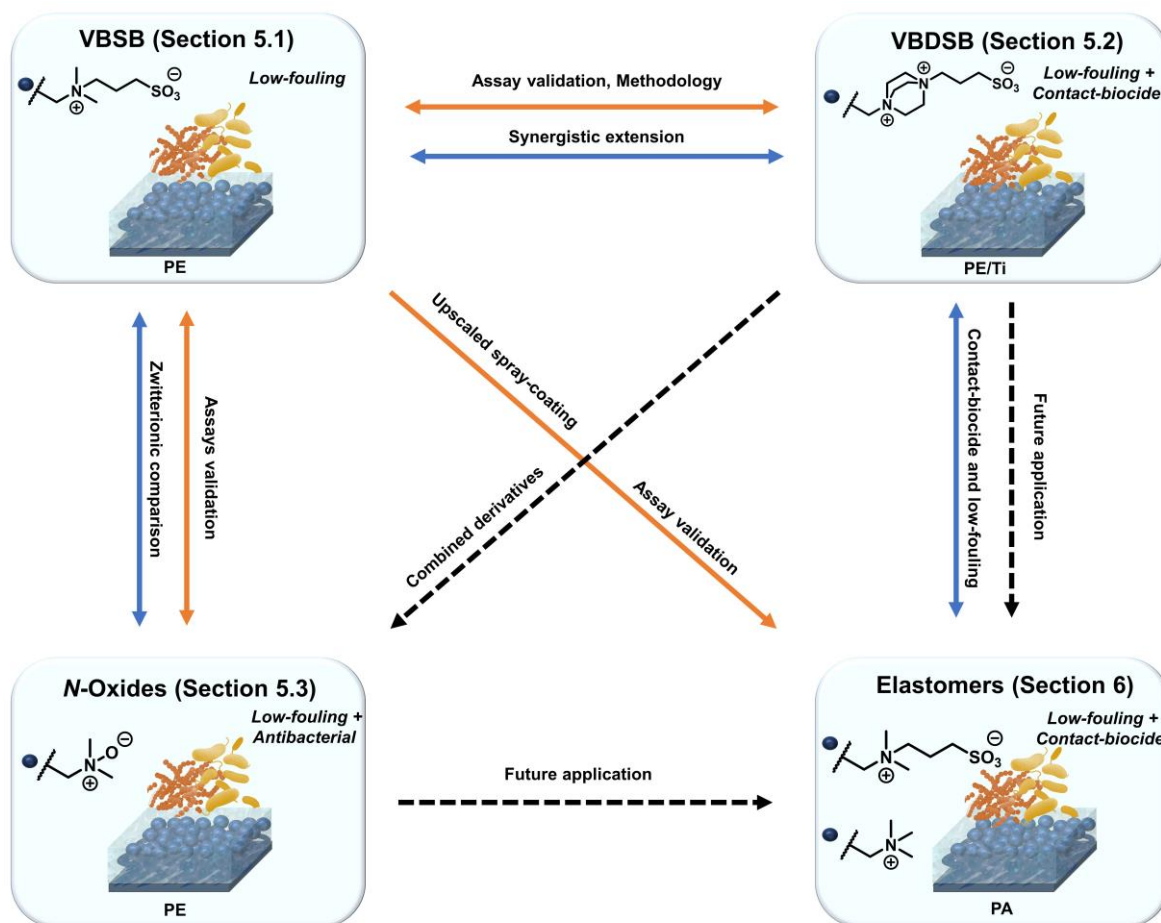


Figure 27: Overview of connections between sections in this work. Orange arrows (\rightarrow) represent methodology validation, blue arrows (\rightarrow) depict activity and principle connections, and black intermittent arrows ($- \rightarrow$) represent prospective implementations of principles.

The evaluation of PE-p-(VBTAC) as a contact biocide and PE-p-(VBSB) as a non-adhesive material facilitated the combination of cationic and zwitterionic moieties towards a bifunctional antifouling material. A scalable synthesis led to the new DABCO-supported styrene derivative (VBDSB) as the first polymerizable “diammonium sulfonate”. It was applied to a graft polymerization from clinically- and industrially-relevant surfaces using different polymerization techniques (section 5.2). The biological efficacy was tested *in vitro* against clinically relevant strains such as Gram-positive *S. aureus* and *E. coli*, and *P. aeruginosa* as Gram-negative examples.

The protocols mentioned above and methodologies have also been applied to the chemical modification of elastomers designed for long-term use in marine biotopes (section 6). A microstructure synergistically enhanced the low-fouling effect in this case. Contact-biocide (p-VBTAC) graft-polymer, zwitterionic (p-VBSB) graft-polymer and the combination of both in one graft-copolymer (p-VBTAC-co-VBSB) demonstrated good to excellent long-term antifouling activity for at least up to nine months in seawater assays.

Along the same lines, polymeric *N*-oxides, as unique zwitterionic structures, were examined (section 5.3). This project revealed a so far unknown antimicrobial effect of these materials. Although not tested in this work, polymeric *N*-oxides and the novel VBDSB bifunctional polymer brushes may prove useful for industrial antifouling applications. An overview of the discussed present and future connections of all studies in this work is depicted in Figure 27.

7.2 Bioactivities

When considering the overall bioactivities of the charged polymer brushes presented in this work, two key points remain to be answered: 1. How do variations in surface modification, including graft polymerization routes, resultant charged polymer brushes and physico-chemical properties, influence microbial colonization patterns and biofilm formation? 2. What induces the (non-exhaustive?) bifunctional biological activity of polymeric *N*-oxides?

To address the first question, it is crucial to analyze the interplay between surface modification and the related biological activity. This includes the analysis of modifications that carry the same charged polymer brush on different bulk materials (*e.g.*, Ti-p-(VBTAC) and PE-p-(VBTAC)). The graft polymers are produced by different polymerization routes (*e.g.*, ATRP for titanium surfaces and FRP for PE and PA surfaces). This results in varying physico-chemical properties (*i.e.*, brush density and layer thickness), which in turn results in different spatial arrangements and charge distribution of the graft polymer chains. All of these factors influence the cell-surface interaction (section 3.2). This is best illustrated by the study of section 5.2. If we look at the results of the contact-biocidal effect of the p-(VBDSB) graft polymers, for example, we see that Ti-p-(VBDSB) has a significantly lower biocidal effect against all tested microorganisms than the PE-p-(VBDSB) modifications. However, the same differences can also be observed in the anti-adhesive effect, where the Ti-p-(VBDSB) modification proves to be superior to the PE modification. Similar differing bioactivities were observed for the other corresponding charged polymer brushes (*e.g.*, p-(VBTAC), p-(VBSB)). In summary, completely different manifestations of charged polymer brushes' bioactivities are observed depending on the bulk material used and the polymerization routes. A selective overview is given in Table 6.

A crucial analytical method to explain these alterations is provided by the colorimetric quantification possibilities of the solvent-accessible charges of the graft polymer. The example of p-(VBDSB) reveals that PE-p-(VBDSB) has a significantly higher number of active, accessible ammonium groups compared to the corresponding titanium modification. Consequently, the Ti-p-(VBDSB) charges can be reached significantly less well by microorganisms compared to the PE-modification. This observation not only explains the difference in the final biocidal activity but also clearly indicates a difference in the spatial

polymer arrangement. Hence, it is critical to consider ToF-SIMS-SPM analysis in this context. The ToF-SIMS-SPM results also provide evidence of different topographies of the loaded polymer brushes. The PE-p-(VBDSB) polymer layer depicted a thicker and more uniform polymer-specific fragment distribution. In contrast, the Ti-p-(VBDSB) brush layer showed a thinner and topographically less homogeneous distribution (section 5.2, Figure 3). Thus, the results of the ToF-SIMS combined with the charge density quantifications reveal apparent differences in the physicochemical nature of the corresponding p-(VBDSB) induced by applying two different polymerization routes. This consequently leads to an entirely different interplay between the polymer brushes and the microorganisms. From these observations, it can, therefore, be concluded that the accessible charge density and its topographical distribution, which ultimately characterize the spatial and elemental distribution of the graft polymer, provide essential information for the assessment of microbiological activity.

Table 6: Selective overview of differing bioactivities against *S. aureus* ATCC29213, focusing on bulk material and applied polymerization route.

Polymerization	Modification	Log ₁₀ reduction ^{a)}	Bacterial adhesion ^{b)}
SI-ATRP	Ti-p-(VBTAC)	2.2 ± 0.3	Not applied
	Ti-p-(VBSB)	Not applied	Not applied
	Ti-p-(VBDSB)	1.6 ± 0.1	28.0 ± 14
SI-FRP	PE-p-(VBTAC)	2.1 ± 0.1	Not applied
	PE-p-(VBSB)	Not applied	8.8 ± 1
	PE-p-(VBDSB)	3.5 ± 0.1	156 ± 69
	T+ p-(VBTAC) ^{c)}	4.0 ± 0.1	Not applied
	T+ p-(VBSB) ^{c)}	Not applied	152 ± 36
	T+p-(VBDSB) ^{c)}	3.2 ± 0.2	Not applied

^{a)} Log₁₀ reduction values for the antimicrobial determination *via* ASTM E2149-13a. Values are presented as mean values ± SD (n ≥ 3). Log₁₀ reduction was calculated as described in the materials and method section of 5.2. ^{b)} Results of the bacterial adhesion assay presented as mean value ± SD in the units of CFU/cm². ^{c)} Rubber base material with added topography *via* a PA 6.6 texture. SI-FRP was performed as described in section 6.1.2.

As necessary for assessment is the choice of microorganisms used for microbiological evaluation in this context. In the presented studies, Gram-negative and Gram-positive strains were used to cover as many varieties as possible, *i.e.*, cell structure and surface (ζ-) potentials.³⁷ Furthermore, the strains used encompassed motile (*e.g.*, *P. aeruginosa*) and non-motile (*e.g.*, *S. aureus*) bacteria, purposely applied to analyze different colonization behaviors. Motile species can specifically recognize surface patterns and interact with the chemical functionalities on the surface. Thus, slight changes in the graft polymer appearance with regard

to spatial chain arrangement or charge distribution can influence microbiological responses significantly. This, for instance, explains again the above-mentioned varying biocidal effects of PE-p-(VBDSB) and Ti-p-(VBDSB). Furthermore, it elucidates the unpredictable anti-adhesive bioactivities of PE-p-(VBDSB) and Ti-p-(VBDSB) against a motile species of *E. coli* and *P. aeruginosa*. The obtained results show a highly anti-adhesive effect for Ti-p-(VBDSB) against both but reduced biocidal activity. In contrast, PE-p-(VBDSB) shows, on the one hand, enhanced biocidal activity against *E. coli* but only anti-adhesive activity against *P. aeruginosa*. Consequently, these varying physical interactions of polymer brushes with the attaching biomaterial and *vice versa* lead to individual colonization patterns for each modified or non-modified material. More clarifying is the view of particular macrofouling patterns. Such selective colonization could be observed for the elastomer modifications (section 6). Figure 24 depicts how different colonization patterns are generated, which are, most likely, dictated by different surface functionality. Regarding the timeline of marine biofouling, this variability in growth can be traced back to different types of initial microbial colonization.

From these varying bioactivities of the graft polymers and the deciphered macrofouling patterns in the long-term seawater test, the hypothesis arises that chemical and physical surface appearances regarding elemental composition and charge distribution might enable controlled colonization patterns. Identifying fundamental principles of selective colonization and surface sensing might enable a deeper understanding of microfouling patterns as a basis for more targeted biofilm prevention. Initial insights can be obtained by analyzing microbial transcriptomes during biofilm formation on surfaces exhibiting minor differences in elemental composition. The first results have been obtained by a comparative colonization analysis of plasma-activated PE and pristine PE. Herein, plasma-activated PE surfaces differ in surface polarity compared to unmodified PE substrates due to the generation of polar oxygen-containing functionalities by the plasma. The materials were incubated with Gram-negative *Vibrio gazogenes* until biofilm formation. Subsequently, transcriptome analyses *via* RNA sequencing (RNAseq) of both colonized surfaces (PE plasma vs. PE) were performed. The results show a significantly altered gene expression of *V. gazogenes* caused by a relatively minor change in surface polarity and elemental composition under otherwise identical growth conditions (Figure 28).

This modified transcription facilitates the identification of phenotypical differences in the resulting biofilms. In addition, these data on altered gene expression also provide a further possible explanation for the above-mentioned varying bioactivities between the charged graft polymers. Further investigations are needed for more detailed structure-activity relations, which support developing targeted and controlled colonization and surface sensing. However, these first experiments highlight the supportive benefit of transcriptome analysis since

molecular aspects of biofilm formation can be derived and explained, and induced bioactivities of the charged surfaces can be elaborated in more detail.

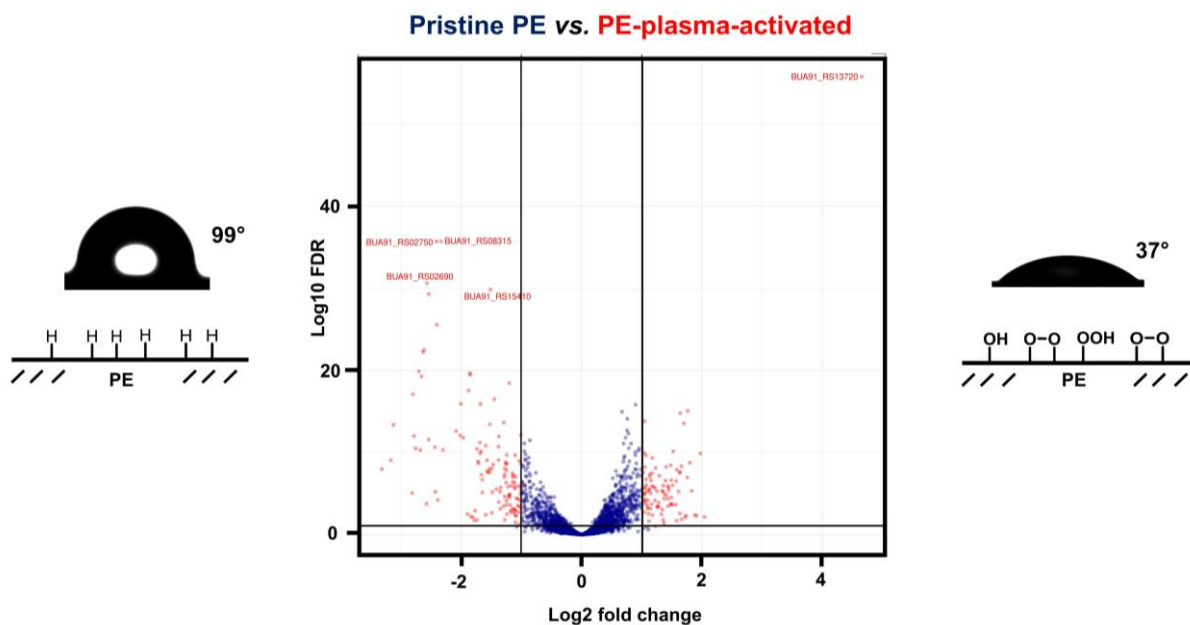


Figure 28: Volcano plots of the transcriptome analysis *via* RNA sequencing performed by Lena Preuss, AG Streit. Only slight changes in the elemental composition are impacting gene regulation significantly. Red dots represent either upregulated gene transcription (positive log₂ fold change) or downregulated transcripts (negative log₂ fold change) of plasma-activated PE compared to pristine PE. Blue dots represent gene regulation that does not differ significantly from pristine PE. Volcano plots of the RNA sequencing of PE vs. plasma-activated PE. According to XPS spectra of plasma-activated PE (Section 9.1.3 (Figure S3), elevated oxygen-containing groups were detected along with higher surface polarity represented by WCA of 37°: Pristine PE displays a relatively hydrophobic surface polarity (WCA ~ 99°).

The development and action of various *N*-oxide graft polymers to modulate biofilms is particularly noteworthy in this context (section 5.3). For the first time, the antibacterial activity of such polymer brushes was reported. Antibacterial activity was drawn back to a radical mechanism *via* the generation of ROS. In addition, repetitive usage of the *N*-oxides suggests that the antibacterial activity is not linked to exhaustive degradation reactions but instead might exhibit a non-limiting and partially regenerative character. Thus, these new classes of *N*-oxides differ from other charged graft polymers and show a combined antifouling effect, including a non-adhesive and an antibacterial component. The latter might be linked to the intrinsic structure of polymeric *N*-oxides and emphasizes how structural manifestations, despite similar antifouling effectors, can affect bioactivity. Results of section 5.3 show an explicit antibacterial activity of poly-styrene (p-VBNOx) and poly-methacrylic (p-MANOx) derivatives but reduced to insufficient antibacterial effectiveness with poly-acrylamide *N*-oxides (p-MAANOx). Such activity differences might be associated with the inter- and intramolecular interaction of the

N^+O^- functionality with the immediate chemical environment. Unlike the other tested graft polymers, the acrylamide species holds an H-bond-donor functionality and additional methylene spacing. These structural differences cause intramolecular H-bonding. This phenomenon was reported to be positively correlated with the low-fouling effect in terms of protein adsorption.¹⁴⁵ In addition, intramolecular H-bonding causes a fixed conformation of the oxygen atom, where its free electron pairs are less available for other interactions, thus generating a differing spatial charge distribution and graft polymer appearance (Figure 29). These differences could cause deviated responsivity when exposed to microbes.

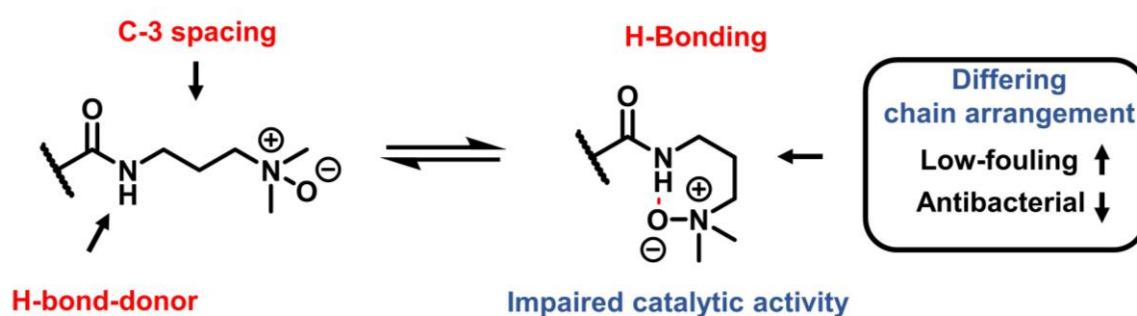


Figure 29: Assumed intramolecular H-bonding of (p-MAANOx).

Moreover, the ROS generation of polymeric *N*-oxides has not been conclusively clarified and requires future investigations. Possible explanations are provided by the latest studies by NAM *et al.*, who observed a photocatalytic transition of triplet oxygen *via* one electron spin flipping to singlet oxygen by the presentation of a hydrophilic polyaminoglycerol-derivative.¹⁴⁶ Similar processes might also be generated by oligomeric or polymeric *N*-oxides, possibly generating catalytic ROS *via* binding and converting dissolved oxygen. Moreover, other redox activities are conceivable. ZHU *et al.* described catalytic electron transfer mediated by pyridine *N*-oxides under the reversible generation of a nitrosyl-radical ($R_3-N^+-O\cdot$).¹⁴⁷ The exact identification of radical species, (by-)products, and the assessment of oxygen influence is part of ongoing investigations. To derive possible structure-activity relationships, the synthesis and evaluation of molecular analogs to the *N*-oxide graft polymers are crucial.

7.3 Novel but Restricted?

Due to their bifunctional activity, *N*-oxide-based graft polymers remain highly interesting for antifouling purposes. Yet, the observed antibacterial ROS generation could be related to so far unrecognized cytotoxicity *in vivo*. However, very limited data is available on applications of oligomeric *N*-oxides involving eukaryotic cells (*i.e.*, tumor cell lines). SHEN *et al.* described a

specific mitochondrial uptake of *N*-oxides. This mitochondrial accumulation in B16F10 cells was also associated with a loss of mitochondrial membrane potential, thus inducing apoptotic events.¹⁴⁸ Similar mitochondrial accumulation in MNNG-HOS cells and induced cell death was reported by TANG *et al.* More importantly, they associated *N*-oxidic micelles (dichloroacetate conjugated to polymeric *N*-oxide) with increased mitochondrial ROS release as superoxide anions ($\bullet\text{O}_2^-$). The latter contributed to cytochrome C mediated-proinflammatory events leading to proptosis.¹⁴⁹ However, the exact interaction of polymeric *N*-oxides with mitochondria in this context has not been elucidated. Until now, a biological target or mechanism of action has neither been clarified for eukaryotic nor for prokaryotic cells. For the latter, detailed transcriptome analysis could contribute to the mechanistic elucidation of biological activity, as mentioned beforehand.

7.4 Future Directions

In conclusion, this work summarizes the synthesis, characterization, and evaluation of established and novel charged monomers and their graft polymerization on different base materials. The obtained charged surfaces exhibit individual physical and chemical properties, which translate into individual biological responses to microorganisms. By considering biofilms' evolutionary causes and vital contribution to earth's biogeochemistry, targeted and thus more symbiotic biofilm prevention should govern the direction of future antifouling strategies. To achieve this objective, further understanding of cell-surface interactions is critical. Both the exact physicochemical elucidation of the surface and the physicochemical properties of the bacteria support the prediction of attachment and subsequent biofilm formation. However, the transducing processes of bacteria to surfaces (*i.e.*, microbial surface sensing) are less well understood. Precisely investigating regulatory responses before, during, and after biofilm formation is an integral part of ongoing and future research. An overarching view of the biological responses of the applied charged polymer brushes in this work can be supportive of developing modifications that specifically modulate biofilms. Furthermore, combining different antifouling effectors is also an opportunity to gain more effective antifouling ability and a deeper understanding of molecular cell-surface interactions. The synthesis and evaluation of the herein presented charged surfaces, in combination with future molecular and transcriptome analysis, could establish valuable structure-activity relationships and lead to more powerful antifouling materials in the future.

8. Literature

- (1) Hall-Stoodley, L.; Costerton, J. W.; Stoodley, P. Bacterial biofilms: from the natural environment to infectious diseases. *Nat. Rev. Microbiol.* **2004**, *2* (2), 95-108. DOI: 10.1038/nrmicro821 From NLM Medline.
- (2) Davey, M. E.; O'Toole G, A. Microbial biofilms: from ecology to molecular genetics. *Microbiol Mol Biol Rev* **2000**, *64* (4), 847-867. DOI: 10.1128/mmbr.64.4.847-867.2000 From NLM.
- (3) Flemming, H. C.; Wingender, J.; Szewzyk, U.; Steinberg, P.; Rice, S. A.; Kjelleberg, S. Biofilms: an emergent form of bacterial life. *Nat. Rev. Microbiol.* **2016**, *14* (9), 563-575. DOI: 10.1038/nrmicro.2016.94 From NLM Medline.
- (4) Costerton, J. W.; Stewart, P. S.; Greenberg, E. P. Bacterial biofilms: a common cause of persistent infections. *Science* **1999**, *284* (5418), 1318-1322. DOI: 10.1126/science.284.5418.1318 From NLM Medline.
- (5) Reardon, S. WHO warns against 'post-antibiotic' era. *Nature* **2014**. DOI: 10.1038/nature.2014.15135.
- (6) Veerachamy, S.; Yarlagadda, T.; Manivasagam, G.; Yarlagadda, P. K. Bacterial adherence and biofilm formation on medical implants: a review. *Proc. Inst. Mech. Eng. H: J. Eng. Med.* **2014**, *228* (10), 1083-1099.
- (7) Daubert, D. M.; Weinstein, B. F. Biofilm as a risk factor in implant treatment. *Periodontol 2000* **2019**, *81* (1), 29-40. DOI: 10.1111/prd.12280 From NLM Medline.
- (8) <https://www.waarschip.info/aktuelles/alles-ueber-antifouling/?lang=de>. (accessed 2023 04.12).
- (9) <https://www.istockphoto.com/de/fotos/pharmaceutical-manufacturing-vials>. (accessed 2023 04.12).
- (10) <https://www.istockphoto.com/de/search/2/image-film?phrase=dental%20implants>. (accessed 2023 04.12).
- (11) Galie, S.; Garcia-Gutierrez, C.; Miguelez, E. M.; Villar, C. J.; Lombo, F. Biofilms in the Food Industry: Health Aspects and Control Methods. *Front Microbiol* **2018**, *9*, 898. DOI: 10.3389/fmicb.2018.00898 From NLM PubMed-not-MEDLINE.
- (12) Araújo, E. A.; de Andrade, N. J.; da Silva, L. H. M.; de Carvalho, A. F.; de Sá Silva, C. A.; Ramos, A. M. Control of Microbial Adhesion as a Strategy for Food and Bioprocess Technology. *Food Bioproc. Tech.* **2010**, *3* (3), 321-332. DOI: 10.1007/s11947-009-0290-z.
- (13) Chambers, L. D.; Stokes, K. R.; Walsh, F. C.; Wood, R. J. K. Modern approaches to marine antifouling coatings. *Surface and Coatings Technology* **2006**, *201* (6), 3642-3652. DOI: <https://doi.org/10.1016/j.surfcoat.2006.08.129>.

- (14) Flemming, H.-C.; Wingender, J. The biofilm matrix. *Nature Reviews Microbiology* **2010**, *8* (9), 623-633. DOI: 10.1038/nrmicro2415.
- (15) Sauer, K.; Stoodley, P.; Goeres, D. M.; Hall-Stoodley, L.; Burmølle, M.; Stewart, P. S.; Bjarnsholt, T. The biofilm life cycle: expanding the conceptual model of biofilm formation. *Nature Reviews Microbiology* **2022**, *20* (10), 608-620. DOI: 10.1038/s41579-022-00767-0.
- (16) Flemming, H.-C.; van Hullebusch, E. D.; Neu, T. R.; Nielsen, P. H.; Seviour, T.; Stoodley, P.; Wingender, J.; Wuertz, S. The biofilm matrix: multitasking in a shared space. *Nature Reviews Microbiology* **2023**, *21* (2), 70-86. DOI: 10.1038/s41579-022-00791-0.
- (17) J W Costerton; K J Cheng; G G Geesey; T I Ladd; J C Nickel; M Dasgupta, a.; Marrie, T. J. Bacterial Biofilms in Nature and Disease. *Annu. Rev. Microbiol.* **1987**, *41* (1), 435-464. DOI: 10.1146/annurev.mi.41.100187.002251.
- (18) Sauer, K.; Camper, A. K.; Ehrlich, G. D.; Costerton, J. W.; Davies, D. G. *Pseudomonas aeruginosa* Displays Multiple Phenotypes during Development as a Biofilm. *J. Bacteriol.* **2002**, *184* (4), 1140-1154. DOI: doi:10.1128/jb.184.4.1140-1154.2002.
- (19) Klausen, M.; Heydorn, A.; Ragas, P.; Lambertsen, L.; Aaes-Jørgensen, A.; Molin, S.; Tolker-Nielsen, T. Biofilm formation by *Pseudomonas aeruginosa* wild type, flagella and type IV pili mutants. *Mol. Microbiol.* **2003**, *48* (6), 1511-1524. DOI: 10.1046/j.1365-2958.2003.03525.x From NLM.
- (20) P. Stoodley; K. Sauer; D. G. Davies; Costerton, J. W. Biofilms as Complex Differentiated Communities. *Annu. Rev. Microbiol.* **2002**, *56* (1), 187-209. DOI: 10.1146/annurev.micro.56.012302.160705.
- (21) Koo, H.; Allan, R. N.; Howlin, R. P.; Stoodley, P.; Hall-Stoodley, L. Targeting microbial biofilms: current and prospective therapeutic strategies. *Nature Reviews Microbiology* **2017**, *15* (12), 740-755. DOI: 10.1038/nrmicro.2017.99.
- (22) Klausen, M.; Heydorn, A.; Ragas, P.; Lambertsen, L.; Aaes-Jørgensen, A.; Molin, S.; Tolker-Nielsen, T. Biofilm formation by *Pseudomonas aeruginosa* wild type, flagella and type IV pili mutants. *Mol. Microbiol.* **2003**, *48* (6), 1511-1524. DOI: <https://doi.org/10.1046/j.1365-2958.2003.03525.x>.
- (23) Zheng, S.; Bawazir, M.; Dhalla, A.; Kim, H. E.; He, L.; Heo, J.; Hwang, G. Implication of Surface Properties, Bacterial Motility, and Hydrodynamic Conditions on Bacterial Surface Sensing and Their Initial Adhesion. *Front Bioeng Biotechnol* **2021**, *9*, 643722. DOI: 10.3389/fbioe.2021.643722 From NLM PubMed-not-MEDLINE.
- (24) Cao, S.; Wang, J.; Chen, H.; Chen, D. Progress of marine biofouling and antifouling technologies. *Chin. Sci. Bull.* **2011**, *56* (7), 598-612. DOI: 10.1007/s11434-010-4158-4.
- (25) Qian, P.-Y.; Cheng, A.; Wang, R.; Zhang, R. Marine biofilms: diversity, interactions and biofouling. *Nature Reviews Microbiology* **2022**, *20* (11), 671-684. DOI: 10.1038/s41579-022-00744-7.

- (26) Apolinario, M.; Coutinho, R. 6 - Understanding the biofouling of offshore and deep-sea structures. In *Advances in Marine Antifouling Coatings and Technologies*, Hellio, C., Yebra, D. Eds.; Woodhead Publishing, 2009; pp 132-147.
- (27) Dobretsov, S. Marine Biofilms. In *Biofouling*, 2009; pp 123-136.
- (28) Qiu, H.; Feng, K.; Gapeeva, A.; Meurisch, K.; Kaps, S.; Li, X.; Yu, L.; Mishra, Y. K.; Adelung, R.; Baum, M. Functional polymer materials for modern marine biofouling control. *Progress in Polymer Science* **2022**, *127*, 101516. DOI: <https://doi.org/10.1016/j.progpolymsci.2022.101516>.
- (29) Rosenhahn, A.; Sendra, G. H. Surface Sensing and Settlement Strategies of Marine Biofouling Organisms. *Biointerphases* **2012**, *7* (1). DOI: 10.1007/s13758-012-0063-5 (accessed 11/9/2023).
- (30) Lord, J. P. Impact of seawater temperature on growth and recruitment of invasive fouling species at the global scale. *Mar. Ecol.* **2017**, *38* (2), e12404. DOI: <https://doi.org/10.1111/maec.12404>.
- (31) Clare, A. S.; Aldred, N. 3 - Surface colonisation by marine organisms and its impact on antifouling research. In *Advances in Marine Antifouling Coatings and Technologies*, Hellio, C., Yebra, D. Eds.; Woodhead Publishing, 2009; pp 46-79.
- (32) Michail, N. A. World economic growth and seaborne trade volume: Quantifying the relationship. *Transportation Research Interdisciplinary Perspectives* **2020**, *4*, 100108. DOI: <https://doi.org/10.1016/j.trip.2020.100108>.
- (33) Callow, J. A.; Callow, M. E. Trends in the development of environmentally friendly fouling-resistant marine coatings. *Nature Communications* **2011**, *2* (1), 244. DOI: 10.1038/ncomms1251.
- (34) Boyer, I. J. Toxicity of dibutyltin, tributyltin and other organotin compounds to humans and to experimental animals. *Toxicology* **1989**, *55* (3), 253-298. DOI: [https://doi.org/10.1016/0300-483X\(89\)90018-8](https://doi.org/10.1016/0300-483X(89)90018-8).
- (35) Brinch, A.; Hansen, S. F.; Hartmann, N. B.; Baun, A. EU Regulation of Nanobiocides: Challenges in Implementing the Biocidal Product Regulation (BPR). *Nanomaterials* **2016**, *6* (2), 33.
- (36) Banerjee, I.; Pangule, R. C.; Kane, R. S. Antifouling coatings: recent developments in the design of surfaces that prevent fouling by proteins, bacteria, and marine organisms. *Adv Mater* **2011**, *23* (6), 690-718. DOI: 10.1002/adma.201001215.
- (37) Wilson, W. W.; Wade, M. M.; Holman, S. C.; Champlin, F. R. Status of methods for assessing bacterial cell surface charge properties based on zeta potential measurements. *Journal of Microbiological Methods* **2001**, *43* (3), 153-164. DOI: [https://doi.org/10.1016/S0167-7012\(00\)00224-4](https://doi.org/10.1016/S0167-7012(00)00224-4).

- (38) Yuan, Y.; Hays, M. P.; Hardwidge, P. R.; Kim, J. Surface characteristics influencing bacterial adhesion to polymeric substrates. *RSC Advances* **2017**, *7* (23), 14254-14261, 10.1039/C7RA01571B. DOI: 10.1039/C7RA01571B.
- (39) Tuson, H. H.; Weibel, D. B. Bacteria–surface interactions. *Soft matter* **2013**, *9* (17), 4368-4380.
- (40) Derjaguin, B. V. Theory of the stability of strongly charged lyophobic sol and of the adhesion of strongly charged particles in solutions of electrolytes. *Acta phys. chim. URSS* **1941**, *14*, 633.
- (41) Overbeek, J. T. G.; Verwey, E. *Theory of the stability of lyophobic colloids: the interaction of sol particles having an electric double layer*, 1948.
- (42) Hermansson, M. The DLVO theory in microbial adhesion. *Colloids and Surfaces B: Biointerfaces* **1999**, *14* (1), 105-119. DOI: [https://doi.org/10.1016/S0927-7765\(99\)00029-6](https://doi.org/10.1016/S0927-7765(99)00029-6).
- (43) Carniello, V.; Peterson, B. W.; van der Mei, H. C.; Busscher, H. J. Physico-chemistry from initial bacterial adhesion to surface-programmed biofilm growth. *Adv Colloid Interface Sci* **2018**, *261*, 1-14. DOI: 10.1016/j.cis.2018.10.005 From NLM.
- (44) van Loosdrecht, M. C. M.; Lyklema, J.; Norde, W.; Zehnder, A. J. B. Bacterial adhesion: A physicochemical approach. *Microb. Ecol.* **1989**, *17* (1), 1-15. DOI: 10.1007/BF02025589.
- (45) Falde, E. J.; Yohe, S. T.; Colson, Y. L.; Grinstaff, M. W. Superhydrophobic materials for biomedical applications. *Biomaterials* **2016**, *104*, 87-103. DOI: 10.1016/j.biomaterials.2016.06.050.
- (46) Absolom, D. R.; Lamberti, F. V.; Policova, Z.; Zingg, W.; Oss, C. J. v.; Neumann, A. W. Surface thermodynamics of bacterial adhesion. *Appl. Environ. Microbiol.* **1983**, *46* (1), 90-97. DOI: doi:10.1128/aem.46.1.90-97.1983.
- (47) Chen, S.; Li, L.; Zhao, C.; Zheng, J. Surface hydration: Principles and applications toward low-fouling/nonfouling biomaterials. *Polymer* **2010**, *51* (23), 5283-5293. DOI: <https://doi.org/10.1016/j.polymer.2010.08.022>.
- (48) Kalia, V. C. Quorum sensing inhibitors: An overview. *Biotechnol. Adv.* **2013**, *31* (2), 224-245. DOI: <https://doi.org/10.1016/j.biotechadv.2012.10.004>.
- (49) Kadam, R. U.; Bergmann, M.; Hurley, M.; Garg, D.; Cacciarini, M.; Swiderska, M. A.; Nativi, C.; Sattler, M.; Smyth, A. R.; Williams, P.; et al. A Glycopeptide Dendrimer Inhibitor of the Galactose-Specific Lectin LecA and of *Pseudomonas aeruginosa* Biofilms. *Angew Chem Int Edit* **2011**, *50* (45), 10631-10635. DOI: <https://doi.org/10.1002/anie.201104342>.
- (50) Bieser, A. M.; Thomann, Y.; Tiller, J. C. Contact-Active Antimicrobial and Potentially Self-Polishing Coatings Based on Cellulose. *Macromol. Biosci.* **2011**, *11* (1), 111-121. DOI: <https://doi.org/10.1002/mabi.201000306>.
- (51) Tiller, J. C.; Liao, C. J.; Lewis, K.; Klibanov, A. M. Designing surfaces that kill bacteria on contact. *Proc Natl Acad Sci U S A* **2001**, *98* (11), 5981-5985. DOI: 10.1073/pnas.111143098.

- (52) Carmona-Ribeiro, A. M.; de Melo Carrasco, L. D. Cationic antimicrobial polymers and their assemblies. *Int J Mol Sci* **2013**, *14* (5), 9906-9946. DOI: 10.3390/ijms14059906.
- (53) Tiller, J. C.; Liao, C.-J.; Lewis, K.; Klibanov, A. M. Designing surfaces that kill bacteria on contact. *Proceedings of the National Academy of Sciences* **2001**, *98* (11), 5981-5985. DOI: 10.1073/pnas.111143098.
- (54) Yasir, M.; Dutta, D.; Hossain, K. R.; Chen, R.; Ho, K. K. K.; Kuppusamy, R.; Clarke, R. J.; Kumar, N.; Willcox, M. D. P. Mechanism of Action of Surface Immobilized Antimicrobial Peptides Against *Pseudomonas aeruginosa*. *Front Microbiol* **2019**, *10*, 3053. DOI: 10.3389/fmicb.2019.03053 From NLM PubMed-not-MEDLINE.
- (55) Bandara, C. D.; Singh, S.; Afara, I. O.; Wolff, A.; Tesfamichael, T.; Ostrikov, K.; Oloyede, A. Bactericidal Effects of Natural Nanotopography of Dragonfly Wing on *Escherichia coli*. *ACS Applied Materials & Interfaces* **2017**, *9* (8), 6746-6760. DOI: 10.1021/acsami.6b13666.
- (56) Ghosh, S.; Mukherjee, S.; Patra, D.; Haldar, J. Polymeric Biomaterials for Prevention and Therapeutic Intervention of Microbial Infections. *Biomacromolecules* **2022**, *23* (3), 592-608. DOI: 10.1021/acs.biomac.1c01528 From NLM Medline.
- (57) Yu, Q.; Cho, J.; Shivapooja, P.; Ista, L. K.; Lopez, G. P. Nanopatterned smart polymer surfaces for controlled attachment, killing, and release of bacteria. *ACS Appl Mater Interfaces* **2013**, *5* (19), 9295-9304. DOI: 10.1021/am4022279.
- (58) Sullivan, T.; O'Callaghan, I. Recent Developments in Biomimetic Antifouling Materials: A Review. *Biomimetics (Basel)* **2020**, *5* (4). DOI: 10.3390/biomimetics5040058.
- (59) Liu, S. Q.; Yang, C.; Huang, Y.; Ding, X.; Li, Y.; Fan, W. M.; Hedrick, J. L.; Yang, Y.-Y. Antimicrobial and Antifouling Hydrogels Formed In Situ from Polycarbonate and Poly(ethylene glycol) via Michael Addition. *Advanced Materials* **2012**, *24* (48), 6484-6489. DOI: <https://doi.org/10.1002/adma.201202225>.
- (60) Sapsford, K. E.; Algar, W. R.; Berti, L.; Gemmill, K. B.; Casey, B. J.; Oh, E.; Stewart, M. H.; Medintz, I. L. Functionalizing nanoparticles with biological molecules: developing chemistries that facilitate nanotechnology. *Chem Rev* **2013**, *113* (3), 1904-2074. DOI: 10.1021/cr300143v From NLM Medline.
- (61) Kyei, S. K.; Darko, G.; Akaranta, O. Chemistry and application of emerging ecofriendly antifouling paints: a review. *Journal of Coatings Technology and Research* **2020**, *17* (2), 315-332. DOI: 10.1007/s11998-019-00294-3.
- (62) Almeida, E.; Diamantino, T. C.; de Sousa, O. Marine paints: The particular case of antifouling paints. *Progress in Organic Coatings* **2007**, *59* (1), 2-20. DOI: <https://doi.org/10.1016/j.porgcoat.2007.01.017>.
- (63) Chien, H.-W.; Chen, X.-Y.; Tsai, W.-P.; Lee, M. Inhibition of biofilm formation by rough shark skin-patterned surfaces. *Colloids and Surfaces B: Biointerfaces* **2020**, *186*, 110738. DOI: <https://doi.org/10.1016/j.colsurfb.2019.110738>.

- (64) Sun, W.; Liu, W.; Wu, Z.; Chen, H. Chemical Surface Modification of Polymeric Biomaterials for Biomedical Applications. *Macromolecular Rapid Communications* **2020**, *41* (8), 1900430. DOI: <https://doi.org/10.1002/marc.201900430>.
- (65) Huang, J. Y.; Koepsel, R. R.; Murata, H.; Wu, W.; Lee, S. B.; Kowalewski, T.; Russell, A. J.; Matyjaszewski, K. Nonleaching antibacterial glass surfaces via "Grafting Onto": The effect of the number of quaternary ammonium groups on biocidal activity. *Langmuir* **2008**, *24* (13), 6785-6795. DOI: 10.1021/la8003933.
- (66) Minko, S. Grafting on Solid Surfaces: "Grafting to" and "Grafting from" Methods. In *Polymer Surfaces and Interfaces: Characterization, Modification and Applications*, Stamm, M. Ed.; Springer Berlin Heidelberg, 2008; pp 215-234.
- (67) Sadeghi, K.; Seo, J. Photografting coating: An innovative approach to "non-migratory" active packaging. *Advanced Functional Materials* **2021**, *31* (28), 2010759.
- (68) Oehr, C.; Müller, M.; Elkin, B.; Hegemann, D.; Vohrer, U. Plasma grafting — a method to obtain monofunctional surfaces. *Surf. Coat. Technol.* **1999**, *116-119*, 25-35. DOI: [https://doi.org/10.1016/S0257-8972\(99\)00201-7](https://doi.org/10.1016/S0257-8972(99)00201-7).
- (69) Kato, K.; Uchida, E.; Kang, E.-T.; Uyama, Y.; Ikada, Y. Polymer surface with graft chains. *Progress in Polymer Science* **2003**, *28* (2), 209-259. DOI: [https://doi.org/10.1016/S0079-6700\(02\)00032-1](https://doi.org/10.1016/S0079-6700(02)00032-1).
- (70) Yuan, S. J.; Pehkonen, S. O.; Ting, Y. P.; Neoh, K. G.; Kang, E. T. Inorganic-organic hybrid coatings on stainless steel by layer-by-layer deposition and surface-initiated atom-transfer-radical polymerization for combating biocorrosion. *ACS Appl Mater Interfaces* **2009**, *1* (3), 640-652. DOI: 10.1021/am800182d.
- (71) Abraham, S.; So, A.; Unsworth, L. D. Poly(carboxybetaine methacrylamide)-Modified Nanoparticles: A Model System for Studying the Effect of Chain Chemistry on Film Properties, Adsorbed Protein Conformation, and Clot Formation Kinetics. *Biomacromolecules* **2011**, *12* (10), 3567-3580. DOI: 10.1021/bm200778u.
- (72) Zoppe, J. O.; Ataman, N. C.; Mocny, P.; Wang, J.; Moraes, J.; Klok, H. A. Surface-Initiated Controlled Radical Polymerization: State-of-the-Art, Opportunities, and Challenges in Surface and Interface Engineering with Polymer Brushes. *Chem Rev* **2017**, *117* (3), 1105-1318. DOI: 10.1021/acs.chemrev.6b00314.
- (73) Huang, J. Y.; Murata, H.; Koepsel, R. R.; Russell, A. J.; Matyjaszewski, K. Antibacterial polypropylene via surface-initiated atom transfer radical polymerization. *Biomacromolecules* **2007**, *8* (5), 1396-1399. DOI: 10.1021/bm061236j.
- (74) Fan, X.; Lin, L.; Messersmith, P. B. Cell fouling resistance of polymer brushes grafted from Ti substrates by surface-initiated polymerization: effect of ethylene glycol side chain length. *Biomacromolecules* **2006**, *7* (8), 2443-2448. DOI: 10.1021/bm060276k.

- (75) Li, M.; Fromel, M.; Ranaweera, D.; Rocha, S.; Boyer, C.; Pester, C. W. SI-PET-RAFT: Surface-Initiated Photoinduced Electron Transfer-Reversible Addition–Fragmentation Chain Transfer Polymerization. *ACS Macro Letters* **2019**, *8* (4), 374-380. DOI: 10.1021/acsmacrolett.9b00089.
- (76) Hawker, C. J.; Bosman, A. W.; Harth, E. New Polymer Synthesis by Nitroxide Mediated Living Radical Polymerizations. *Chem. Rev.* **2001**, *101* (12), 3661-3688. DOI: 10.1021/cr990119u.
- (77) Fu, Y.; Zhang, L.; Huang, L.; Xiao, S.; Chen, F.; Fan, P.; Zhong, M.; Yang, J. Salt- and thermo-responsive polyzwitterionic brush prepared via surface-initiated photoiniferter-mediated polymerization. *Appl Surf Sci* **2018**, *450*, 130-137. DOI: <https://doi.org/10.1016/j.apsusc.2018.04.112>.
- (78) Deng, J.; Wang, L.; Liu, L.; Yang, W. Developments and new applications of UV-induced surface graft polymerizations. *Progress in Polymer Science* **2009**, *34* (2), 156-193. DOI: <https://doi.org/10.1016/j.progpolymsci.2008.06.002>.
- (79) plasma. 3.0.1 ed.; International Union of Pure and Applied Chemistry (IUPAC), 2019.
- (80) Quintana, R.; Jańczewski, D.; Vasantha, V. A.; Jana, S.; Lee, S. S. C.; Parra-Velandia, F. J.; Guo, S.; Parthiban, A.; Teo, S. L.-M.; Vancso, G. J. Sulfobetaine-based polymer brushes in marine environment: Is there an effect of the polymerizable group on the antifouling performance? *Colloids and surfaces B: Biointerfaces* **2014**, *120*, 118-124.
- (81) Schonemann, E.; Laschewsky, A.; Rosenhahn, A. Exploring the Long-Term Hydrolytic Behavior of Zwitterionic Polymethacrylates and Polymethacrylamides. *Polymers (Basel)* **2018**, *10* (6). DOI: 10.3390/polym10060639 From NLM PubMed-not-MEDLINE.
- (82) Hirata, T.; Kashiwagi, T.; Brown, J. E. Thermal and oxidative degradation of poly (methyl methacrylate): weight loss. *Macromolecules* **1985**, *18* (7), 1410-1418.
- (83) Fox, R. B.; Isaacs, L. G.; Stokes, S. Photolytic degradation of poly(methyl methacrylate). *Journal of Polymer Science Part A: General Papers* **1963**, *1* (3), 1079-1086. DOI: <https://doi.org/10.1002/pol.1963.100010321>.
- (84) Lomakin, S. M.; Brown, J. E.; Breese, R. S.; Nyden, M. R. An investigation of the thermal stability and char-forming tendency of cross-linked poly(methyl methacrylate). *Polym. Degradation Stab.* **1993**, *41* (2), 229-243. DOI: [https://doi.org/10.1016/0141-3910\(93\)90048-N](https://doi.org/10.1016/0141-3910(93)90048-N).
- (85) Funt, B. L.; Tan, S.-R. The photoelectrochemical initiation of polymerization of styrene. *Journal of Polymer Science: Polymer Chemistry Edition* **1984**, *22* (3), 605-608. DOI: <https://doi.org/10.1002/pol.1984.170220310>.
- (86) Prohaska, G. W.; Johnson, E. D.; Evans, J. F. Preparation and characterization of plasma-polymerized styrene thin films. *Journal of Polymer Science: Polymer Chemistry Edition* **1984**, *22* (11), 2953-2972. DOI: <https://doi.org/10.1002/pol.1984.170221119>.

- (87) Kaur, R.; Liu, S. Antibacterial surface design - Contact kill. *Prog Surf Sci* **2016**, *91* (3), 136-153. DOI: 10.1016/j.progsurf.2016.09.001.
- (88) Khalil, F.; Franzmann, E.; Ramcke, J.; Dakischew, O.; Lips, K. S.; Reinhardt, A.; Heisig, P.; Maison, W. Biomimetic PEG-catecholates for stable antifouling coatings on metal surfaces: applications on TiO₂ and stainless steel. *Colloids and Surfaces B: Biointerfaces* **2014**, *117*, 185-192. DOI: 10.1016/j.colsurfb.2014.02.022.
- (89) Han, S.; Kim, C.; Kwon, D. Thermal/oxidative degradation and stabilization of polyethylene glycol. *Polymer* **1997**, *38* (2), 317-323. DOI: [https://doi.org/10.1016/S0032-3861\(97\)88175-X](https://doi.org/10.1016/S0032-3861(97)88175-X).
- (90) Shao, Q.; Jiang, S. Molecular understanding and design of zwitterionic materials. *Adv Mater* **2015**, *27* (1), 15-26. DOI: 10.1002/adma.201404059.
- (91) Huang, H.; Zhang, C.; Crisci, R.; Lu, T.; Hung, H. C.; Sajib, M. S. J.; Sarker, P.; Ma, J.; Wei, T.; Jiang, S.; et al. Strong Surface Hydration and Salt Resistant Mechanism of a New Nonfouling Zwitterionic Polymer Based on Protein Stabilizer TMAO. *J Am Chem Soc* **2021**, *143* (40), 16786-16795. DOI: 10.1021/jacs.1c08280 From NLM Medline.
- (92) Shao, Q.; Jiang, S. Effect of carbon spacer length on zwitterionic carboxybetaines. *J Phys Chem B* **2013**, *117* (5), 1357-1366. DOI: 10.1021/jp3094534 From NLM Medline.
- (93) Tolba, S. A.; Xia, W. Molecular insights into the hydration of zwitterionic polymers. *Molecular Systems Design & Engineering* **2023**, *8* (8), 1040-1048. DOI: 10.1039/d3me00020f.
- (94) Ostuni, E.; Chapman, R. G.; Holmlin, R. E.; Takayama, S.; Whitesides, G. M. A Survey of Structure-Property Relationships of Surfaces that Resist the Adsorption of Protein. *Langmuir* **2001**, *17* (18), 5605-5620. DOI: 10.1021/la010384m.
- (95) Chapman, R. G.; Ostuni, E.; Takayama, S.; Holmlin, R. E.; Yan, L.; Whitesides, G. M. Surveying for surfaces that resist the adsorption of proteins. *Journal of the American Chemical Society* **2000**, *122* (34), 8303-8304. DOI: DOI 10.1021/ja000774f.
- (96) Chang, Y. Designs of zwitterionic polymers. *Journal of Polymer Research* **2022**, *29* (7). DOI: 10.1007/s10965-022-03041-2.
- (97) Xie, X.; Cong, W.; Zhao, F.; Li, H.; Xin, W.; Hou, G.; Wang, C. Synthesis, physicochemical property and antimicrobial activity of novel quaternary ammonium salts. *J Enzyme Inhib Med Chem* **2018**, *33* (1), 98-105. DOI: 10.1080/14756366.2017.1396456.
- (98) Damodaran, V. B.; Murthy, N. S. Bio-inspired strategies for designing antifouling biomaterials. *Biomaterials research* **2016**, *20* (1), 1-11.
- (99) Du, H.; Qian, X. The hydration properties of carboxybetaine zwitterion brushes. *J Comput Chem* **2016**, *37* (10), 877-885. DOI: 10.1002/jcc.24234 From NLM Medline.
- (100) Asha, A. B.; Chen, Y.; Narain, R. Bioinspired dopamine and zwitterionic polymers for non-fouling surface engineering. *Chem Soc Rev* **2021**, *50* (20), 11668-11683. DOI: 10.1039/d1cs00658d From NLM Medline.

- (101) Dilly, S. J.; Beecham, M. P.; Brown, S. P.; Griffin, J. M.; Clark, A. J.; Griffin, C. D.; Marshall, J.; Napier, R. M.; Taylor, P. C.; Marsh, A. Novel Tertiary Amine Oxide Surfaces That Resist Nonspecific Protein Adsorption. *Langmuir* **2006**, *22* (19), 8144-8150. DOI: 10.1021/la060743j.
- (102) Li, B.; Jain, P.; Ma, J.; Smith, J. K.; Yuan, Z.; Hung, H. C.; He, Y.; Lin, X.; Wu, K.; Pfaendtner, J.; et al. Trimethylamine N-oxide-derived zwitterionic polymers: A new class of ultralow fouling bioinspired materials. *Sci Adv* **2019**, *5* (6), eaaw9562. DOI: 10.1126/sciadv.aaw9562 From NLM Medline.
- (103) Sonnenschein, L.; Seubert, A. Synthesis of a series of monomeric styrene sulfobetaine precursors. *Tetrahedron Letters* **2011**, *52* (10), 1101-1104. DOI: 10.1016/j.tetlet.2010.12.100.
- (104) O'Neil, I. *Science of Synthesis*; Thieme Chemistry, 2009.
- (105) Cao, B.; Tang, Q.; Cheng, G. Recent advances of zwitterionic carboxybetaine materials and their derivatives. *J Biomater Sci Polym Ed* **2014**, *25* (14-15), 1502-1513. DOI: 10.1080/09205063.2014.927300 From NLM Medline.
- (106) Maan, A. M. C.; Hofman, A. H.; Vos, W. M.; Kamperman, M. Recent Developments and Practical Feasibility of Polymer-Based Antifouling Coatings. *Adv. Funct. Mater.* **2020**, *30* (32). DOI: 10.1002/adfm.202000936.
- (107) <https://biomimeticdesign.wordpress.com/2008/08/27/lotus-effect-efecto-lotus/> (accessed 2023 04.12).
- (108) <https://www.nationalgeographic.com/animals/article/rare-footage-three-female-great-white-sharks>. (accessed 2023 04.12).
- (109) <https://marinesanctuary.org/blog/sea-wonder-purple-sea-urchin/>. (accessed 2023 04.12).
- (110) <https://www.nationalgeographic.com/animals/invertebrates/facts/dragonflies-insects>. (accessed 2023 04.12).
- (111) Rauner, N.; Mueller, C.; Ring, S.; Boehle, S.; Strassburg, A.; Schoeneweiss, C.; Wasner, M.; Tiller, J. C. A Coating that Combines Lotus-Effect and Contact-Active Antimicrobial Properties on Silicone. *Adv. Funct. Mater.* **2018**, *28* (29), 1801248. DOI: <https://doi.org/10.1002/adfm.201801248>.
- (112) Genzer, J.; Efimenko, K. Recent developments in superhydrophobic surfaces and their relevance to marine fouling: a review. *Biofouling* **2006**, *22* (5-6), 339-360. DOI: 10.1080/08927010600980223.
- (113) Georgakopoulos-Soares, I.; Papazoglou, E. L.; Karmiris-Obratański, P.; Karkalos, N. E.; Markopoulos, A. P. Surface antibacterial properties enhanced through engineered textures and surface roughness: A review. *Colloids and Surfaces B: Biointerfaces* **2023**, *231*, 113584. DOI: <https://doi.org/10.1016/j.colsurfb.2023.113584>.

- (114) Wu, S.; Zhang, B.; Liu, Y.; Suo, X.; Li, H. Influence of surface topography on bacterial adhesion: A review (Review). *Biointerphases* **2018**, *13* (6), 060801. DOI: 10.1116/1.5054057.
- (115) Brzozowska, A. M.; Parra-Velandia, F. J.; Quintana, R.; Xiaoying, Z.; Lee, S. S.; Chin-Sing, L.; Janczewski, D.; Teo, S. L.; Vancso, J. G. Biomimicking micropatterned surfaces and their effect on marine biofouling. *Langmuir* **2014**, *30* (30), 9165-9175. DOI: 10.1021/la502006s.
- (116) Shao, Q.; He, Y.; White, A. D.; Jiang, S. Difference in Hydration between Carboxybetaine and Sulfobetaine. *The Journal of Physical Chemistry B* **2010**, *114* (49), 16625-16631. DOI: 10.1021/jp107272n.
- (117) Fu, Y.; Wang, Y.; Huang, L.; Xiao, S.; Chen, F.; Fan, P.; Zhong, M.; Tan, J.; Yang, J. Salt-Responsive "Killing and Release" Antibacterial Surfaces of Mixed Polymer Brushes. *Industrial & Engineering Chemistry Research* **2018**, *57* (27), 8938-8945. DOI: 10.1021/acs.iecr.8b01730.
- (118) Shao, Q.; Jiang, S. Molecular understanding and design of zwitterionic materials. *Adv. Mater.* **2015**, *27* (1), 15-26. DOI: <https://doi.org/10.1002/adma.201404059>.
- (119) Quintana, R.; Jańczewski, D.; Vasantha, V. A.; Jana, S.; Lee, S. S. C.; Parra-Velandia, F. J.; Guo, S.; Parthiban, A.; Teo, S. L.-M.; Vancso, G. J. Sulfobetaine-based polymer brushes in marine environment: Is there an effect of the polymerizable group on the antifouling performance? *Colloids Surf. B. Biointerfaces* **2014**, *120*, 118-124.
- (120) Zhang, Z.; Chao, T.; Chen, S.; Jiang, S. Superlow Fouling Sulfobetaine and Carboxybetaine Polymers on Glass Slides. *Langmuir* **2006**, *22* (24), 10072-10077. DOI: 10.1021/la062175d.
- (121) Diefenbeck, M.; Muckley, T.; Hofmann, G. O. Prophylaxis and treatment of implant-related infections by local application of antibiotics. *Injury* **2006**, *37 Suppl 2*, S95-104. DOI: 10.1016/j.injury.2006.04.015 From NLM Medline.
- (122) Zhang, S. B.; Yang, X. H.; Tang, B.; Yuan, L. J.; Wang, K.; Liu, X. Y.; Zhu, X. L.; Li, J. N.; Ge, Z. C.; Chen, S. G. New insights into synergistic antimicrobial and antifouling cotton fabrics via dually finished with quaternary ammonium salt and zwitterionic sulfobetaine. *Chem. Eng. J.* **2018**, *336*, 123-132. DOI: 10.1016/j.cej.2017.10.168.
- (123) Fu, Y.; Yang, Y.; Xiao, S.; Zhang, L.; Huang, L.; Chen, F.; Fan, P.; Zhong, M.; Tan, J.; Yang, J. Mixed polymer brushes with integrated antibacterial and antifouling properties. *Prog Org Coat* **2019**, *130*, 75-82. DOI: <https://doi.org/10.1016/j.porgcoat.2019.01.038>.
- (124) Wu, T.; Beyer, F. L.; Brown, R. H.; Moore, R. B.; Long, T. E. Influence of Zwitterions on Thermomechanical Properties and Morphology of Acrylic Copolymers: Implications for Electroactive Applications. *Macromolecules* **2011**, *44* (20), 8056-8063. DOI: 10.1021/ma201211j.

- (125) Zhang, K.; Drummey, K. J.; Moon, N. G.; Chiang, W. D.; Long, T. E. Styrenic DABCO salt-containing monomers for the synthesis of novel charged polymers. *Polym Chem-Uk* **2016**, 7 (20), 3370-3374, 10.1039/C6PY00426A. DOI: 10.1039/C6PY00426A.
- (126) Meisenheimer, J. Über eine eigenartige Umlagerung des Methyl-allyl-anilin-N-oxyds. *Berichte der deutschen chemischen Gesellschaft (A and B Series)* **1919**, 52 (8), 1667-1677. DOI: <https://doi.org/10.1002/cber.19190520830>.
- (127) Grierson, D. The Polonovski Reaction. In *Organic Reactions*, 2004; pp 85-295.
- (128) Cope, A. C.; LeBel, N. A. Amine Oxides. VII. The Thermal Decomposition of the N-Oxides of N-Methylazacycloalkanes^{1,2}. *Journal of the American Chemical Society* **2002**, 82 (17), 4656-4662. DOI: 10.1021/ja01502a052.
- (129) *Energy Maritime Associates Pte Ltd, Floating Production Systems Quarterly Report*; 2019.
- (130) van de Lagemaat, M.; Grotenhuis, A.; van de Belt-Gritter, B.; Roest, S.; Loontjens, T. J. A.; Busscher, H. J.; van der Mei, H. C.; Ren, Y. Comparison of methods to evaluate bacterial contact-killing materials. *Acta Biomater* **2017**, 59, 139-147. DOI: 10.1016/j.actbio.2017.06.042.
- (131) Priester, J. H.; Horst, A. M.; Van de Werfhorst, L. C.; Saleta, J. L.; Mertes, L. A.; Holden, P. A. Enhanced visualization of microbial biofilms by staining and environmental scanning electron microscopy. *J Microbiol Methods* **2007**, 68 (3), 577-587. DOI: 10.1016/j.mimet.2006.10.018 From NLM.
- (132) *ASTM D6990-20 Standard Practice for Evaluating Biofouling Resistance and Physical Performance of Marine Coating Systems*; 2020. DOI: 10.1520/D6990-20
- (133) *Standard Test Method for Subjecting Marine Antifouling Coating to Biofouling and Fluid Shear Forces in Natural Seawater*; 2020. DOI: 10.1520/D4939-89R20
- (134) Seto, F.; Muraoka, Y.; Sakamoto, N.; Kishida, A.; Akashi, M. Surface modification of synthetic fiber nonwoven fabrics with poly(acrylic acid) chains prepared by corona discharge induced grafting. *Angew Makromol Chem* **1999**, 266 (1), 56-62, [https://doi.org/10.1002/\(SICI\)1522-9505\(19990501\)266:1<56::AID-APMC56>3.0.CO;2-0](https://doi.org/10.1002/(SICI)1522-9505(19990501)266:1<56::AID-APMC56>3.0.CO;2-0). DOI: 10.1002/(sici)1522-9505(19990501)266:1<56::Aid-apmc56>3.0.Co;2-0 (accessed 2020/12/30).
- (135) Kliewer, S.; Wicha, S. G.; Broker, A.; Naundorf, T.; Catmadim, T.; Oellingrath, E. K.; Rohnke, M.; Streit, W. R.; Vollstedt, C.; Kipphardt, H.; et al. Contact-active antibacterial polyethylene foils via atmospheric air plasma induced polymerisation of quaternary ammonium salts. *Colloids and Surfaces B* **2020**, 186, 110679. DOI: 10.1016/j.colsurfb.2019.110679.
- (136) Burmeister, N.; Vollstedt, C.; Kröger, C.; Friedrich, T.; Scharnagl, N.; Rohnke, M.; Zorn, E.; Wicha, S. G.; Streit, W. R.; Maison, W. Zwitterionic surface modification of polyethylene via atmospheric plasma-induced polymerization of (vinylbenzyl)-sulfobetaine and evaluation of

- antifouling properties. *Colloids and Surfaces B: Biointerfaces* **2023**, 224. DOI: 10.1016/j.colsurfb.2023.113195.
- (137) Zorn, E.; Knaack, J. I. H.; Burmeister, N.; Scharnagl, N.; Rohnke, M.; Wicha, S. G.; Maison, W. Contact-Biocide TiO(2) Surfaces by Surface-Initiated Atom Transfer Radical Polymerization with Chemically Stable Phosphonate Initiators. *Langmuir* **2023**. DOI: 10.1021/acs.langmuir.3c01366 From NLM Publisher.
- (138) Manakhov, A.; Zajíčková, L.; Eliáš, M.; Čechal, J.; Polčák, J.; Hnilica, J.; Bittnerová, Š.; Nečas, D. Optimization of Cyclopropylamine Plasma Polymerization toward Enhanced Layer Stability in Contact with Water. *Plasma Processes and Polymers* **2014**, 11 (6), 532-544. DOI: <https://doi.org/10.1002/ppap.201300177>.
- (139) Weiss, I. M.; Muth, C.; Drumm, R.; Kirchner, H. O. K. Thermal decomposition of the amino acids glycine, cysteine, aspartic acid, asparagine, glutamic acid, glutamine, arginine and histidine. *BMC Biophys* **2018**, 11, 2. DOI: 10.1186/s13628-018-0042-4.
- (140) Archer, G. L. Staphylococcus aureus: A Well-Armed Pathogen. *Clinical Infectious Diseases* **1998**, 26 (5), 1179-1181. DOI: 10.1086/520289 (accessed 4/16/2023).
- (141) Biokorrosion, D. B. P. G. I. f. A. u. *Antifouling-Wirksamkeit von Testsystemen der Eddelbüttel & Schneider GmbH im Jahr 2022 im Roten Meer*, 2022.
- (142) de Messano, L. V. R.; Sathler, L.; Reznik, L. Y.; Coutinho, R. The effect of biofouling on localized corrosion of the stainless steels N08904 and UNS S32760. *Int. Biodeterior. Biodegrad.* **2009**, 63 (5), 607-614. DOI: <https://doi.org/10.1016/j.ibiod.2009.04.006>.
- (143) Moretto, E. Quantification of the charge density of surface-grafted N-oxides by acid fuchsin. Master Thesis, University of Hamburg, 2024.
- (144) Burmeister, N.; Zorn, E.; Farooq, A.; Preuss, L.; Vollstedt, C.; Friedrich, T.; Mantel, T.; Scharnagl, N.; Rohnke, M.; Ernst, M.; et al. Surface Grafted N-Oxides have Low-Fouling and Antibacterial Properties. *Adv. Mater. Interfaces* **2023**, 10, 2300505. DOI: 10.1002/admi.202300505.
- (145) Dobrzanska, D. A.; Cooper, A. L.; Dowson, C. G.; Evans, S. D.; Fox, D. J.; Johnson, B. R.; Biggs, C. I.; Randev, R. K.; Stec, H. M.; Taylor, P. C.; et al. Oxidation of tertiary amine-derivatized surfaces to control protein adhesion. *Langmuir* **2013**, 29 (9), 2961-2970. DOI: 10.1021/la4003719 From NLM Medline.
- (146) Nam, J. S.; Hong, Y.; Lee, C. G.; Kim, T. I.; Lee, C.; Roh, D. H.; Lee, I. S.; Kweon, S.; Ahn, G.; Min, S. K.; et al. Singlet Oxygen Generation from Polyaminoglycerol by Spin-Flip-Based Electron Transfer. *JACS Au* **2022**, 2 (4), 933-942. DOI: 10.1021/jacsau.2c00050 From NLM PubMed-not-MEDLINE.
- (147) Zhu, Y.; Liu, G.; Zhao, R.; Gao, H.; Li, X.; Sun, L.; Li, F. Photoelectrochemical water oxidation improved by pyridine N-oxide as a mimic of tyrosine-Z in photosystem II. *Chem Sci* **2022**, 13 (17), 4955-4961. DOI: 10.1039/d2sc00443g From NLM PubMed-not-MEDLINE.

- (148) Geng, Y.; Xiang, J.; Shao, S.; Tang, J.; Shen, Y. Mitochondria-targeted polymer-celastrol conjugate with enhanced anticancer efficacy. *J Control Release* **2022**, *342*, 122-133. DOI: 10.1016/j.jconrel.2022.01.002 From NLM Medline.
- (149) Jin, J.; Yuan, P.; Yu, W.; Lin, J.; Xu, A.; Xu, X.; Lou, J.; Yu, T.; Qian, C.; Liu, B.; et al. Mitochondria-Targeting Polymer Micelle of Dichloroacetate Induced Pyroptosis to Enhance Osteosarcoma Immunotherapy. *ACS Nano* **2022**, *16* (7), 10327-10340. DOI: 10.1021/acsnano.2c00192.
- (150) Gestis Substance Database. Insitut für Arbeitsschutz der Deutschen Gesetzlichen Unfallversicherung

9. Appendix

9.1 Supplementary Materials

9.1.1 Zwitterionic surface modification of polyethylene *via* atmospheric plasma-induced polymerization of (vinylbenzyl-)sulfobetaine and evaluation of antifouling properties

Zwitterionic surface modification of polyethylene *via* atmospheric plasma-induced polymerization of (vinylbenzyl-)sulfobetaine and evaluation of antifouling properties

Nils Burmeister^a, Christel Vollstedt^b, Cathrin Kröger^b, Timo Friedrich^a, Nico Scharnag^f, Marcus Rohnke^d, Eilika Zorn^a, Sebastian G. Wicha^a, Wolfgang R. Streit^b, Wolfgang Maison^a

^aUniversität Hamburg, Department of Chemistry, Bundesstrasse 45, 20146 Hamburg, Germany

^bUniversität Hamburg, Department of Microbiology and Biotechnology, Ohnhorststrasse 18, 22609 Hamburg, Germany.

^cHelmholtz-Zentrum Hereon GmbH, Institute of Surface Science, Max-Planck-Strasse 1, 21502 Geesthacht, Germany.

^dJustus-Liebig-Universität Gießen, Institute of Physical Chemistry, Heinrich-Buff-Ring 17, 35392 Giessen, Germany.

Outline

1. Contact angles after polymerization and Soxhlet extraction	4
2. Investigation of polymerization with the crosslinking additive divinylbenzene (DVB)	5
3. Weight loss after Soxhlet extraction (gravimetry).....	5
4. Contact angles after bacterial adhesion tests and biofilm adhesion tests in natural seawater.....	6
5. XPS survey spectra	7
6. Determination of grafting density by adsorption and desorption of crystal violet.....	8
7. Gravimetric determination of pVBSB grafting yield.....	10
8. Bacterial adhesion assay – growth control	11
9. Biofilm adhesion in natural seawater.....	12
11. Synthetic procedures	13
12. NMR spectra	15

1. Contact angles after polymerization and Soxhlet extraction

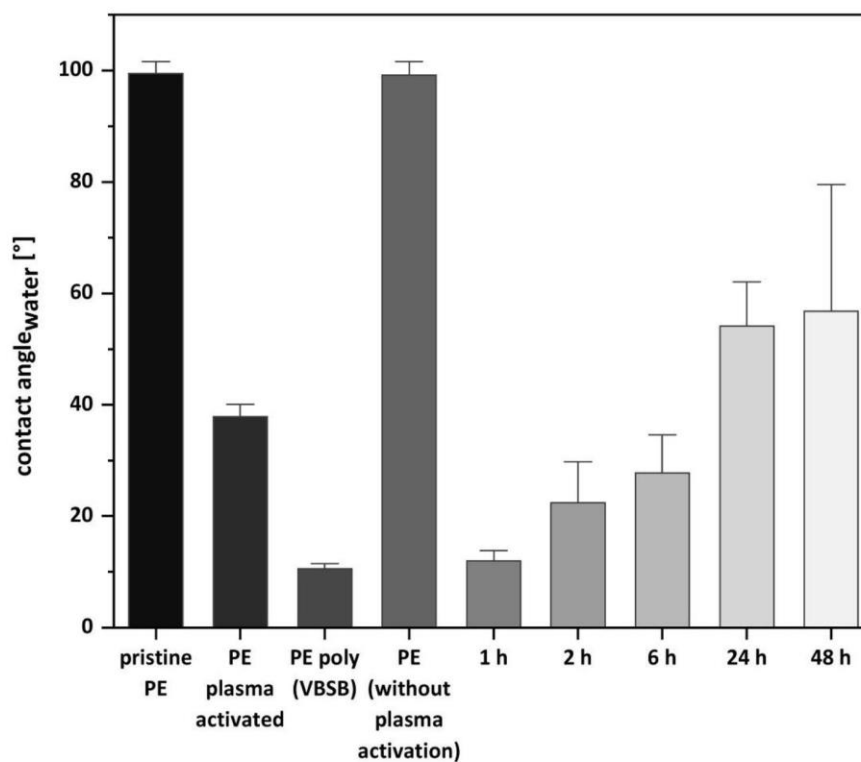


Fig.1: Contact angles after Soxhlet extraction with demin. water and initial contact angles after polymerization including the negative control of non-activated PE.

2. Investigation of polymerization with the crosslinking additive divinylbenzene (DVB)

Table 1: Comparison of contact angles between PE-poly-(VBSB) and PE-poly-(VBSB-DVB) and resultant charge density according to crystal violet adsorption/desorption assay. Polymerization conditions for PE-poly-(VBSB): 20 wt% (vinylbenzyl)sulfobetaine (VBSB) in water with 1.0 wt% ammoniumperoxodisulfate (APS), 85 C, 2 h. Subsequent washing: 3x30 min with 70 %water/ethanol mixture in an ultrasonic bath followed by drying at 50°C. Polymerization conditions for PE-poly-(VBSB-DVB): 20 wt% (vinylbenzyl)sulfobetaine (VBSB) in water/acetonitrile (80:20) with 1.0 wt% ammoniumperoxodisulfate (APS) and divinylbenzene (0.2 wt%), 85 C, 2 h. Subsequent washing: 3x30 min with 70 %water/ethanol mixture in an ultrasonic bath followed by drying at 50°C.

Entry	CA [°] of PE-poly- (VBSB)	CA [°] of PE-poly-(VBSB-DVB)	Zwitterions/cm ² of PE-poly-(VBSB-DVB)
1	12.51	22.41	6.20*10 ¹³
2	11.52	13.86	4.22*10 ¹⁴
3	9.53	18.41	5.47*10 ¹⁴
4	11.67	19.44	6.13*10 ¹³
5	10.68	27.26	7.80*10 ¹³
6	15.67	20.76	3.01*10 ¹⁴

3. Weight loss after Soxhlet extraction (gravimetry)

Table 2: Weight loss after applying Soxhlet extraction to three different PE-poly-(VBSB) modifications with an area of 1 cm². Polymerization conditions for PE-poly-(VBSB): 20 wt% (vinylbenzyl)sulfobetaine (VBSB) in water with 1.0 wt% ammoniumperoxodisulfate (APS), 85 C, 2 h. Subsequent washing: 3x30 min with 70 %water/ethanol mixture in an ultrasonic bath followed by drying at 50°C

Hours of extraction	Initial	1	2	6	24	48
PE-poly- (VBSB) extract [g]	0.0000	±0.0003	±0.0000	±0.0002	±0.0000	±0.0001

4. Contact angles after bacterial adhesion tests and biofilm adhesion tests in natural seawater

Table 3: Water contact angle measurements of PE-poly-VBSB as synthesized, after bacterial adhesion test in MHB medium and after biofilm adhesion test in natural seawater. For each value, a triplicate measurement at three different points on the surface of the test specimen was performed. After biological assays, the respective samples were sterilized and washed with iPrOH (70 vol% in demin. water) followed by drying the test specimen at 50°C. Polymerization conditions for PE-poly-(VBSB): 20 wt% (vinylbenzyl)sulfobetaine (VBSB) in water with 1.0 wt% ammoniumperoxodisulfate (APS), 85 C, 2 h. Subsequent washing: 3x30 min with 70 %water/ethanol mixture in an ultrasonic bath followed by drying at 50°C.

Initial PE-poly-(VBSB)	<i>Bacterial adhesion test (after 48 hours at 37°C)</i>	<i>Biofilm adhesion test (after 21 days at 20°C)</i>
9.93± 2°	10.71 ± 3°	9.26 ± 1°

5. XPS survey spectra

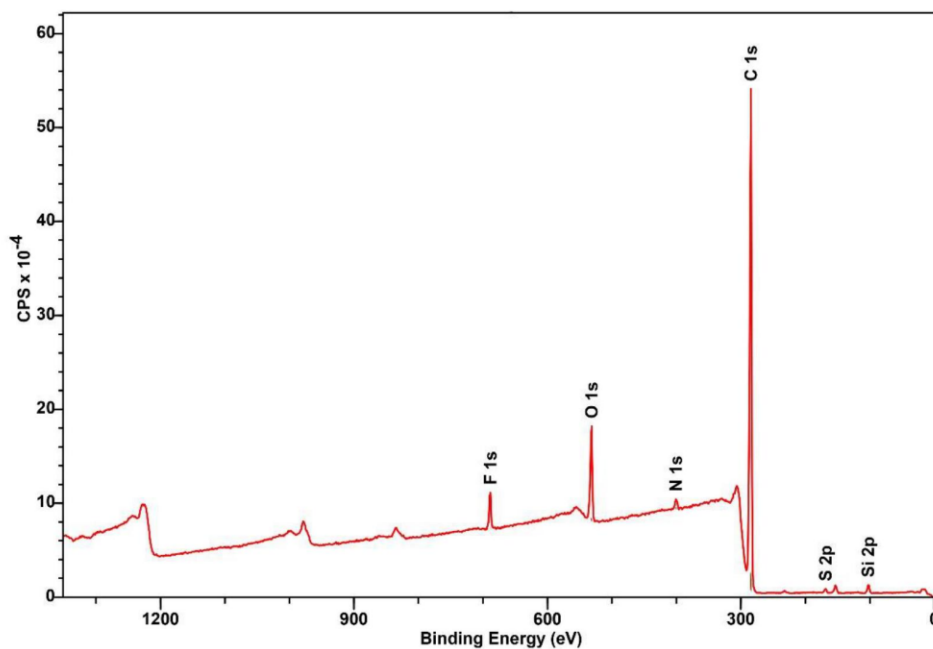


Fig 2: XPS survey spectra of pristine PE.

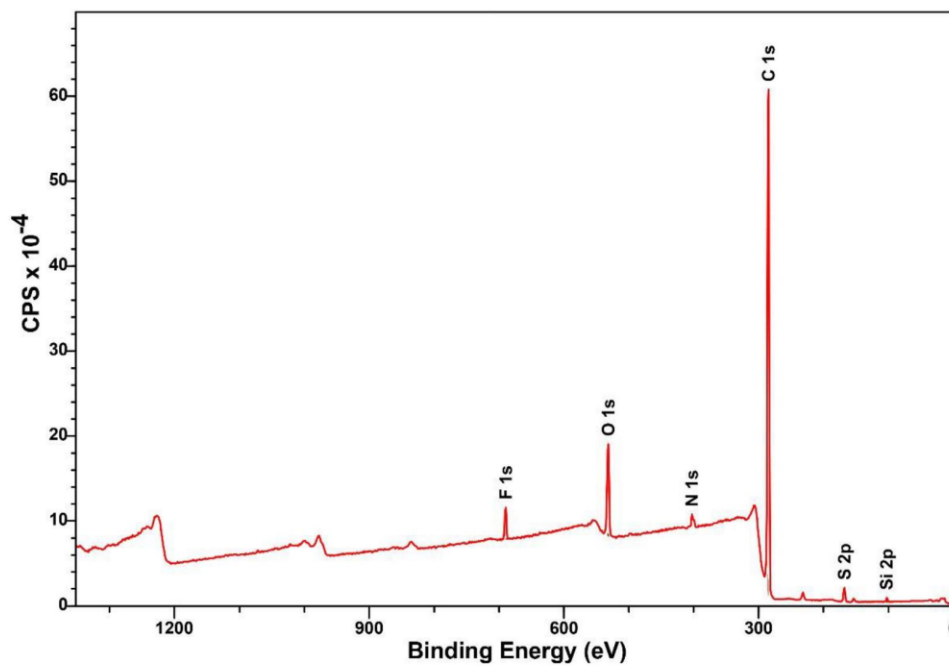


Fig. 3: XPS survey spectra of PE-poly-(VBSB). Polymerization conditions for PE-poly-(VBSB): 20 wt% (vinylbenzyl)sulfobetaine (VBSB) in water with 1.0 wt% ammoniumperoxodisulfate (APS), 85 C, 2 h. Subsequent washing: 3x30 min with 70 %water/ethanol mixture in an ultrasonic bath followed by drying at 50°C

6. Determination of grafting density by adsorption and desorption of crystal violet

For analysis of grafted polymer and determination of the charge density, an ion exchange assay in combination with UV/vis quantification was used. PE foils were rinsed with an isopropanol/water mixture of 70% (v/v) and stored in an ultrasonic bath for 10 min prior to use. PE foils were cut into squares of 1.0 cm² and were immersed into 1 wt% of aqueous crystal violet solution for 30 min on a shaker at 100 rpm at room temperature. PE foils were rinsed once with demin. water, transferred into 10 mL of demin. water and stored in an ultrasonic bath for 3 x 10 min with the renewal of the solvent in between to remove any residual non-bound dye. The PE foils were then treated with 10.0 mL of an aqueous 0.1 wt% sodium dodecyl sulfate solution for 30 min. The resulting solution containing the desorbed dye was analyzed by UV/vis spectroscopy at 590 nm. The resulting UV/vis absorbance was correlated to the concentration of desorbed crystal violet using the Beer-Lambert law:

$$c = \frac{A}{\epsilon * l}$$

A: measured absorbance

ϵ : extinction coefficient of crystal violet = 87000 M⁻¹cm⁻¹ [62]

l: optical path length [cm]

c: concentration of desorbed crystal violet [mol/L]

For calculation of the charge density, a blank value of pristine PE, treated under equivalent conditions was subtracted. Triplicate measurements of modified and pristine PE samples were performed.

Table 4: Raw data and calculation of charge density from crystal violet absorption assay. Absorbance was measured in triplicates using constant parameters: Optical path length $l = 1$ cm, crystal violet extinction coefficient of $87000 \text{ [M}^{-1}\cdot\text{cm}^{-1}\text{]}$, molecular mass of VBSB repeating unit of polymer: 283.12 g/mol . The calculation was based on an assumed adsorption ratio of 1:1 crystal violet per zwitterion.

VBSB [wt%]	Absorbance a.u.	Concentration of desorbed CV [mol/l]	Zwitterions [mol/cm ²]	Charge density [SO ₃ ⁻ /cm ²]
	0,0044	5,05747E-08	5,05747E-10	3,04561E+14
1	0,008	9,1954E-08	9,1954E-10	5,53747E+14
	0,007	8,04598E-08	8,04598E-10	4,84529E+14
	0,0039	4,48276E-08	4,48276E-10	2,69952E+14
5	0,0013	1,49425E-08	1,49425E-10	8,99839E+13
	0,025	2,87356E-07	2,87356E-09	1,73046E+15
	0,0279	3,2069E-07	3,2069E-09	1,93119E+15
10	0,053	6,09195E-07	6,09195E-09	3,66857E+15
	0,046	5,28736E-07	5,28736E-09	3,18405E+15
	0,167	1,91954E-06	1,91954E-08	1,15595E+16
20	0,145	1,66667E-06	1,66667E-08	1,00367E+16
	0,158	1,81609E-06	1,81609E-08	1,09365E+16
	0,1236	1,42069E-06	1,42069E-08	8,55539E+15
40	0,143	1,64368E-06	1,64368E-08	9,89823E+15
	0,1261	1,44943E-06	1,44943E-08	8,72844E+15
	0,046	5,28736E-07	5,28736E-09	3,18405E+15
55	0,0491	5,64368E-07	5,64368E-09	3,39862E+15
	0,131	1,50575E-06	1,50575E-08	9,06761E+15
	0,0294	3,37931E-07	3,37931E-09	2,03502E+15
80	0,03	3,44828E-07	3,44828E-09	2,07655E+15
	0,0287	3,29885E-07	3,29885E-09	1,98657E+15

7. Gravimetric determination of pVBSB grafting yield

To determine the grafting yield of modified PE-poly-(VBSB) samples gravimetric measurements using an ultra-micro balance of a TGA 2 from Mettler Toledo (Giessen, Germany) was performed. Briefly, a PE sample of 0.25 cm² was weighed before and after polymerization (conditions as specified below). For calculation, a quintuplet measurement was performed. The overall grafting yield was determined using the following equation and an average grafting yield of 264.5 ± 19 µg per cm² was determined.

$$GY = \frac{W_{\text{grafted}} - W_{\text{pristine}}}{A} : 1000$$

GY: Grafting yield of PE-(poly)-VBSB [µg/cm²]

***W_{pristine}*:** Weight of pristine PE sample [mg]

***W_{grafted}*:** Weight of PE-poly-(VBSB) sample [mg]

***A*:** Area of measured PE sample [cm²]

Table 5: Gravimetric determination of poly-VBSB grafting yield. Polymerization conditions for PE-poly-(VBSB): 20 wt% (vinylbenzyl)sulfobetaine (VBSB) in water with 1.0 wt% ammoniumperoxodisulfate (APS), 85 C, 2 h. Subsequent washing: 3x30 min with 70 %water/ethanol mixture in an ultrasonic bath followed by drying in vacuo at 50°C for three hours.

entry	W_{pristine} (PE pristine) [mg]	W_{grafted} (PE-poly-(VBSB)) [mg]	grafting yield [µg/cm ²]
1	8.0018	8.0679	264.4
2	8.0163	8.0789	250.4
3	8.0180	8.0809	251.6
4	8.0128	8.0768	256.0
5	8.0029	8.0781	300.8
		average:	264.5 ± 19

8. Bacterial adhesion assay – growth control

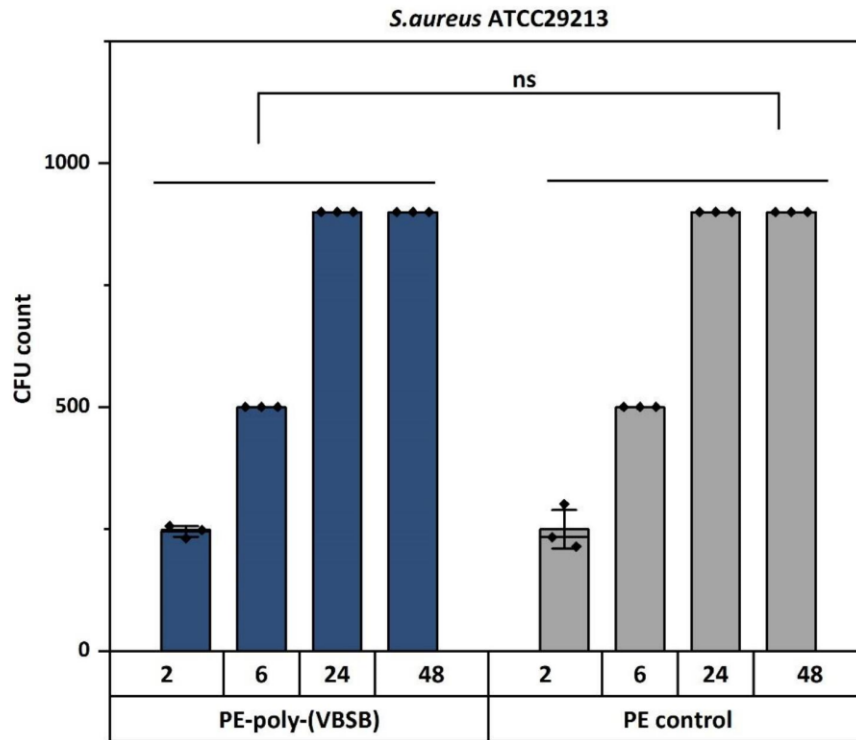


Fig 4: Growth control of each bacterial suspension to confirm non-antibacterial effects. Statistical non-significance (ns) was calculated via pairwise comparison. A p-value of higher than 0.05 was considered not significant (ns).

9. Biofilm adhesion in natural seawater

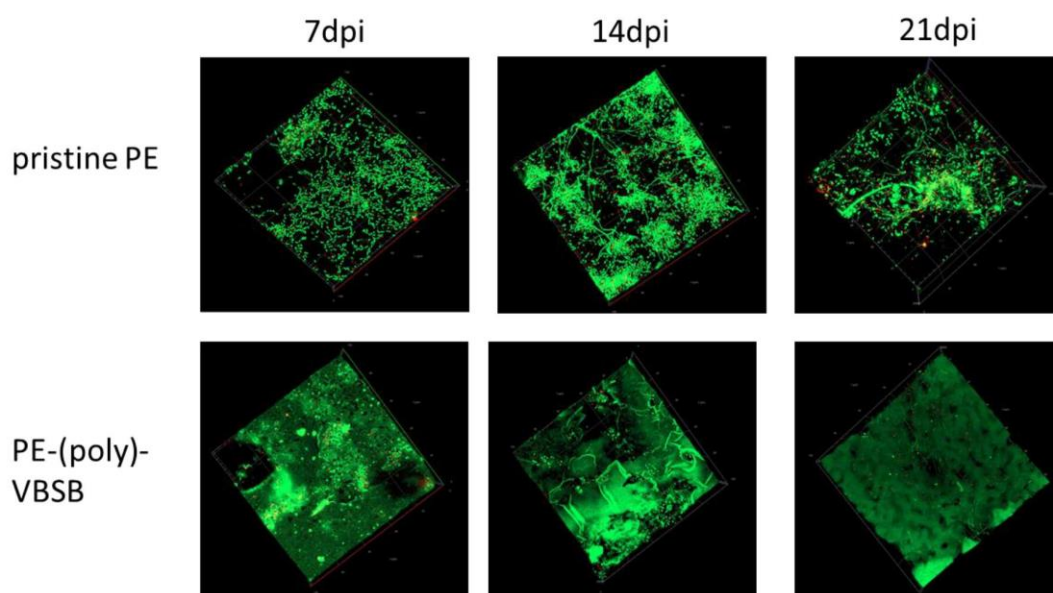
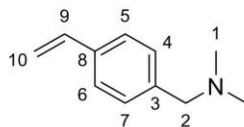


Fig 5: Confocal fluorescence microscopy images of biofilm formation after 7, 14- and 21-days past seawater incubation (dpi). Live/Dead staining: living microorganisms appear light green, dead microorganisms appear red; background autofluorescence of poly-VBSB brushes is visible as a laminar homogenous green layer.

11. Synthetic procedures

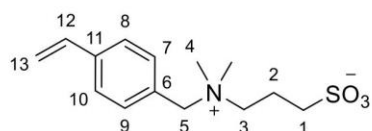
N,N-dimethyl-1-(4-vinylbenzylamine) (VBDMA):



K₂CO₃ (1 eq, 176 mmol, 24.70 g) was added to a dimethylamine solution (33 wt%) in EtOH (7 eq, 1.24 mol, 221.14 mL). The resulting suspension was cooled to 0 °C and vinylbenzylchloride (1 eq, 176.91 mmol, 27.78 mL) was added dropwise within 30 min. The reaction mixture was stirred for 18 h at room temperature. All volatile components were removed under reduced pressure. The crude product was dissolved in 200 mL of EtOAc and 200 mL of H₂O. The two layers were separated and the aqueous layer was extracted 3 times with each 100 mL of EtOAc. The combined organic layers were dried over Mg₂SO₄. Removal of the solvent under reduced pressure gave 26.29 g (163 mmol, 92 %) of the title compound as an orange-red-colored oil.

¹H NMR (500 MHz, MeOD): δ [ppm] = 7.42 (³J_{HH} = 7.9 Hz, 2H, 4-H, 7-H), 7.29 (³J_{HH} = 8.3 Hz, 2H, 5-H, 6-H), 6.78 (dd, ³J_{HH} = 10.8, 18.0 Hz, 1H, 9-H), 5.79 (dd, ³J_{HH} = 1.1, 17.9 Hz, 1H, 10a-H), 5.23 (dd, ³J_{HH} = 1.2, 10.8 Hz, 1H, 10b-H), 3.47 (s, 2H, 2-H), 2.25 (s, 6H, 1-H)

¹³C NMR (126 MHz, MeOD): δ [ppm] = 138.4 (C3), 138.3 (C9), 130.9 (C4, C7), 126.6 (C5, C6), 114.0 (C10) 64.6 (C2), 44.4 (C1).

(Vinylbenzyl)sulfobetaine (VBSB)

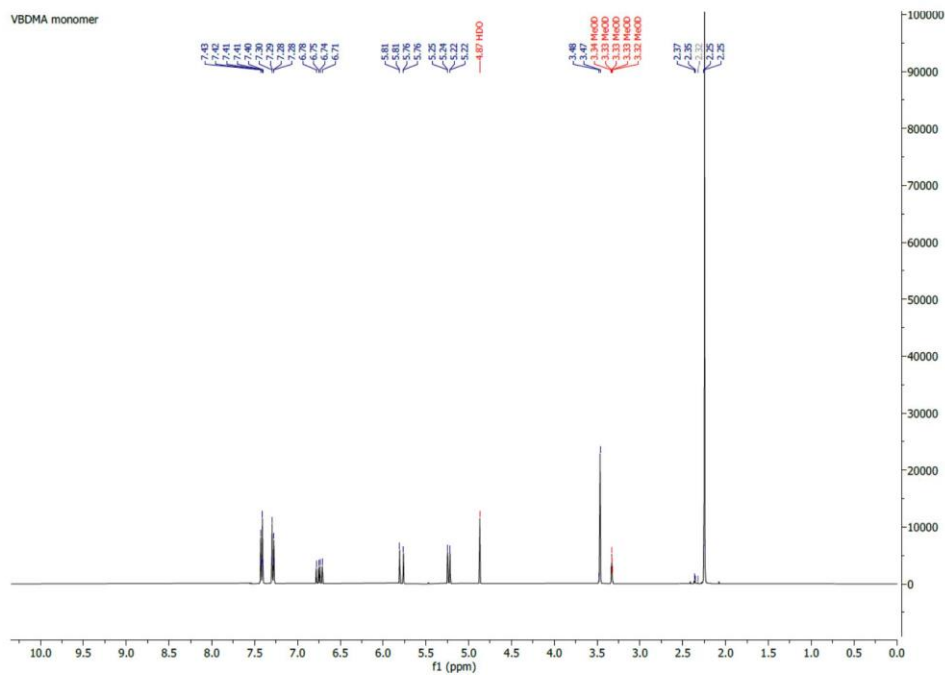
1,3 propanesultone (1.5 eq, 139.54 mmol, 8.73 mL) was dissolved in 100 mL EtOAc at room temperature and VBDMA (1 eq, 93.02 mmol, 15.00 g) was added dropwise within 30 min. The reaction mixture was vigorously stirred at 50°C for 20 h. The resultant precipitant was washed with ethyl acetate to obtain the colorless crude product. The crude product was crystallized from ethanol to obtain 23.16 g (81.73 mmol, 88%) of the title compound as a colorless solid.

^1H NMR (500 MHz, D_2O): δ [ppm] = 7.63 ($^3J_{\text{HH}} = 8.3$ Hz, 2H, 7-H, 9-H), 7.53 ($^3J_{\text{HH}} = 8.3$ Hz, 2H, 8-H, 10-H), 6.85 (dd, $^3J_{\text{HH}} = 11.13$, 7.4 Hz, 1H, 12-H), 5.96 (d, $^3J_{\text{HH}} = 17.8$ Hz, 2H, 13a-H), 5.44 (d, $^3J_{\text{HH}} = 11.1$ Hz, 1H, 13b-H), 4.52 (s, 1H, 5-H), 3.46 (m, 2H, H-3), 3.07 (m, 6H, 4-H), 2.99 (t, $^3J_{\text{HH}} = 7.3$ Hz, 2H, 1-H), 2.34 (m, 2H, 2-H).

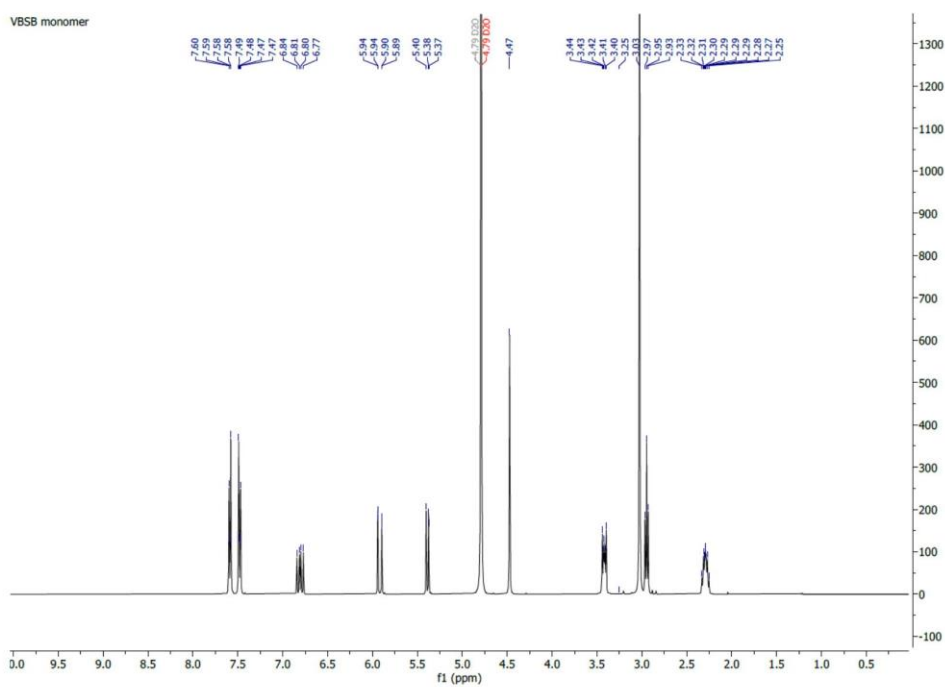
^{13}C NMR (101 MHz, D_2O): δ [ppm] = 139.7 (C6), 137.1 (C13), 133.6 (C8, C10), 127.4 (C7, C9), 125.8 (C11), 116.3 (C12), 67.9 (C5), 61.3 (C3), 50.4 (C4), 44.0 (C1), 16.9 (C2).

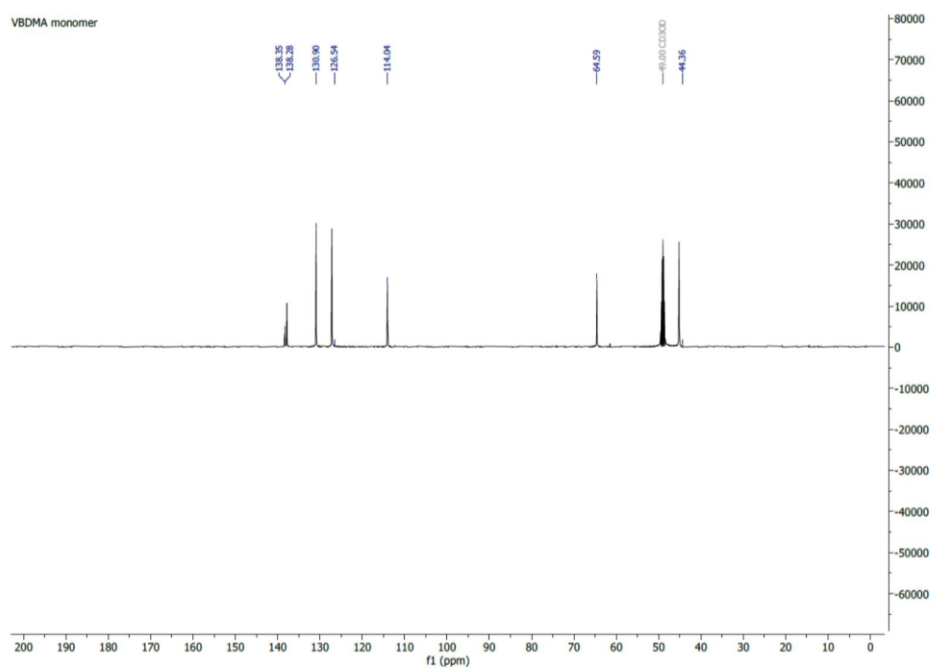
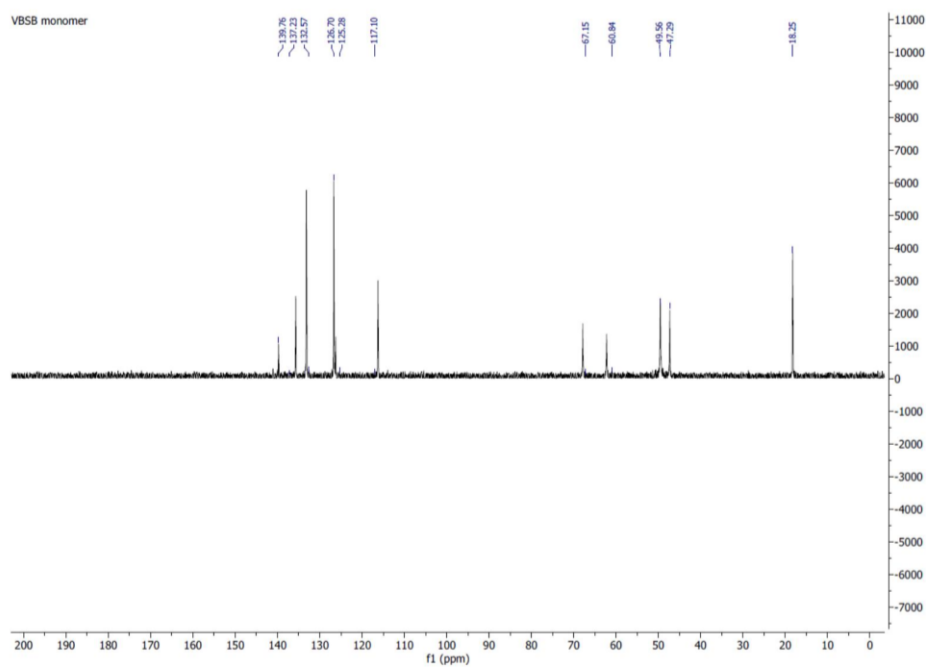
12. NMR spectra

¹H-NMR of *N,N*-dimethyl-1-(4-vinylbenzylamine)



¹H-NMR of (Vinylbenzyl)sulfobetaine



^{13}C -NMR of *N,N*-dimethyl-1-(4-vinylbenzylamine) **^{13}C -NMR of (Vinylbenzyl)sulfobetaine**

9.1.2 Low-fouling and antibacterial polymer brushes *via* surface-initiated polymerization of a mixed zwitterionic and cationic monomer

Supporting information for

Low-fouling and antibacterial polymer brushes via surface-initiated polymerization of a mixed zwitterionic and cationic monomer

Nils Burmeister^{‡,a}, Eilika Zorn^{‡,a}, Lena Preuss^b, Donovan Timm^a, Nico Scharnagl^c, Marcus Rohnke^d, Sebastian G. Wicha^a, Wolfgang R. Streit^b, Wolfgang Maison^a

^aUniversität Hamburg, Department of Chemistry, Bundesstrasse 45, 20146 Hamburg, Germany

^bUniversität Hamburg, Department of Microbiology and Biotechnology, Ohnhorststrasse 18, 22609 Hamburg, Germany.

^cHelmholtz-Zentrum Hereon GmbH, Institute of Surface Science, Max-Planck-Strasse 1, 21502 Geesthacht, Germany.

^dJustus-Liebig-Universität Gießen, Institute of Physical Chemistry, Heinrich-Buff-Ring 17, 35392 Giessen, Germany.

* corresponding author: Wolfgang Maison. Email: wolfgang.maison@uni-hamburg.de

Table of content

Thermogravimetric measurement	3
ATR-FTIR spectra of TiO₂-p-(VBDSB)	6
Fluorescein-and Crystal violet assay for charge density determination	7
Stability test (Soxhlet extraction)	8
XPS analysis	9
Results of the ASTM E2149-13a	12
Results of the Bacterial Adhesion Assay	13
Growth controls of the Bacterial Adhesion Assay	14
Results of the Agar plate diffusion test (DIN EN ISO 20645:2002-02)	16
Assessment of Antimicrobial-Activity of p-(VBDSB)	18

NMR spectra	19
References	21

Thermogravimetric measurement

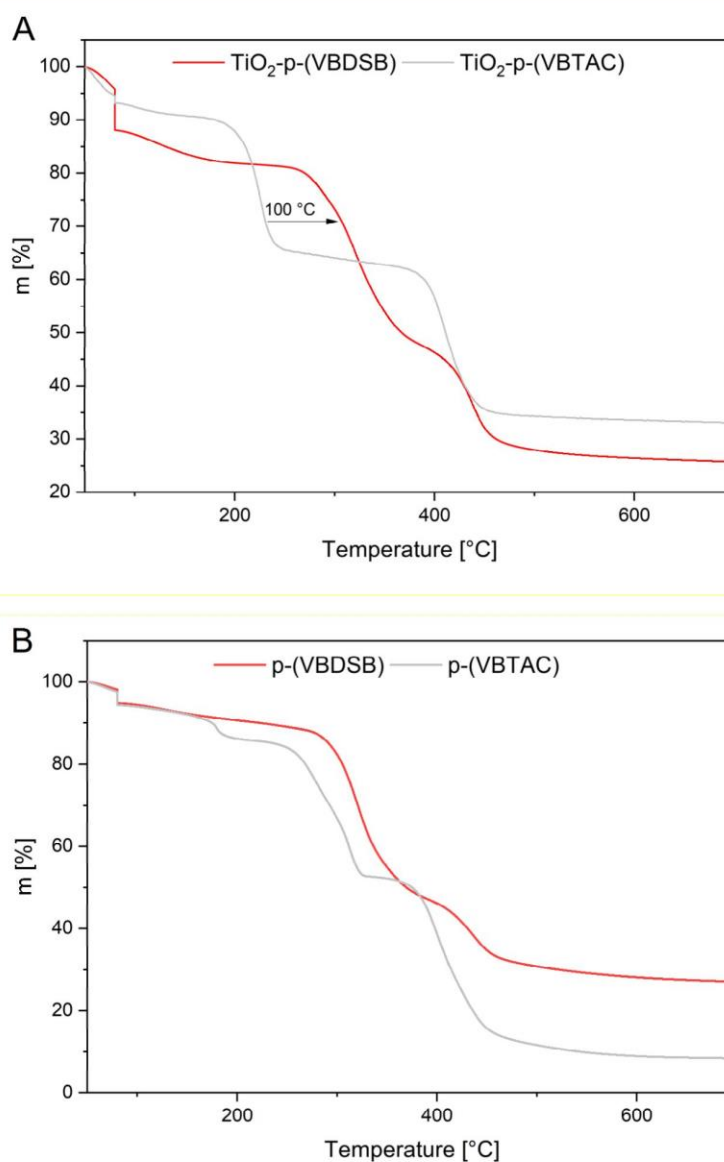


Figure S1. TGA results of A) TiO₂-p-(VBTAC), TiO₂-p-(VBDSB) and B) p-(VBTAC) and p-(VBDSB) homopolymers. Overall weight loss Δm [%] over two steps and plotted shift for the degradation of the grafted polymers.

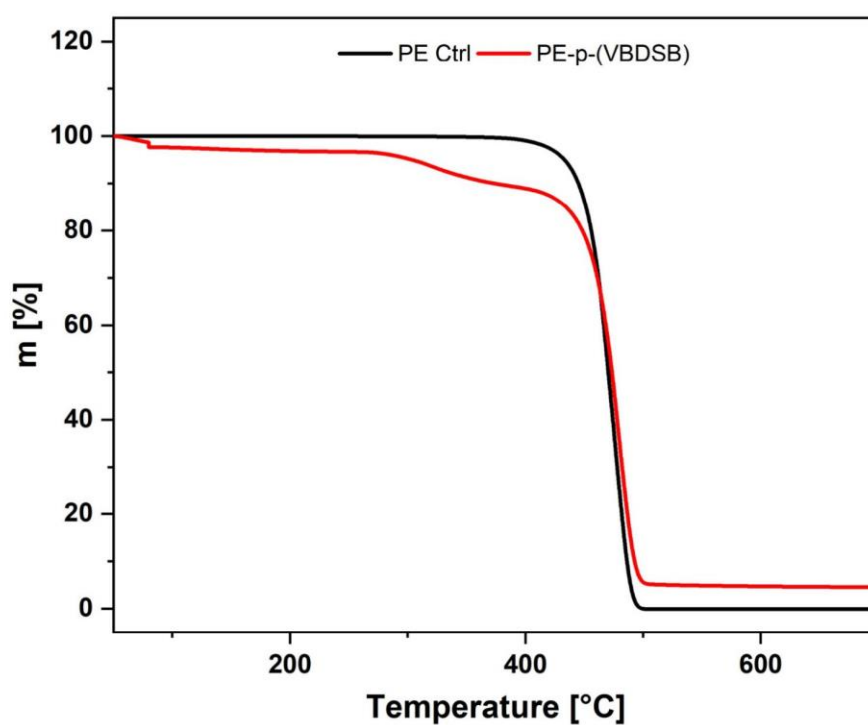


Figure S2. TGA results for PE foils, PE ctrl and PE-p-(VBDSB).

The grafting yield was calculated from the estimated layer thickness from ToF-SIMS analysis with Equation S1.

$$\text{Equation S1} \quad \sigma(pVBDSB) = d * 1 \text{ cm}^2 * \rho$$

With d = layer thickness estimated from ToF-SIMS analysis.

The density of the styrene polymer $\rho = 1.05 \text{ g*cm}^{-3}$

N^+ per cm^2 can be calculated out of the grafting yield with Equation S1.

Equation S1
$$\frac{N^+}{cm^2} = \frac{\sigma(pVBDSB) * N_A}{M(VBDSB) * 10^4}$$

With $M(VBDSB)$ = molecular weight of the Monomer VBDSB $351.17 \text{ g}^*\text{mol}^{-1}$.

And $M(VBTAC)$ = molecular weight of the monomer VBTAC: $211.73 \text{ g}^*\text{mol}^{-1}$.

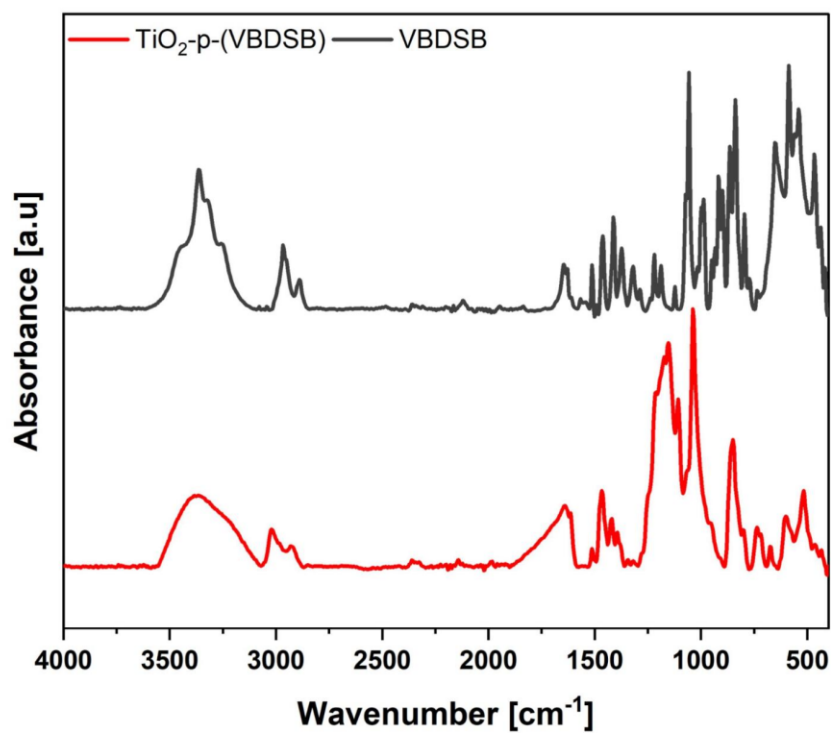
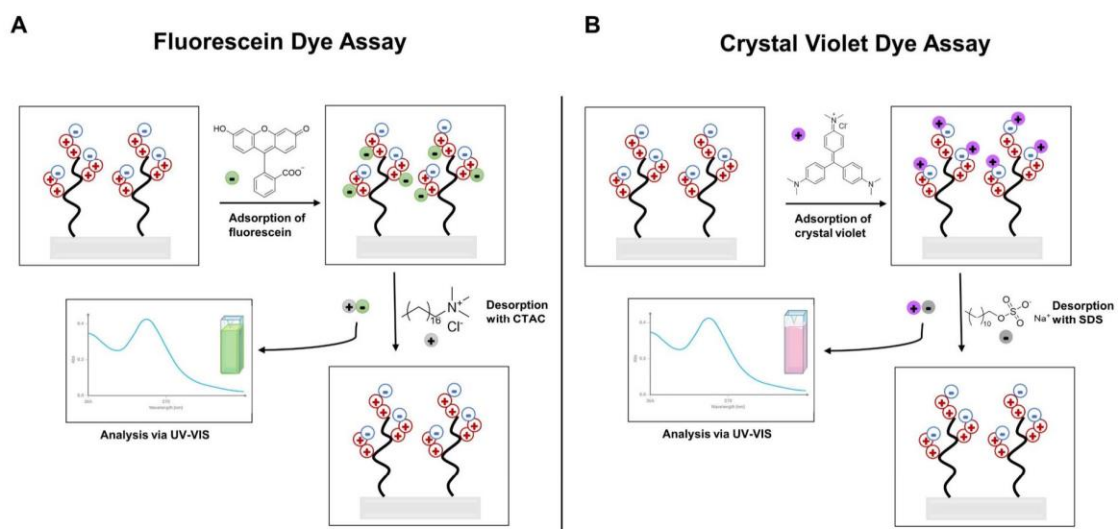
ATR-FTIR spectra of TiO₂-p-(VBDSB)

Figure S3. ATR-FTIR spectra of VBDSB monomer (black line) and grafted nanoparticle TiO₂-p-(VBDSB) (red line). ATR-FTIR measurements were carried out as described in the experimental section.

Fluorescein-and Crystal violet assay for charge density determination

XPS analysis

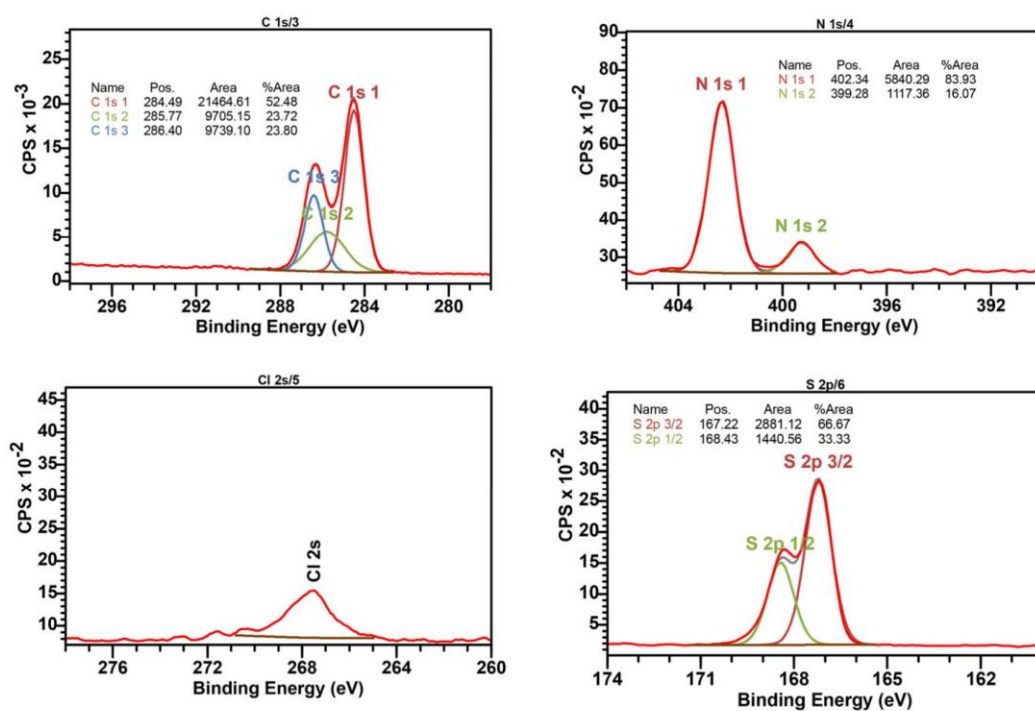


Figure S5. Deconvoluted XPS spectra of PE-p-(VBDSB).

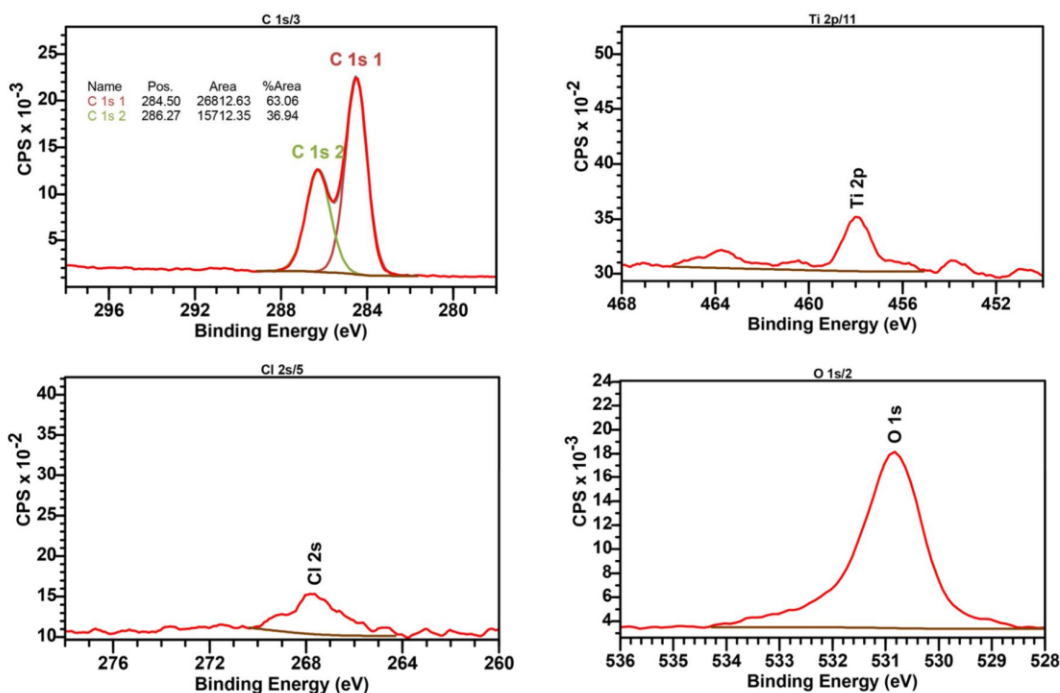


Figure S6. Deconvoluted XPS-spectra of Ti-p-(VBDSB)

The high-resolution spectra of C 1s for both materials show two overlapping peaks. For PE-p-(VBDSB) the C 1s spectra were deconvoluted into three peaks at 284.5 eV, 285.8 eV and 286.4 eV. In the C 1s spectra of Ti-p-(VBDSB) peaks are presented at 284.5 eV and 286.3 eV. The peaks with higher energy can be assigned to the CN^+ and CSO_3^- bonding. The lower peaks can be assigned to aliphatic C-C and C-H binding of the polymer formed on the surface.³ Peak at 530.8 eV with high-energy tailing in the high resolution spectra of O 1s for both materials correlate to the sulfonate oxygen.⁴

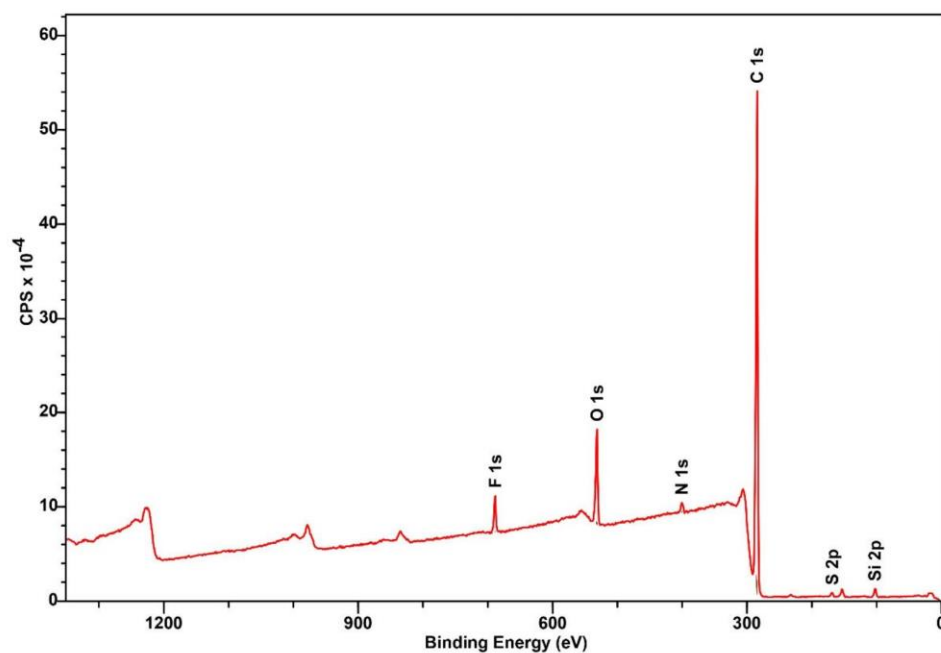


Figure S7. XPS-survey spectra of non-modified PE

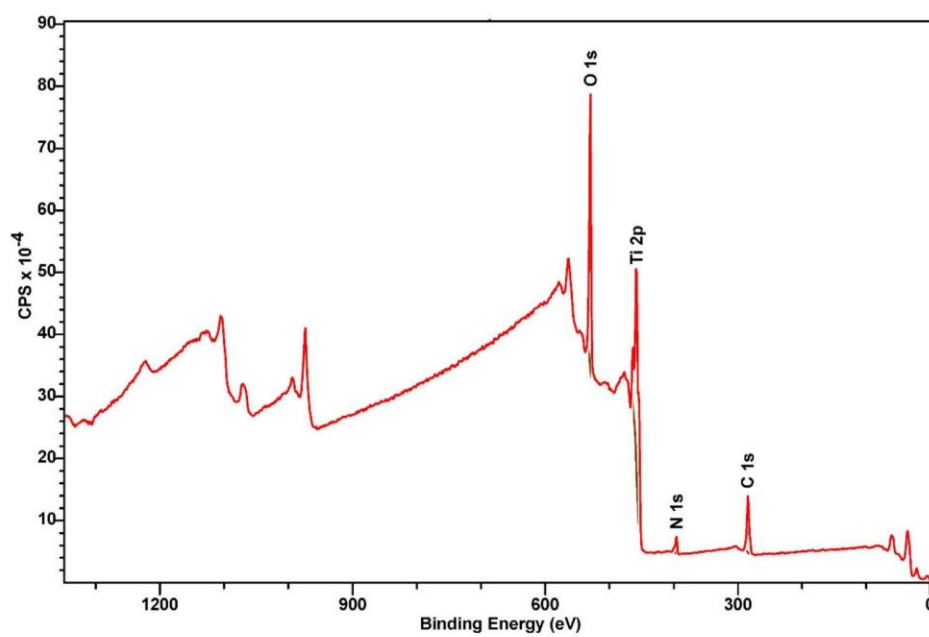


Figure S8. XPS-survey spectra of non-modified titanium.

Results of the ASTM E2149-13a

Table S2. Results of the antimicrobial determination via ASTM E2149 13a of Titanium modifications. Log₁₀ reduction was calculated as described in the experimental section. Values are given as mean values (n = 3) ± SD.

Sample	Bacterial strain	Log (N ₀ /N) reduction
Ti-p-(VBDSB)	<i>E. coli</i> ATCC 25922	2.6 ± 0.1
Ti-p-(VBDSB)	<i>S. aureus</i> ATCC 29213	1.6 ± 0.1
Ti-p-(VBDSB)	<i>P. aeruginosa</i> PA01	1.6 ± 0.0
Ti-p-(VBDSB)	<i>S. aureus</i> ATCC 25923	3.0 ± 0.1
Ti-p-(VBTAC)	<i>E. coli</i> ATCC 25922	4.5 ± 0.0
Ti-p-(VBTAC)	<i>S. aureus</i> ATCC 29213	2.2 ± 0.3
Ti-p-(VBTAC)	<i>P. aeruginosa</i> PA01	1.5 ± 0.1
PE-p-(VBDSB)	<i>S. aureus</i> ATCC 25923	3.1 ± 0.0
PE-p-(VBDSB)	<i>P. aeruginosa</i> PA01	1.3 ± 0.1
PE-p-(VBTAC)	<i>P. aeruginosa</i> PA01	1.5 ± 0.1

Results of the Bacterial Adhesion Assay

Table S3. Results of the bacterial adhesion assay of PE modifications compared to non-modified PE (Ctrl). Values declared as colony-forming units (CFU) per mm² are given as mean values (n = 3) ± SD.

Sample	Bacterial strain	CFU/cm ²
PE-p-(VBDSB)	<i>E. coli</i> ATCC 25922	94 ± 35
PE-p-(VBDSB)	<i>S. aureus</i> ATCC 29213	156 ± 69
PE-p-(VBDSB)	<i>P. aeruginosa</i> PA01	(no attachment)
PE Ctrl	<i>E. coli</i> ATCC 25922	> 250 (TNTC)
PE Ctrl	<i>S. aureus</i> ATCC 29213	> 250 (TNTC)
PE Ctrl	<i>P. aeruginosa</i> PA01	> 250 (TNTC)

Growth controls of the Bacterial Adhesion Assay

Table S4: Growth controls for the incubation solution of the bacterial adhesion assays after 24 hours at 37°C in MHB medium. For evaluation, 100 µL of the suspension were aliquoted on Columbia Agar and incubated overnight prior cell counting. Cell counts above 250 were set as too numerous to count (TNTC). Values declared as colony-forming units (CFU) are presented as mean values (n =3) ± SD.

Sample	Bacterial strain	CFU
PE-p-(VBDSB)	<i>E. coli</i> ATCC 25922	> 250 (TNTC)
PE-p-(VBDSB)	<i>S. aureus</i> ATCC 29213	> 250 (TNTC)
PE-p-(VBDSB)	<i>P. aeruginosa</i> PA01	> 250 (TNTC)
PE Ctrl	<i>E. coli</i> ATCC 25922	> 250 (TNTC)
PE Ctrl	<i>S. aureus</i> ATCC 29213	> 250 (TNTC)
PE Ctrl	<i>P. aeruginosa</i> PA01	> 250 (TNTC)
Ti-p-(VBDSB)	<i>E. coli</i> ATCC 25922	> 250 (TNTC)
Ti-p-(VBDSB))	<i>S. aureus</i> ATCC 29213	> 250 (TNTC)
Ti-p-(VBDSB))	<i>P. aeruginosa</i> PA01	> 250 (TNTC)
Ti Ctrl	<i>E. coli</i> ATCC 25922	> 250 (TNTC)

Ti Ctrl	<i>S. aureus</i> ATCC 29213	> 250 (TNTC)
Ti Ctrl	<i>P. aeruginosa</i> PA01	> 250 (TNTC)

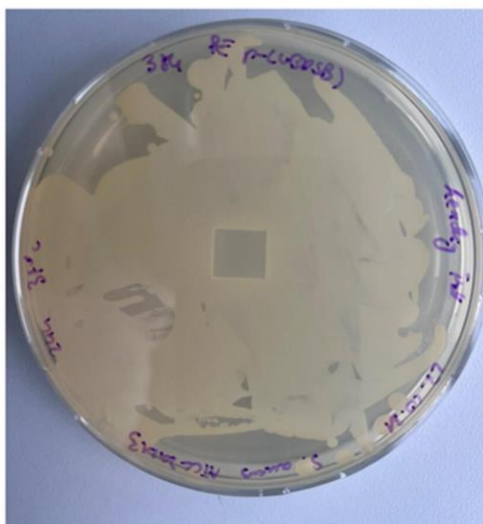
Results of the Agar plate diffusion test (DIN EN ISO 20645:2002-02)

Figure S9: Exemplary image of the agar plate diffusion test (DIN EN ISO 20645:2002-02) of PE-p-(VBDSB) against *S. aureus* ATCC29213, with no inhibition zone detected after 20 h of incubation. At 37°C.

Table S4. Results of the Agar plate diffusion test (DIN EN ISO 20645:2002-02). Briefly, test specimens (with the size of 1.0 cm²) were placed with the p-(VBDSB)-grafted surface facing downwards in a two-layer agar plate (Columbia agar). The top agar layer was previously covered with 200 µL of 1.5*10⁸ CFU/mL of either *S. aureus* (strain ATCC29213) or *E. coli* (strain ATCC25922) suspension. Plates were incubated for 20 h at 37 °C. The plates were then assessed for the development of an inhibition zone surrounding the test specimen. Inhibition zones were presented as mean values (n = 3) ± SD.

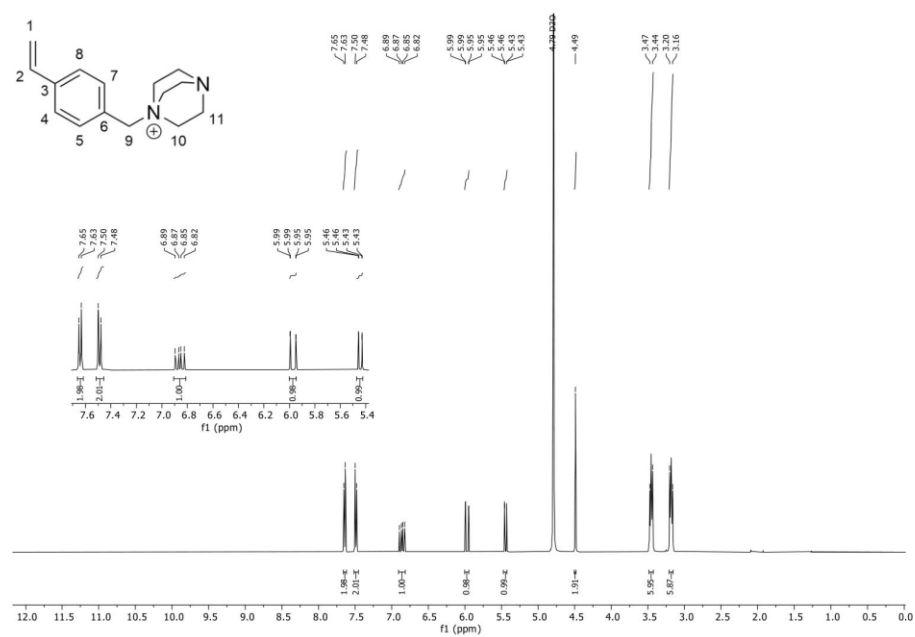
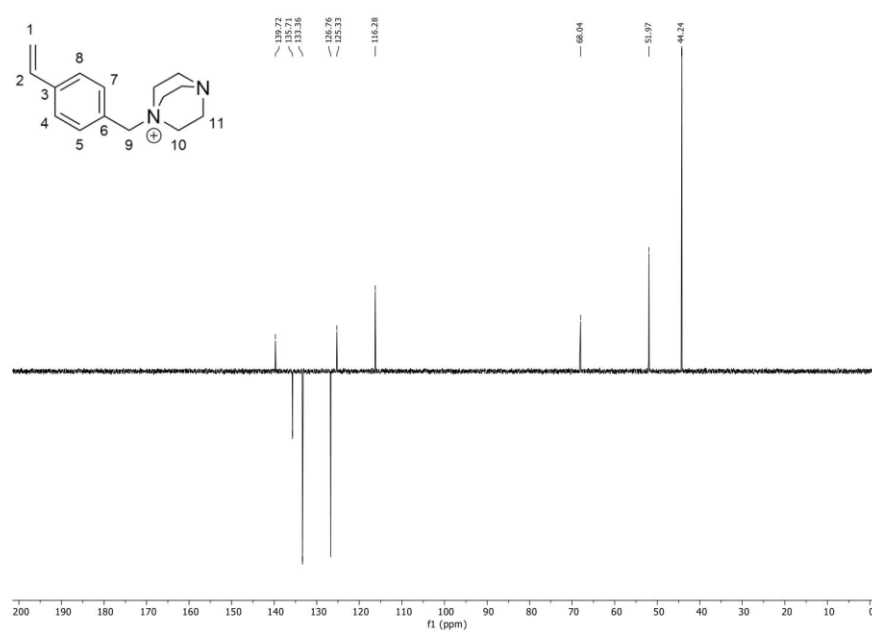
Sample	Bacterial strain	Inhibition zone [mm]
PE-p-(VBDSB)	<i>E. coli</i> ATCC 25922	No inhibition zone
PE-p-(VBDSB)	<i>S. aureus</i> ATCC 29213	No inhibition zone
PE Ctrl	<i>E. coli</i> ATCC 25922	No inhibition zone
PE Ctrl	<i>S. aureus</i> ATCC 29213	No inhibition zone

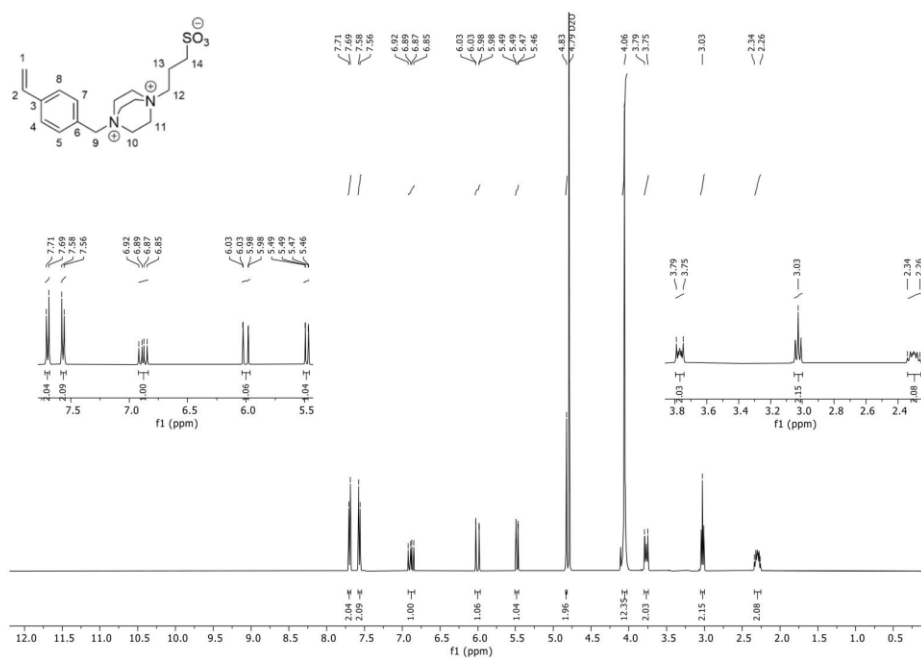
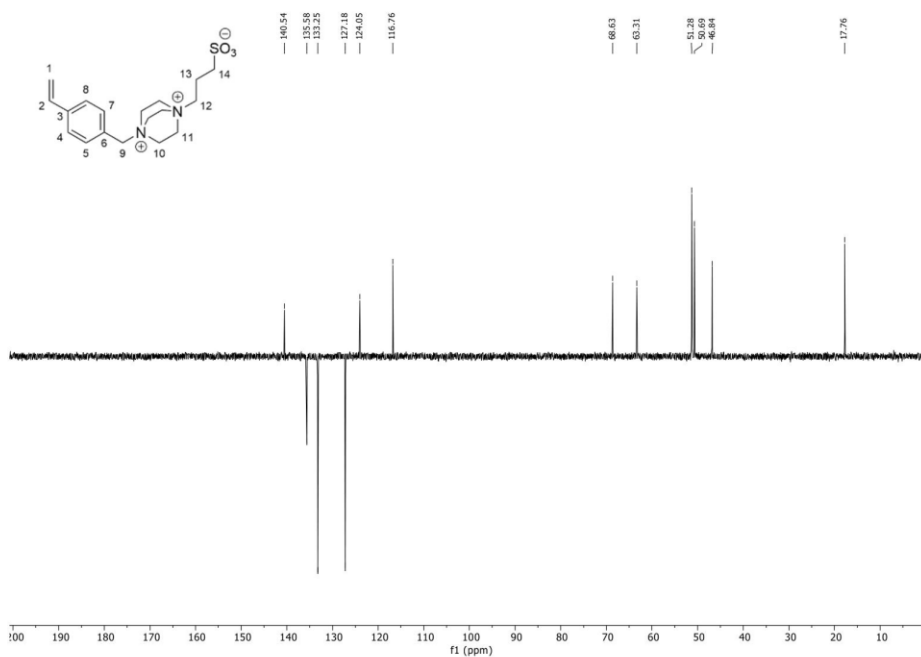
Assessment of Antimicrobial-Activity of p-(VBDSB)

Table S6. The minimum inhibitory concentration (MIC) of p-(VBDSB) against *S. aureus* (strain ATCC29213) and *E. coli* (strain ATCC25922) was determined by the microdilution method (Methods for Dilution Antimicrobial Susceptibility Tests for Bacteria That Grow Aerobically; Approved Standard—Ninth Edition. CLSI document M07-A9. Wayne, PA: Clinical and Laboratory Standards Institute; 2012). As the upper limit, a concentration of 78.5 µg/mL was selected, which reflects the maximum amount of leaching polymer according to the determined grafting yield. Preparation of p-(VBDSB): VBDSB monomer (2.00 g, 5.17 mmol, 1.0 eq.) was dissolved with AIBN (8.5 mg, 0.052 mmol, 0.01 eq.) in demin. water (5 mL) and was purged with nitrogen for 30 min. The obtained solution was heated to 80 °C for 1 h. The viscous solution was lyophilized to obtain a colorless powder, which was washed excessively with water and *i*-PrOH.

Polymer	Bacterial strain	MIC ₉₀
p-(VBDSB)	<i>S. aureus</i> ATCC 29213	> 78.75µg/mL
p-(VBDSB)	<i>E. coli</i> ATCC 25922	> 78.75µg/mL

NMR spectra

 ^1H spectra of VBD ^{13}C (^1H) Spectra of VBD

¹H spectra of VBDSB¹³C (1H) spectra of VBDSB

References

- (1) Murata, H.; Koepsel, R. R.; Matyjaszewski, K.; Russell, A. J. Permanent, non-leaching antibacterial surface--2: how high density cationic surfaces kill bacterial cells. *Biomaterials* **2007**, *28* (32), 4870-4879. DOI: 10.1016/j.biomaterials.2007.06.012.
- (2) Burmeister, N.; Vollstedt, C.; Kröger, C.; Friedrich, T.; Scharnagl, N.; Rohnke, M.; Zorn, E.; Wicha, S. G.; Streit, W. R.; Maison, W. Zwitterionic surface modification of polyethylene via atmospheric plasma-induced polymerization of (vinylbenzyl-)sulfobetaine and evaluation of antifouling properties. *Colloids and Surfaces B: Biointerfaces* **2023**, *224*. DOI: 10.1016/j.colsurfb.2023.113195.
- (3) Zhang, Z.; Chao, T.; Chen, S.; Jiang, S. Superlow Fouling Sulfobetaine and Carboxybetaine Polymers on Glass Slides. *Langmuir* **2006**, *22* (24), 10072-10077. DOI: 10.1021/la062175d.
- (4) Shan, B.; Yan, H.; Shen, J.; Lin, S. Ozone-induced grafting of a sulfoammonium zwitterionic polymer onto low-density polyethylene film for improving hemocompatibility. *J. Appl. Polym. Sci.* **2006**, *101* (6), 3697-3703. DOI: <https://doi.org/10.1002/app.20860>.

9.1.3 Surface grafted N-Oxides have Low-Fouling and Antibacterial Properties



Supporting Information

for *Adv. Mater. Interfaces*, DOI 10.1002/admi.202300505

Surface Grafted N-Oxides have Low-Fouling and Antibacterial Properties

*Nils Burmeister, Eilika Zorn, Aneeq Farooq, Lena Preuss, Christel Vollstedt, Timo Friedrich, Tomi Mantel, Nico Scharnagl, Marcus Rohnke, Mathias Ernst, Sebastian G. Wicha, Wolfgang R. Streit and Wolfgang Maison**

WILEY-VCH

Supporting Information

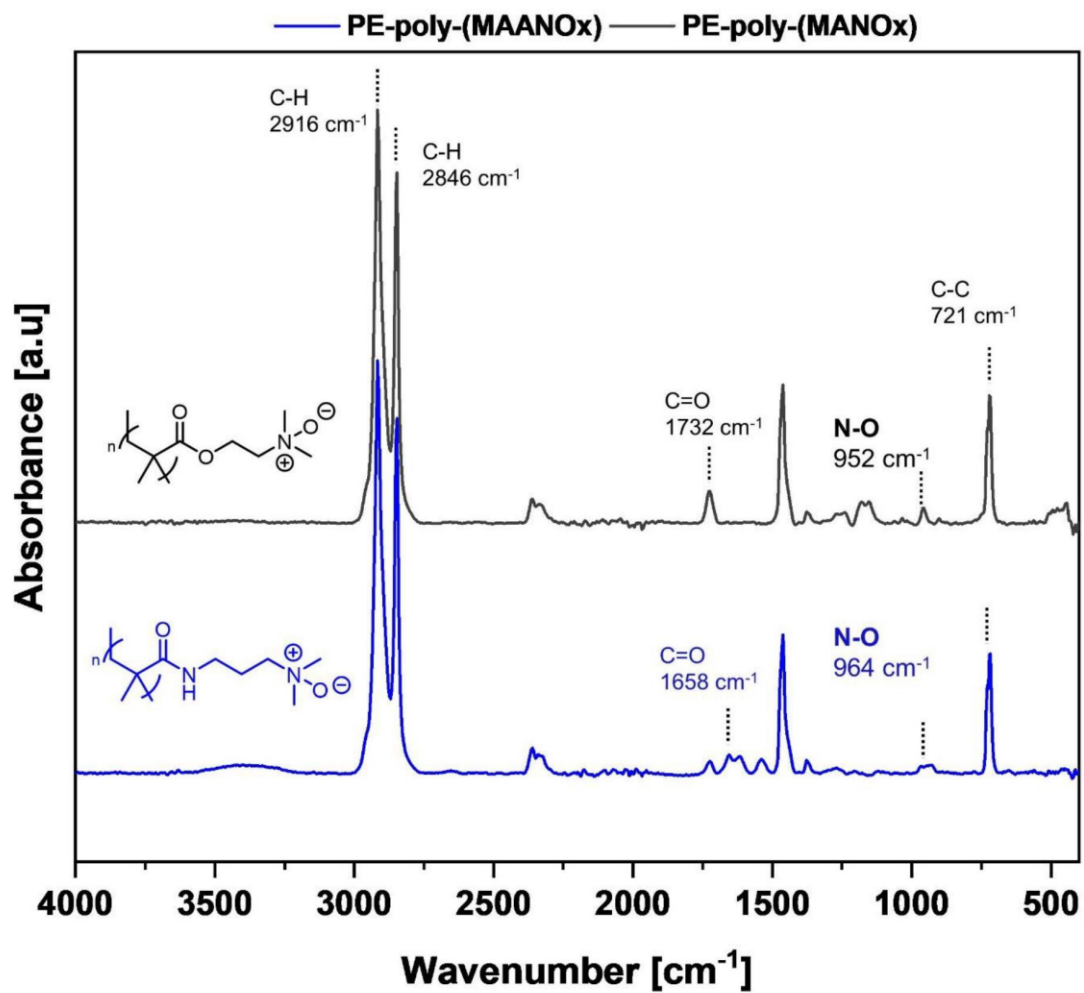
Surface grafted *N*-Oxides have low-fouling *and* antibacterial properties

*Nils Burmeister, Eilika Zorn, Aneeq Farooq, Lena Preuss, Christel Vollstedt, Timo Friedrich, Tomi Mantel, Nico Scharnagl, Marcus Rohnke, Mathias Ernst, Sebastian G. Wicha, Wolfgang R. Streit, Wolfgang Maison**

Content

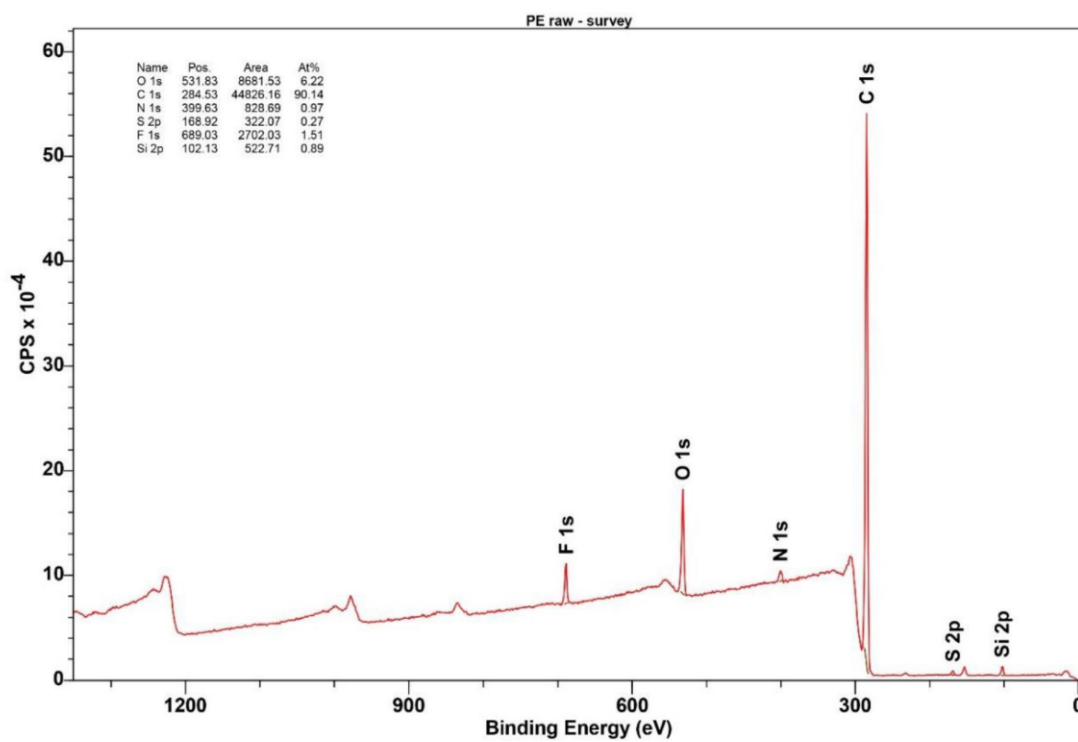
Figure S1. ATR-FTIR-spectra of PE-poly (MANOx) and PE-poly (MAANOx).....	2
Figure S2. XPS survey spectra of pristine PE.....	3
Figure S3. XPS survey spectra of plasma-activated PE.....	4
Figure S4. Deconvoluted XPS spectra of plasma-activated PE.....	5
Figure S5. XPS survey spectra of PE-poly-(VBNOx).....	6
Figure S6. Deconvoluted XPS spectra: N1s region of PE-poly-(VBNOx).....	7
Table S1. MIC-Tests of <i>N</i> -oxide derivatives.....	8
Figure S7. Agar plate diffusion test (DIN EN ISO 20645:2002-02).....	9
Figure S8. Bacterial adhesion assay of poly- <i>N</i> -Oxide materials.....	10
Figure S9. Bacterial adhesion assay – growth controls.....	11
Figure S10. HRP assay of PE-poly-(VBNOx).....	12
Figure S11. DPPH assay: Overview of DPPH-assay at 70°C in benzene for 24 hours of incubation.....	13
Figure S12. Control experiments of the EPR spectroscopy.....	14
Figure S13. Water contact angles, Zeta potential and ATR-FTIR spectra after repeated ASTM E2149-13a (three times).....	15
Estimated grafting yield of PE-poly-(VBNOx).....	16
Synthetic procedures.....	17
NMR-spectra.....	18

WILEY-VCH

Figure S1. ATR-FTIR-spectra of PE-poly (MANOx) and PE-poly (MAANOx)

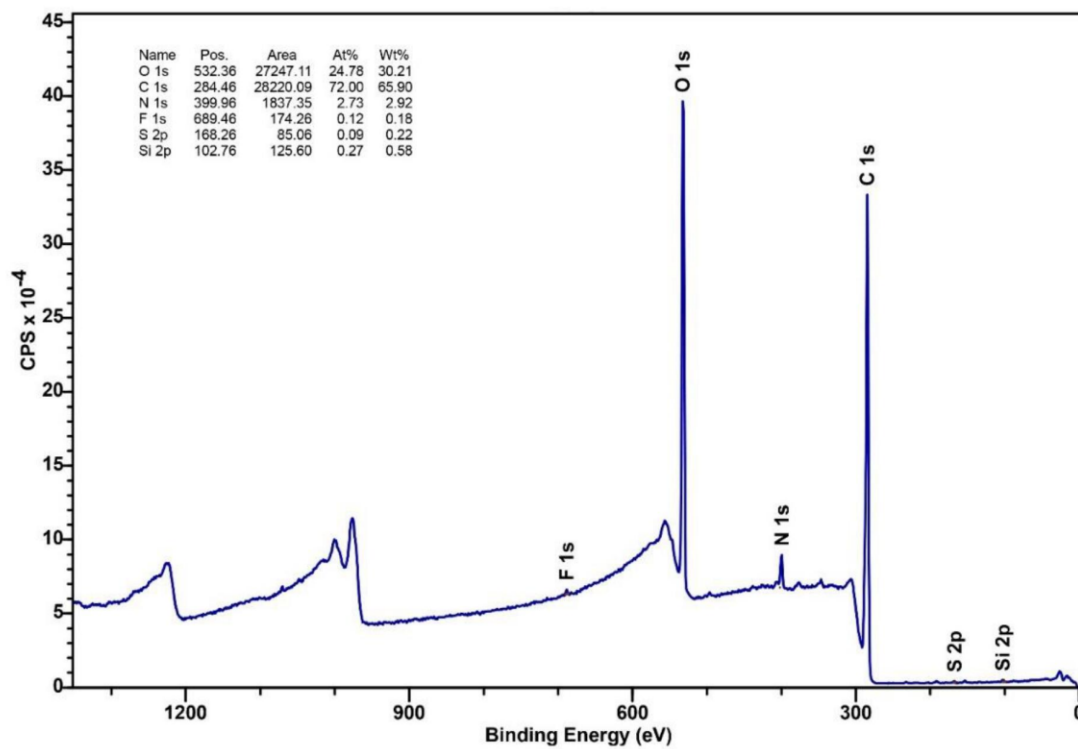
WILEY-VCH

Figure S2. XPS survey spectra of pristine PE



WILEY-VCH

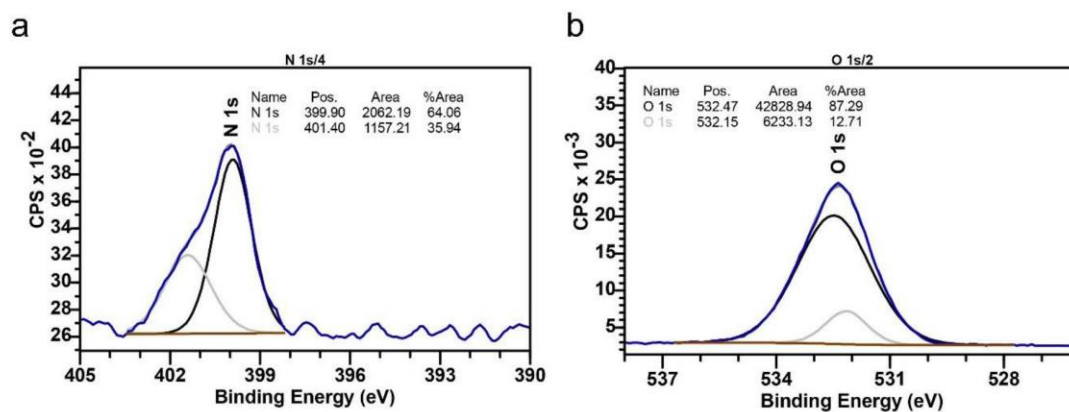
Figure S3. XPS survey spectra of plasma-activated PE. Spectra were recorded 72 h after plasma activation.



WILEY-VCH

Figure S4. Deconvoluted XPS spectra of plasma-activated PE.

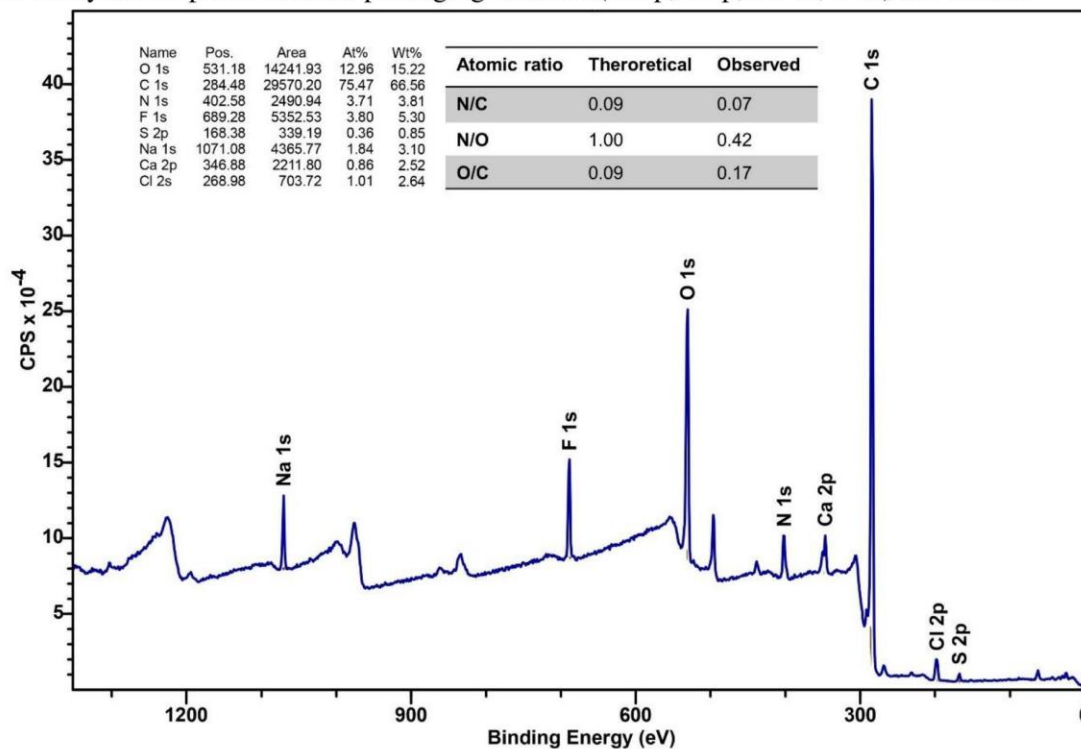
a) Deconvoluted N1s region of plasma-activated PE and b) Deconvoluted XPS region of the O1s region of plasma-activated PE. Plasma activation was carried out as described in the experimental section. Spectra were recorded 72 h after plasma activation. Plasma-activated PE samples were stored under nitrogen atmosphere prior XPS measurements.



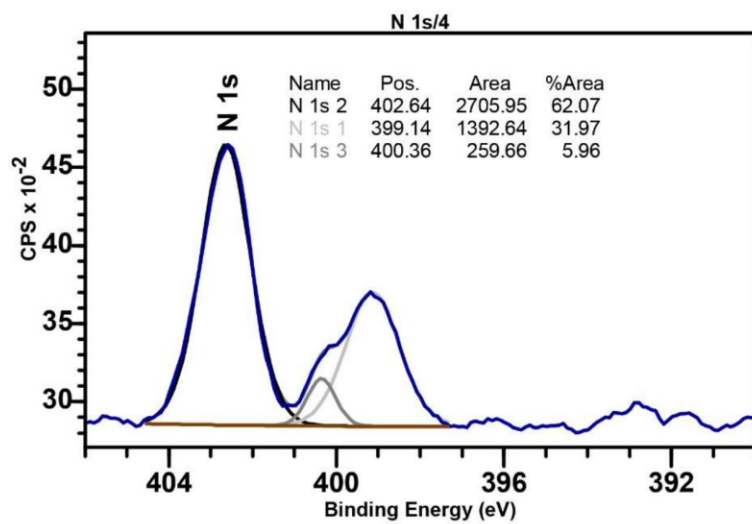
WILEY-VCH

Figure S5. XPS survey spectra of PE-poly-(VBNOx).

Synthesis and polymerization protocols were carried out as described in the experimental section. Atomic ratio for N/C is similar to the theoretical ratio. The deviation of the N/O and C/O ratio were assigned to non-identified impurities, most likely absorbed CO. Residues of sodium hydroxide species from the decomposition process of the material as well as artifacts of the synthetic procedure and packaging material (Si 2p, S 2p, Ca 1s, F 1s) are visible.



WILEY-VCH

Figure S6. Deconvoluted XPS spectra: N1s region of PE-poly-(VBNOx).

WILEY-VCH

Table S1. MIC-Tests of *N*-oxide derivatives.

Molecule	MIC, <i>E. coli</i> ATCC 25922	MIC, <i>S. aureus</i> ATCC 29213
VBNOx	>1024 µg/mL	>1024 µg/mL
MANOx	>1024 µg/mL	>1024 µg/mL
MAANOx	>1024 µg/mL	>1024 µg/mL
Benzalkoniumchloride	<16 µg/mL	<16 µg/mL

WILEY-VCH

Figure S7. Agar plate diffusion test (DIN EN ISO 20645:2002-02).

Exemplary images of the agar plate diffusion test (DIN EN ISO 20645:2002-02) a) PE-poly-(VBNOx) sample and b) pristine PE after 20 hours at 37°C incubation against *S. aureus* ATC29213.

$$IZ = \frac{D - d}{2} \quad (1)$$

IZ: Inhibition zone [mm]

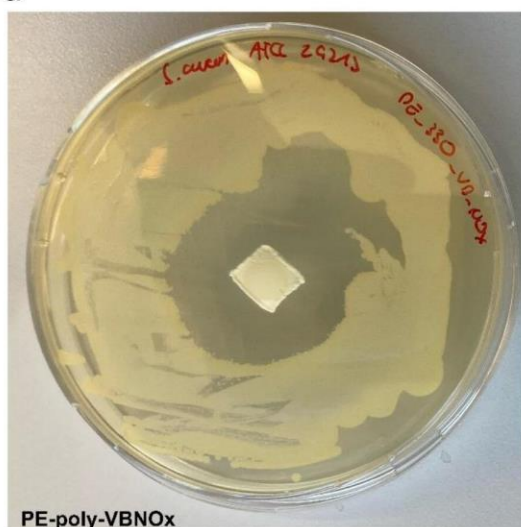
D: Diameter of sample and inhibition zone [mm]

d: Diameter of sample [mm]

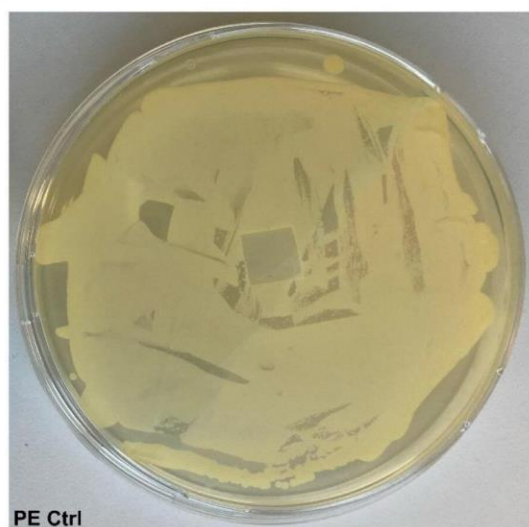
material	IZ [mm], <i>E. coli</i> ATCC 25922	IZ [mm], <i>S. aureus</i> ATCC 29213
PE-poly-(VBNOx)	11.8 ± 2.2	14.1 ± 1.6
PE Ctrl	No inhibition zone	No inhibition zone

IZ-values were determined using equation (1) and are given as mean value ± SD of three independent measurements.

a



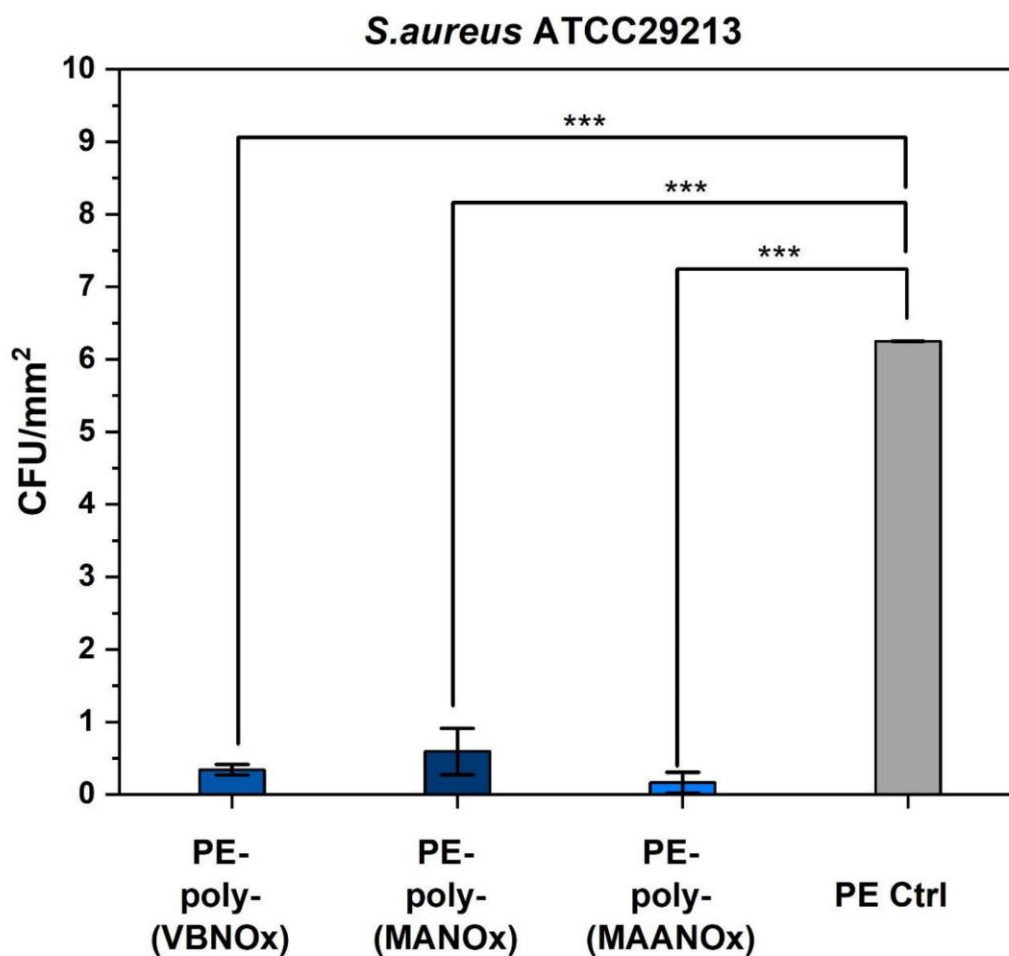
b



WILEY-VCH

Figure S8. Bacterial adhesion assay of poly-N-Oxide materials.

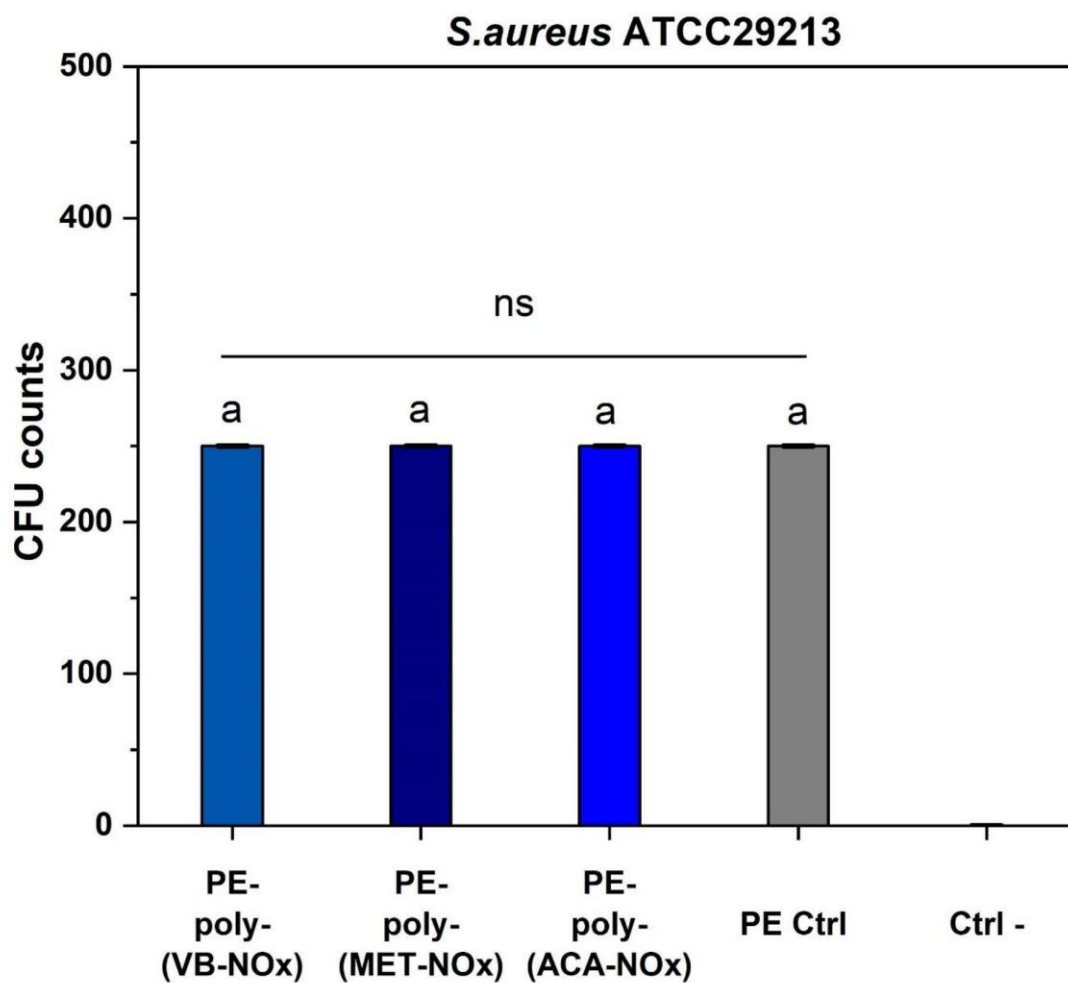
Bacterial adhesion assay of PE-poly-(VBNOx) compared to PE-poly-(MANOx) and PE-poly-(MAANOx). To all experiments, positive controls of pristine PE were added (PE Ctrl) as well as negative controls of pure MHB. Bars are represented as mean values \pm SD of three independent measurements. Statistical significance was determined using the Tukey test *via* pairwise comparison $p \leq 0.001$ (***)



WILEY-VCH

Figure S9. Bacterial adhesion assay – growth controls.

Growth control experiments of the bacterial adhesion assay of PE-poly-(VBNO_x), PE-poly-(MANO_x), PE-poly-(MAANO_x) and the pristine PE (PE Ctrl) incubated media. All growth controls were validated against one negative control of pure MHB (Ctrl -). Colony counts above 250 were set as too numerous to count (TNTC) (a). Statistical significance was determined using the Tukey test *via* pairwise comparison. A p-value above 0.05 (*) was considered non-significant (ns).

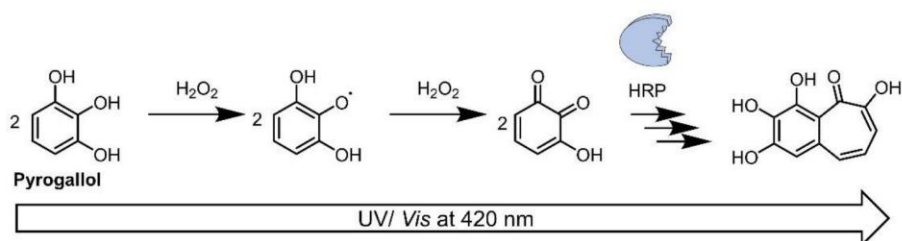


WILEY-VCH

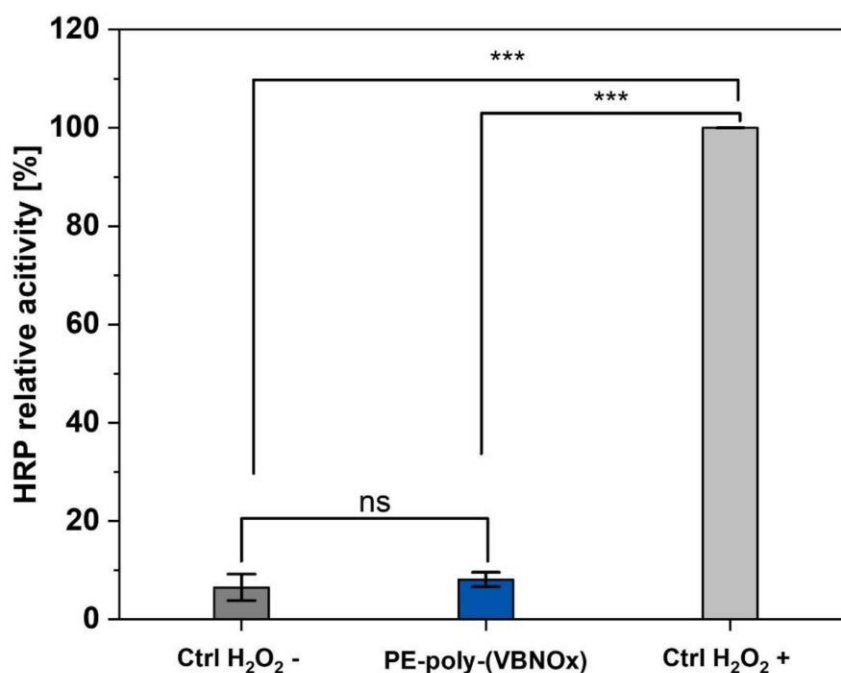
Figure S10. HRP assay of PE-poly-(VBNOx).

Horseradish-peroxidase assay: A) Scheme of horseradish peroxidase (HRP) catalyzed dimerization of pyrogallol in presence of H_2O_2 and its detection via UV/vis measurements at 420 nm. B) Results of the HRP assay: Assay was carried out and HRP relative was calculated as described in the experimental section. For comparison, an H_2O_2 containing positive control (Ctrl H_2O_2 +) with a final H_2O_2 concentration of 0.1 mM was added. Furthermore, a negative control without H_2O_2 (Ctrl H_2O_2 -) was added. Bars are represented as mean values \pm SD of at least three independent measurements. Statistical significance was determined using the Tukey test *via* pairwise comparison $p \leq 0.001$ (***) and a p-value above 0.05 (*) was considered as non-significant (ns).

A



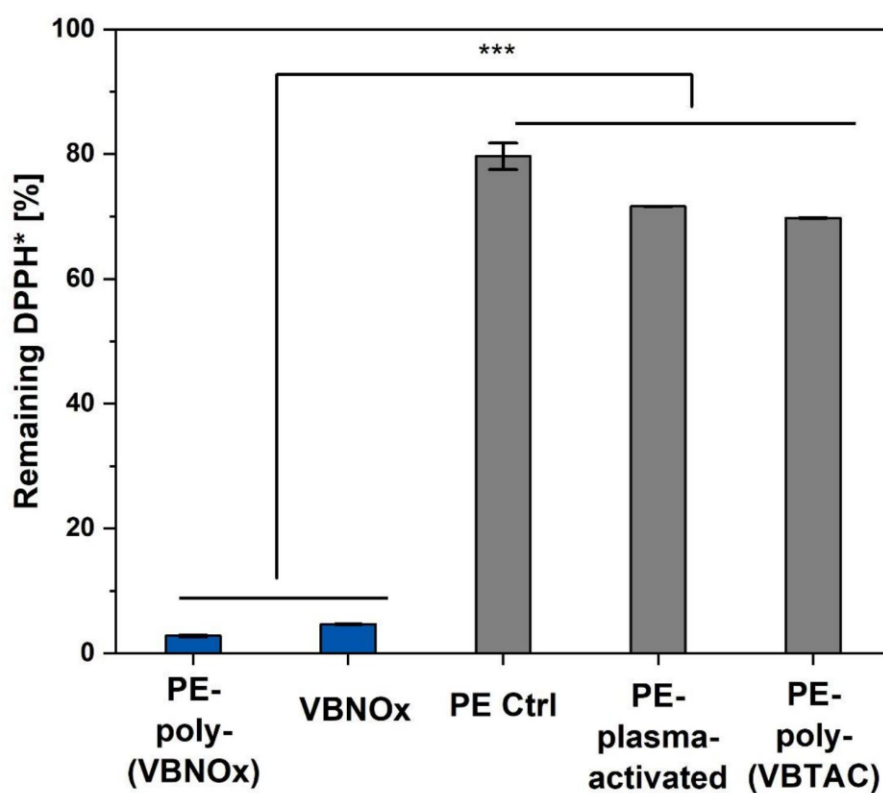
B



WILEY-VCH

Figure S11. DPPH assay: Overview of DPPH-assay at 70°C in benzene for 24 hours of incubation.

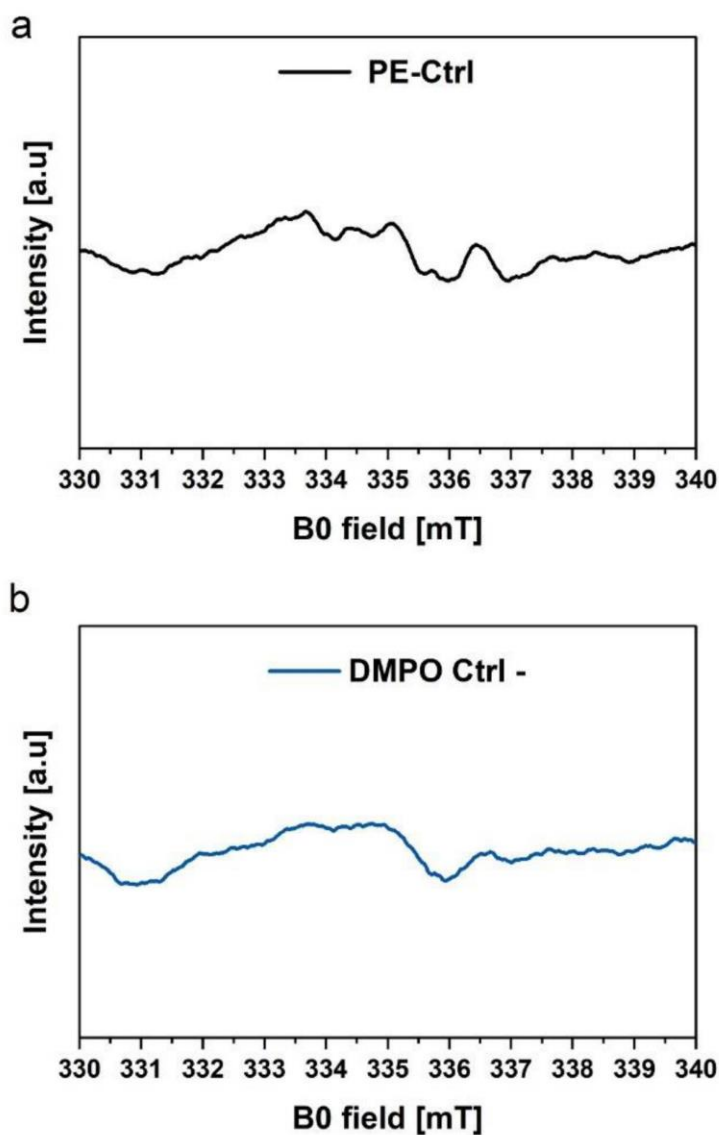
The assay was carried out as described in the experimental section. As control experiments pristine PE (PE Ctrl), plasma-activated PE and grafted poly-vinylbenzyltrimethylammonium-chloride PE-poly-(VBTAC) were added. Bars are represented as mean values \pm SD of at least three independent measurements. Statistical significance was determined using the Tukey test *via* pairwise comparison $p \leq 0.001$ (***).



WILEY-VCH

Figure S12. Control experiments of the EPR spectroscopy.

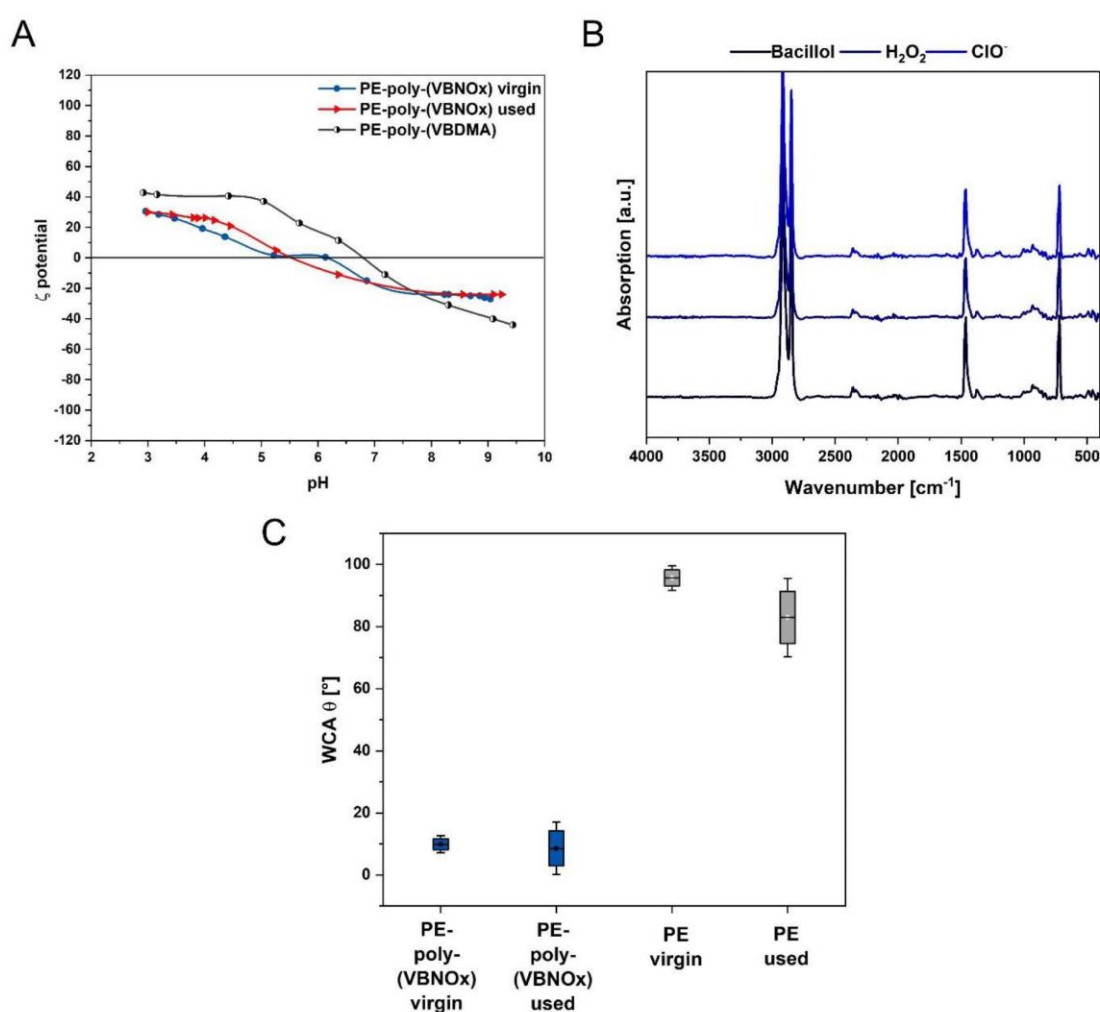
a) pristine PE incubated with spin trapping DMPO (PE-Ctrl) showing no radical formation. b) PE-poly-(VBNOx) incubated without spin trapping DMPO (DMPO Ctrl -).



WILEY-VCH

Figure S13. Water contact angles, Zeta potential and ATR-FTIR spectra after repeated ASTM E2149-13a (three times).

A) Zeta potential measurements of PE-poly-(VBNOx) before and after the antibacterial activity test (ASTM e2149-13a), for further comparison the precursor tertiary amine containing material PE-poly(VBDMA) was added. B) ATR-FTIR spectra after the 3rd ASTM e2149-13a repetition with subsequent cleaning in water/*i*PrOH and drying at room temperature. C) Advancing water contact angles (WCAs) of PE-poly-(VBNOx) before (virgin) and after the 3rd ASTM E2149-13a repetition (used). Pristine PE was used for comparison.



WILEY-VCH

Estimated grafting yield of PE-poly-(VBNOx)

The grafting yield σ of PE-poly-(VBNOx) was calculated to be $10.5 \mu\text{g}\cdot\text{cm}^{-2}$ using the following equation:

$$\sigma(\text{poly} - \text{VBNOx}) = d * 1 \text{ cm}^2 * \rho$$

σ (poly-VBNOx): Grafting yield of poly-VBNOx [$\mu\text{g}\cdot\text{cm}^{-2}$]

d: Layer thickness calculated by ToF-SIMS-SPM analysis was 100 nmp: Density of a styrene-based-polymer = $1.05 \text{ g}\cdot\text{cm}^{-3}$

WILEY-VCH

Synthetic procedures

PE-poly-(VBTAC) was prepared according to a previously reported method.^[1]

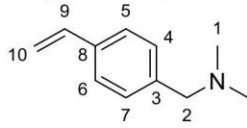
N,N-Dimethyl-1-(4-vinylbenzylamine-*N*-oxide) (VBNOx): *N,N*-Dimethyl-1-(4-vinylbenzylamine) VBDMA (1eq, 12.40 mmol, 2.00 g) was added dropwise at 0°C to a solution of aqueous hydrogen peroxide (30% w/w) (8 eq, 99.23 mmol, 10.14 mL). The reaction mixture was stirred for 10 hours at room temperature. Activated carbon was added to the solution at 0°C for decomposition of excess hydrogen peroxide. The decomposition of hydrogen peroxide was tracked using peroxide test stripes. After completed decomposition, the reaction mixture was filtered and all volatile compounds were removed under reduced pressure. Freeze drying of the crude product gave 2.15 g (12.13 mmol, 98%) of the title compound VBNOx as a colorless powder. ¹H NMR (400 MHz, D₂O): [δ ppm] = 7.59 (d, ³J_{HH} = 8.3 Hz, 2H, 4-H, 7-H), 7.52 (d, ³J_{HH} = 8.3 Hz, 2H, 5-H, 6-H), 6.85 (dd, ³J_{HH} = 11.0, 17.8 Hz, 1H, 9-H), 5.94 (dd, ²J_{HH} = 0.9, 17.7 Hz, 1H, 10a-H), 5.40 (dd, ²J_{HH} = 0.9, 17.7 Hz, 1H, 10b-H), 4.44 (s, 2H, 2-H), 3.16 (s, 6H, 1-H). ¹³C NMR (150 MHz, D₂O): [δ ppm] = 138.9 (C9), 135.9 (C8), 132.9 (C, C7), 128.9 (C3), 126.3 (C5, C6), 115.6 (C10) 73.5 (C2), 56.7 (C1). HRMS (ESI): m/z calculated for C₁₁H₁₅NO: 178.1226, found 178.1227 [M-H]⁺.

3-Methacrylamido-*N,N*-dimethylpropan-1-amine oxide (MAANOx): *N*-[3-(Dimethylamino)propyl]methacrylamide (1 eq, 11.63 mmol, 2.00 g) was dissolved in 5 mL demineralized water and was added dropwise at 0°C to a solution of aqueous hydrogen peroxide (30% w/w) (8 eq, 93.04 mmol, 9.50 mL). The reaction mixture was stirred for 6 hours at 0°C. Activated carbon was added to the solution at 0°C for decomposition of excess hydrogen peroxide. The decomposition of hydrogen peroxide was confirmed with peroxide test stripes. After completed decomposition, the reaction mixture was filtered and all volatile compounds were removed under reduced pressure. The final lyophilization of the crude product gave 1.98 g (10.63mmol, 91 %) of the title compound MAANOx as a colorless viscous liquid. ¹H NMR (400 MHz, D₂O): [δ ppm] = 5.73-5.71 (m, 1H, 7a-H), 5.49-5.46 (m, 1H, 7b-H), 3.41-3.35 (m, 4H, 4-H, 6-H), 3.04 (s, 6H, 9-H), 2.13-2.04 (m, 2H, 5-H), 1.78 (t, ³J_{HH} = 2.6 Hz, 8-H). ¹³C NMR (100 MHz, D₂O): [δ ppm] = 171.9 (C2), 138.9 (C1), 121.5 (C7), 67.9 (C6), 57.3 (C9), 36.6 (C4), 23.0 (C5), 17.6 (C8). HRMS (ESI): m/z calculated for C₉H₁₈N₂O₂: 187.1441, found 187.1431 [M-H]⁺.

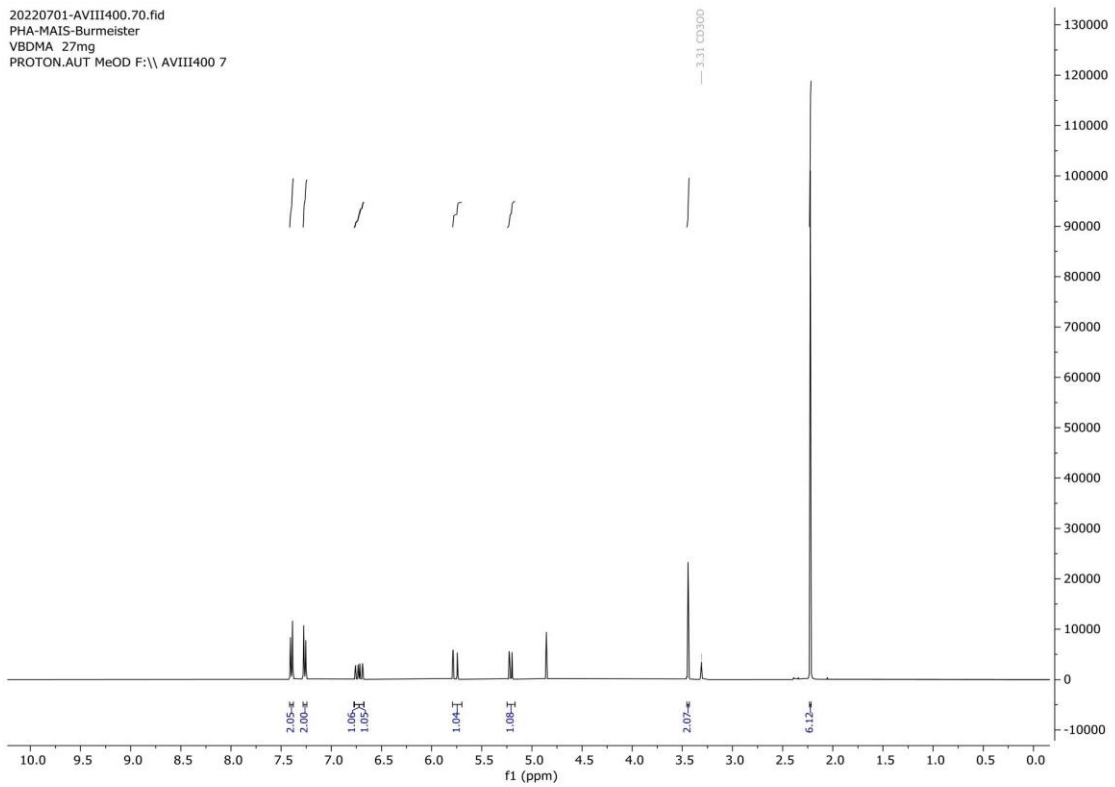
2-(Methacryloyloxy)-*N,N*-dimethylethan-1-amine oxide (MANOx): 2-(Dimethylamino)ethyl methacrylate (1eq, 12.59 mmol, 2.00 g) was dissolved in 5 mL demineralized water and was added dropwise at 0°C to a solution of aqueous hydrogen peroxide (30% w/w) (8 eq, 100.76 mmol, 10.29 mL). The reaction mixture was stirred for 10 hours at 0°C. Activated carbon was added to the solution at 0°C to decompose excess hydrogen peroxide. The decomposition of hydrogen peroxide was confirmed with peroxide test stripes. After completed decomposition, the reaction mixture was filtered and all volatile compounds were removed under reduced pressure. The crude product was dissolved in 10 mL of demineralized water. The pH was adjusted with 0.1M NaOH to 12 and 10 mL of Et₂O were added. Layers were separated and the aqueous layer was extracted 3 times with each 10 mL of Et₂O. Freeze drying of the aqueous phase gave 2.01 g (11.60 mmol, 92 %) of the title compound MANOx as a colorless viscous liquid. ¹H NMR (500 MHz, D₂O): [δ ppm] = 5.60-5.58 (m, 1H, 7a-H), 5.29-5.27 (m, 1H, 7b-H), 3.94 (t, ³J^{HH} = 5.1 Hz, 2H, 4-H), 3.40 (t, ³J^{HH} = 5.1 Hz, 2H, 3-H), 3.18 (s, 6H, 5-H), 1.82 (t, ³J^{HH} = 1.2 Hz, 3H, 7-H). ¹³C NMR (126 MHz, D₂O): [δ ppm] = 142.3 (C2), 120.3 (C7), 71.6 (C4), 58.1 (C5), 56.0 (C3), 18.9 (C6). HRMS (ESI): m/z calculated for C₈H₁₅NO₃: 174.1124, found 174.1104 [M-H]⁺.

WILEY-VCH

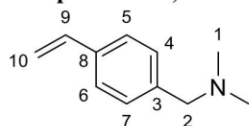
NMR-spectra

¹H Spectra of *N,N*-dimethyl-1-(4-vinylbenzylamine) (VBDMA):

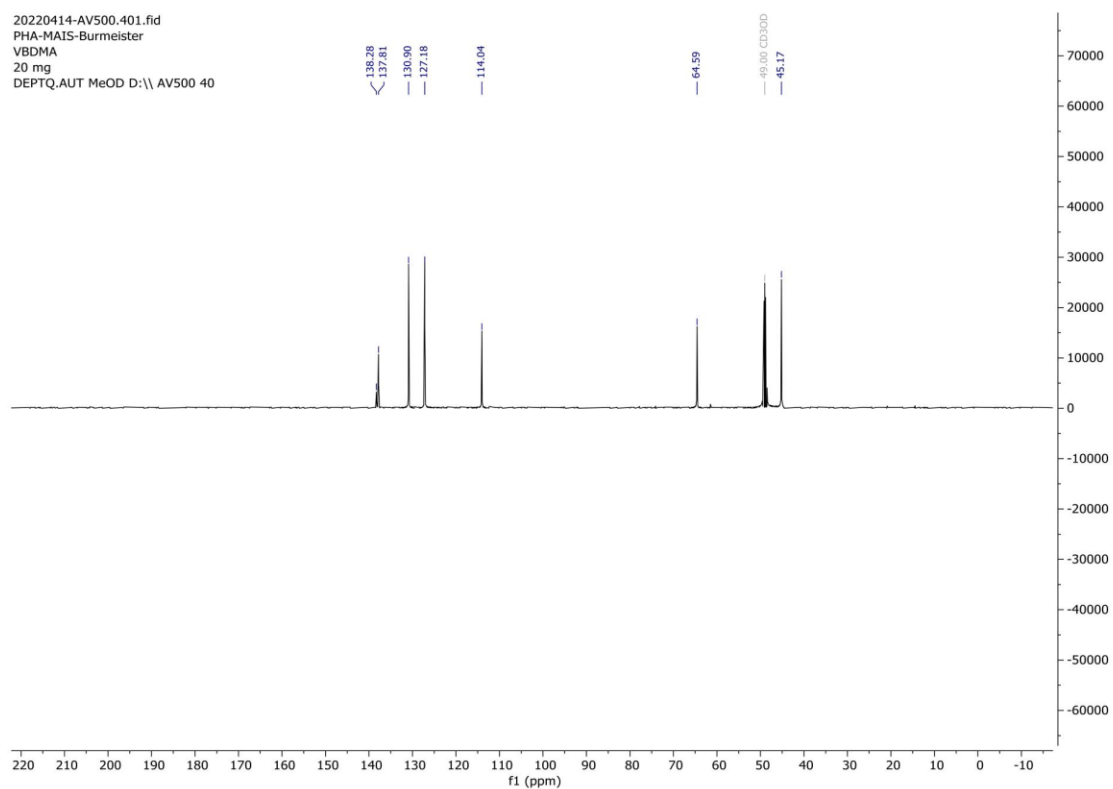
20220701-AVIII400.70.fid
PHA-MAIS-Burmeister
VBDMA 27mg
PROTON.AUT MeOD F:\ AVIII400 7



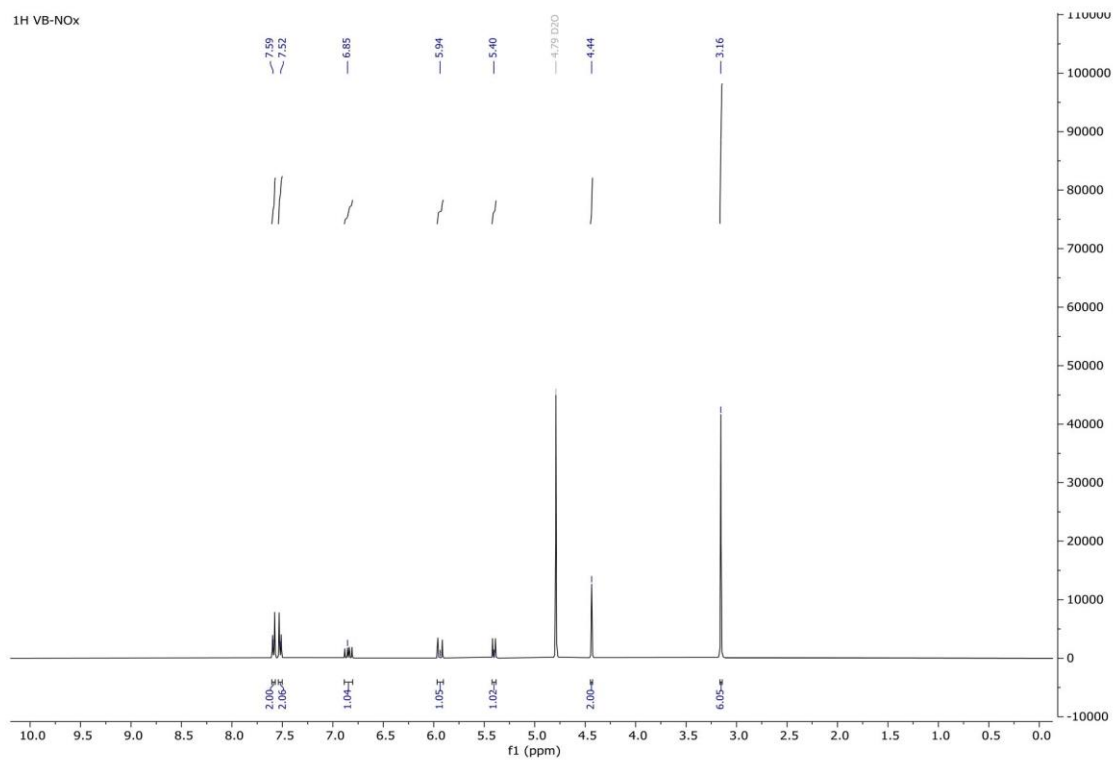
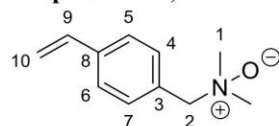
WILEY-VCH

 ^{13}C Spectra of *N,N*-dimethyl-1-(4-vinylbenzylamine) (VBDMA):

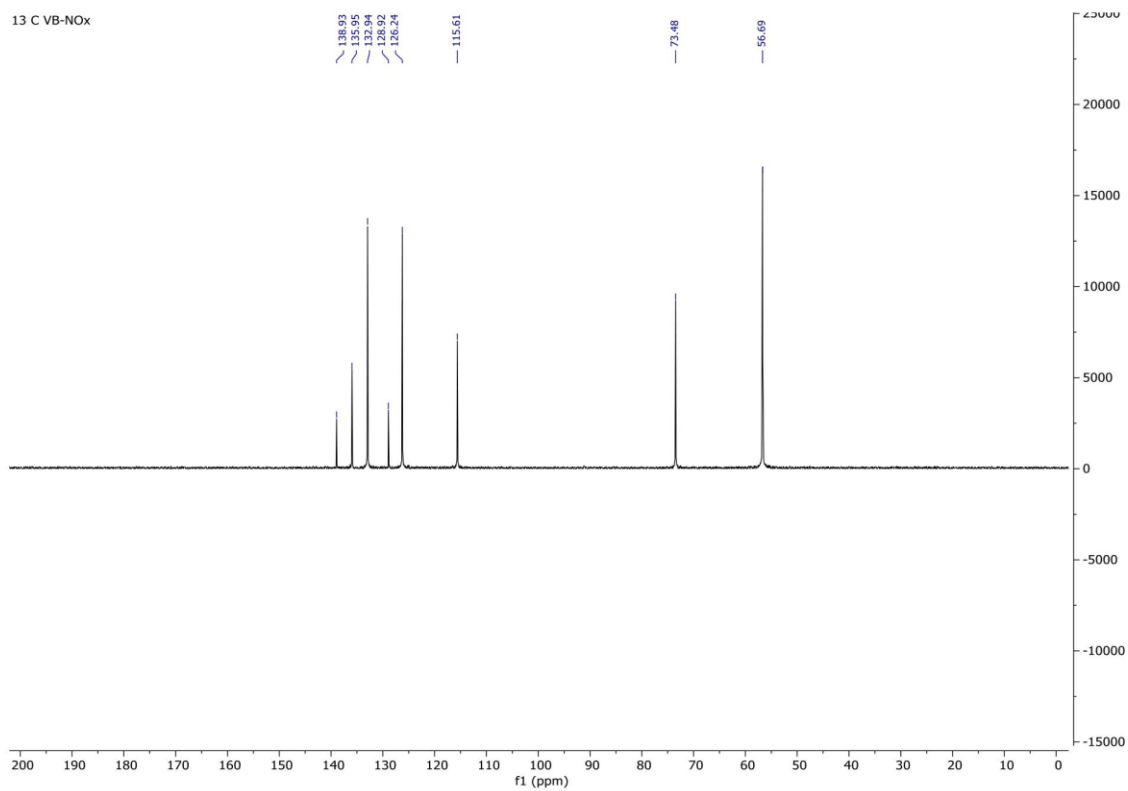
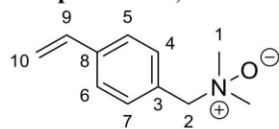
20220414-AV500.401.fid
PHA-MAIS-Burmeister
VBDMA
20 mg
DEPTQ.AUT MeOD D:\ AV500 40



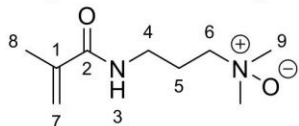
WILEY-VCH

¹H Spectra of N, N-Dimethyl-1-(4-vinylbenzylamine-N-oxide) (VBNOx):

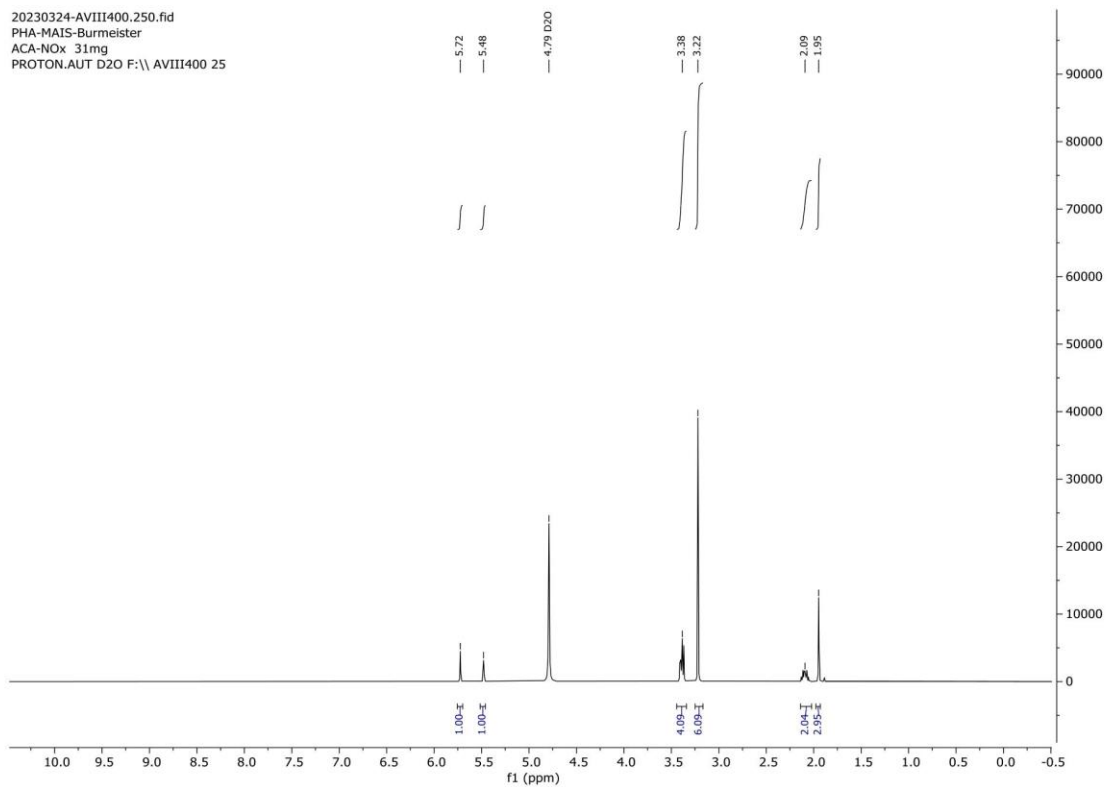
WILEY-VCH

 ^{13}C Spectra of N, N-Dimethyl-1-(4-vinylbenzylamine-N-oxide) (VBNOx):

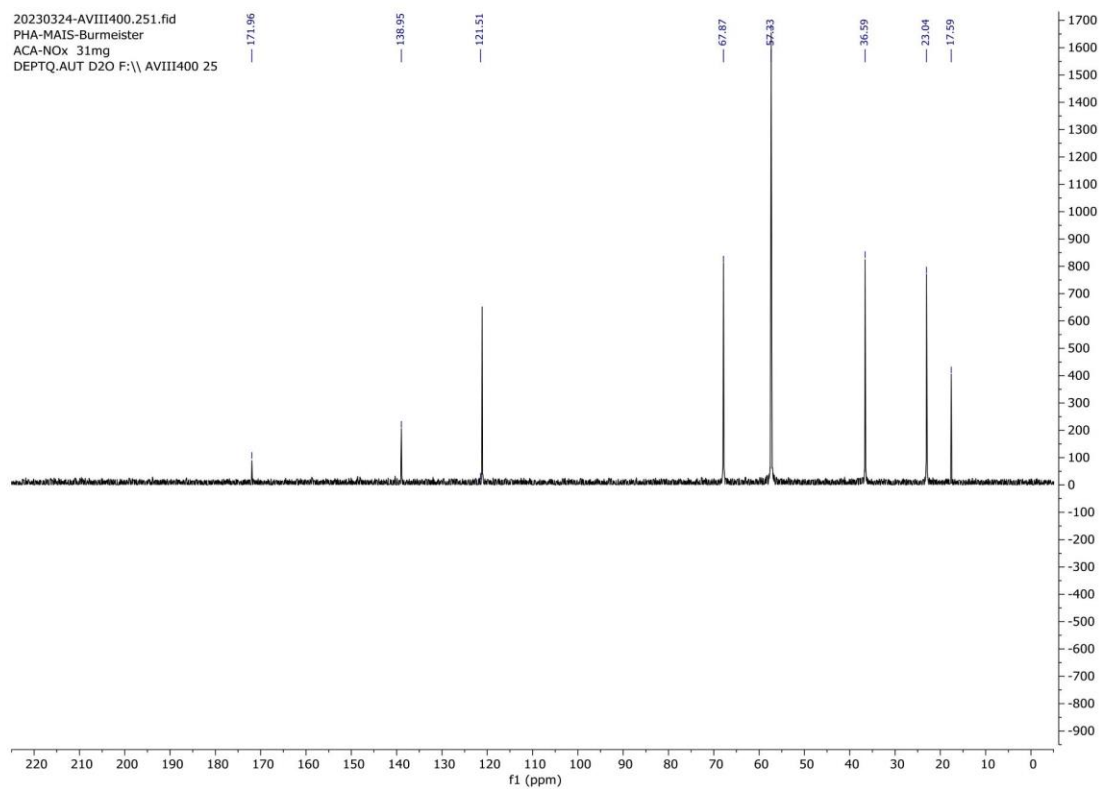
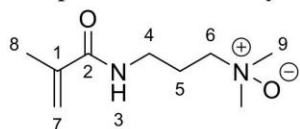
WILEY-VCH

¹H Spectra of 3-methacrylamido-*N,N*-dimethylpropan-1-amine oxide (MAANOx):

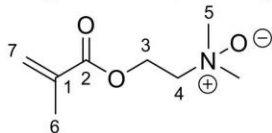
20230324-AVIII400.250.fid
PHA-MAIS-Burmeister
ACA-NOx 31mg
PROTON.AUT D2O F:\ AVIII400 25



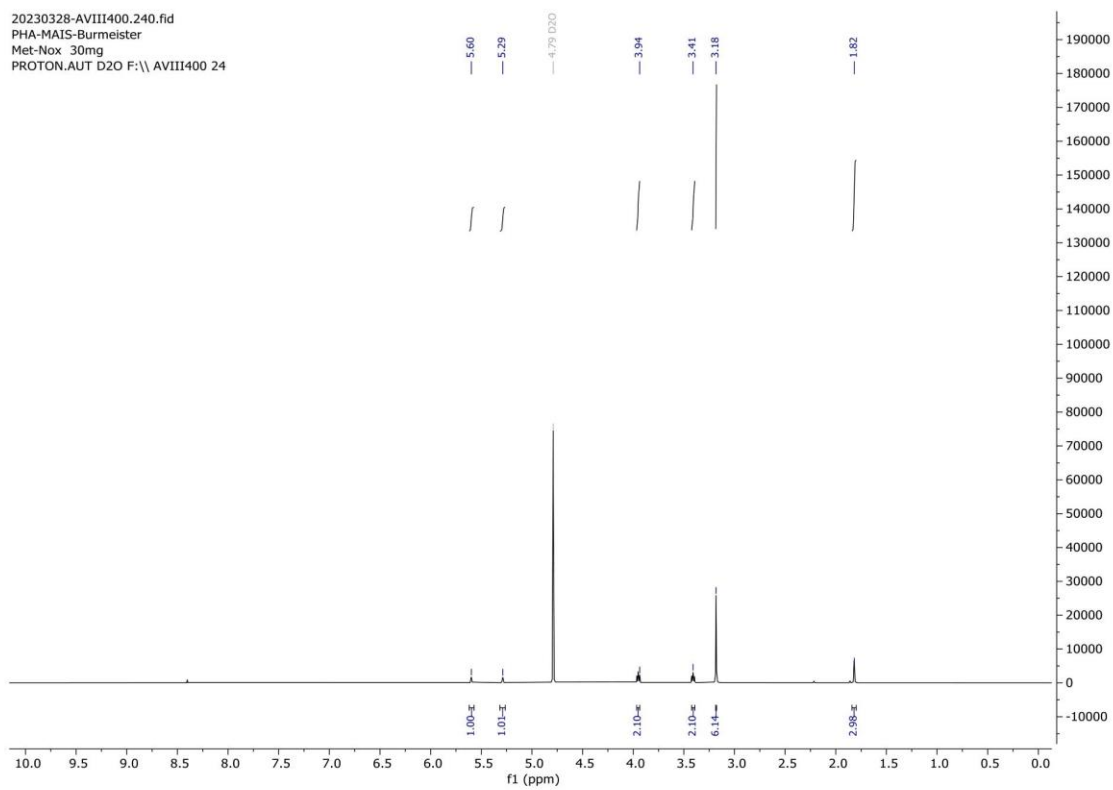
WILEY-VCH

 ^{13}C Spectra of 3-methacrylamido-*N,N*-dimethylpropan-1-amine oxide (MAANOx):

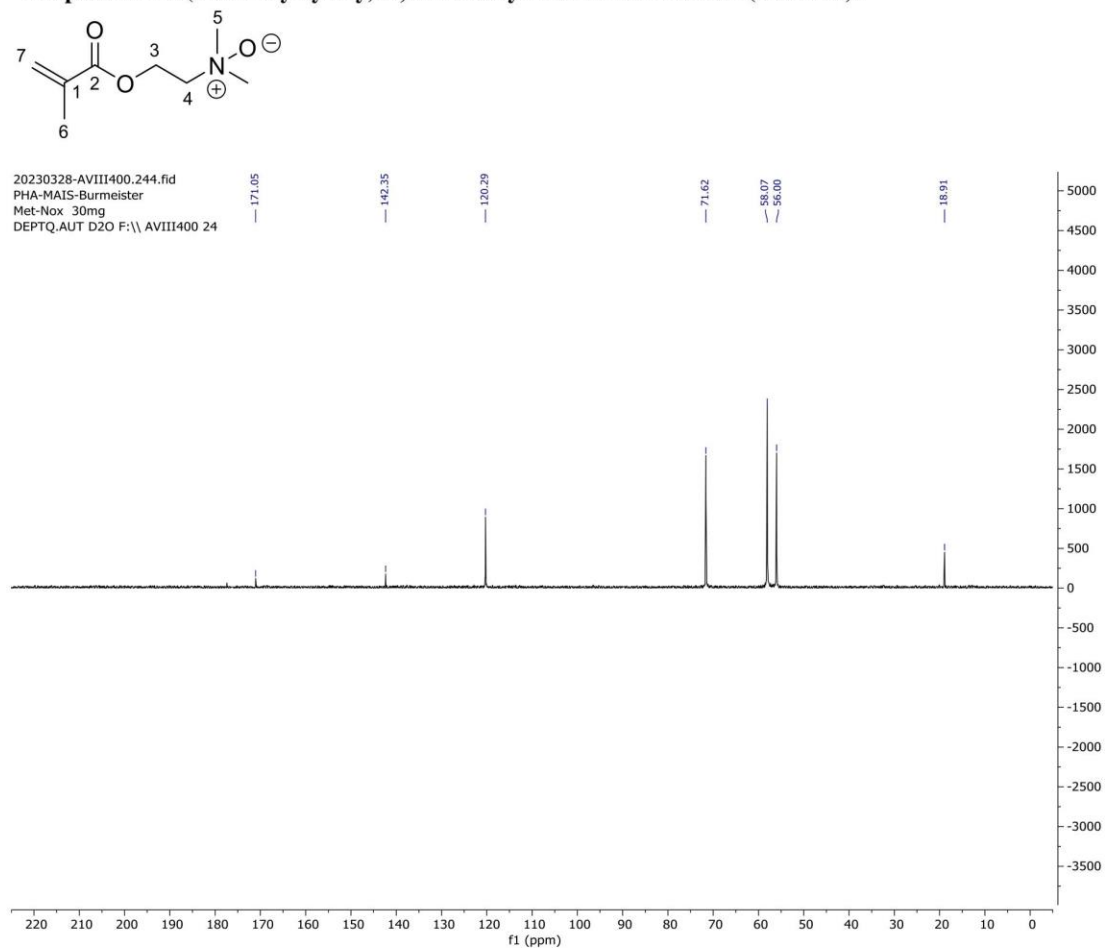
WILEY-VCH

¹H Spectra of 2-(methacryloyloxy)-*N,N*-dimethylethan-1-amine oxide (MAOx):

20230328-AVIII400.240.fid
PHA-MAIS-Burmeister
Met-Nox 30mg
PROTON.AUT D2O F:\ AVIII400 24



WILEY-VCH

 ^{13}C Spectra of 2-(methacryloyloxy)-*N,N*-dimethylethan-1-amine oxide (MANOx):

- [1] S. Kliewer, S. G. Wicha, A. Broker, T. Naundorf, T. Catmadim, E. K. Oellingrath, M. Rohnke, W. R. Streit, C. Vollstedt, H. Kipphardt, W. Maison, *Colloids Surf., B* **2020**, *186*, 110679.

9.2 Supplementary Experimental Section

9.2.1 Transcriptome analysis

As colonization substrates, plasma-activated and pristine PE foils (1 cm²) were considered. The plasma activation of PE was performed by an atmospheric air plasma system from Plasmamatreat GmbH (Steinhagen, Germany). The activation step was conducted as described in the experimental sections 5.1 and 5.3. For the observation of gene expression of *V. gazogenes* under early-stage biofilm conditions, PE substrates (1 cm²) were placed in 6 well plates and submerged in 4 mL of artificial seawater medium. Overnight precultures were used for the inoculation at OD_{600 nm} = 0.05. The plates were incubated at 22 °C under gentle shaking (80 rpm) for 8 h. Cells were scratched off the surface of the PE substrate to get rid of the planktonic cells. Only harvesting cells were attached to the surface. 2 ml of 20% stop mix consisting of 95 % ethanol and 5% phenol was added to the cells. The mixture was centrifuged for 20 min at 4 °C. Supernatant was discarded and the pellet was washed three times in PBS buffer and afterward immediately frozen in liquid nitrogen and stored at -70°C. The pellets were sent to Vertis Biotechnologie AG, Freising, Germany. The company conducted the next steps of RNAseq. The NGS libraries were single-read sequenced on an Illumina NextSeq 500 system using 75 bp read length. The NGS library pool was analyzed on a Shimadzu MultiNA microchip electrophoresis system.

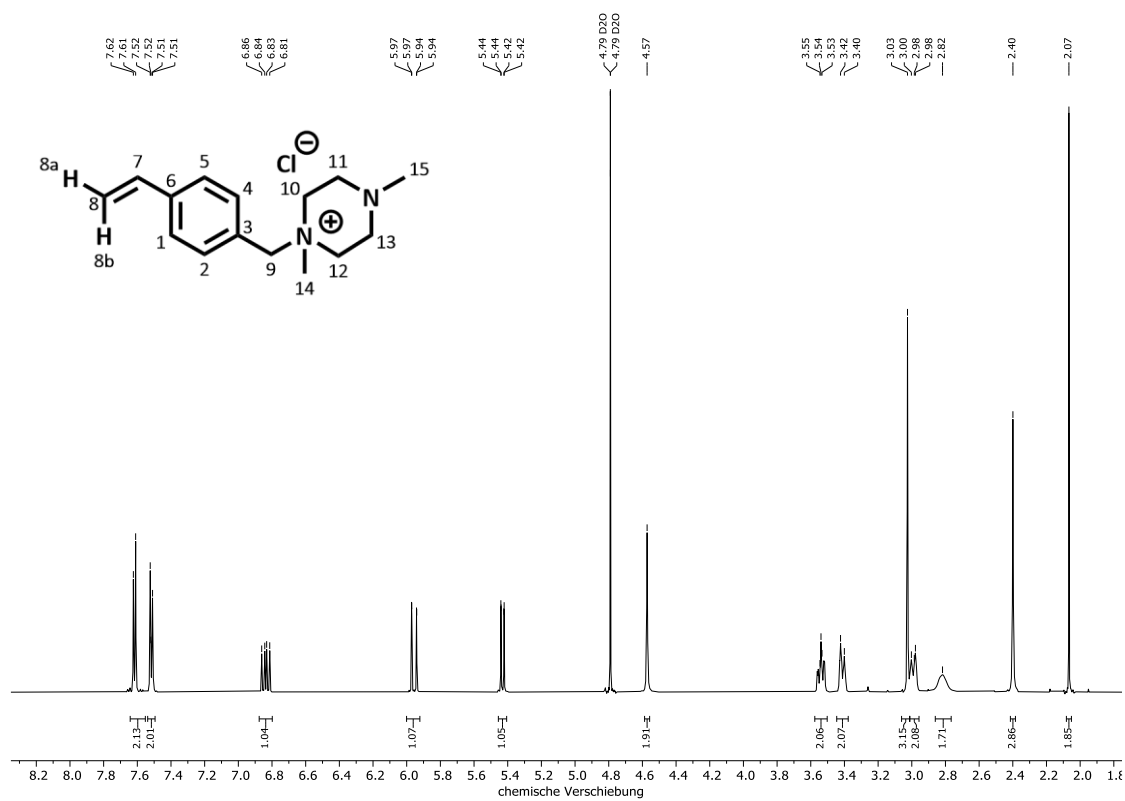
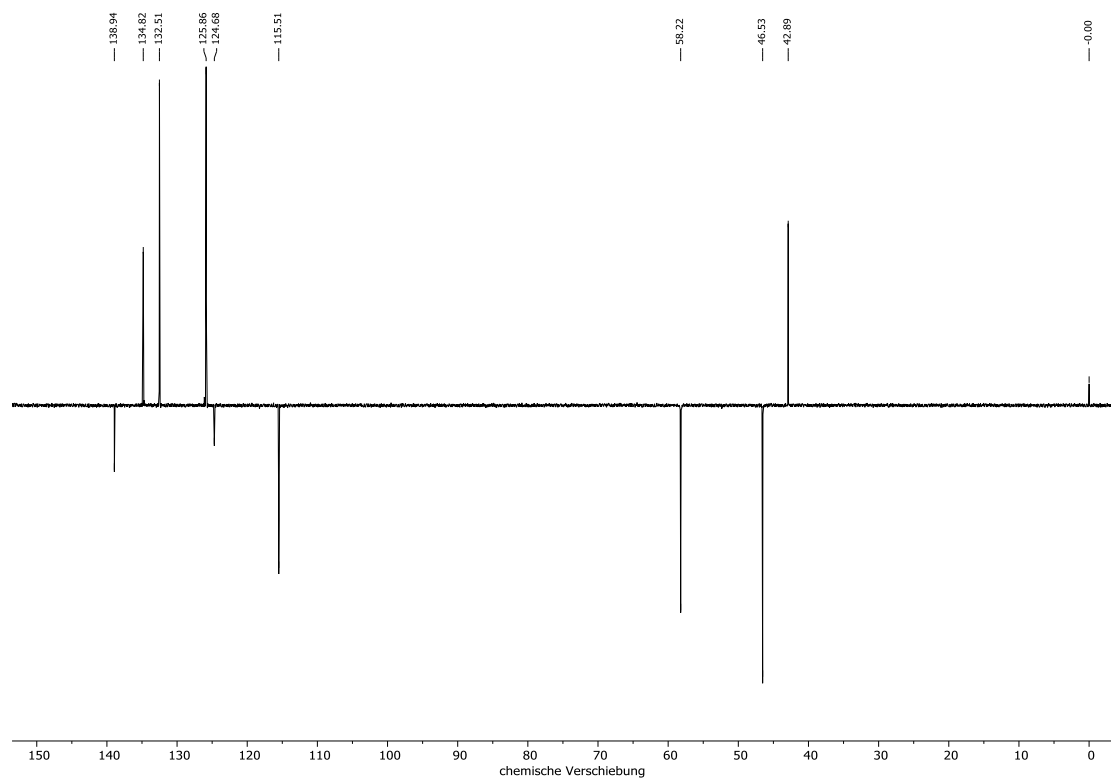
9.2.2 Synthesis of 1,4-dimethyl-1-(4-vinylbenzyl) piperazin-1-ium chloride (VB-DMP):

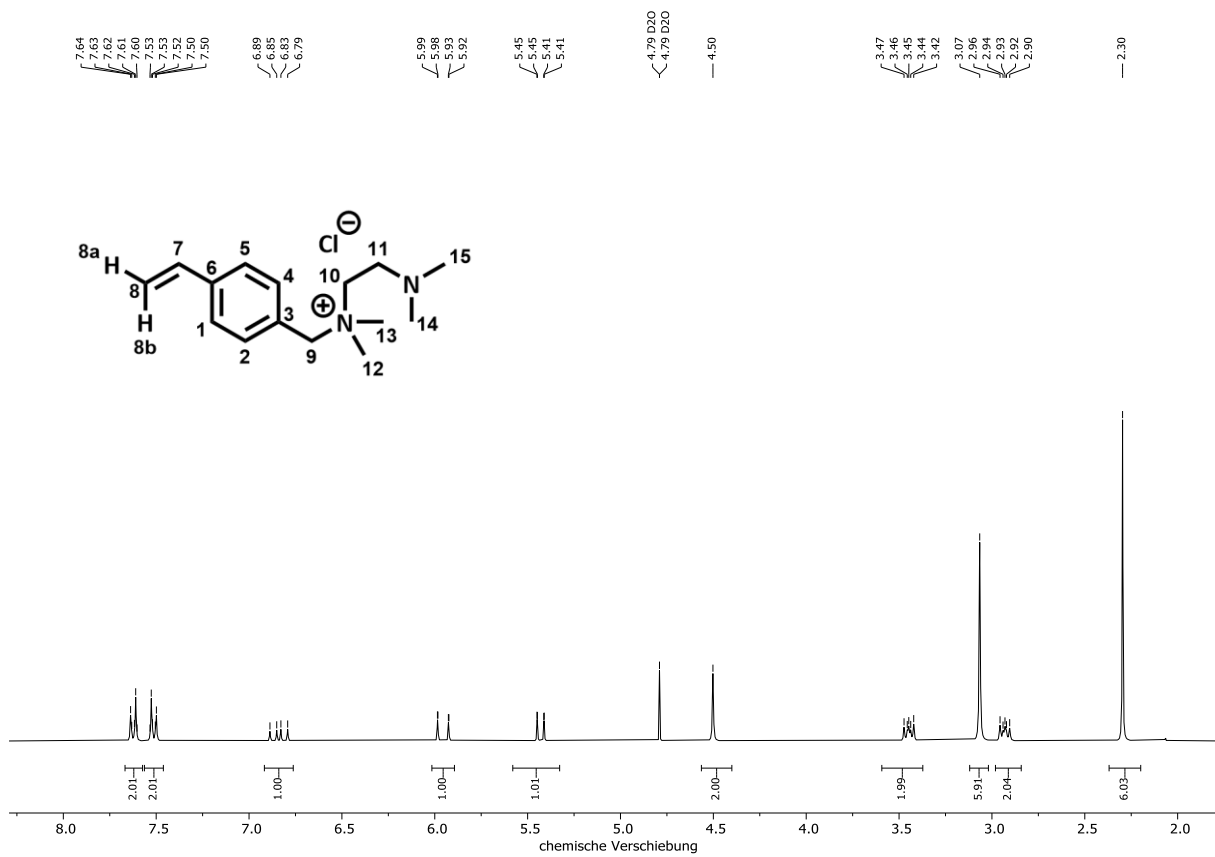
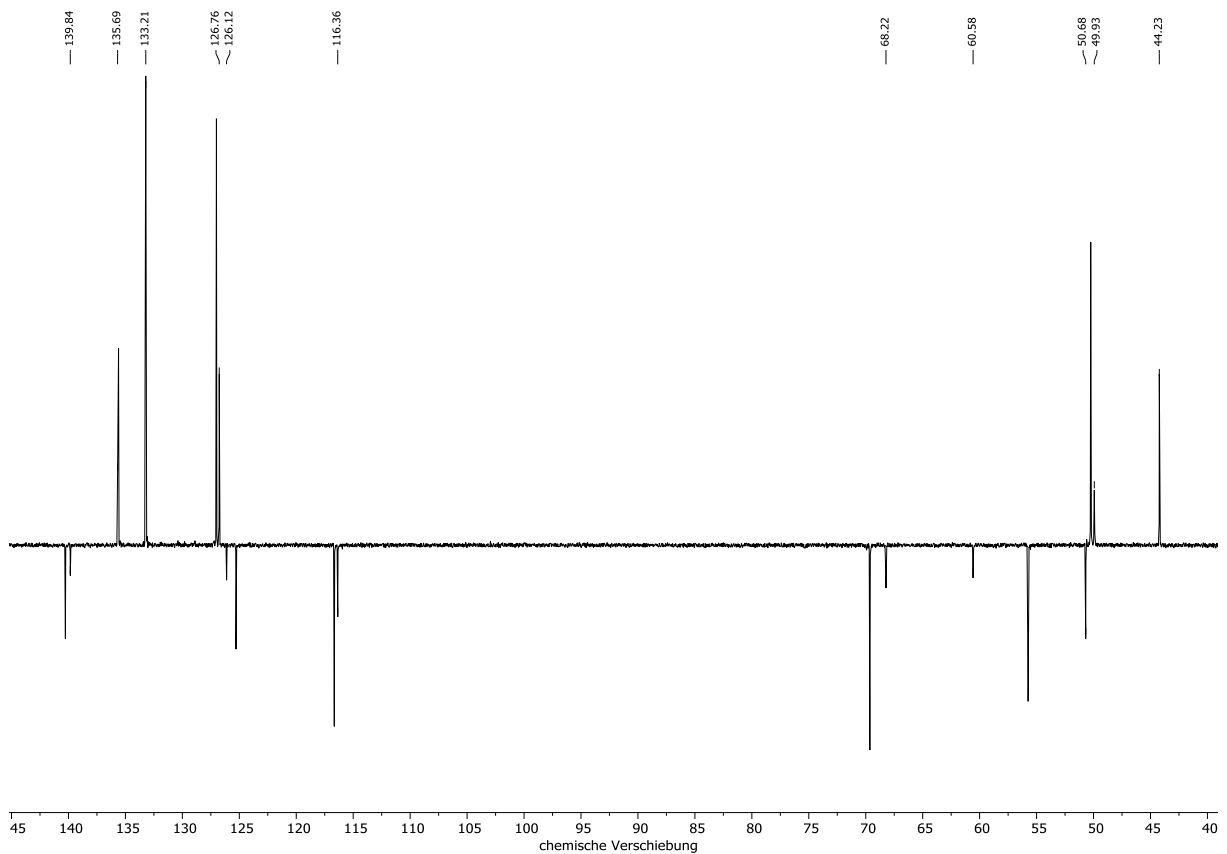
To a stirring solution of dimethyl piperazine (17.4 mL, 128 mmol, 2.0 eq.) in acetonitrile (100 mL) was added *p*-vinylbenzyl chloride (10 mL, 63.9 mmol, 1 eq.) over 5 min. The resulting yellowish solution was stirred for 18 h at room temperature. The resulting suspension was filtered, the colorless crystalline solid was washed with cold acetonitrile (3 x 10 mL) under reduced pressure. The product **VB-DMP** (15.20 g, 56.95 mmol, 89%) was obtained as a colorless amorphous solid. **IR:** ν [cm⁻¹] = 3098, 2968, 2814, 2358, 2251, 1365, 1138, 891. **¹H-NMR:** (600 MHz, D₂O, 298 K): δ [ppm] = 7.64-7.60 (m, 2H, H-2, H-4), 7.56-7.49 (m, 2H, H-1, H-5), 6.84 (dd, ³J_{H,H} = 17.7 Hz, ³J_{H,H} = 11.0 Hz, 1H, H-7), 5.96 (dd, ²J_{H,H} = 17.7 Hz, ²J_{H,H} = 0.8 Hz, 1H, H-8b), 5.43 (dd, ²J_{H,H} = 11.0 Hz, ²J_{H,H} = 0.8 Hz, 1H, H-8a), 4.57 (s, 2H, H-9), 3.58 – 3.50 (m, 2H, H-10, H-12), 3.45 – 3.38 (m, 2H, H10, H-12), 3.03 (s, 3H, H-14), 3.02 – 2.96 (m, 2H, H-11, H-13), 2.83 – 2.80 (m, 2H, H-11, H-13), 2.40 (s, 3H, H-15). Impurities: 2.07 (s, 2H) (Acetonitrile) **¹³C-NMR:** (151 MHz, D₂O, 298 K): δ [ppm]= 138.94 (C6), 134.82 (C7), 132.51 (C1, C5), 125.86 (C2, C4), 124.68 (C3), 115.51 (C8), 58.22 (C10, C12), 46.53 (C11, C13), 42.89 (C15). **HRMS (ESI+):** (*m/z*) [M]⁺ = 232.1891 (calculated) und 232.1895 (found).

9.2.3 Synthesis of 2-(dimethyl amino)-N, N-dimethyl-N-(4-vinylbenzyl) ethan-1-aminium chloride (VB-TMEDA):









To a stirring solution of TMEDA (19.3 mL, 128 mmol, 2.0 eq.) in acetonitrile (80 mL), *p*-vinylbenzyl chloride (10 mL, 63.9 mmol, 1 eq.) was added over 5 min. The resulting yellowish solution was stirred for 25 min at room temperature. The solution was concentrated under reduced pressure and an orange oil was obtained. This was taken up in acetonitrile (20 mL) and crystallized. The resulting suspension was filtered and the colorless crystalline solid was washed with cold acetonitrile (3 x 10 mL) and dried under reduced pressure. The product **VB-TMEDA** (16.25 g, 60.58 mmol (95%)). was obtained as a colorless amorphous solid. **IR:** ν [cm⁻¹] = 2966, 2822, 2767, 1454, 860 cm⁻¹. **¹H-NMR:** (300 MHz, D₂O, 298 K): δ [ppm]= 7.67 – 7.46 (m, 4H, H-1, H-2, H-4, H-5), 6.84 (dd, ³J_{H,H} = 17.7 Hz, ³J_{H,H} = 11.0 Hz, 1-H, H-7), 5.95 (dd, ²J_{H,H} 17.7, 0.8 Hz, 1H, H-8b), 5.43 (dd, ²J_{H,H} = 11.0, 0.8 Hz, 1H, H-8a), 4.50 (s, 2H, H-9), 3.59 – 3.37 (m, 2H, H-10), 3.07 (s, 6H, H-12,H-13), 2.98 – 2.84 (m, 2H, H-11), 2.30 (s, 6H, H-14, H-15). **¹³C-NMR:** (151 MHz, D₂O, 298 K) δ [ppm] = 139.84 (C6), 135.69 (C7), 133.21 (C1, C5), 126.76 (C2, C4), 126.12 (C3), 116.36 (C8), 68.22 (C9), 60.58(C10), 50.68 (C11), 49.93 (C12, C13), 44.23 (C14, C15). **HRMS (ESI+):** (*m/z*) für [M]⁺ = 233.2013 (calculated) und 233.2009 (found).











9.2.4 NMR Spectra





















 $^1\text{H-NMR}$ VB-DMP in D_2O , 600 MHz. $^{13}\text{C-NMR}$ VB-DMP in D_2O , 151 MHz.

$^1\text{H-NMR}$ VB-TMEDA in D_2O , 300 MHz. $^{13}\text{C-NMR}$ VB-TMEDA in D_2O , 151 MHz

9.3. Hazardous Material

Substance	Hazard pictograms	Hazard Statement	Precautionary Statements ¹⁵⁰
1,3-Propanesultone		H301, H312, H315, H318, H350	P201, P202, P280, P301+P310, P302+P352+P312, P305+P351+P338
1,4 dimethyl piperazine		H225, H302, H314	P210, P233, P280; P305+361+353, P305+P351+P338, P402+P235
1,4-Diaza-bicyclo [2.2.2] octane		H228, H302, H315, H318	P210, P240, P280, P301+P312, P302, P305+P351+P338
2,2'-Azobis(2- methylpropionitrile)		H242; H302+H332, H412, EUH044	P210, P235, P273, P304+P340+P312, P370+P378, P403
2,2-Diphenyl-1- picrylhydrazyl		H242, H302+H312+H332, H315, H317, H319, H334	P210, P215, P280, P302+P352+P312, P370 +P378, P403
4-Toluenesulfonyl chloride		H290, H315, H317, H318	P234, P261, P264, P280, P302+P352, P305+P351+P338
4-Vinylbenzyl chloride		H302, H311, H314, H317	P261, P270, P280, P301+P312, P303+P361+P353, P305+P351+P338
Acetic acid		H226, H314	P210, P233, P240, P280, P303+P361+P353, P305+P351+P338

Substance	Hazard pictograms	Hazard Statement	Precautionary Statements ¹⁵⁰
Acetone		H225, H319, H336, EUH066	P210, P240, P305+P351+P338, P403+P233
Acetonitrile		H225, H302+H312+H332, H319	P210, P280, P301+P312, P303+P361+P353, P304+P340+P312, P305+P351+P338
Ammonium persulfate		H272, H302, H315, H317, H319, H334, H335	P210, P280, P301+P312, P302+P352, P304+P340+P312, P304+P351+P338
Copper-(I)-bromide		HZ302+H312, H315, H318, H410	P264, P273, P280, P301+P312, P302+P352+P312, P305+P351+P338
Crystal violet		H302, H318, H351, H410	P202, P273, P280, P301+P312, P305+P351+P338, P308+P313
Ethanol		H225, H319	P210, P233, P240, P241, P242, P305+P351+P338
Ethyl acetate		H225, H319, H336, EUH066	P210, P233, P240, P305+P351, P338, P403+P235
Hydrochloric acid		H290, H314, H335	P280, P303+P361+P353, P303+P361+P353, P350+P351, P310
Hydrogen peroxide 30%		H272, H302, H332, H318	P220, P261, P280, P305+P351+P338
Isopropanol		H225, H319, H336	P210, P240, P305+p351+P338, P403+P233

Substance	Hazard pictograms	Hazard Statement	Precautionary Statements ¹⁵⁰
Methanol	  	H225, H301+H311+H331, H370	P210, P233, P280, P301+P310, P303+P361+P353, P304+P340+P311
<i>N, N, N', N', N''</i> - Pentamethyl- diethylenetriamine	 	H302, H311, H314	P280, P301+P312+P330, P303+P361+P353, P305+P351+P338+P310
Pentane	   	H225, H304, H336, H411, EUH066	P210, P273, P301+P310+P331
Sodium-dodecylsulfate	  	H228, H302+H332, H315, H318, H335, H412	P210, P261, P280, P301+P312+P330, P305+P351+P338+P310, P370+P378
Sodium-hydroxide		H290, H314	P280, P301+P330+P331, P305+P351+P338, P308+P310
Sulfuric acid		H290, H314	P280, P301+P330+P331, P303+P361+P353, P305+P351+P310
Tetramethyl- ethylenediamine	  	H225, H332, H302, H314	P210, P280; P301+P330+P331, P303+361+353, P304+P340+P312, P404+P351+P338
Triethylamine	  	H225, H302, H311+H331, H314, H335	P210, P280, P301+P312, P303+P361+P353, P304+P340+P311, P305+P351+P338+P310

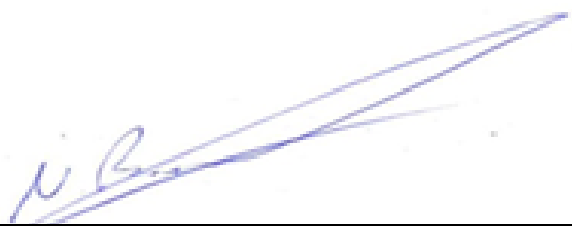
Declaration

I hereby declare that I have written this thesis myself and that I have not used any auxiliaries other than those indicated. The submitted thesis with the title: "Charged Polymer Brushes: Design, Synthesis and Microbiological Evaluation" corresponds to the one on the electronic storage medium. I hereby affirm that this thesis was not submitted in a previous doctoral procedure.

Eidstaatliche Versicherung

Hiermit versichere ich an Eides statt, die vorliegende Dissertation mit dem Titel: "Charged Polymer Brushes: Design, Synthesis and Microbiological Evaluation" selbst verfasst und keine anderen als die angegebenen Hilfsmittel benutzt zu haben. Die eingereichte schriftliche Fassung entspricht der auf dem elektronischen Speichermedium. Ich versichere, dass die Dissertation nicht in einem früheren Promotionsverfahren eingereicht wurde.

22.02.2024



Datum, Unterschrift